



THE HONG KONG
POLYTECHNIC UNIVERSITY

香港理工大學

Pao Yue-kong Library

包玉剛圖書館

Copyright Undertaking

This thesis is protected by copyright, with all rights reserved.

By reading and using the thesis, the reader understands and agrees to the following terms:

1. The reader will abide by the rules and legal ordinances governing copyright regarding the use of the thesis.
2. The reader will use the thesis for the purpose of research or private study only and not for distribution or further reproduction or any other purpose.
3. The reader agrees to indemnify and hold the University harmless from and against any loss, damage, cost, liability or expenses arising from copyright infringement or unauthorized usage.

IMPORTANT

If you have reasons to believe that any materials in this thesis are deemed not suitable to be distributed in this form, or a copyright owner having difficulty with the material being included in our database, please contact lbsys@polyu.edu.hk providing details. The Library will look into your claim and consider taking remedial action upon receipt of the written requests.

Pao Yue-kong Library, The Hong Kong Polytechnic University, Hung Hom, Kowloon, Hong Kong

<http://www.lib.polyu.edu.hk>

**FINE PARTICULATE MATTER POLLUTION IN SELECTED
CITIES OF EASTERN AND SOUTHERN CHINA:
COMPOSITIONS, SOURCES, AND IMPACTS**

XIE JIAWEN

PhD

The Hong Kong Polytechnic University

2021

The Hong Kong Polytechnic University

Department of Civil and Environmental Engineering

**Fine Particulate Matter Pollution in Selected Cities of Eastern and
Southern China: Compositions, Sources, and Impacts**

Xie Jiawen

**A thesis submitted in partial fulfilment of the requirements for
the degree of Doctor of Philosophy**

Dec 2020

Certificate of Originality

I hereby declare that this thesis is my own work and that, to the best of my knowledge and belief, it reproduces no material previously published or written, nor material that has been accepted for the award of any other degree or diploma, except where due acknowledgement has been made in the text.

_____ **(Signed)**

Xie Jiawen _____ **(Name of student)**

Abstract

Fine particulate matter (PM_{2.5}) pollution has become a perennial environmental issue and triggered health problems in China, especially in densely populated regions such as the Yangtze River Delta (YRD) in the east and the Pearl River Delta (PRD) in the south. For health-oriented pollution control, it is necessary to dissect PM_{2.5} from both the chemical and the biological perspective and further identify the key toxic components and source contributors of adverse health effects. However, integrated investigation of PM_{2.5} composition and closed-loop analysis from sources to impacts have not yet been completed. Towards this end, PM_{2.5} was collected simultaneously for one year across geographical locations under different land-use impacts in selected typical cities of the YRD and PRD regions, to characterise the inter/intra-regional differentiation of chemical and biological features of PM_{2.5} with linkage to emission sources and the resultant health impacts.

First, the chemical composition profile (*e.g.*, organic carbon and elemental carbon, water-soluble ions, and metals) of PM_{2.5} showed notable regional differences, while the intra-regional heterogeneity was more exhibited by trace metal profiles, with the highest concentrations of anthropogenically enriched metals at industrial sites. Incorporating the speciation and bioaccessibility information, a population-based risk assessment of chronic exposure to metal was conducted. Chromium and arsenic were major contributors of the estimated metal-induced carcinogenic risk (CR) over the safety level in both regions, whereas the non-carcinogenic risk (NCR) within the threshold was largely attributed to manganese. Traffic emission and combustion (coal/waste/biomass burning) were identified as two common dominant sources of metal-induced CR to be controlled in both regions, besides an elevated contribution from industrial emissions in the YRD

sites. The differentiation of source profiles between environmental risk and the total mass of metals further implied the necessity of a regulatory control shift from a mass concentration-based to a risk-based framework for public health benefit.

Second, investigations on the biological components of PM_{2.5} focused on bacteria and embedded antibiotic resistance genes (ARGs) for their potential as microbial hazards to humans and provided the following findings: (1) more pronounced seasonal variations in bacterial and ARG abundance at the (semi)rural site compared with other land-use types in both regions; (2) inter-regional differentiation in ARG profiles in contrast to similar intra-regional antibiotic resistance patterns independent of land-use types and seasonal cycles; (3) the targeted ARGs associated with limited bacterial genera and their relative abundance commonly correlated to mobile genetic elements (MGEs) across regions; (4) ARG and MGE enrichment in PM_{2.5} with high variability covering the span of terrestrial/aquatic samples from natural to engineered environments and human/animal excreta; and (5) PM_{2.5} as a unique exposure pathway for bacteria and ARGs via inhalation with region-specific importance, compared with ingestion of drinking water and food.

To further quantify the contributions of anthropogenic sources to PM_{2.5}-associated bacteria and ARGs, a metagenomics-based study was conducted in a wastewater treatment plant (WWTP) in Hong Kong, supplemented with analysis of literature data on other potential sources. As evidenced by the more distinct disparities in bacterial and ARG profiles across environmental matrices (PM_{2.5} and sewage/sludge/effluent) compared with sampling locations (PM_{2.5} in WWTP and urban/coastal sites), PM_{2.5} was reaffirmed as a unique bacterial and ARG reservoir. Dominated by multidrug resistance, the increasing ARG enrichment in PM_{2.5} along the coastal–urban–WWTP gradient

illustrated the impacts of human activities on the atmospheric accumulation of ARGs. However, a co-occurrence analysis suggested that the horizontal transfer of ARGs, especially to pathogens, could hardly occur in the atmosphere. Finally, ~18% of the bacteria and >36% of the relevant ARGs in urban and WWTP PM_{2.5} were attributable to sewage/sludge/effluent in WWTP. The results showed the differences in source profiles between chemical and microbial hazards in PM_{2.5} and indicated WWTPs as an important source of airborne bacteria and ARGs to be controlled.

Collectively, the current integrated study on PM_{2.5} from both chemical and (micro)biological dimensions quantitatively links geographical disparities in chemical-induced health risk (*e.g.*, metal) and microbial components (*e.g.*, bacteria and associated ARGs) to their sources. The results contribute to a better understanding of PM_{2.5} pollution and provide valuable information for health-oriented pollution control that can be adapted for regional-specific circumstances, thus helping to improve regional air quality and protect public health.

Acknowledgement

The PhD study is not only an impressive start for research careers, but also a valuable journey about persistence. During the entire endeavour, many people have more or less provided their kind support and help to me, without which this thesis may not have been finished.

First and foremost, I would like to convey my most sincere appreciation to my supervisor Prof. Xiangdong Li, for his continued guidance and support for my PhD study. His immense passion and high standards towards research have always inspired and motivated me during my study.

I would also like to express my deep gratitude to Dr Ling Jin for his constructive suggestions and instructions on the design of my research project and the writing of relevant manuscripts. My thanks also go to other members and alumni of Prof. Li's research group, including Dr Jinli Cui, Dr Tangtian He, Dr Dong Wu, Dr Xinyu Du, Dr Lili Ming, Dr Siyuan Liang, Dr Nan Xiang, Dr Yanping Zhao, Ms Jue Zhao, Mr Xiaohua Zhang, and Ms Yihua Wang, for their support during my study. I would like to give my thanks to our technicians, Mr W.S. Lam, Dr Hang Liu, and Ms Celine Che, for their assistance with my laboratory work. In addition, I am grateful to Prof. Xiaosan Luo from Nanjing University of Information Science and Technology and Dr Jun Li from Guangzhou Institute of Geochemistry, Chinese Academy of Sciences, as well as their students, for helping with sample collection. My appreciation also extends to all of my friends during my life at The Hong Kong Polytechnic University for their friendship and support.

I must acknowledge the Research Grant Council of Hong Kong for funding my research project.

Last but not least, I must give my deepest thanks to my beloved family for their selfless love and full support.

Table of Content

Certificate of Originality	I
Abstract	II
Acknowledgement.....	V
Table of Content	VII
Abbreviations	XII
List of Figures	XV
List of Tables.....	XXIII
Chapter 1 Introduction	1
1.1 Background.....	1
1.2 Research objectives	4
1.3 Organisation.....	5
Chapter 2 Literature Review	7
2.1 PM _{2.5} pollution, a health-threatening environmental issue.....	7
2.2 Chemical characteristics of PM _{2.5}	9
2.2.1 Major chemical components and potential sources	9
2.2.2 Spatiotemporal variations and regional patterns	11
2.2.3 Trace metals as critical components with health relevance.....	12
2.2.3.1 Metal bioaccessibility and molecular speciation	13
2.2.3.2 Risk assessment and related sources	15
2.3 Biological perspectives of airborne particulates.....	16
2.3.1 Microorganisms in airborne particles	17

2.3.1.1 Microbial distribution in particles with different sizes	17
2.3.1.2 Concentration, community structure, and spatiotemporal variations	18
2.3.1.3 Putative sources and transport of bacteria in the atmosphere	21
2.3.1.4 Survival, viability, and health concerns	22
2.3.2 ARGs as a kind of emerging pollutant	24
2.3.2.1 Origin, acquisition, and development of antibiotic resistance in the environment	24
2.3.2.2 Dissemination of ARGs via airborne particles	25
2.3.3 Aerosolisation potential of bacteria and ARGs from key anthropogenic sources	28
2.3.4 Detection methods of airborne microbes and relevant genetic elements – development and challenges	30
2.4 Summary and outlook	32
Chapter 3 Methodology	34
3.1 General information of the studied regions	34
3.2 Description of the sampling strategy and sampling sites	35
3.2.1 Sample collection for the regional comparative study	40
3.2.2 Sample collection in typical sources of PM _{2.5} -associated bacteria and ARGs	45
3.3 Chemical-based analysis	51
3.3.1 WSI and carbonaceous material analysis	51
3.3.2 Total metal(loid) and bioaccessible metal(loid) analysis	51
3.3.3 Source apportionment	53
3.3.4 Analysis of arsenic speciation by X-ray absorption near edge structures (XANES)	55
3.3.5 Metal-based health risk assessment	56
3.3.6 Modification on the calculation of arsenic-induced health risks based on speciation distribution	59

3.3.7 Data analysis.....	61
3.4 Molecular biological analysis	61
3.4.1 Sample pretreatment	62
3.4.2 DNA extraction.....	63
3.4.3 Absolute quantification of target genes (16S rRNA gene, ARGs, and MGEs) by qPCR.....	66
3.4.3.1 Construction of qPCR standards.....	66
3.4.3.2 qPCR detection of target genes	69
3.4.3.3 Assessment of inhalational contribution to the daily intake of bacteria and ARGs	71
3.4.4 16S rRNA gene amplicon sequencing.....	72
3.4.4.1 Sample preparation and sequencing strategy.....	72
3.4.4.2 Taxonomy annotation and source tracking.....	73
3.4.5 Metagenomic sequencing	74
3.4.5.1 Sequencing strategy	74
3.4.5.2 Bioinformatic analysis	75
3.4.6 Statistical analysis.....	77

Chapter 4 Chemical Characterisation and Metal-based Health Risk-oriented Source Apportionment of PM_{2.5} across Geographical Locations in the YRD and PRD

79

4.1 Inter-regional and intra-regional comparisons of the concentrations and chemical composition profiles of PM _{2.5}	79
4.2 Regional comparisons of the characteristics of PM _{2.5} -associated metal(loid)s	85
4.2.1 Total metal(loid) concentrations.....	85
4.2.2 Bioaccessibility and bioaccessible concentrations of targeted metal(loid)s	89
4.3 Speciation-adjusted risk assessment of metal(loid)s	92
4.4 Contribution of emission sources to metal-induced health risks	96

4.4.1 Identification of emission sources of major chemical components in PM _{2.5} , with a particular focus on trace metals	96
4.4.2 Source-resolved metal-induced risk profiles based on PMF results.....	99
4.5 Summary.....	103
Chapter 5 Biological Components of PM_{2.5}, from Associated Airborne Bacteria to ARGs in the YRD and PRD	107
5.1 Regional differences in PM _{2.5} -associated bacterial loads and community structure	107
5.1.1 Intra-regional urban–rural contrast of PM _{2.5} -associated bacterial loads .	107
5.1.2 Inter-regional comparisons of PM _{2.5} -associated bacteria in urban areas .	110
5.1.3 Relationship between chemical components and bacterial community structures in PM _{2.5}	113
5.2 Regional fingerprints of ARG profiles with relevance to potential hosts	115
5.2.1 Regional comparisons of the concentration and composition of PM _{2.5} -associated ARGs.....	115
5.2.2 Relationship between airborne bacteria and the detected ARGs.....	119
5.3 Enrichment of ARGs and MGEs in PM _{2.5} in the studied regions	123
5.4 Human exposure to environmental ARGs from inhalation and other pathways in the YRD and PRD	126
5.5 Summary.....	128
Chapter 6 Typical Urban Anthropogenic Sources of PM_{2.5}-associated Bacteria and ARGs – A Case Study in a WWTP in Hong Kong	131
6.1 Distinctive features of the microbial community structure among PM _{2.5} , sewage, sludge, and effluent.....	132
6.2 Discrimination of ARG profiles across environmental matrices and sampling locations.....	134

6.3 Co-occurrence patterns of ARGs, MGEs, and potential hosts to indicate the environmental resistome risks	140
6.3.1 Overview of the co-occurrence relationship of ARGs, MGEs and bacteria	141
6.3.2 Evaluation of resistome risks across sample types and sampling locations	144
6.3.3 Exploration of ARG-associated priority pathogens in urban and WWTP PM _{2.5}	145
6.4 Contributions of WWTP and other potential sources to airborne bacteria and ARGs	148
6.5 Summary.....	151
Chapter 7 Conclusions and Recommendations	155
7.1 Overall summary and major conclusions	155
7.2 Limitations of the current study and future perspectives	158
Appendix 1.....	163
Appendix 2.....	166
References.....	186
Publications from the Research Project	208

Abbreviations

Abbreviations	Full names
ANOSIM	Analysis of similarities
ANOVA	Analysis of variance
ARB	Antibiotic-resistant bacteria
ARG(s)	Antibiotic resistance gene(s)
BLASTn	Basic Local Alignment Search Tool for nucleotide sequence
BF	Barge facility
CCA	Correspondence canonical analysis
CEPT	Chemically enhanced primary treatment
CFU	Colony-forming unit
CH	Conghua (Guangzhou, Guangdong Province)
CI	Confidence interval
CR	Carcinogenic risk
DNA	Deoxyribonucleic acid
EC	Elemental carbon
EC _{IR1.5}	Effect concentration with an induction ratio of 1.5
EF(s)	Enrichment factor(s)
ESBL	Extended-spectrum β -lactamase
ESKAPE	<i>Enterococcus faecium</i> , <i>Staphylococcus aureus</i> , <i>Klebsiella pneumoniae</i> , <i>Acinetobacter baumannii</i> , <i>Pseudomonas aeruginosa</i> , and <i>Enterobacter</i> spp.
FT	Flocculation tank
GDP	Gross domestic product
HGT	Horizontal gene transfer
HQ	Hazard quotient
HS	Heshan (Jiangmen, Guangdong Province)
HT	Hok Tsui (Hong Kong)
HG-AFS	Hydride generation and atomic fluorescence spectrometry
HPLC	High-performance liquid chromatography
ICP-MS	Inductively coupled plasma mass spectrometry

Abbreviations	Full names
IDBA-UD	Iterative de Bruijn graph <i>de novo</i> assembler for short reads sequencing data with highly uneven sequencing depth
IUR	Inhalation unit risk
LCA	Lowest common ancestor
LCF	Linear combination fitting
LDA	Linear discriminant analysis
LEfSe	Linear discriminant analysis effect size
LOQ	Limit of quantification
LS	Lishui (Nanjing, Jiangsu Province)
MDL	Method detection limit
MGE(s)	Mobile genetic element(s)
NAAQS	National Ambient Air Quality Standard
NCBI	National Center for Biotechnology Information
NCR	Non-carcinogenic risk
NMDS	Non-metric multidimensional scaling
OC	Organic carbon
OEHHA	Office of Environmental Health Hazard Assessment (California Environmental Protection Agency)
PAH	Polycyclic aromatic hydrocarbon
PBS	Phosphate-buffered saline
PCR	Polymerase chain reaction
PERMANOVA	Permutational multivariate analysis of variance
PERMDISP	Permutational analysis of multivariate dispersions
PES	Polyethersulfone
PK	Pukou (Nanjing, Jiangsu Province)
PM-ARGs	Potentially mobile antibiotic resistance genes
PM _{2.5}	Atmospheric particulate matter with an aerodynamic diameter of or less than 2.5 μm
PMF	Positive matrix factorization
PRD	Pearl River Delta
PU	The Hong Kong Polytechnic University
qPCR	Quantitative polymerase chain reaction

Abbreviations	Full names
RDA	Redundancy analysis
RfC	Reference concentration
ROS	Reactive oxygen species
rRNA	Ribosomal ribonucleic acid
RSD	Relative standard deviation
SCISTW	Stonecutters Island Sewage Treatment Work
SST	Sludge storage tank
ST	Sedimentation tank
TH	Tianhe (Guangzhou, Guangdong Province)
TSP	Total suspended particles
USEPA	United States Environmental Protection Agency
VPA	Variation partitioning analysis
WHO	World Health Organization
WSI	Water-soluble ions
WWTP(s)	Wastewater treatment plant(s)
XANES	X-ray absorption near edge structures
XAS	X-ray absorption spectroscopy
XW	Xuanwu (Nanjing, Jiangsu Province)
YRD	Yangtze River Delta

List of Figures

Figure 1-1 A flowchart of the objectives and structure of the thesis.....	5
Figure 2-1 Number of death caused by PM _{2.5} in 2019 (plot by country) (Health Effects Institute, 2020). The original data are retrieved from The Institute for Health Metrics and Evaluation (2019).	8
Figure 2-2 Deposition of airborne particulate matter in the human respiratory system with regard to particle size. This figure was adapted from Li et al. (2018c) (Copyright 2018 Chinese Medical Association; production and hosting by Elsevier B.V. on behalf of KeAi Communications Co., Ltd.; open access under the CC BY-NC-ND license [https://creativecommons.org/licenses/by-nc-nd/4.0/]).	9
Figure 2-3 Spatiotemporal variations in surface PM _{2.5} concentration (seasonal mean) over China from December 2013 to November 2019. The figure was adapted from Jiang et al. (2020) (Copyright 2020 the authors; published by Elsevier B.V.; open access under the CC BY-NC-ND license [https://creativecommons.org/licenses/by-nc-nd/4.0/]).	12
Figure 2-4 Spatial variations of aerosol-associated microbial/bacterial load (Bertolini et al., 2013; Bowers et al., 2009; Gao et al., 2017; Gao et al., 2016; Gat et al., 2017; Harrison et al., 2005; Hospodsky et al., 2012; Lee et al., 2010; Li et al., 2020; Ling et al., 2013; Lymperopoulou et al., 2016; Xu et al., 2016a; Xu et al., 2019; Zhen et al., 2017). Filled boxes/dots represent sites in the vicinity of typical sources (e.g., clinical, poultry, and municipal solid waste treatment system). Those unfilled represent ambient sites with land-use types distinguished by colour.....	20
Figure 2-5 Putative natural (blue arrow) and anthropogenic (red arrow) emission sources of airborne bacteria.	22
Figure 2-6 Geographical comparisons of absolute abundance of selected ARGs that are prevalent in aerosol particles (copy m ⁻³) (Gao et al., 2016; Gat et al., 2017; Ling et al., 2013; Wang et al., 2019) assuming equal DNA extraction efficiency across studies. ...	28
Figure 3-1 Geographical locations of the YRD and PRD (created using ArcGIS (2012)).	35
Figure 3-2 Satellite map of the sampling sites (created using ArcGIS (2012) with the World Imagery base map (Esri, 2009)).	42

Figure 3-3 Map of three sampling locations in Hong Kong.....	47
Figure 3-4 Sampling sites in the SCISTW and sample types collected along the treatment process. (A) An overall layout of the SCISTW, with the PM _{2.5} sampling sites marked with stars; (B) an aerial view of the SCISTW; (C) the general sewage treatment process in the SCISTW, with the sampling sites and the corresponding sample types collected marked.	47
Figure 3-5 Wind direction and wind speed during the sampling period in the SCISTW.	48
Figure 3-6 Rarefaction curves of (A) bacterial genera and (B) ARG subtype diversity analysed using the “vegan” package in R.....	75
Figure 4-1 Spatiotemporal variations in PM _{2.5} concentrations at the studied sites in the PRD (TH, CH, and HS) and YRD (XW, PK, and LS). The red dashed line represents the WHO guideline value for PM _{2.5} concentrations (25 µg m ⁻³) based on short-time monitoring (24 h), while the grey dashed line is the Grade II level (75 µg m ⁻³) for 24-h sampling according to China’s Air Quality Standard.....	81
Figure 4-2 Annual average PM _{2.5} concentrations at the studied sites in the PRD (TH, CH, and HS) and YRD (XW, PK, and LS). Line and error bars represent the mean with the 95% CI. Non-parametric Kruskal–Wallis tests were conducted in GraphPad Prism 7 (* <i>p</i> < 0.05; ** <i>p</i> < 0.01). The red dashed line represents the WHO guideline value for PM _{2.5} concentrations (10 µg m ⁻³) on an annual average basis, while the grey dashed line indicates the Grade II level (35 µg m ⁻³) for annual mean according to the Chinese NAAQS.	81
Figure 4-3 Seasonal variations in major chemical components analysed in PM _{2.5} in the PRD and YRD. The pie charts are divided according to the proportion of each analysed component over the total analysed components regarding their concentrations in PM _{2.5} samples.	83
Figure 4-4 Comparisons of the (A) total and (B) bioaccessible metal/metalloid concentrations in PM _{2.5} in the PRD and YRD region based on annual average figures. The concentration value of each element was normalised independently prior to plotting figures in R using the pheatmap package. The original data can be found in Table 4-2 and Table 4-3. Metals presented here were grouped based on the mean value of the EFs in all the sampling sites.....	87

Figure 4-5 EFs of the analysed trace elements (Fe concentration as reference), shown as their annual average. 89

Figure 4-6 Bioaccessible metal concentrations extracted by Gamble’s solution and their corresponding bioaccessibility (%) in PM_{2.5} in the PRD and YRD. The orange box plots represent the bioaccessible concentrations (left Y-axis), while the blue dots indicate the bioaccessibility (right Y-axis). The box plots with whiskers cover data from the 10th to 90th percentile. The error bars for dot plots represent the 95% CI. Non-parametric Kruskal–Wallis tests were conducted in GraphPad Prism 7 (* $p < 0.05$; ** $p < 0.01$; *** $p < 0.001$; **** $p < 0.0001$). 90

Figure 4-7 Toxicity potency of metals with regard to their speciation. Panel (A) presents the correlation (spearman r and p values are shown) between the effect concentration for reactive oxygen species (ROS) induction (EC_{IR1.5}; units: M) of different metals (Jin et al., 2019) and the IUR ($\mu\text{g m}^{-3}$)⁻¹, as well as the inhalation-relevant RfC (mg m^{-3}) of various metals specified in the documents of the USEPA (2018a) and other national standards (Oosthuizen et al., 2015) that are given in Table 3-8. The EC_{IR1.5} data of different metals used here are based on certain kinds of speciation, *i.e.*, Pb(II), V(V), Ni(II), As(V), Mn(II), Cr(III), Cd(II), Fe(III), Cu(II), and Zn(II). Panel (B) presents the dominant speciation of arsenic in three PM_{2.5} samples with high concentrations of arsenic in the semirural-industrial site (HS) in the PRD and one in the suburban-industrial site (PK) in the YRD, illustrated by XANES spectra (black solid line). The red dotted lines represent the LCF results. The spectra of two standards (As(III) and As(V)) were obtained from a previous study (Cui et al., 2013). 93

Figure 4-8 The CR and NCR posed by PM_{2.5}-associated metals in the PRD and YRD. Panel (A) presents the CR and NCR posed by metals across geographical locations under different land-use impacts in the two studied regions, based on annual bioaccessible metal concentrations with modifications according to As and Cr speciation. The box plots with whiskers cover data from the 10th to 90th percentiles, with outliers marked by crosses. The red dashed lines stand for the acceptable risk level for a carcinogen (10^{-6}) and the reference HQ level (1.0) for non-cancer effects recommended by the USEPA. The grey box plots show the original assessment results without speciation adjustment. Panel (B) indicates the relative contributions of various metals to the total CR and NCR in the six sampling sites. 94

Figure 4-9 CR and NCR (presented as the HQ) values from different metals in PM _{2.5} based on their bioaccessible concentrations. The red dotted lines represent the acceptable risk levels for a carcinogen (10 ⁻⁶) and the reference HQ level (1.0) for non-cancer effects recommended by the USEPA.	95
Figure 4-10 Element-resolved metal mass profile and risk (CR and NCR) profile in the PRD and YRD (absolute abundance).	96
Figure 4-11 Resolved source profiles of major chemical components in PM _{2.5} for: (A) the urban TH site in the PRD, (B) the semirural-industrial HS site in the PRD, (C) the urban XW site in the YRD, and (D) the suburban-industrial PK site in the YRD. The coloured bar represents the percentage of certain species contributed by different sources (left Y-axis), while the circle indicates the corresponding concentration of species that originated from these sources (right Y-axis). Error bars represent the 95% CI estimated by the bootstrap method in PMF.	99
Figure 4-12 Contribution of different emission sources to the mass and risk profile of PM _{2.5} -associated metals in the PRD and YRD. Panel (A) highlights the urban–industrial contrast in source-specific health risks posed by trace metals in the PRD and YRD. Panel (B) supplements the source-resolved mass profiles of PM _{2.5} and risk-inducing trace metals (Mn, As, Cd, Cr, V, Co, Ni, Pb, Fe, Cu, and Zn).	102
Figure 4-13 Source-resolved metal mass profile and risk (CR and NCR) profile in the PRD and YRD (absolute abundance).	102
Figure 5-1 Intra-regional rural–urban contrasts of PM _{2.5} -associated 16S rRNA gene abundance (an indicator of bacteria) in the YRD and PRD.	109
Figure 5-2 (A) Relationship between the abundance of the 16S rRNA gene and the concentration of PM _{2.5} and (B) the bacterial weight proportion of PM _{2.5}	109
Figure 5-3 Inter-regional comparisons of PM _{2.5} -associated 16S rRNA gene abundance in urban areas in the YRD and PRD, with an urban site in the temperate zone (Beijing) as a comparison.	111
Figure 5-4 Comparisons of the 16S rRNA gene abundance in PM _{2.5} of different regions in different climate zones. Data for comparisons were sought from the literature (Gao et al., 2017; Hospodsky et al., 2012; Wei et al., 2019; Xu et al., 2019). BD: Baoding, Hebei; YC: Yucheng, Shandong; Mt. Tai: Mountain Tai, Shandong.	112

Figure 5-5 Spatiotemporal patterns of PM _{2.5} -associated bacterial communities at the phylum level in the YRD and PRD in the subtropical zone, compared with bacterial communities in Beijing (the temperate zone).....	112
Figure 5-6 Seasonal variations in the contribution from terrestrial sources (soil/dust) in different sampling sites predicted by SourceTracker2.	113
Figure 5-7 RDA reveals the relationship between the bacterial community and chemical compositions in PM _{2.5} (999 permutations, * <i>p</i> < 0.05). Here only the top 20 bacterial genera were used for analysis. The “adjusted R ² ” on the figures represents the proportion of variance explained by the explanatory variables (chemical components) in the total variance of response variables (bacterial taxa). The percentage marked in the axis means the proportion of variance explained by the certain RDA component in the total explained variance.....	114
Figure 5-8 Annual average (the first four seasons included) concentrations of (A) ARGs and (B) MGEs in the YRD and PRD (subtropical) compared with urban Beijing (temperate) (* <i>p</i> < 0.05; **** <i>p</i> < 0.0001).	117
Figure 5-9 NMDS analysis (Bray–Curtis dissimilarity) based on (A) bacterial communities at the genus level and (B) ARGs profiles, respectively; the ellipse represents the 95% confidence level.....	117
Figure 5-10 Regional signatures of airborne ARG profiles. The relative percentage of each gene is an annual average of all of the samples.	118
Figure 5-11 Seasonal variability of relative abundance of airborne ARGs normalised to the 16S rRNA gene.....	119
Figure 5-12 RDA identifying the relationships between bacterial genera and ARGs in PM _{2.5} (<i>p</i> < 0.05).....	121
Figure 5-13 Spearman correlation matrices (A) between targeted ARGs and (B) between dominant genera (>5%). The asterisks indicate the significant levels (* <i>p</i> < 0.05; ** <i>p</i> < 0.01; *** <i>p</i> < 0.001).....	122
Figure 5-14 Relationships between ARGs and MGEs in PM _{2.5} across the studied sites.	124
Figure 5-15 Relative abundance of ARGs normalised to the 16S rRNA gene in different environmental matrices. Panel (A) was adapted from Li et al. (2015a) (Copyright 2015	

International Society for Microbial Ecology). Note that the data in (A) are based on metagenomic sequencing, while the data in (B) are based on qPCR analyses from this study..... 125

Figure 5-16 Comparisons of *intI1* copy number per cell (assuming on average 4.2 copies of the 16S rRNA gene per cell) between different environmental matrices. Panel (A) was adapted from Ma et al. (2017) (Copyright 2017 American Chemical Society). In (A), *intI1* was identified based on metagenomic sequencing, while in (B) the gene was quantified by qPCR in the current study..... 125

Figure 5-17 Regional comparisons of the human daily intake of ARGs and the 16S rRNA genes between inhalation and ingestion, coupled with a contrast with the U.S. situation. The calculations are based on Equation 3-13, Equation 3-14, and Equation 3-15. Annual average concentrations of targeted genes in the PRD, the YRD, and Beijing generated in this study were used to estimate the daily intake via inhalation. The raw data on the concentrations of the targeted genes in tap water in the YRD and PRD were from Shi et al. (2013) and Su et al. (2018b), respectively. The raw data for samples of shrimp intestines and washed vegetable leaves in the PRD were from Su et al. (2018a) and He et al. (2016), respectively. The U.S. data were obtained from Hospodsky et al. (2012), Xi et al. (2009), Huang (2014), and Echeverria-Palencia et al. (2017)..... 127

Figure 6-1 Relative abundance of microbial communities at the domain level assigned by kraken2 (read-based). 133

Figure 6-2 (A) The number of shared bacterial genera revealed by a Venn diagram and (B) comparisons of PM_{2.5}-associated bacterial loads among different sampling locations. 133

Figure 6-3 Shift in bacterial community structure among sample types: (A) the relative abundance of the profiled bacteria at the phylum level; (B) the NMDS results of the bacterial community at the phylum and genus levels; (C) the taxonomic differentiation among different sample types at the statistically significant level of 0.05 using LEfSe analysis (LDA score > 4.6)..... 134

Figure 6-4 The number of shared ARG subtypes of samples (A) from different environmental matrices and (B) among PM_{2.5} samples collected in different locations. 137

Figure 6-5 Antibiotic resistance profiles of samples across environmental matrices and sampling locations according to the drug class. In (A), ARGs at the type level with the relative abundance no less than 0.5 (normalised to the 16S rRNA gene) are marked with asterisks in the corresponding cells. The correlation-based distance was considered in average-linkage clustering. Panel (B) presents the relative abundance of total identified ARGs normalised to the 16S rRNA gene among sample types and sampling locations. The brown line represents the mean value. Panel (C) shows the contributions of various ARG types to the total ARG abundance in different samples. 138

Figure 6-6 Profiles of the top 100 ARGs with the highest relative abundance (normalised to the 16S rRNA gene) in samples across environmental matrices and sampling locations at the ARG subtype level. ARGs with a relative abundance no less than 0.1 (normalised to the 16S rRNA gene) are marked with asterisks. The correlation-based distance was considered in average-linkage clustering. 139

Figure 6-7 Major significantly discriminative ARGs and resistance types between different sample types revealed by LEfSe analysis (LDA score > 3.3). 140

Figure 6-8 Co-occurrence patterns of ARGs, MGEs, and potential bacterial hosts at the phylum level based on assembled scaffolds (analysed by NanoARG). Panel (A) shows the differences between the ARG profile and the mobile ARG profile, while (B) presents the differences in their host profiles. Panel (C) and (D) demonstrate the detailed co-occurrence patterns of ARGs and mobile ARGs with their potential hosts in Sankey diagrams, respectively. In (C), the left column shows whether the identified ARGs are co-localised with MGEs on the assembled scaffolds, whereas the middle and right columns are the profiles of ARGs and their potential hosts, respectively, the same as the left panel of (A) and (B). Analogously, the first and second column of each subfigure in (D) exhibit the mobile ARG profile and their potential hosts, the same as shown in the right side of (A) and (B), respectively. 143

Figure 6-9 Estimated dissemination risks of ARGs proposed by MetaCompare. The X-, Y- and Z-axes in (A) represent the co-occurrence probability of the targeted components – ARGs, ARGs–MGEs, ARGs–MGEs–putative pathogens, respectively – identified in the samples. This information is expressed as the scaffold number with critical components divided by the total assembled scaffold number. The normalised risk scores evaluating the dissemination potential of ARGs and their latent association with putative

pathogens are shown in (B). Detailed information of the relevant algorithms could be found in a previous study (Oh et al., 2018). 145

Figure 6-10 (A) Antibiotic-resistant pathogens and (B) the corresponding resistance profile at the ARG type level identified based on the co-occurrence pattern of critical pathogens (ESKAPE and WHO priority pathogens) and ARGs in different samples via NanoARG. The Y-axis of (A) represents the relative abundance of antibiotic-resistant pathogens described in the unit of “ppm”, which means the hit number of these antibiotic-resistant pathogens found in one million assembled scaffolds. Panel (B) shows the distribution of ARGs identified in critical pathogens..... 148

Figure 6-11 NMDS analysis of (A) the bacterial community structure at the genus level and (B) the ARG profile at the subtype level of different sample types used in source tracking. 151

Figure 6-12 Contributions of various potential sources to (A) PM_{2.5}-associated bacteria and (B) ARGs in coastal, urban, and SCISTW sites analysed by SourceTracker2..... 151

List of Tables

Table 3-1 Description of the sampling sites.	37
Table 3-2 Demographic and economic information of the sampling districts.....	39
Table 3-3 Sampling period, frequency, and sample size in the regional sampling campaign, as well as the analytical assays that were applied.	43
Table 3-4 Detailed information of the samples collected in the SCISTW and urban and coastal Hong Kong.	49
Table 3-5 Recovery of targeted elements by acid digestion in the analysis of total metal concentration.	53
Table 3-6 Chemical composition of Gamble’s Solution (pH 7.4).....	53
Table 3-7 Method detection limit of the analysed chemical species in this study.....	55
Table 3-8 Parameters used in the calculation of CR and NCR (presented as HQ) in this study.....	59
Table 3-9 List of DNA samples from the SCISTW and urban and coastal areas in Hong Kong for downstream analysis.	65
Table 3-10 Information about the primer sets used in the present study.	68
Table 3-11 Minimum quantifiable copy number (qPCR) and LOQ of different target genes in the current method (normalised to air volume).	70
Table 4-1 Comparisons of chemical compositions of PM _{2.5} in the PRD and YRD in different studies (µg m ⁻³).	84
Table 4-2 The average concentrations of trace elements in PM _{2.5} in the PRD and YRD in different studies (ng m ⁻³).	88
Table 4-3 Annual average bioaccessible concentrations of metal(loid)s in PM _{2.5} in the PRD and YRD.	91
Table 5-1 PERMANOVA (Bray–Curtis dissimilarity) test results of the regional differentiation in bacterial and ARG profiles (* <i>Pr</i> < 0.05; ** <i>Pr</i> < 0.01; *** <i>Pr</i> < 0.001).	118

Table 5-2 PERMDISP test (“betadisper” and “PERMUTEST” function in the “vegan” package) on the dispersion effects in NMDS analysis of regional differentiation in bacterial and ARG profiles. For the pairwise comparisons, observed and permuted *p*-value are presented below and above diagonal, respectively. 118

Table 6-1 List of priority pathogens with increasing concern of antimicrobial resistance proposed by the WHO, categorised by the urgency of the need for novel antibiotics. 147

Chapter 1 Introduction

1.1 Background

Air pollution has become a global environmental issue relevant to human health. Among the air pollutants, fine particulate matter $\leq 2.5 \mu\text{m}$ in aerodynamic diameter (generally abbreviated as $\text{PM}_{2.5}$) is considered a principal culprit of death caused by air pollution. Owing to its small size, $\text{PM}_{2.5}$ can enter the respiratory tract and later penetrate the bronchi upon inhalation. The ultrafine portion is even capable of penetrating deep into the alveoli and entering the bloodstream, a phenomenon that can have adverse effects on human health.

China, located in eastern Asia, is undergoing frequent $\text{PM}_{2.5}$ pollutions, especially for the densely populated regions under rapid urbanisation and industrialisation – the Yangtze River Delta (YRD) and the Pearl River Delta (PRD) – where effective control of $\text{PM}_{2.5}$ pollution is required for public health benefit. Previous studies pointed out that the spatial differentiation in $\text{PM}_{2.5}$ composition and different underlying toxicity between components could lead to unequal exposure risk per unit $\text{PM}_{2.5}$ mass across geographical locations (Li et al., 2019b). Hence, to better control pollution from health-oriented perspectives, it is of significance to first dissect $\text{PM}_{2.5}$ and determine the key components that may elicit negative health impacts, rather than only be concerned about the total concentrations of $\text{PM}_{2.5}$.

According to previous studies, $\text{PM}_{2.5}$ is a heterogeneous mixture of various chemical and biological components (Jin et al., 2017). The chemical fractions of $\text{PM}_{2.5}$, including the major compositions (*e.g.*, elemental carbon [EC], organic carbon [OC], heavy metals, and water-soluble ions [WSI]) and their potential sources (*e.g.*, dust resuspension, vehicular

exhaust, coal combustion, and industrial emissions) have been extensively explored (Chang et al., 2017; Cong et al., 2011; Qi et al., 2016; Tan et al., 2014). Meanwhile, some researchers assessed the exposure risks of various hazardous components under their environmental concentrations to find out the key health-relevant species. On top of this, heavy metals accounting for low mass proportions in PM_{2.5} were confirmed to pose significant adverse effects on human health via inhalation (Lu et al., 2008; Sørensen et al., 2005). Many studies have analysed the health outcome of airborne metals, such as carcinogenic risk (CR) and non-carcinogenic risk (NCR) estimated by the population-based assessment model from the United States Environmental Protection Agency (USEPA), using total metal or bioaccessible metal concentrations (Cong et al., 2011; Huang et al., 2016b; Huang et al., 2016d; Ming et al., 2017). However, few studies incorporated metal speciation information into risk assessment for bias control and further apportioned the predicted risks to the identified metal sources, so as to differentiate the contributions of various sources to the consequent health risks. Continuous efforts on this issue are needed to figure out the key sources of metal-induced risk, which can help with the formulation of risk-based source control strategies.

Compared with the chemical composition, the biological part of PM_{2.5} has been less explored but could be far more critical than previously thought. A large number of microorganisms have been found in PM_{2.5} (*e.g.*, bacteria, fungal spores, viruses, and pollen debris), in which some are allergens or pathogens responsible for infection when exposed to individuals. Thus, PM_{2.5} is increasingly recognised as an important vector for the transmission of potential microbial hazards with relevance to human health via inhalation (Cao et al., 2014; Schaeffer et al., 2017; Zhou et al., 2018b). In addition, the spread of some hazardous genetic elements carried by airborne microbes, such as

bacteria-associated antibiotic resistance genes (ARGs) that can encode resistance to drugs for infection treatment, have provoked increasing research (Li et al., 2018a; Ling et al., 2013; Pal et al., 2016). Standing at the intersection between fine inhalable particulates and antibiotic resistance, PM_{2.5}-associated ARGs have become an important issue, considering their potential to be transferred to pathogens from benign bacteria and deposit into the human airway via inhalation. However, the composition and spatiotemporal characteristics of these biological components in PM_{2.5}, including ARGs and the associated bacteria (no matter benign or bad) as potential ARG carriers, remain elucidations at local or regional scales before geographical differences in latent exposure risks are revealed. In addition, previous studies have qualitatively identified various potential sources of airborne bacteria and ARGs, including livestock farms, clinical settings, and wastewater treatment plants (WWTPs) (He et al., 2020; Smets et al., 2016; Yang et al., 2018). Further quantifications of source contributions could help to pinpoint the key sources of these biological fractions in PM_{2.5} to be controlled.

Collectively, systematic investigations of the spatiotemporal variations in PM_{2.5} across geographical locations in two densely populated regions in China – the YRD and PRD – from both chemical and (micro)biological perspectives, would contribute to an integrated understanding of the regional and local characteristics of PM_{2.5} pollution. Further attempts to identify their emission sources from these two dimensions and conduct pertinent exposure risk assessments could provide valuable information for health-oriented pollution control adaptive to regional/local-specific circumstances, thus helping to improve air quality.

1.2 Research objectives

This study aims to compare PM_{2.5} pollutions from chemical and biological dimensions in two densely populated regions in China – the YRD and PRD – with linkage to emission sources and resultant health impacts. An annual-based PM_{2.5} sampling campaign was thus deployed in multiple sites under different land-use impacts in selected typical cities in these two regions, coupled with a case study in a typical anthropogenic source of PM_{2.5}-associated microbes as a supplement, to better fill in the aforementioned research gaps.

The major objectives (Figure 1-1) are:

- 1) to study the inter-regional differentiation and intra-regional variations in chemical compositions of PM_{2.5}, including OC, EC, WSI, and heavy metals;
- 2) to identify the emission sources of major chemical components of PM_{2.5} and the source-resolved risk profiles posed by PM_{2.5}-associated metals based on their bioaccessible concentrations with combinations of metal speciation;
- 3) to characterise the regional features of the key biological components in PM_{2.5}, such as bacteria and associated ARGs that could be potential biohazards, including their concentrations and community structures, and estimate the relative contribution of the inhalation pathway to ARG daily intake; and
- 4) to quantify the contributions of specific emission sources to PM_{2.5}-associated bacteria and ARGs in the ambient atmosphere, based on a case study in a WWTP in Hong Kong in the PRD region.

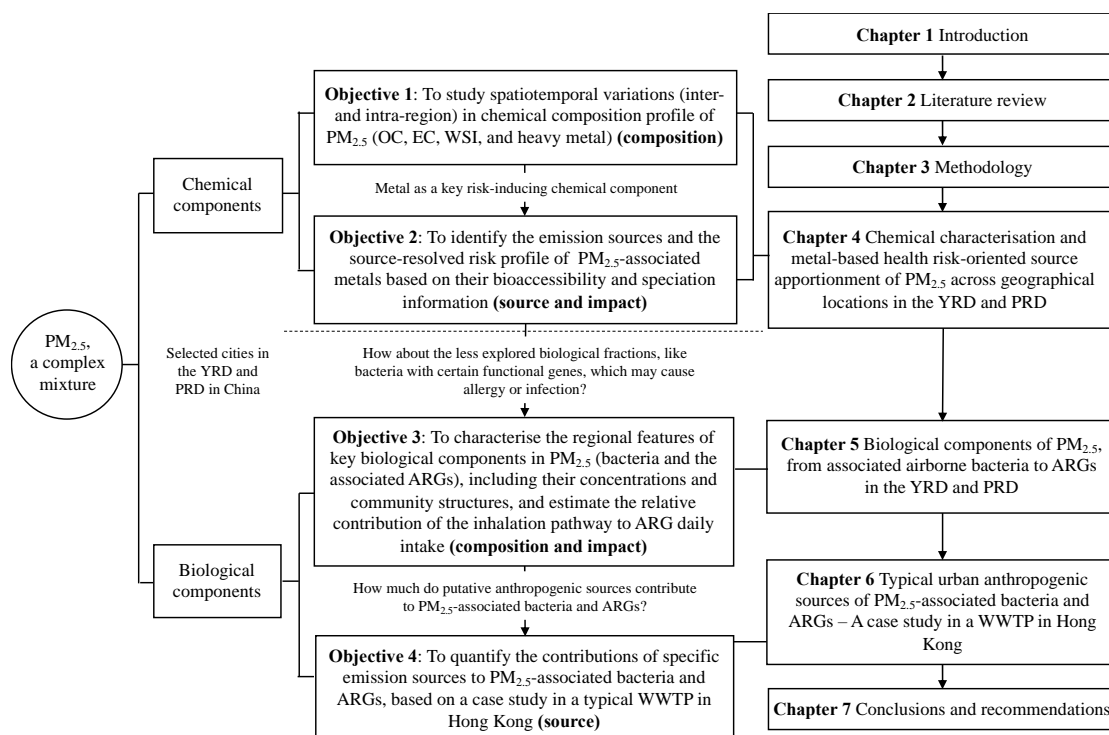


Figure 1-1 A flowchart of the objectives and structure of the thesis.

1.3 Organisation

This thesis comprises seven chapters (Figure 1-1). The present chapter provides the background information on PM_{2.5} pollution, clarifies the gaps in identifying health-related PM_{2.5} components and their emission sources from both chemical and biological perspectives, and states the purpose of this PhD project. Chapter 2 gives a holistic review of current work in dissecting the compositions of airborne particles and advances in detection techniques, especially for biological components, accompanied by elucidations of critical research gaps in linking emission sources and potential risks of health-related fractions in PM_{2.5}. Subsequently, Chapter 3 presents the sampling settings and the experimental approach to achieving the research objectives. The following three chapters describe and discuss the acquired results. Specifically, Chapter 4, targeting chemical characterisations of PM_{2.5}, demonstrates the regional differences of PM_{2.5} chemical compositions and source-resolved risk profiles based on metal content between the PRD

and YRD (based on selected cities). With a shift to biological components, Chapter 5 discusses the seasonal variations in PM_{2.5}-associated bacterial concentrations and community structures, the importance of PM_{2.5} in disseminating bacteria and ARGs, and the relevant contributions of inhalation to the daily intake of these biological components. As an extension of Chapter 5 and based on a case study in a WWTP (a typical anthropogenic source of airborne bacteria and ARGs) in Hong Kong in the PRD, Chapter 6 characterises the bacterial community and ARG structure across sample types (*e.g.*, PM_{2.5}, sewage, sludge, and effluent) and that in PM_{2.5} across sampling locations (*e.g.*, WWTP, urban, and coastal) and estimates the relative contributions of various potential sources to the ambient bacteria and ARGs. Finally, Chapter 7 summarises the major conclusions and limitations of the current project and provides recommendations for future studies.

Chapter 2 Literature Review

Given that PM_{2.5} is a complex mixture with negative impacts on human health, this chapter provides an overview of the chemical and microbiological components of PM_{2.5} along with innovations in detection techniques. From a health perspective, this review mainly focuses on the major health-relevant components in both dimensions, such as heavy metals and bacteria coupled with ARGs, and extends to their spatiotemporal variations, sources, and risk assessment, thus enhancing the understanding of the current research gaps and helping to address the research needs.

2.1 PM_{2.5} pollution, a health-threatening environmental issue

With rapid urbanisation and industrialisation, air pollution has become an evolving problem worldwide and there is an urgent need for mitigation regarding its impacts on human health. According to the World Health Organization (WHO), approximately 91% of the world's population was exposed to polluted air that exceeded the level of the WHO's safety guideline value in 2016 (WHO, 2018). In 2019, air pollution climbed to be the fourth biggest cause of death (Health Effects Institute, 2020). Among the currently known atmospheric pollutants, PM_{2.5} could be a major culprit for up to 4.2 million premature deaths worldwide per year (WHO, 2018), besides its influence on regional and global climate (Menon et al., 2002) and deterioration of the environment. Revealed by a global report from Health Effects Institute (2020), China, located in eastern Asia, is one of the epicentres of PM_{2.5} pollution with a consequent death up to 1.42 million in 2019 (Figure 2-1) and thus deserves more research focus.

According to myriad epidemiological studies, the escalating hospital admissions in relation to respiratory and cardiovascular diseases could be ascribed to short-term and

long-term exposure to PM_{2.5}, which poses acute and chronic effects on human health (Atkinson et al., 2014; Thurston et al., 2016). Previous studies have highlighted the nonuniform deposition pattern of PM_{2.5} (after it is inhaled into the respiratory tract) regarding the particle size (Li et al., 2019a). The larger fractions of PM_{2.5} (>1 μm) are likely to sediment in the tracheobronchial regions (Wang et al., 2002); whereas the ultrafine portion is capable of penetrating deep into the alveoli by Brownian diffusion and even transferring to extrapulmonary organs (Li et al., 2019a), in addition to getting access to the human body via trans-synaptic mechanisms (Li et al., 2018c) (Figure 2-2). PM_{2.5} can be associated with a number of pollutants due to its large specific surface areas, thus significantly increasing its mutagenic and carcinogenic risks. To deploy health-based control of PM_{2.5} pollution, it is imperative to dissect and characterise PM_{2.5} components from the beginning.

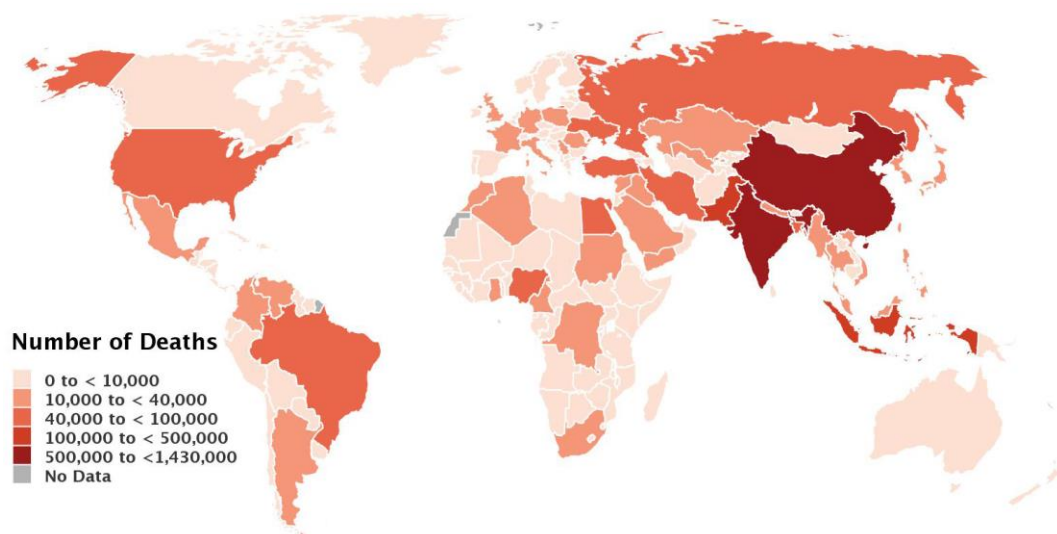


Figure 2-1 Number of death caused by PM_{2.5} in 2019 (plot by country) (Health Effects Institute, 2020). The original data are retrieved from The Institute for Health Metrics and Evaluation (2019).

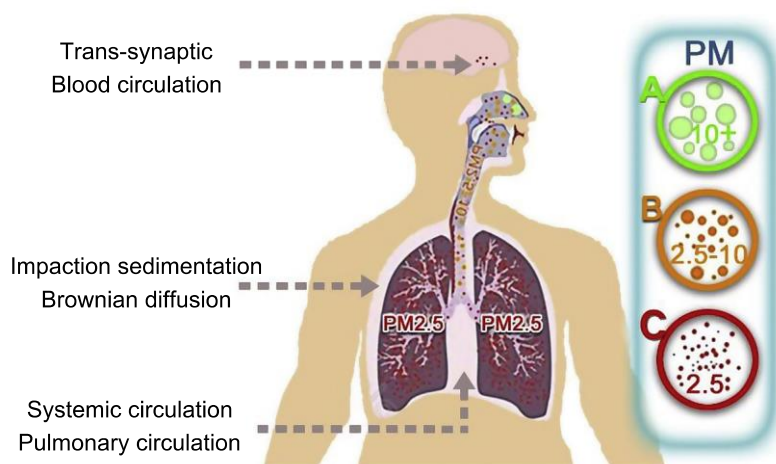


Figure 2-2 Deposition of airborne particulate matter in the human respiratory system with regard to particle size. This figure was adapted from Li et al. (2018c) (Copyright 2018 Chinese Medical Association; production and hosting by Elsevier B.V. on behalf of KeAi Communications Co., Ltd.; open access under the CC BY-NC-ND license [<https://creativecommons.org/licenses/by-nc-nd/4.0/>]).

2.2 Chemical characteristics of PM_{2.5}

2.2.1 Major chemical components and potential sources

Chemical fractions of PM_{2.5} are characterised as a diverse mixture of carbonaceous substances (EC, OC, and their derivatives), WSI (*e.g.*, SO₄²⁻, NO₃⁻, NH₄⁺, Na⁺, K⁺, and Cl⁻), metals/metalloids (*e.g.*, Al, Fe, Ca, Zn, Pb, Cu, V, Mn, Co, Cr, and Ni), and other minor constituents. Generally, aerosols can be emitted directly from sources (primary aerosol) like plants, soils, mineral dust, sea salts, and fuel combustions, or generated through physical or chemical processes with conversion of gases to particles (secondary aerosol) (Seinfeld et al., 2016). It has been reported that severe haze episodes in China are mainly driven by the formation of secondary aerosols with high levels of PM_{2.5} (Guo et al., 2014), and both secondary organic and inorganic aerosols contribute over 30% to the mass of PM_{2.5} (Huang et al., 2014b). Inorganic aerosols chiefly contain sulphate,

nitrate, and ammonium, but have less amount of inorganic carbon and trace metals. Compared with inorganic aerosols, it could be more difficult and complex to dissect organic aerosols because of the diversity of organic molecules and the complicated organic reactions in the atmosphere. However, advances in online monitoring instruments, like aerosol mass spectrometer, and offline techniques, including gas/liquid chromatography–mass spectrometry, nuclear magnetic resonance, and Fourier transform infrared spectroscopy, have gradually allowed chemical speciation of this fraction.

A variety of methods have been established to identify the sources of PM_{2.5} and its embedded components. For example, water-soluble potassium and levoglucosan (C₆H₁₀O₅) are widely considered indicators of biomass burning (Urban et al., 2012). Compared with the rough estimation of carbon sources based on the source-specific OC/EC ratio, radiocarbon (¹⁴C) can be a robust measure to differentiate the sources of carbonaceous substances more accurately and unambiguously (Liu et al., 2014). For trace elements, the enrichment factor (EF) is conveniently and extensively used to distinguish their origins from natural or anthropogenic sources (Chen et al., 2008). Other methods based on mathematical applications like the chemical mass balance model, multilinear engine, and positive matrix factorisation (PMF) can distinguish and calculate the contributions of specific sources to trace metal and PM_{2.5} (Chang et al., 2017; Qi et al., 2016; Rizzo et al., 2007; Tan et al., 2014), by which various sources, such as coal combustion, vehicular exhaust, dust resuspension, and industrial emissions have been identified.

2.2.2 Spatiotemporal variations and regional patterns

Chemical compositions and concentrations of PM_{2.5} often exhibit spatial and temporal variations in China (Figure 2-3) due to differentiation in contributions from various sources under the effect of fickle meteorological conditions. In general, the PM_{2.5} concentration shows a decreased trend from the Beijing–Tianjin–Hebei region in north China, with a higher burden of coal-based industries, to the YRD in the east and the PRD in the south, with favourable weather conditions for pollutant dilution (Ma et al., 2020). According to the nationwide survey of PM_{2.5} concentration, higher loads of PM_{2.5} in winter and lower loads in summer across China have been common and affected by the meteorological conditions (Ye et al., 2018), except some region-specific pollution episodes like dust storms in the spring in west China and biomass burning in the autumn in east China that have been accompanied by a higher abundance of crustal elements and OC/Cl⁻/K⁺ in PM_{2.5}, respectively (Tao et al., 2013; Zhang et al., 2015). These spatiotemporal variations in PM_{2.5} concentrations indicate the heterogeneous distributions of pollution sources between regions, which may also result in changes in chemical compositions of PM_{2.5}. Besides the regional patterns, some studies conducted in intra-regional and even intra-city level have revealed the spatial differences of PM_{2.5} pollution between land-use types or functional zones, highlighting the important role that local emission sources play in shaping the pollution patterns on a rather fine scale, particularly regarding some specific components. For example, the authors of an investigation within a city in south China observed a higher level of carbonaceous aerosols in roadside and urban sites compared with rural sites; these findings point to the significant contribution from local traffic sources, while similar levels of sulphate in these three locations hint at the regional contribution (So et al., 2007). The combined effect of regional and local sources complicates the characterisation of PM_{2.5} pollution and

warrants further studies to identify the major source contributor to mitigate PM_{2.5} pollution effectively.

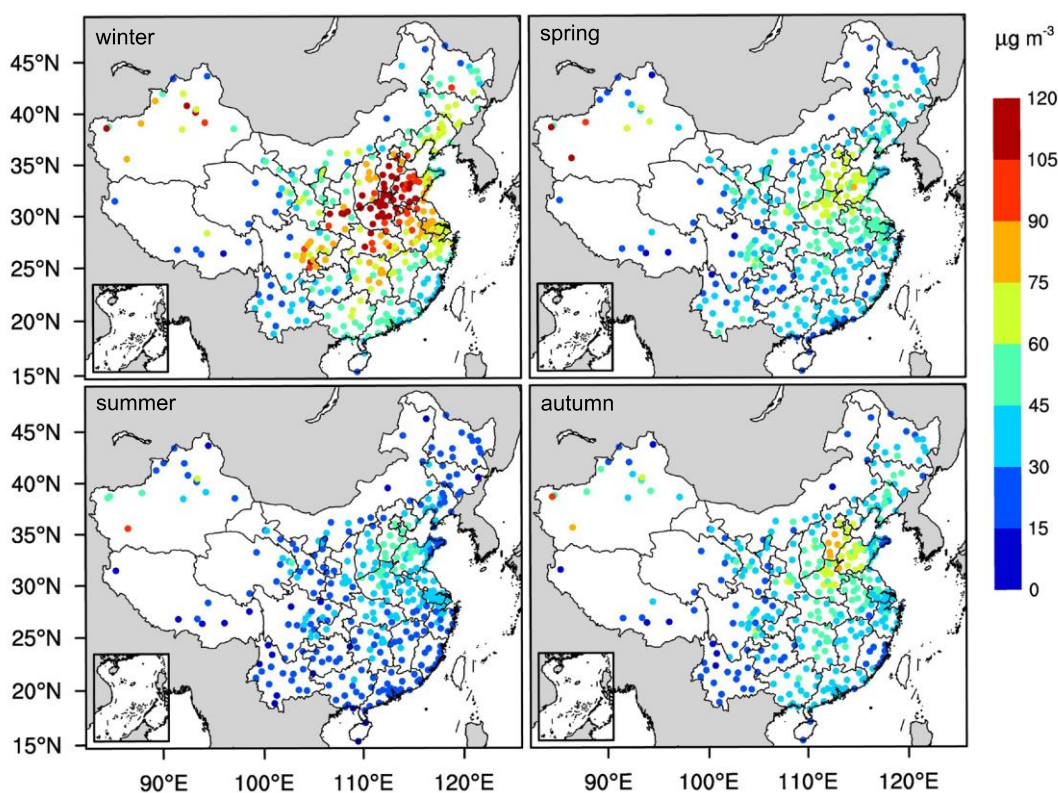


Figure 2-3 Spatiotemporal variations in surface PM_{2.5} concentration (seasonal mean) over China from December 2013 to November 2019. The figure was adapted from Jiang et al. (2020) (Copyright 2020 the authors; published by Elsevier B.V.; open access under the CC BY-NC-ND license [<https://creativecommons.org/licenses/by-nc-nd/4.0/>]).

2.2.3 Trace metals as critical components with health relevance

As mentioned in the previous section, the deposition location of airborne particles inside the human body is related to their sizes. Hence, the health effects posed by chemical components in airborne particulates could be associated with their distribution in different size fractions besides their own toxic potency. Consider metal(loid)s: Al and Fe from crustal origins are usually concentrated in coarse particles, while toxic elements with a high EF such as Cu, Zn, As, Se, Cd, and Pb tend to accumulate in fine fractions (Pan et

al., 2015), a phenomenon that intensifies the health risks they cause considering the size distribution and the resultant deposition site. Accumulated evidence has demonstrated that transition metals in fine particles can result in oxidative DNA damage, even though those elements only account for a minor mass proportion of the hosted particles compared with other components (Lu et al., 2008; Sørensen et al., 2005). A suite of studies based on either long-term or transitory monitoring strategy have been conducted to investigate the spatiotemporal variations in the metal concentrations and compositions in PM_{2.5} so as to evaluate the resultant toxicity (Kendall et al., 2011; Liu et al., 2017; Wang et al., 2018; Wang et al., 2015). However, explorations beyond the total metal concentrations, like the identification of their active and toxic fractions, as well as the key source contributors of the derived risks, are still much in demand to ensure effective health risk mitigation.

2.2.3.1 Metal bioaccessibility and molecular speciation

Not all the trace elements could be available for biochemical reactions after entering the human body via PM_{2.5}. Some studies have regarded the exchangeable and reducible fractions of inhaled metals determined by sequential extraction as the bioavailable part readily available to influence health directly (Feng et al., 2009; Huang et al., 2018); others have utilised simulated lung fluids to extract the bioaccessible fractions of metals to deduce their *in vivo* bioavailability for risk assessment. In general, neutral Gamble's solution and acidic artificial lysosomal fluid are widely applied in *in vitro* bioaccessibility tests of metals in atmospheric particles (Cong et al., 2011; Huang et al., 2016a; Huang et al., 2016c; Ming et al., 2017; Zereini et al., 2012). The solubility of metals can be determined and regulated by multiple factors, including their own characteristics relevant to emission sources (*e.g.*, the metal-aerosol bond and metal speciation), environmental

parameters (*e.g.*, pH and temperature), and operationally defined conditions (*e.g.*, the selected extraction solution) (Smichowski et al., 2005).

Besides its bioavailability, the toxic potency of a metal is highly dependent upon its valence state, which can be another key factor to determine the health impact it poses (Egorova et al., 2017; Jan et al., 2015), like Fe(II)/Fe(III), Cr(III)/Cr(VI), and As(III)/As(V). Arsenic and chromium are notable examples that present huge disparities in toxicity between different forms. However, little information regarding their valence states in PM_{2.5} is available from the literature. In some urban areas, including Guangzhou in the PRD and Beijing in north China, inorganic As(V) as the predominant species could account for over 80% of the total arsenic content in PM_{2.5} and total suspended particles (TSP) (Huang et al., 2014a; Sánchez-Rodas et al., 2007; Yang et al., 2012). By contrast, even fewer studies have reported chromium speciation in PM_{2.5} in non-source sites. A study at a traffic site in Poland showed that chromium was often present in the less poisonous form of Cr(III) in fine particles no matter in summer or winter (Widziewicz et al., 2016). For metal quantification with requirements for speciation information, complex pretreatment processes are often needed in metal extraction before separations of metals in different forms using chromatography-based instruments like high-performance liquid chromatography (HPLC), coupled with other downstream detection equipment such as hydride generation and atomic fluorescence spectrometry (HG-AFS) and inductively coupled plasma mass spectrometry (ICP-MS) for their high sensitivity (Nocoń et al., 2018). However, avoiding species transformation during the pretreatment process is always a nodus when using the detection methods mentioned above. An increasing number of studies have also reported the adoption of X-ray absorption spectroscopy (XAS) to determine the speciation of heavy metals, including Cr, As, Zn,

Cu, Mn, and Ni in atmospheric particulates. These data have been collected from the indoor or outdoor environment and the ambient atmosphere or emission sources (Galbreath et al., 2004; Godelitsas et al., 2011; Lu et al., 2015; Wang et al., 2007). Compared with other methods, the highly specific XAS technique can be conveniently applied in raw environmental samples like PM_{2.5}, although it is possibly limited by its relatively high detection limit.

2.2.3.2 Risk assessment and related sources

Risk assessment of PM_{2.5}-associated metals based on either their total concentrations or bioaccessible concentrations has been widely conducted using the USEPA's guidelines to estimate the CR and NCR under lifelong exposure. Along with the differentiation of airborne metal characteristics in different sampling locations, the risk contribution profiles of metals present spatial variations. However, As, Cr, and Pb – as the major culprits of CR – and Mn – as one of the important contributors of NCR – have been commonly found in many (sub)urban areas in China (Huang et al., 2018; Huang et al., 2016d; Liu et al., 2018; Ming, 2017; Wang et al., 2015). This finding is probably because of the high toxic potency of these anthropogenically enriched elements as well as their similar dominant sources, like traffic emission, in cities. However, it is a general practice in the current risk assessment model to use the inhalation unit risk (IUR) and reference concentration (RfC) of metals given by the USEPA, while such parameters typically consider either the most toxic form of metals or are based on metal bulk concentration without speciation information. This often results in large deviations from reality due to the toxicity discrepancy between different metal speciation and leads to unmeasurable biases when carrying out geographical comparisons of inhalational risks posed by metals.

After determining the metal-resolved risk profiles, a few studies have attempted to further assign the resultant health risks to the potential emission sources of metals, so as to obtain the source-resolved profile of metal-induced risks. Following this strategy, researchers have found that in Beijing in winter, coal combustion and traffic emissions were primarily responsible for the inhalational risks posed by bioavailable metals (Huang et al., 2018), while soil dust was the predominant source of both the CR and NCR resulting from total PM_{2.5}-associated metals in Huzhou, a city in Zhejiang province in east China (Peng et al., 2017). Although these researchers either considered total metal concentrations or used bioaccessible metal concentrations over a short-term period, they still aimed to assess specific key sources for health-oriented controls of PM_{2.5} pollution.

2.3 Biological perspectives of airborne particulates

Atmospheric primary biological particles include plant debris, pollens, algae, fungi, bacteria, viruses, and other cellular substances like proteins and polysaccharides, ranging in sizes from millimetres to nanometres (Jaenicke, 2005). Some of them are small enough to be suspended in air and cluster in clumps to form bioaerosols due to their micron-level size. It is alarming that part of them could be somehow responsible for human respiratory diseases. In contrast to the majority of microorganisms in airborne particles being benign to human beings, the pathogenic bacteria might only account for less than 0.02%–0.2% in non-polluted days (Zhang et al., 2019a). However, some microbial allergens and pathogens in airborne particles significantly enriched along with the increase in pollution level could make up 1.7% of total microbes in PM_{2.5} and 4.5% in PM₁₀ during polluted days (Cao et al., 2014). Meanwhile, some specific genetic elements such as ARGs can be inhaled along with aerosol-associated bacteria and are likely to pose risks to human health if they can be transferred from benign bacteria to respiratory pathogens. Considering the

potential health impact, it is of significance to firstly investigate the biological components of PM_{2.5}, including microorganism (no matter whether pathogenic or not) and the associated ARGs, of which the current understanding will be summarised below.

2.3.1 Microorganisms in airborne particles

Microorganisms are ubiquitous in the atmospheric environment despite the lack of nutrition, high burden of radiation, and strong turbulence compared with other environmental compartments. Accumulated evidence indicates that airborne microbes play important roles in mediating physical and chemical processes in the atmosphere, including cloud formation, precipitation, and biotransformation of organic and inorganic compounds (Ariya et al., 2009; Ariya et al., 2002); these microbes also pose implications for human health.

2.3.1.1 Microbial distribution in particles with different sizes

Considering that some microbes in the atmosphere present negative effects on human health (*e.g.*, allergy, bacterial infection, and viral infection) and ecosystem functions, studies on airborne microbes have skyrocketed in pace with the development of high-throughput sequencing. Based on previous research, the community structures of airborne microbes are dissimilar in different sizes of aerosol particles (Bertolini et al., 2013; Bowers et al., 2013; Franzetti et al., 2011). As revealed by the results of high-throughput sequencing, bacteria are the most dominant domain in airborne particles. They generally occupy a higher proportion of the total microbial community in PM_{2.5} compared with PM₁₀, although the taxon richness and diversity seem to be higher in coarse particles (Bowers et al., 2013; Cao et al., 2014). It is not difficult to understand that microorganisms distribute unevenly in atmospheric particles with different sizes

considering the diverse aerodynamic diameters of different kinds of airborne microbes. Most eukaryotes like fungi and algae as well as plant debris larger than 2.5 μm tend to attach to PM_{10} and TSP. In contrast, the higher diversity of bacteria in coarser fractions could be partially attributed to the greater abundance of nutrients and better shelter effect from environmental stress (like ultraviolet radiation) in larger particles, as proposed by Bowers et al. (2013).

2.3.1.2 Concentration, community structure, and spatiotemporal variations

Several studies have mainly focused on airborne bacteria because they are small enough to penetrate the respiratory tract and some of them (*e.g.*, allergenic and pathogenic species) can exert adverse health effects. The concentration of airborne bacteria presents obvious spatial variations spanning several orders of magnitude in the outdoor near-surface atmosphere, most of which range from 10^3 to 10^6 copies m^{-3} of the 16S ribosomal ribonucleic acid (rRNA) gene (Bertolini et al., 2013; Gao et al., 2017; Lympelopoulou et al., 2016) based on quantitative polymerase chain reaction (qPCR), or from 10^4 to 10^6 cells m^{-3} quantified by cell-based approaches like flow cytometry or fluorescence microscopy (Bowers et al., 2011b; Murata et al., 2016). A summary of geographical disparities in bacterial load in airborne particles is provided in Figure 2-4. Consistently, the airborne bacterial community presents great diversity and also distinct spatial variability across land-use types and between cities (Bowers et al., 2013; Bowers et al., 2011a; Gandolfi et al., 2015). However, there are still some commonalities of certain kinds of bacteria, a factor that could be due to the selection pressure of the atmospheric environment and contributions from similar sources. For example, Actinobacteria, Firmicutes, Proteobacteria, and Bacteroidetes are generally the most abundant phyla in airborne particles regardless of particle sizes (Bowers et al., 2013; Cao et al., 2014; Liang

et al., 2020; Lympelopoulou et al., 2016). Some specific taxa like Actinobacteridae at the subclass level (Bertolini et al., 2013; Bowers et al., 2013) and Actinomycetales at the order level (Cao et al., 2014; Gandolfi et al., 2015), which originate from terrestrial sources and dominate in the bacterial community under their corresponding classification rank, are prevalent in different sampling locations. Relevant studies have also highlighted the strong seasonal variability and even diurnal fluctuation of airborne bacteria in a certain site and different seasonal patterns across geographical locations (Bertolini et al., 2013; Bowers et al., 2013; Chen et al., 2012; Fang et al., 2007; Gandolfi et al., 2011; Gusareva et al., 2019). Such spatiotemporal variations in airborne bacteria could be regulated by multiple factors, like the emission sources, environmental stress, and other meteorological conditions. A suite of studies has emphasised the shift of contributions from different sources as a determining factor on the changes in the concentration and composition of airborne bacteria. For example, bacterial loads are higher in summer and decrease in winter, variations that are concordant with the seasonal changes in vegetation, which release less relevant bacteria in winter due to plant senescence especially in agricultural sites (Bertolini et al., 2013; Bowers et al., 2013). On the contrary, marine-related microbes may be universal in the air in coastal areas. Detailed information about the sources of airborne bacteria is provided in Section 2.3.1.3. Meteorological conditions including temperature, relative humidity, wind speed, precipitation, and possibly ultraviolet flux are also partially responsible for the short-term variations in airborne bacteria; these factors regulate the contributions from different sources and provide selection pressure in shaping the bacterial community (Bowers et al., 2013; Sun et al., 2020). Besides, variations in airborne microbes are also found correlated with other environmental factors like chemical pollutants (Gandolfi et al., 2015) because they can be either nutrients or toxic compounds for microbes. However, there is still a lack of

evidence to justify whether it is the actual effect of these chemicals or just a result of the co-selection effect of meteorological conditions on both the chemical and biological components. Owing to the highly dynamic nature of the atmospheric environment and the intricate relationships among influential factors, it seems difficult to quantify the contributions of different factors on microbial concentrations and community structure in the atmosphere. Robust approaches from a more biological perspective are warranted in the future, in addition to the current mathematical methods like correspondence canonical analysis (CCA), redundancy analysis (RDA), and variation partitioning analysis (VPA) (Zhen et al., 2017).

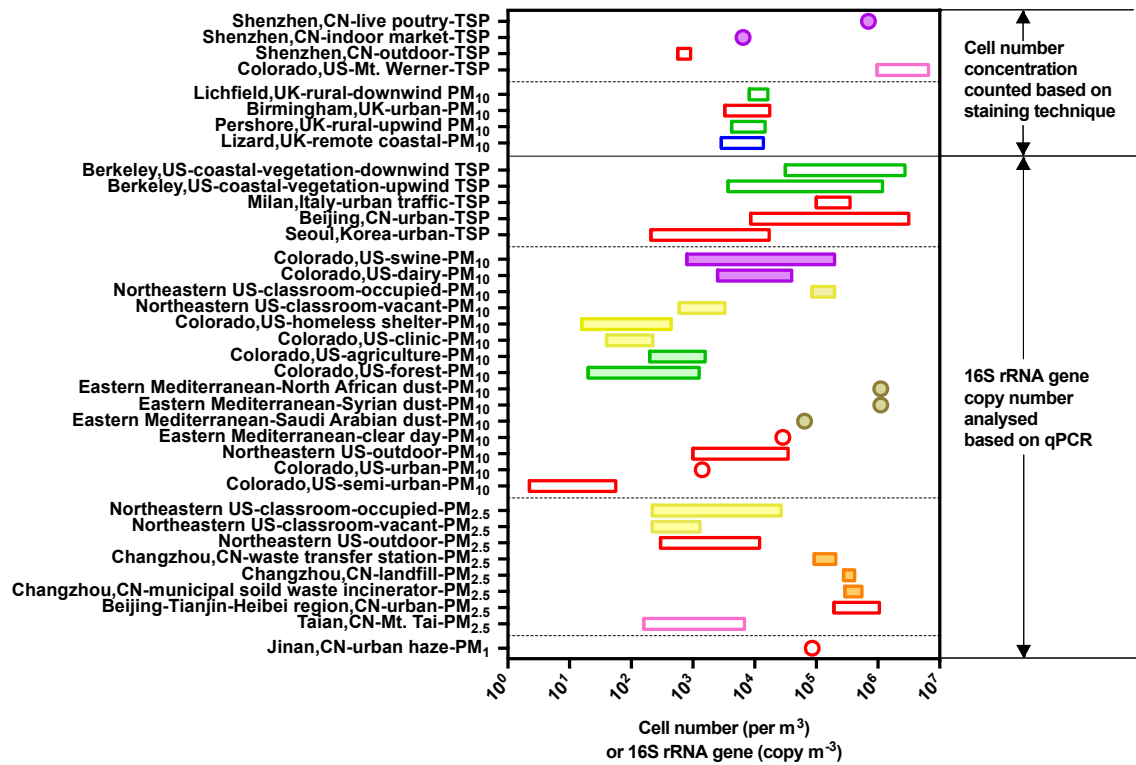


Figure 2-4 Spatial variations of aerosol-associated microbial/bacterial load (Bertolini et al., 2013; Bowers et al., 2009; Gao et al., 2017; Gao et al., 2016; Gat et al., 2017; Harrison et al., 2005; Hospodsky et al., 2012; Lee et al., 2010; Li et al., 2020; Ling et al., 2013; Lympelopoulou et al., 2016; Xu et al., 2016a; Xu et al., 2019; Zhen et al., 2017). Filled boxes/dots represent sites in the vicinity of typical sources (e.g., clinical, poultry, and

municipal solid waste treatment system). Those unfilled represent ambient sites with land-use types distinguished by colour.

2.3.1.3 Putative sources and transport of bacteria in the atmosphere

Respectable studies have tried to identify the putative sources and quantify their contributions to airborne bacteria (Figure 2-5). Soils, vegetation, faecal materials, and (local/foreign) dust could be important terrestrial origins of bacteria in near-surface aerosols (Bowers et al., 2013; Bowers et al., 2011a; Bowers et al., 2011b; Gat et al., 2017), as well as the aquatic environments like marine and freshwater with non-negligible contributions (Cao et al., 2014). Previous studies have highlighted that microorganisms in water bodies can be ejected into the atmosphere along with the bubble breakage in the air–water microlayer, which is responsible for the distribution of ocean-related microbiota in the air in coastal areas (Aller et al., 2005). Other identified anthropogenic sources, including WWTPs (Bauer et al., 2002), composting and bio-solid treatment facilities (Wéry, 2014), livestock farms (Bakutis et al., 2004), hospitals, and humans (Hospodsky et al., 2012), could probably account for a greater contribution in urban areas and other locations under intense human activities. To quantify the contributions of various sources, source tracking methods have been developed based on the sequencing data of samples. By comparisons with the indicative taxa in samples from potential sources, the methods adopted by Bowers et al. (2013) and Cao et al. (2014) allow assigning DNA sequences of targeted samples to different sources and thus provide an estimated source contribution profile. In recent years an improved method – SourceTracker2, based on Bayesian approach – has been extended to atmospheric studies to calculate the contribution of various sources to airborne bacteria (Knights et al., 2011; Uetake et al., 2019; Yang et al., 2019).

After emission from the surface of sources, bacteria can be transported to downwind areas through airflow and even participate in continental-scale movements along with dust storms and cyclones. Scientists have found that bacteria that originated from livestock farms can be isolated from the air plumes in downwind areas more than 100 m away from the sources (Gibbs et al., 2006). In addition, the local airborne microbial communities changed after the attack of a dust storm in the Eastern Mediterranean (Mazar et al., 2016) and the microbial communities in the rainfall collected during the dusty days were more diverse than those in the clean rains (Itani et al., 2016). Such observations indicate the possibility of long-range dispersal of airborne microbes, for which dust serves as an important carrier.

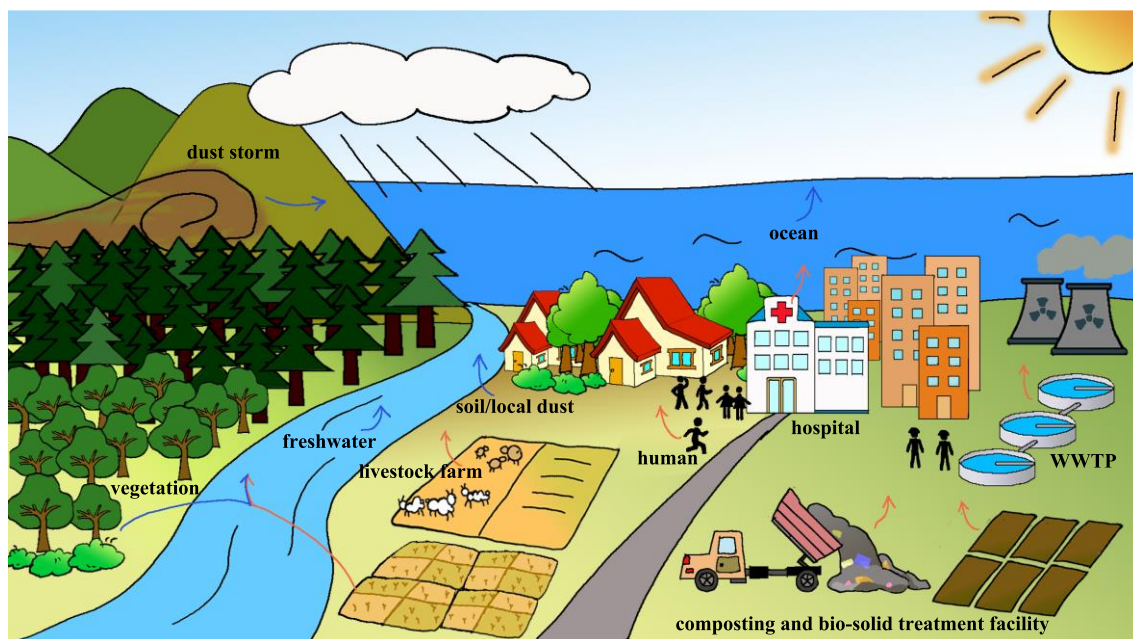


Figure 2-5 Putative natural (blue arrow) and anthropogenic (red arrow) emission sources of airborne bacteria.

2.3.1.4 Survival, viability, and health concerns

Compared with other habitats like soil and water bodies, the atmosphere used to be considered a harsh environment for microorganisms to live and proliferate due to the

scarcity of nutrients and moisture and the existence of solar radiation and myriad gaseous pollutants. However, investigations of airborne microbes by culture-based technique have revealed the viability of some airborne microbes (Fang et al., 2007; Gao et al., 2015). Pigmentation is a powerful mechanism by which airborne bacteria protect themselves from solar radiation damage; this strategy could be prevalent in bacteria dwelling in the atmospheric boundary layer (Imshenetsky et al., 1978). Tong et al. (1997) reported an increased proportion of pigmented bacteria in the outdoor environment because the intensification of solar radiation exerted selective pressure on non-pigmented bacteria. Another way for microbes to survive the tough atmospheric environment is to go dormant. Morphologically, they are transformed into spores that enjoy high resistance to external pressures. During this stage, their metabolic rates reduce greatly as multiplication and cell division cease (Bär et al., 2002). Once they encounter suitable conditions, they can readily reside in their new habitats and become active again. The successful recovery of culturable microbes in the free troposphere in North America during a storm from Asia verified the tenacious vitality of airborne bacteria even after a cross-continental transport (Smith et al., 2012), a phenomenon that raises concern about the spread of microbes via atmospheric dispersal, especially for pathogens. Moreover, although most of the microbes detected in the atmospheric particles are non-pathogenic to humans, the relative abundance of the diagnosed microbial allergens and pathogens have increased in pace with the pollution level of airborne particles (Cao et al., 2014; Sun et al., 2020). These findings in China indicate the role of haze episodes in promoting the proliferation of pathogens and opportunistic pathogens.

2.3.2 ARGs as a kind of emerging pollutant

2.3.2.1 Origin, acquisition, and development of antibiotic resistance in the environment

ARGs refer to genetic elements that encode resistance to antibiotics. As a matter of fact, antibiotic resistance is an intrinsic attribute of some environmental microorganisms. They harbour certain ARGs so as to protect themselves from the surrounding, naturally existing antibiotics or their endogenous metabolites to inhibit the growth of other microbes that compete with them for niches (Martinez et al., 2009). Some soil microbes with intrinsic ARGs can even gain nutrition by degrading the antibiotics in the surrounding environment (Allen et al., 2010). Such intrinsic ARGs are ubiquitously present in the environment as a kind of functional gene in ecosystems. For other microorganisms, ARGs can be acquired by horizontal gene transfer (HGT) or mutation, which can occur spontaneously (Martinez et al., 2000). However, human activities can provide a high selection pressure that accelerates the formation and dissemination of antibiotic resistance in the environment, like overuse or abuse of antibiotics in human therapy and in husbandry (Witte, 1998). The antibiotic residuals can be subsequently retained in the soil or released to the aquatic environment in a sub-inhibitory concentration due to ineffective removal in WWTPs.

Antibiotic resistance used to be a health concern in the clinical environment, the rapid development of which in recent decades has been confirmed by the progressive ineffectiveness of traditional antibiotics and an increased detection rate of pathogens resistant to some novel antibiotics of last resort, like vancomycin. However, a growing body of research has shown that ARGs, including those with high clinical-relevance like *bla_{NDM-1}* and *mcr-1*, are becoming prevalent and enriched in non-clinical environments

such as some anthropogenic hotspots (*e.g.*, WWTPs, landfills, and livestock) and then the receiving environment (*e.g.*, soil, surface water, and sediment), compared with low abundance in relatively pristine places (Chen et al., 2013b; Chen et al., 2016; Ji et al., 2012; Ouyang et al., 2015; Schages et al., 2020; Wu et al., 2017; Yang et al., 2016; Zhu et al., 2017b). Meanwhile, mobile genetic elements (MGEs) (*e.g.*, integrons, transposons, plasmids, and bacteriophages) able to mobilise DNA either within a given cell or between bacterial cells are widely detected in the environment. The capability for MGEs to either capture ARGs or transfer them between bacteria – and the aptitude of bacteria under certain conditions to uptake extracellular DNA – can facilitate the dissemination of ARGs in bacterial communities in the environment (Berglund, 2015; Salyers et al., 1997; Van Hoek et al., 2011). Thus, all of the aforementioned facts urge the need to treat ARGs as a kind of emerging environmental pollutant (Pruden et al., 2006).

2.3.2.2 Dissemination of ARGs via airborne particles

Compared with the considerable amount of studies on the source, dissemination, and distribution of ARGs in the terrestrial and aquatic environment, the situations in the atmosphere have been far less explored. This situation is concerning because airborne particles may also be important vectors for the dissemination of ARGs.

Aerosol-associated bacteria showing resistance to different antibiotics like macrolides, beta-lactams, tetracyclines, fluoroquinolones, and sulphonamides, have been continuously isolated from clinical settings and animal farms where a variety of antibiotics have been applied (Fan et al., 2014; Gibbs et al., 2006; Gilbert et al., 2010), as well as in the urban atmospheric environment (Gandolfi et al., 2011; Liang et al., 2020; Mao et al., 2019; Zhang et al., 2019b; Zhao et al., 2020). This isolation indicates the

ubiquitous presence of airborne ARGs encoding the corresponding antibiotic resistance. Aerosol-associated bacteria and ARGs that withstand long-range transport via air movements and dust storms are likely to influence the local airborne bacterial and ARG profiles of downwind locations (Gat et al., 2017; McEachran et al., 2015). Using culture-independent methods, researchers have shown that the absolute and relative abundance of airborne ARGs can evolve frequently over times and across geographical gradients (Li et al., 2018a; Liang et al., 2020; Wang et al., 2019; Zhang et al., 2019b). However, studies on spatiotemporal variations in airborne ARGs, especially for their absolute abundance used for exposure estimation, are still quite limited over the world. Figure 2-6 provides a geographical comparison of certain prevalent ARGs detected in the atmosphere. The observed ARG variations over times and spaces could be under the combined influence of host bacterial communities, meteorological conditions, and anthropogenic activities (Hu et al., 2018b; Liang et al., 2020). Some recent studies providing comparisons on airborne bacteria and ARGs between hazy and non-hazy days have revealed that the diversity and abundance of airborne ARGs seem to increase with the deterioration of PM pollution (Sun et al., 2020; Zhao et al., 2020). These findings highlight the growing exposure risks of airborne ARGs on polluted days. In addition, the higher abundance of MGEs like *intI1* and *tnpA* found in PM_{2.5} pollution episodes is consistent with studies in other environmental compartments from a certain perspective that *intI1* could be a candidate indicator of anthropogenic pollutions (Gillings et al., 2015). Such observations triggered our concern about the acceleration of ARG dissemination via HGT in the atmosphere since urban PM_{2.5} is likely to promote the frequency of conjugative transfer (Xie et al., 2019).

Emerging evidence distinguished PM_{2.5}-associated antibiotic resistomes from those in terrestrial and marine systems (Pal et al., 2016). These observations suggest that the atmospheric environment is a unique reservoir of antibiotic resistance, with varying stresses shaping their structures. Accumulating data have enabled qualitative comparisons of antibiotic resistome profiles between potential source matrices and nearby aerosol-bound ARGs, as well as comparisons of the abundance of aerosol-bound ARGs between the potential source points and their ambient environments. On such a basis, various typical sources including natural sources such as marine and soil dust (Gat et al., 2017; Liang et al., 2020) and other anthropogenic hotspots like animal faeces in livestock, WWTPs, hospitals, and solid waste treatment systems (He et al., 2020; Li et al., 2020; Yang et al., 2018), were identified to contribute ARGs to the ambient atmosphere.

Although a growing number of investigations have provided valuable information on airborne ARGs near potential emission sources and in urban areas, most of them either mainly focused on coarser particles (*e.g.*, TSP and PM₁₀) (Gat et al., 2017; Li et al., 2018a; Ling et al., 2013; Mazar et al., 2016) or considered a short-term snapshot or limited analyses to certain small-scale areas (Hu et al., 2018b; Sun et al., 2020; Zhang et al., 2019b). In addition, compared with water and food that are generally well-processed before ingestion, ambient air is inhaled directly with aerosol-bound pollutants subject to virtually no treatments before entering the respiratory tract. This fact sets the inhalation of airborne particulates as an important exposure pathway for ARGs and bacteria (see Section 2.3.1). Hence, spatiotemporally resolved dynamics of aerosol-associated antibiotic-resistant bacteria (ARB) and ARGs, especially for the PM_{2.5}-bound fraction,

are still required to assess long-term human exposures via inhalation on a larger scale like regional, national, and even global scope.

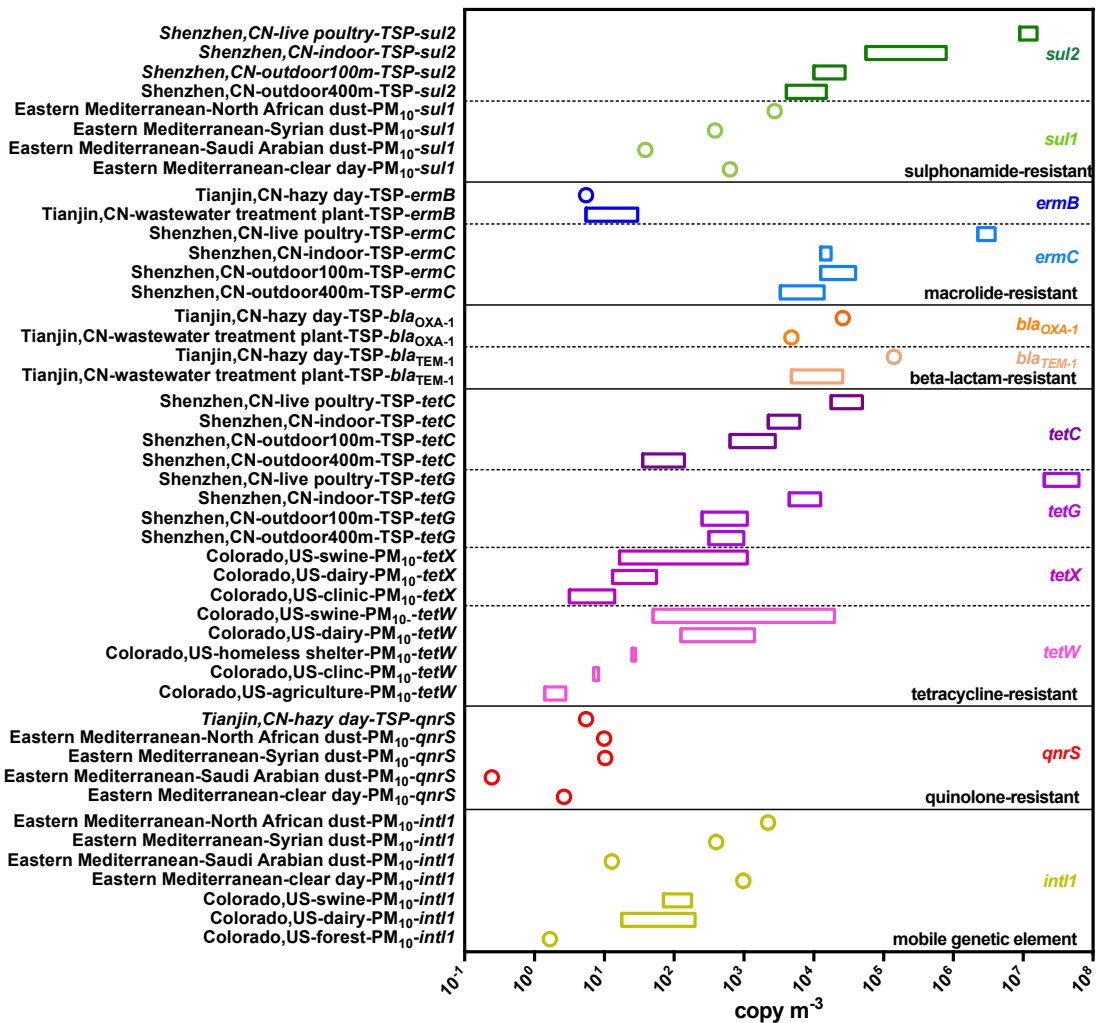


Figure 2-6 Geographical comparisons of absolute abundance of selected ARGs that are prevalent in aerosol particles (copy m^{-3}) (Gao et al., 2016; Gat et al., 2017; Ling et al., 2013; Wang et al., 2019) assuming equal DNA extraction efficiency across studies.

2.3.3 Aerosolisation potential of bacteria and ARGs from key anthropogenic sources

As described in previous sections, livestock farms, WWTPs, composite lands, and hospitals are considered to be critical anthropogenic reservoirs of ARGs and bacteria – especially opportunistic pathogens; hence, occupational exposure risks at these locations merit close attention. The importance of investigations on microbial emissions has

already been emphasised by many researchers who have revealed the frequent occurrence of respiratory symptoms in workers in WWTPs and farms with high levels of airborne microbes (Eduard et al., 2001; Melbostad et al., 1994). Previous papers have reported that the concentrations of source-indicative bacterial and ARG species in the atmosphere are in descending order by the increased distance away from bacteria- and ARGs-rich environment like poultry manure and municipal solid wastes, which probably hints at the emission of microbes and ARGs from solid/water matrices to ambient air in bioaerosol forms (Gao et al., 2016; Li et al., 2020).

Most of the extant research on the aerosolisation potential of bacteria from potential sources have been conducted in WWTPs. Bioaerosol emission levels in WWTPs subject to a strong impact by agitation methods could vary along with the treatment phases (Fathi et al., 2017; Gotkowska-Płachta et al., 2013; Li et al., 2016a), during which time the aeration process can generate bioaerosols less than 1 μm in size with a unimodal pattern peaking at the nanometre scale, as reported in a laboratory-based study (Han et al., 2019). Bauer et al. (2002) also found that most of the emitted bioaerosols from wastewater were less than 2 μm , with the aerosolisation ratio of culturable bacteria ranging from $8.4\text{E-}11$ to $4.9\text{E-}9$ (expressed as colony-forming units [CFU] m^{-3} air/CFU m^{-3} wastewater). These findings demonstrate the need for concern about the exposure risks in these key sites. Other possible methods to measure the emission rate of microorganisms could be based on dispersal models using meteorological parameters and concentrations of bioaerosols away from sources at different downwind distances (Li et al., 2013). Researchers have recently started to use the robust source tracking software (SourceTracker2) in airborne bacterial studies. Based on this method, Yang et al. (2019) attributed 4%–17% of airborne bacteria within the WWTP to wastewater and sludge; these data provide quantitative

information of contributions from WWTP by-products to airborne bacteria. However, the authors used air samples from sites downwind of the WWTP as a potential source of the indoor airborne microbes in the WWTP, a design that ignored the influence of the WWTP on the downwind air and could result in unknown uncertainty to the contribution profile.

Compared with airborne bacteria in WWTPs, only a few studies have touched the field of ARG emission from wastewater and sludge. Some studies have isolated opportunistic pathogens with antibiotic resistance from bioaerosols collected in WWTPs (Zhang et al., 2018), while others based on metagenomic sequencing have only compared the ARG profiles between activated/dewatered sludge and bioaerosol in WWTPs without further quantitative estimations of the contributions (Han et al., 2020). Fortunately, the feasibility of SourceTracker2 in predicting the contributions of different ARG sources has been verified in sediment and urban stream samples (Baral et al., 2018; Li et al., 2018b). This ability could possibly be extended to airborne ARGs in the future.

2.3.4 Detection methods of airborne microbes and relevant genetic elements – development and challenges

Traditional detection methods of airborne microbes are culture-based, with the embedded antibiotic resistance generally evaluated by disc diffusion tests. However, <1% of the viable microorganisms in any environment are cultivable according to previous studies (Amann et al., 1995; Pace, 1997). Hence, the abundance and diversity of microbes and ARB could be largely underestimated using traditional methods.

To overcome the drawbacks, various molecular biological methods have been established. Sebat et al. (2003) analysed designated gene contents from genomic libraries of

environmental samples with DNA microarray technology. Polymerase chain reaction (PCR) has been utilised to amplify and detect ARGs that encode resistance to tetracycline (Schmitt et al., 2006), erythromycin (Patterson et al., 2007), and sulphonamides (Agero et al., 2007). Denaturing gradient gel electrophoresis and 16S rDNA clone library were once used to analyse the microbial communities in different matrices (Zhang et al., 2000; Zhang et al., 2005). In recent years, metagenomic analysis has been revolutionised with rapid developments in sequencing techniques. Next-generation sequencing (*e.g.*, HiSeq and Miseq platforms from Illumina), characterised by high throughput and low cost, and third-generation sequencing (*e.g.*, PacBio and Nanopore sequencing), which features long reads, have been widely used in environmental analysis to profile the microbial communities and explore the interactions between microbes and other genetic elements (*e.g.*, ARGs and MGEs). Besides the above-mentioned qualitative methods, qPCR is a competitive and highly sensitive technique for quantifying target genes and their expression efficacy. The recently developed high-throughput qPCR can even parallelly quantify hundreds of genes or pathogens. The applications of these newly established techniques facilitate the identification of target gene context and the exploration of metabolic pathways of microbes for different environmental substances and their roles in environmental processes.

However, the main problem we face now in atmospheric microbiome studies is how to get enough DNA from airborne particles before downstream analysis, especially for metagenomic sequencing. The extremely low biological content in airborne particulates compared with other environment matrices (*e.g.*, water and soil) and the limited DNA extraction efficiency make it difficult to study extensively the microbial and ARG community in the atmosphere. Whole genome amplification (*e.g.*, multiple displacement

amplification), a promising method to amplify DNA amounts with acceptable biases, has been successfully used before metagenomic analysis in urban aerosol surveillance (Nicholas et al., 2015). On the other hand, some scientists are concentrating on improving DNA extraction efficiency in order to get enough DNA from airborne particles for downstream analysis. For example, a modified protocol of DNA extraction and metagenomic sequencing with low DNA input has been developed (Jiang et al., 2015) for metagenomic analysis of the airborne microbiome.

2.4 Summary and outlook

PM_{2.5} pollution has become an environmental issue with high relevance to human health around the world, especially in developing countries like China. The YRD and PRD – located in east and south China, respectively – have been and continue to be subject to intensive anthropogenic impacts due to urbanisation and industrialisation, thus resulting in severe PM_{2.5} pollution. To better control the pollution from health-oriented perspectives, it is necessary to dissect the composition of PM_{2.5} and find out the key components with negative health effects.

Previous studies have extensively explored the spatiotemporal variations and potential sources of major chemical compositions in PM_{2.5}, including carbonaceous materials, WSI, and metal(loid)s. Among the widely identified components, heavy metals accounting for low mass proportions in PM_{2.5} could pose significant adverse effects on human health via inhalation. Although a variety of studies have investigated the mass contribution of different sources to PM_{2.5}-associated metals and estimated the metal-induced CR and NCR based on either their total or bioaccessible concentrations, limited efforts have been made to incorporate the information of metal speciation into risk assessment and further

apportion the predicted risks to the identified metal sources, so as to differentiate the contributions of various sources of emissions to the consequent health risks under prolonged exposures. An integrated and comprehensive study to close the loop of metal exposure via PM_{2.5} from sources to health implications is needed, especially in highly urbanised and industrialised regions like the YRD and PRD.

Compared with the chemical compositions of PM_{2.5}, understanding the (micro)biological fractions like the PM_{2.5}-associated bacteria and ARGs is still in its infancy; inhalation of these fractions may cause allergies and infections. The airborne particulate matter is an important vector that is responsible for the dissemination of bacteria and ARGs in the atmosphere. Analogous to chemical components, many studies in independent geographical locations on the seasonal and spatial variations in airborne bacterial concentration as well as the community structures have emerged. However, there is still a lack of simultaneous studies to explore the biological features of PM_{2.5} at inter-regional scales from a health-relevant perspective. Standing at the intersection between fine inhalable particulates and antibiotic resistance, PM_{2.5}-associated ARGs have aroused increasing research interest, but it has been quite limited with regard to identifying certain ARG subtypes on small scales. The spatial and seasonal characteristics of airborne ARGs with linkage to PM_{2.5}-associated bacteria at regional scales remain to be elucidated, as well as the contributions of putative sources to airborne bacteria and ARGs. A comparative study considering both the chemical and (micro)biological components of PM_{2.5} between regions could sharpen our current understanding of the regional characteristics of PM_{2.5} pollution from an integrated perspective and further help with the health-oriented pollution control that can be adapted to regional-specific circumstances.

Chapter 3 Methodology

This section provides the general information of the studied sites, sampling strategy, and detailed descriptions of the chemical and biological analyses applied in this study.

3.1 General information of the studied regions

This study was conducted in two of the most economically developed and densely populated regions in China, namely, the YRD and PRD (Figure 3-1).

The YRD is located in eastern China. It has a population of around 225 million and covers a total area of 358000 km², which integrates the whole area of Jiangsu province, Zhejiang province, Anhui province, and Shanghai (State Council of the People's Republic of China, 2019). Twenty-seven central cities such as Shanghai, Nanjing in Jiangsu province, and Hangzhou in Zhejiang province – all with a robust economy – are expected to take leading positions to drive the development of the entire region. As a coastal region lying on the west of the Pacific Ocean, the YRD is situated across low and middle latitudes and subjected to the subtropical monsoon climate. Hence, the YRD enjoys clear seasonal features characterised by hot and humid summers under the influence of southeastern winds and cold and dry winters with northwestern winds.

In contrast, the PRD lies in southeastern China and faces the South China Sea; it includes nine cities in Guangdong province, Macau, and Hong Kong. Similarly to the YRD, the PRD is located in the subtropical zone with most areas south of the Tropic of Cancer. Under the impact of a subtropical monsoon climate, rainfall in the PRD mainly falls between April and September (from spring to late summer). Compared with the YRD,

winter in the PRD tends to be more temperate. Being a highly developed region in China, the PRD has around 70 million people dwelling in a total area of 56000 km².

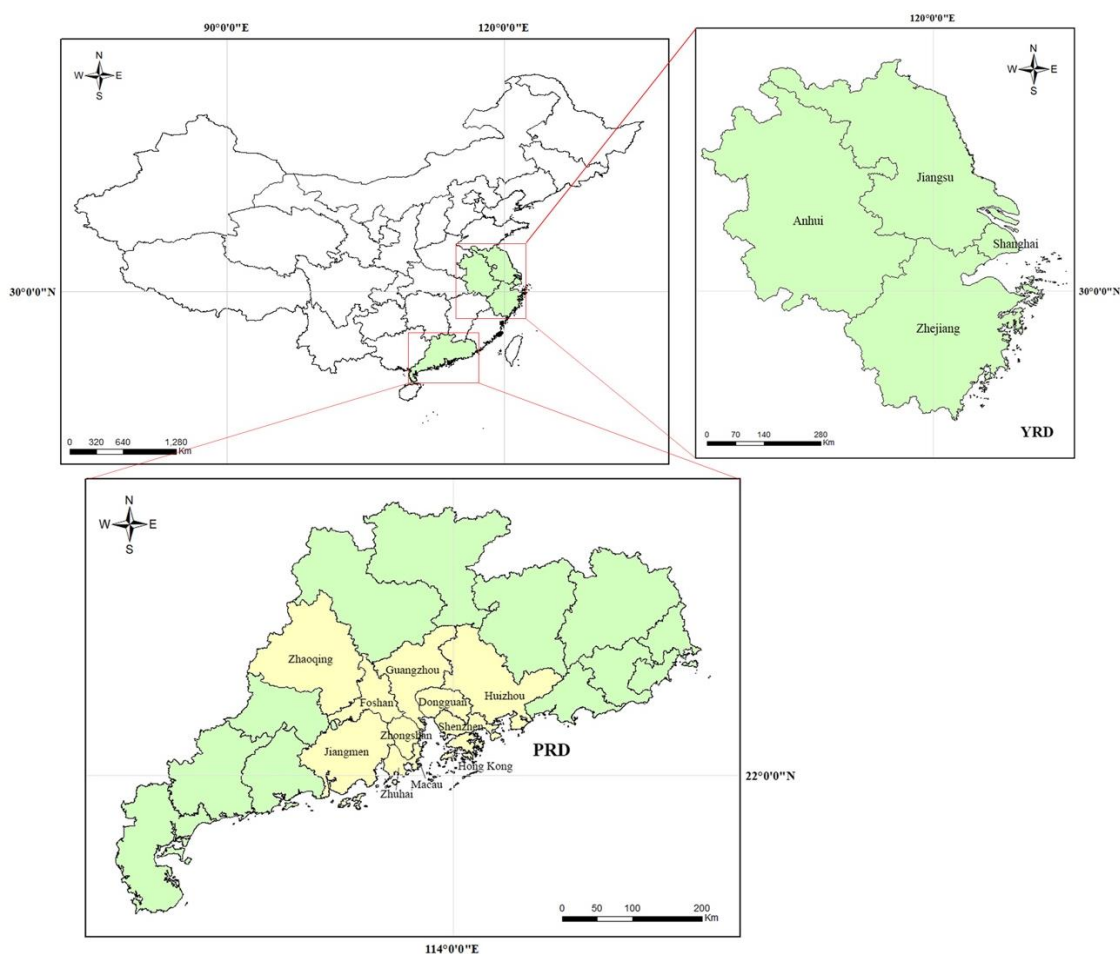


Figure 3-1 Geographical locations of the YRD and PRD (created using ArcGIS (2012)).

3.2 Description of the sampling strategy and sampling sites

In this study, sample collection was first conducted in multiple sites under different land-use impacts in selected typical cities in the YRD and PRD to investigate the inter-/intra-regional differences of PM_{2.5} pollution from both chemical and biological perspectives. Unlike the relatively extensive study on the climate effect on chemical pollution, the climate influence on the airborne biological fraction has been less explored. Therefore, additional samples were collected simultaneously in a representative urban Beijing site (temperate continental climate) for biological studies and further comparisons with the

subtropical YRD and PRD. Then, a short-term case study on a small scale was deployed in a WWTP in Hong Kong of the PRD region, a representative source of airborne bacteria and ARGs, to explore the quantitative contributions of potential urban sources to the biological components of ambient PM_{2.5}. Details of all the sampling sites in this study, including the description of the surrounding environment and the demographic and economic information of their located districts, are listed in Table **3-1** and Table **3-2**. Further information of the two sampling campaigns is introduced in Section 3.2.1 and 3.2.2, respectively.

Table 3-1 Description of the sampling sites.

Region	Climate zone	District/City (Abbreviated site name)	Type	Sampling site	Description
Beijing (northern China)	Temperate	Haidian, Beijing (BJ)	Urban	Institute of Atmospheric Physics, Chinese Academy of Sciences	Sampling site at the rooftop of a two-floor building; located between the North 3 rd Ring Road and the North 4 th Ring Road; surrounded by heavy traffic, residential buildings and a public park; covered with certain amounts of vegetation
		Pukou, Nanjing (PK)	Suburban-industrial	Nanjing University of Information Science and Technology	Sampling site at the rooftop of a twelve-floor building; surrounded by petrochemical plants, steel plants and highways; mixed industrial-residential areas
YRD (eastern China)	Subtropical	Xuanwu, Nanjing (XW)	Urban	Institute of Soil Science, Chinese Academy of Sciences	Sampling site at the rooftop of a five-floor building; downtown area surrounded by school, residential, and commercial buildings, with complex traffic networks
		Lishui, Nanjing (LS)	Rural	A botanical garden	Sampling site on the ground; distant from main roads, with massive vegetation cover; no obvious industrial emissions around
PRD (southern China)	Subtropical	Tianhe, Guangzhou (TH)	Urban	Guangzhou Institute of Geochemistry, Chinese Academy of Sciences	Sampling site at the rooftop of a five-floor building; adjacent to two expressways with heavy traffic, and surrounded by dwellings and schools
		Conghua, Guangzhou (CH)	Suburban	Tianhu Park	Sampling site on the ground upon a hill; located in a recreation area around 60 km northeast from Guangzhou downtown areas
		Heshan, Jiangmen (HS)	Semirural-industrial	Guangdong Atmospheric Monitoring Supersite of China	Sampling site at the rooftop of a four-floor building; located on a hill surrounded by vegetation, farmlands and country roads in the vicinity, as well as some industrial activities and highways in the outer space
		Hok Tsui, Hong Kong (HT)	Coastal	Hok Tsui Background Air Monitoring Station	Sampling site on the ground upon a hill; located in southeast Hong Kong and facing the South China Sea; approximately 10 km away from the urban areas

Region	Climate zone	District/City (Abbreviated site name)	Type	Sampling site	Description
PRD (southern China)	Subtropical	Hong Kong (PU)	Hung, Kong Urban	The campus of the Hong Kong Polytechnic University	Sampling site on the ground; at the roadside and next to a crowded footbridge; located in the highly urbanised city centre with heavy traffic and human flow
		Stonecutters Island, Hong Kong (SCISTW)	WWTP	Stonecutters Island Sewage Treatment Work	Sampling sites on the ground next to different treatment facilities within the SCISTW; located in the Stonecutters Island in West Kowloon with the West Kowloon Refuse Transfer Station on the northeast side.

Table 3-2 Demographic and economic information of the sampling districts.

Region	Types of land use	District	Area (km ²)	Residential population (1000 capita)	Population density (capita km ⁻²)	Urbanisation ratio (population) (%)	GDP ^a (billion RMB)	Percentage of GDP (%)			GDP density (million RMB km ⁻²)		
								Primary industry	Secondary industry	Tertiary industry	Primary industry	Secondary industry	Tertiary industry
Beijing (northern China)	Urban	Haidian	430	3593	8342	98.16	539.5	0.03	11.14	88.82	0.38	139.77	1114.38
	Urban	Xuanwu	75	634	8646	100	79.6	0	4.48	95.52	0.00	47.55	1013.79
YRD (east China)	Suburban-industrial	Pukou	910	769	823	69.87	88.5	4.68	47.96	47.37	4.55	46.64	46.07
	Rural	Lishui	1063	432	399	25.69	64.2	6.23	51.15	42.62	3.76	30.89	25.74
PRD (south China)	Urban	Tianhe	96	1631	16931	100	380	0.02	9.96	90.03	0.79	394.25	3563.69
	Suburban	Conghua	1974	635	322	44.81	37.5	6.75	43.83	49.43	1.28	8.33	9.39
	Semirural-industrial	Heshan	1082	505	344	61.01	28.7	8.05	52.12	39.83	2.14	13.82	10.56
		Hong Kong	1106	7337	6777	100	2491 ^b	0.1	7.7	92.2	2.25 ^b	173.42 ^b	2076.58 ^b

The statistical data were obtained from Beijing Municipal Bureau of Statistics (2017a,2017b), Nanjing Municipal Statistics Bureau (2017), Guangdong Statistics Bureau (2017), Jiangmen Statistics Bureau (2017), and Census and Statistics Department (2017,2018).

^a GDP, gross domestic product

^b HK\$ billion; revised data of 2016

3.2.1 Sample collection for the regional comparative study

For regional comparisons of the chemical and biological features of PM_{2.5} pollution, our PM_{2.5} sampling campaign was conducted simultaneously in selected cities in the YRD and PRD from spring 2016 to spring 2017. The seasons were demarcated as follows: March–May as spring, June–August as summer, September–November as autumn, and December–February as winter, in accordance with the China Meteorological Administration. In each region, three sampling sites under different land-use impacts within a city or two close cities were selected: for the YRD, these were Pukou (PK, representing a suburban-industrial area), Xuanwu (XW, representing an urban area), and Lishui (LS, representing a rural area) of Nanjing; for the PRD, these were Tianhe (TH, representing an urban area) and Conghua (CH, representing a suburban area) of Guangzhou, and Heshan (HS, representing a semirural-industrial area) of Jiangmen (Figure 3-2). The site classification was based on the major land-use type, population density, economic development, and industrial activities of the district where each sampling site is located (Table 3-1 and Table 3-2). The Nanjing and Guangzhou city selected here were typical megacity with a large population in the YRD and PRD, respectively, while the Jiangmen city, enjoying about one fourth of the agricultural land in the PRD, was under rapid industrial development at the same time. In addition, an urban site in Beijing (Haidian district) with sample collection during the same aforementioned period was added as a supplement – but merely for comparisons of biological features of PM_{2.5} between the subtropical and the temperate zones. As mentioned before, regarding the representativeness of the sites selected, detailed information of the surrounding environments for the sampling sites and the possible influence from human activities can be found in Table 3-1. One 24-hour PM_{2.5} sample per week was collected with high-volume samplers (TH-1000C II, Wuhan Tianhong

Instruments Co., Ltd., China) at a flow rate of around 1 m³/min in the above-mentioned studied sites, with the exception of TH and LS, where samples were collected every three days and on a monthly basis, respectively. The current sampling method for biological study has been widely used, of which the appropriateness was tested in previous studies. Although there could be a gradual loss of DNA content as the sampling time increases (Luhung et al., 2015), it is a trade-off to obtain enough biological materials for downstream analysis by the one-day sampling strategy. By applying the same sampling method, errors from DNA loss during the sampling period can be regarded as systematic errors. Additionally, it must be mentioned that, unlike the biological analysis in which all the samples were used, only the samples collected from March 2016 to February 2017 in the YRD and PRD were used for chemical analysis. Approximately four samples from each month in TH during this one-year period were randomly selected for chemical analysis. For better quality control, a filter placed in the air sampler not operating throughout the sampling campaign served as a field blank for each site. Tissuquartz filters (8 × 10 in, PALL, United States) pre-baked at 500°C for 5 h were used, weighed before and after sampling with a sensitivity of ± 0.0001 g. Before weighing, filters were equilibrated at 25°C and at 40%–50% relative humidity. Meanwhile, surface soil samples (1–2 cm depth) were collected in triplicate in the Beijing site, the PK and XW site in the YRD, and the TH site in the PRD, respectively, using a sterilised trowel (wiped with 70% ethanol). The possibility of fine surface fraction of soil being resuspended into the atmosphere makes soil a potential source for airborne microorganisms. These soil samples were only used for part of biological tests to help with source tracking of airborne bacteria. Since space was found to play a far more important role than season in shaping the microbial community in soil (Zhang et al., 2020b), it is still reasonable to collect soil samples once in this study. However, it should be cautious that the soil sampling time did

not fully match the PM_{2.5} sampling period, which could partially affect the relevant results. All of the filter and soil samples after collection were stored at -20 °C until subsequent treatment. A summary of the total number of samples, sampling frequency in each site over the sampling period, and the succeeding analyses that samples were subjected to is given in Table 3-3.

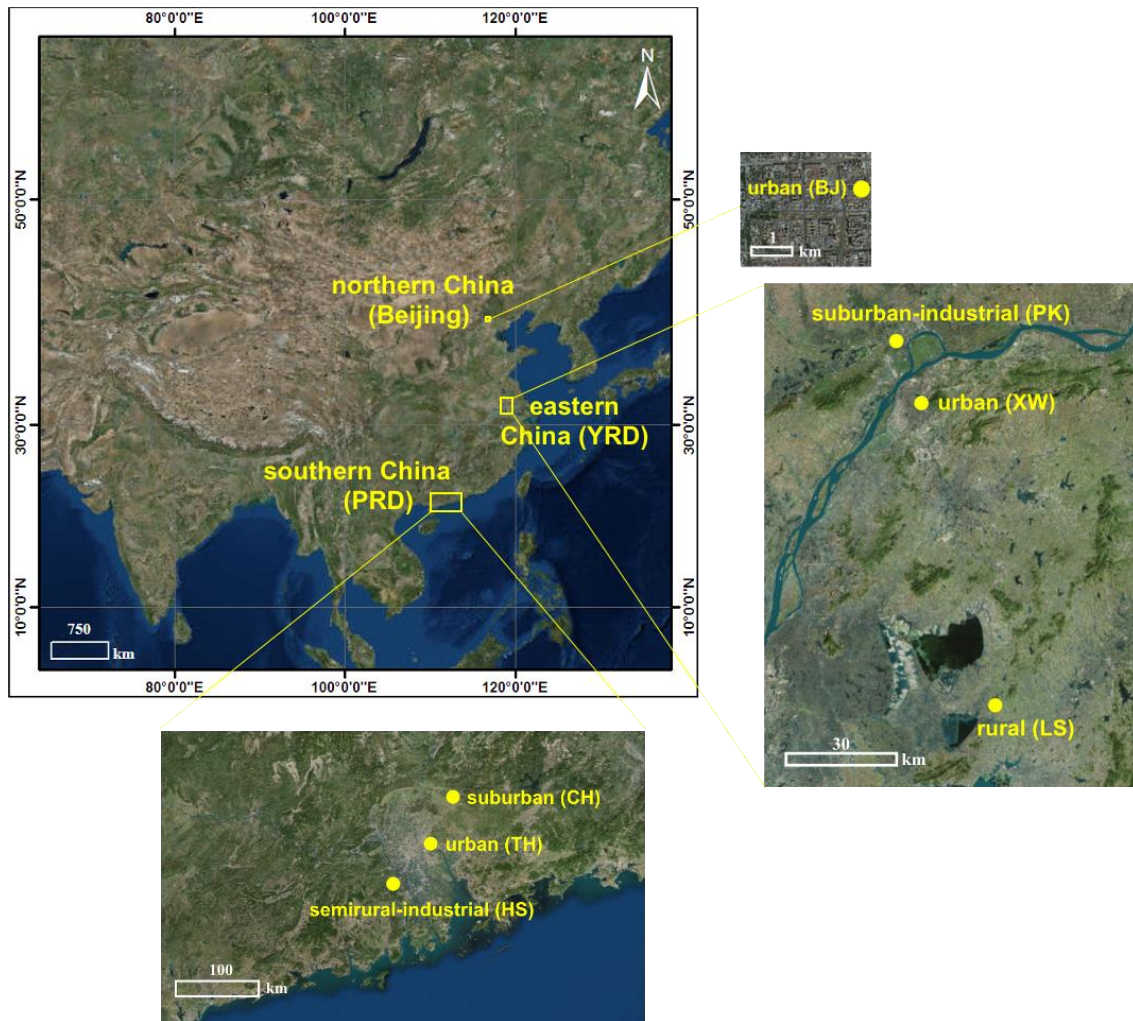


Figure 3-2 Satellite map of the sampling sites (created using ArcGIS (2012) with the World Imagery base map (Esri, 2009)).

Table 3-3 Sampling period, frequency, and sample size in the regional sampling campaign, as well as the analytical assays that were applied.

Region	Land-use type	Sampling site	Sample type	Sampling period	Sampling frequency	Sample size	Experimental analysis
Beijing (northern China)	Urban	Haidian (BJ)	PM _{2.5}	March 2016–May 2017	Weekly	61	Biological (DNA extraction; qPCR analysis; 16S rDNA sequencing)
			Soil	April 2018	N/A**	3	Biological (DNA extraction; 16S rDNA sequencing)
	Suburban- industrial	Pukou (PK)	PM _{2.5}	March 2016–May 2017	Every 7–10 days	46 (36*)	Chemical (OC/EC, WSI, total/bioaccessible metal); Biological (DNA extraction; qPCR analysis; 16S rDNA sequencing)
			Soil	July 2017	N/A**	3	Biological (DNA extraction; 16S rDNA sequencing)
YRD (eastern China)	Urban	Xuanwu (XW)	PM _{2.5}	March 2016–May 2017	Every 7–10 days	48 (37*)	Chemical (OC/EC, WSI, total/bioaccessible metal); Biological (DNA extraction; qPCR analysis; 16S rDNA sequencing)
			Soil	July 2017	N/A**	3	Biological (DNA extraction; 16S rDNA sequencing)
	Rural	Lishui (LS)	PM _{2.5}	April 2016–May 2017	Every 20–30 days	18 (15*)	Chemical (OC/EC, WSI, total/bioaccessible metal); Biological (DNA extraction; qPCR analysis; 16S rDNA sequencing)
PRD (southern China)	Urban	Tianhe (TH)	PM _{2.5}	March 2016–May 2017	Around every 3 days	122 (51*)	Chemical (OC/EC, WSI, total/bioaccessible metal); Biological (DNA extraction; qPCR analysis; 16S rDNA sequencing)
			Soil	February 2018	N/A**	3	Biological (DNA extraction; 16S rDNA sequencing)

Region	Land-use type	Sampling site	Sample type	Sampling period	Sampling frequency	Sample size	Experimental analysis
PRD (southern China)	Suburban	Conghua (CH)	PM _{2.5}	March 2016–May 2017	Every 7–10 days	52 (41 [*])	Chemical (OC/EC, WSI, total/bioaccessible metal); Biological (DNA extraction; qPCR analysis; 16S rDNA sequencing)
	Semirural- industrial	Heshan (HS)	PM _{2.5}	March 2016–May 2017	Weekly	65 (51 [*])	Chemical (OC/EC, WSI, total/bioaccessible metal); Biological (DNA extraction; qPCR analysis; 16S rDNA sequencing)

^{*} All the samples collected were used in biological analysis, while the specified number with an asterisk in the bracket refers to the sample size used in chemical analysis.

^{**} N/A, not applicable; soil samples were only collected once in this study.

3.2.2 Sample collection in typical sources of PM_{2.5}-associated bacteria and ARGs

To explore the quantitative contributions from potential urban sources to the biological components of PM_{2.5}, a typical WWTP in Hong Kong (a representative city in the PRD) was selected for further study, with an urban and a coastal site in Hong Kong as comparisons. In detail, the PM_{2.5} sampling campaign was deployed in the Stonecutters Island Sewage Treatment Work (SCISTW), the campus of The Hong Kong Polytechnic University (PU), and Hok Tsui (HT) (Figure 3-3; Table 3-1). Serving half of the population, the SCISTW is the largest sewage treatment plant in Hong Kong, with daily a capacity for treating 2.45 million m³ sewage and featured by its application of chemically enhanced primary treatment (CEPT) without biological treatment before the effluent is discharged. To reduce the emission of odour and the impact on nearby residents, all the flocculation tanks and sedimentation tanks in the SCISTW are equipped with covers. In addition, the West Kowloon Refuse Transfer Station is located on the northeast of the SCISTW, where the sludge generated from the SCISTW is temporarily stored and gathered with other municipal solid wastes before being transported for landfilling and incineration. PU is located in the highly urbanised city centre with heavy traffic and human flow. The sampling site in PU is located at the roadside and next to a crowded footbridge. By contrast, HT in southeast Hong Kong faces the South China Sea and is approximately 10 km away from the urban areas. Hence, these three locations were selected as the representatives of WWTP, urban, and coastal areas, respectively.

The sampling period lasted from 24 to 30 October 2016 in the SCISTW and HT, and from 28 October to 4 November 2016 in PU. Twenty-four-hour PM_{2.5} samples were collected daily on pre-baked (500 °C for 5 h) quartz filters (8 × 10 in², PALL) using high-volume air samplers (TH-1000C II, Wuhan Tianhong Instruments Co., Ltd., China) at a flow rate

of around $1 \text{ m}^3 \text{ min}^{-1}$. Unlike PU and HT – where only a single sampler was set – four sites were selected to collect $\text{PM}_{2.5}$ samples simultaneously in the SCISTW, including the flocculation tank (FT), sedimentation tank (ST), sludge storage tank (SST), and the barge facility (BF) (Figure 3-4A and Figure 3-4B). One sampler was placed beside each of the above-mentioned sites, except the BF site equipped with two samplers in 2 m intervals as duplicates. A blank filter was placed in a non-operating sampler at the flocculation tank, PU, and HT for quality control. Correspondingly, sewage including screened influent (daily flow ranging from 1.9 to 2.0 million m^3 during the sampling period), flocculation tank sewage, sedimentation tank effluent, and final effluent after de-chlorination, as well as CEPT sludge before centrifugation and sludge cake ready for transport to be landfilled, were collected daily from 24 to 28 October 2016 in the SCISTW (Figure 3-4C). Samples were kept at $4 \text{ }^\circ\text{C}$ and sent back to the laboratory immediately. $\text{PM}_{2.5}$ samples were stored at $-80 \text{ }^\circ\text{C}$ until further treatment, while sewage/effluent/sludge samples were subjected to pretreatment (Section 3.4.1) upon arrival at the laboratory. In addition, to monitor the meteorological parameters, a weather station (Vantage Pro2TM, Davis, UK) was set above the sedimentation tank. The major wind direction and wind speed during the sampling period are shown in a wind rose graph (Figure 3-5). The West Kowloon Refuse Transfer Station, which might pose certain impacts on nearby airborne microbes and ARGs, was never upwind of the SCISTW during the course of sampling. Detailed information of the collected samples, including the sampling period, sample size, and the downstream analytical assays applied, is summarised in Table 3-4.



Figure 3-3 Map of three sampling locations in Hong Kong.

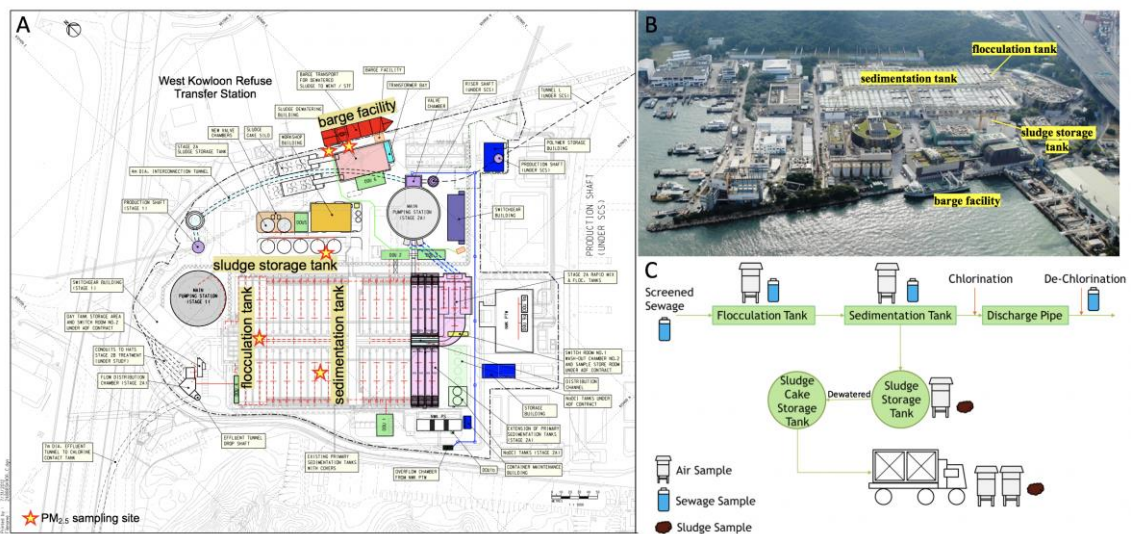


Figure 3-4 Sampling sites in the SCISTW and sample types collected along the treatment process. (A) An overall layout of the SCISTW, with the PM_{2.5} sampling sites marked with stars; (B) an aerial view of the SCISTW; (C) the general sewage treatment process in the SCISTW, with the sampling sites and the corresponding sample types collected marked.

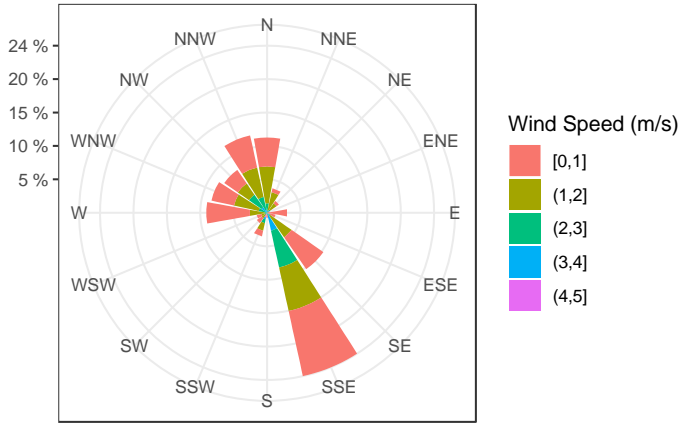


Figure 3-5 Wind direction and wind speed during the sampling period in the SCISTW.

Table 3-4 Detailed information of the samples collected in the SCISTW and urban and coastal Hong Kong.

Region	Land-use type	Sampling site	Sample type	Sampling period	Sampling frequency	Sample size	Experimental analysis
Hong Kong, PRD (southern China)	Coastal	Hok Tsui (HT)	PM _{2.5}	24–30 October 2016	Daily	5 (4 for 24 h; 1 for 72 h*)	Biological (DNA extraction; qPCR analysis; metagenomic sequencing)
	Urban	Roadside of the PU campus (PU)	PM _{2.5}	28 October–4 November 2016	Daily	6 (5 for 24 h; 1 for 72 h*)	Biological (DNA extraction; qPCR analysis; metagenomic sequencing)
	WWTP	Floculation tank (FT), SCISTW	Sewage (influent)	24–28 October 2016	Daily	3 (24-h composite)	Biological (DNA extraction; qPCR analysis; metagenomic sequencing)
			PM _{2.5}	27–30 October 2016	Daily	2 (1 for 24 h; 1 for 72 h*)	Biological (DNA extraction; qPCR analysis; metagenomic sequencing)
		Sedimentation tank (ST), SCISTW	Sewage	24–28 October 2016	Daily	5	Biological (DNA extraction; qPCR analysis; metagenomic sequencing)
			PM _{2.5}	24–30 October 2016	Daily	5 (4 for 24 h; 1 for 72 h*)	Biological (DNA extraction; qPCR analysis; metagenomic sequencing)
		Sludge storage tank (SST), SCISTW	Effluent	24–28 October 2016	Daily	3 (24-h composite)	Biological (DNA extraction; qPCR analysis; metagenomic sequencing)
			PM _{2.5}	24–30 October 2016	Daily	5 (4 for 24 h; 1 for 72 h*)	Biological (DNA extraction; qPCR analysis; metagenomic sequencing)
		Barge facility_1 (BFN), SCISTW	Sludge	24–28 October 2016	Daily	3	Biological (DNA extraction; qPCR analysis; metagenomic sequencing)
			PM _{2.5}	24–26 October 2016	Daily	3	Biological (DNA extraction; qPCR analysis; metagenomic sequencing)

Region	Land-use type	Sampling site	Sample type	Sampling period	Sampling frequency	Sample size	Experimental analysis
Hong Kong, PRD (southern China)	WWTP	Barge facility_2 (BFF), SCISTW	PM _{2.5}	25–30 October 2016	Daily	4 (3 for 24 h; 1 for 72 h*)	Biological (DNA extraction; qPCR analysis; metagenomic sequencing)
		Discharge pipe (post de-chlorination)	Effluent	24–28 October 2016	Daily	3 (24-h composite)	Biological (DNA extraction; qPCR analysis; metagenomic sequencing)
		Truck (for sludge transport)	Sludge (de-watered)	24–28 October 2016	Daily	3	Biological (DNA extraction; qPCR analysis; metagenomic sequencing)

* Due to the inaccessibility to the SCISTW during weekends, the collection of PM_{2.5} samples that started on Friday lasted for 72 h until the next Monday. For consistency, the corresponding PM_{2.5} samples in HT and PU were collected for 72 h as well.

3.3 Chemical-based analysis

This section describes the wet lab experiments for basic analysis of the chemical components of PM_{2.5}, including WSI, OC, EC, total metal(loid)s, and bioaccessible metal(loid)s, as well as the subsequent risk-calculation model for source apportionment. For chemical analysis, only the PM_{2.5} samples collected from March 2016 to February 2017 in the YRD and PRD with impact from different types of land use were used (Table 3-3).

3.3.1 WSI and carbonaceous material analysis

One thirty-second of each filter sample was extracted twice in 15 mL Milli-Q water (18.2 MΩ cm at 25 °C) using sonication (20 min for each) in an ice-water bath. The sample was filtered through a 0.45-μm membrane and stored at 4 °C and measured within one week for anions (Cl⁻, NO₃⁻, and SO₄²⁻) and cations (Na⁺, K⁺ and NH₄⁺) with IonPac AS14 and CS12 (Dionex, United States) columns, respectively, using ion chromatography (Dionex). All the samples were cut using ceramic scissors, which was wiped and sterilised with 70% ethanol between cuts. With regard to the carbonaceous materials, 0.526 cm² of each filter was used for OC and EC analysis by a Desert Research Institute (DRI) Model 2001 Thermal/Optical Carbon Analyzer (Atmoslytic Inc., United States), the result of which was calculated based on the thermal optical reflectance protocol.

3.3.2 Total metal(loid) and bioaccessible metal(loid) analysis

For total metal(loid) analysis, one sixteenth of each sample was cut and submerged within a mixture of HNO₃ and HClO₄ at a ratio of 4:1 in test tubes, followed by digestion in a heating block with a progressive temperature increase programme up to 190 °C until it was dried. Then a 10 mL aliquot of 5% (v/v) HNO₃ was added and the mixture was

incubated at 70 °C for 1 h. The final solutions were filtrated through 0.45- μ m membranes and kept at 4 °C until detection of the total concentration of various elements by ICP-MS (Agilent model 7700, United States). For quality control, a standard reference matter (NIST 1648a), filter blank, and reagent blank were treated with the same procedure and detection method as the samples. Replicates were applied to 5% of samples (randomly selected) to test the precision of the digestion and analysis (relative standard deviation [RSD] < 5%). Using the method in this study, the recovery of most metals in the reference materials ranged from 80% to 105%, with the exception of Al and Cr, both of which displayed unsatisfactory recovery due to incomplete dissolution limited by the current digestion method (Table 3-5).

To investigate the bioaccessibility of metal(loid)s in PM_{2.5}, Gamble's solution was applied to extract the bioaccessible metal(loid) fractions in samples. The composition of Gamble's solution is shown in Table 3-6; the chemicals were added to 18.2 M Ω cm Milli-Q water following the sequence specified in previous studies (Colombo et al., 2008; Marques et al., 2011). One sixteenth of each sample was combined with 30 mL Gamble's solution and shaken at 100 rpm and 37 °C for 24 h. A portion of the solution (15 mL in this study) was digested with the addition of 2 mL HNO₃, heated at 120 °C until it was dried, and subsequently leached by 5% HNO₃ following the aforementioned method for total metal(loid) digestion. The leachate was kept at 4 °C before further analysis by ICP-MS. Filter blank and reagent blank were treated following the same procedure at the same time. RSD < 5% was consistently achieved for the replicates of samples (5% of samples randomly selected). In addition, all the test tubes used in metal analyses in this study were submerged in 10% nitric acid overnight, washed with Milli-Q water, and dried before use, to reduce external contaminations as much as possible.

Table 3-5 Recovery of targeted elements by acid digestion in the analysis of total metal concentration.

Element	Al	Ca	Mg	Fe	As	Cd	Co
Mean (%)	51.50	101.16	81.23	92.64	104.66	91.14	81.71
SD (%)	2.50	3.32	1.85	2.00	4.16	3.28	3.73
Element	Cr	Cu	Ni	Pb	V	Zn	Mn
Mean (%)	21.67	88.65	81.54	98.84	81.79	95.86	80.59
SD (%)	2.39	2.34	1.49	2.85	1.44	2.20	5.31

Table 3-6 Chemical composition of Gamble's Solution (pH 7.4).

Chemicals	Concentration (g L ⁻¹)
Magnesium chloride, MgCl ₂	0.095
Sodium chloride, NaCl	6.019
Potassium chloride, KCl	0.298
Disodium hydrogen phosphate, Na ₂ HPO ₄	0.126
Sodium sulphate, Na ₂ SO ₄	0.063
Calcium chloride dihydrate, CaCl ₂ ·2H ₂ O	0.368
Sodium acetate, C ₂ H ₃ O ₂ Na	0.574
Sodium hydrogen carbonate, NaHCO ₃	2.604
Sodium citrate dihydrate, C ₆ H ₅ Na ₃ O ₇ ·2H ₂ O	0.097

3.3.3 Source apportionment

The EFs of metal(loid)s in PM_{2.5} were calculated using Fe as the reference element, with comparisons to the geochemical background values of metal(loid)s in soils in Guangzhou and Jiangmen in the PRD (Guangdong Geological Survey, 2010) and Nanjing in the YRD (Liao et al., 2011). Then, the PMF model from the USEPA (PMF 5.0) was applied to explore the more specific sources of PM_{2.5} (Norris et al., 2014b) in the areas with intense

human activities, including two urban sites (TH and XW) and another two sites under industrial impacts (HS and PK), using the concentrations of PM_{2.5} and its major chemical components. Briefly, the PMF model that is extensively used in the source apportionment of pollutants in ambient air can resolve the input data (multiple pollutant data arranged in a matrix) into a factor contribution matrix and a factor profile matrix. The exhaustive explanations of this mathematical model can be found in its user guide (Norris et al., 2014a). In this study, the input data under the method detection limit (MDL; refer to Table 3-7 for details) were replaced by half of the MDL beforehand. The species-specific uncertainties for each sample were calculated following either Equation 3-1 or Equation 3-2.

$$Unc = \sqrt{(10\% \times concentration)^2 + (0.5 \times MDL)^2}, \text{ if concentration} > MDL$$

Equation 3-1

$$Unc = \frac{5}{6} \times MDL, \text{ if concentration} \leq MDL$$

Equation 3-2

Various tests were conducted to determine the optimal factor numbers according to the criteria provided in a previous study (Lyu et al., 2016), mainly based on the model fitness and the interpretability of the source profile results. Different starting seeds were examined, and an approximate Q value was obtained. After removing the data that resulted in out-of-range points, the scaled residuals ranged from -3 to +3 (the percentage of the valid data was >90%). The ratio of Q(robust) to Q(true) was close to 1 (<1.5). For most species, the slope and correlation coefficient (R²) between the predicted data and the input data were 0.82–1.16 and 0.80–0.99, respectively, meaning a good fit for the model. The only exceptions were As, Cr, and Ni, all of which showed a relatively lower slope (0.6–0.83) and R² (0.55–0.76), possibly due to the limited sample size used and the complex mixing sources of these elements (Zeng et al., 2019). For uncertainty assessment

of the modelled results, 100 bootstrap runs were conducted after the base run to estimate the errors, which were used for the calculation of the 95% confidence interval (CI). The G-space plot generated by a subsequent run of the F-peak model showed a poor correlation between various factors, which meant there was little rotational ambiguity.

Table 3-7 Method detection limit of the analysed chemical species in this study.

Chemical species	Detection limit ($\mu\text{g m}^{-3}$)	Chemical species	Detection limit ($\mu\text{g m}^{-3}$)
Na ⁺	0.0441	Mg	0.0223
NH ₄ ⁺	0.0333	As	0.0020
K ⁺	0.0161	Cd	0.0001
Cl ⁻	0.0642	Cr	0.0026
SO ₄ ²⁻	0.0350	Cu	0.0017
NO ₃ ⁻	0.1138	Mn	0.0011
OC	0.205	Ni	0.0016
EC	0.0475	Pb	0.0017
Al	0.1134	V	0.0007
Fe	0.0406	Zn	0.0235
Ca	0.2065	Co	0.0001

3.3.4 Analysis of arsenic speciation by X-ray absorption near edge structures (XANES)

Considering that arsenic and chromium with high toxicity under their specific valence state – As(III) and Cr(VI) – and the more significant disparities in toxicity between their different valence states compared with other metals, a lack of speciation information of these two metals could result in bias in downstream risk assessment. Hence, the speciation information of As and Cr were attempted to be acquired by the XANES technique. However, the low mass content of Cr in PM_{2.5} samples did not support its analysis via

XANES. Therefore, only the analytical method for the molecular speciation of arsenic in airborne fine particulate matter was provided in this section.

The As K-edge (11,867 eV) XANES spectra of four selected PM_{2.5} filter samples (*i.e.*, 3 from HS in the PRD and 1 from PK in the YRD) with a high arsenic concentration were acquired in fluorescence mode on beamline 01C1 at the National Synchrotron Radiation Research Center, Taiwan, coupled with reference standards, such as NaAsO₂ and Na₂HAsO₄. For the XANES analysis, PM_{2.5} filter samples were directly used without pretreatment, while standard compounds were ground into powder. Multiple scans for each sample were merged and processed using Athena software (Ravel et al., 2005) according to methods specified in previous studies (Cui et al., 2018; Cui et al., 2013) before downstream linear combination fitting (LCF) was conducted, where all weights were constrained to between 0 and 1 with a final sum of 1.

3.3.5 Metal-based health risk assessment

To determine the chronic inhalation risks caused by the airborne trace metals of interest, a health risk assessment following guidelines from the USEPA was conducted for adults based on the bioaccessible concentrations of metals detected in the sampling sites. In light of the significant disparities in toxicity between different speciation of arsenic and chromium, a slightly modified risk assessment was conducted. The distribution of arsenic speciation determined by the XANES analysis was incorporated into the calculation of CR and NCR (refer to Section 3.3.6). One seventh of the bioaccessible chromium concentration (assumed to be bioaccessible Cr(VI)) was used in the risk assessment, on the assumption that the ratio of Cr(VI) to Cr(III), two major species of Cr, is around 1:6

in the air as proposed by the USEPA (2018b) and applied in other studies (Park et al., 2008; Zhang et al., 2017).

Specifically, the exposure concentration ($\mu\text{g m}^{-3}$) was normalised according to Equation 3-3 at the start of the analysis. The CR and NCR indicated by the hazard quotient (HQ) were calculated using Equation 3-4 and Equation 3-5, respectively (USEPA, 2009).

$$EC = (BC \times ET \times EF \times ED)/AT$$

Equation 3-3

In Equation 3-3, EC ($\mu\text{g m}^{-3}$) indicates the exposure concentration; BC ($\mu\text{g m}^{-3}$) is the annual average of bioaccessible metal concentration; and ET, EF, and ED represent exposure time (h day^{-1}), frequency (days year^{-1}), and duration (years), respectively. AT is the averaging time, which means the total number of hours in a lifetime when calculating CR, but it is only considered as the number of hours in the exposure duration while calculating HQ.

$$CR = IUR \times EC$$

Equation 3-4

$$HQ = EC/(RfC_i \times 1000 \mu\text{g}/\text{mg})$$

Equation 3-5

In Equation 3-4 and Equation 3-5, IUR means inhalation unit risk ($\mu\text{g m}^{-3}$)⁻¹ and RfC_{*i*} refers to reference concentration (mg m^{-3}) of a specific metal (*i*) via inhalation. The values of other parameters are shown in Table 3-8. Here the arsenic concentrations used for risk calculation were modified according to its speciation information. The modification model based on speciation distribution is explained in Section 3.3.6.

Subsequently, the CR caused by metals from each source in different locations was determined according to Equation 3-6, while the NCR was based on Equation 3-7.

$$CR_{s,l} = \sum_i (CR_{i,l} \times RC_{i,s,l}) \quad (i = \text{Co, Ni, As, Cd, Pb, and Cr})$$

Equation 3-6

$$HQ_{s,l} = \sum_i (HQ_{i,l} \times RC_{i,s,l}) \quad (i = \text{V, Mn, Co, Ni, As, Cd, Pb, Cr, Fe, Cu, and Zn})$$

Equation 3-7

In the above equations, s is the emission sources and l represents the sampling locations (TH, CH, and HS in the PRD and PK, XW, and LS in the YRD). $CR_{i,l}$ and $HQ_{i,l}$ are the CR and NCR induced by each metal(loid) in a specific sampling location, calculated from the aforementioned Equation 3-4 and Equation 3-5, respectively. $RC_{i,s,l}$ stands for the relative contribution of a certain source to individual metal(loid)s in a targeted location, which can be obtained from the source profile determined by the PMF model.

Finally, the contribution of individual sources to the CR and NCR of metal(loid)s via inhalation were evaluated using Equation 3-8 and Equation 3-9, respectively.

$$Con_{CR_{s,l}} = \frac{CR_{s,l}}{\sum_s CR_{s,l}}$$

Equation 3-8

$$Con_{HQ_{s,l}} = \frac{HQ_{s,l}}{\sum_s HQ_{s,l}}$$

Equation 3-9

In the above equations, s represents an individual source category and l represents an individual sampling location. $CR_{s,l}$ and $HQ_{s,l}$ are the CR and NCR induced by all the identified metal(loid)s from a certain source (s) in a certain sampling location (l), which were calculated in the previous step.

Table 3-8 Parameters used in the calculation of CR and NCR (presented as HQ) in this study.

Parameter	Adult	Metal(loid)	IUR ^a ($\mu\text{g m}^{-3}$) ⁻¹	RfC ^a (mg m^{-3})
ED (years)	20	V	-- ^g	1.00E-04
ET (h day ⁻¹)	8	Mn	-- ^g	5.00E-05
EF (days year ⁻¹)	350	Co	9.00E-03	6.00E-06
AT-non-carcinogens (h)	175200 (20 years)	Ni	2.60E-04 ^b	9.00E-05
		As	4.30E-03	1.50E-05
AT-carcinogens (h)	613200 (70 years)	Cd	1.80E-03 ^c	1.00E-05
		Pb	1.20E-05 ^d	5.00E-04 ^e
		Cr(VI)	8.40E-02	1.00E-04
		Fe	-- ^g	5.00E+00 ^{e, f}
		Cu	-- ^g	1.00E+00 ^e
		Zn	-- ^g	5.00E-01 ^e

^a IUR (inhalation unit risk) and RfC (reference concentration) obtained from the USEPA (2018a)

^b IUR estimated from data of soluble nickel salts

^c IUR estimated from cadmium data in diet and water

^d IUR estimated from lead phosphate data

^e benchmark value obtained from other standards (Oosthuizen et al., 2015)

^f RfC estimated from data of iron oxide in dusts

^g stands for a scarcity of relevant information

3.3.6 Modification on the calculation of arsenic-induced health risks based on speciation distribution

According to documents from the USEPA (USEPA, 2007), the IUR of arsenic was deduced from previous epidemiological studies conducted near the Anaconda smelter and Asarco smelter. Meanwhile, the RfC of arsenic for NCR assessment was established by the California Environmental Protection Agency's Office of Environmental Health Hazard Assessment (OEHHA) from a study on child exposure to arsenic in well water in Bangladesh (OEHHA, 2014; USEPA, 1994), due to a lack of relevant study on chronic effects of As exposure via inhalation. The estimate of RfC of As for air exposure assessment was based on the assumption that the lowest As dose to have an observed toxic or adverse effect under chronic exposure via inhalation should be the same as that from ingestion of drinking water. Regrettably, these studies – carried out in places with

heavy arsenic pollution – only considered the total concentration of arsenic regardless of their speciation. With reference to relevant studies, As(III) concentration was found to be at least one time higher than that of As(V) in Bangladesh groundwater (Rahman et al., 2008) and at a similar level to As(V) in West Bengal, which neighbours Bangladesh (Samanta et al., 1999). In contrast, As(V) was the dominant arsenic species in the surface soil near the Asarco smelter, with As(III) also detected (Impellitteri, 2005). Given the much higher toxic potency of trivalent compared with pentavalent arsenic, the PM_{2.5} arsenic criteria recommended by the USEPA could be less suitable for risk assessment of ambient air in places that are distant from smelters or without groundwater consumption by residents, as the speciation distribution of arsenic could be different in ordinary ambient environments from heavily polluted environments.

As such, a modified model for arsenic risk assessment based on its speciation distribution was applied, as shown in Equation 3-10 for the CR and Equation 3-11 for the NCR.

$$CR_{cur} = \frac{CR_{ori}}{R_{ori,As(V)} * TR_{As(V)/As(III)} + R_{ori,As(III)}} \times (R_{cur,As(V)} * TR_{As(V)/As(III)} + R_{cur,As(III)})$$

Equation 3-10

$$HQ_{cur} = \frac{HQ_{ori}}{R_{ori,As(V)} * TR_{As(V)/As(III)} + R_{ori,As(III)}} \times (R_{cur,As(V)} * TR_{As(V)/As(III)} + R_{cur,As(III)})$$

Equation 3-11

In the above equations, CR_{cur} and CR_{ori} are the modified and original cancer risks, respectively, based on data from the USEPA. R_{cur} means the proportion of As(V) or As(III) in total arsenic in the current study, while R_{ori} represents those in the studies referenced by the USEPA. TR_{As(V)/As(III)} refers to the ratio of As(V) toxicity to As(III). Of note, the toxic potency of trivalent arsenic is at least one order of magnitude higher than pentavalent arsenic (Jacobson-Kram et al., 1985; USEPA, 2007); thus TR_{As(V)/As(III)}= 0.1 was adopted in this study. Given that there is a lack of literature that provides the

distribution information of arsenic speciation in air particles near the Anaconda smelter (copper) and the Asarco smelter (lead), here the ratio of As(V) to As(III) in PM_{2.5} in another copper smelter (de la Campa et al., 2008), which was estimated to be around 5 based on average concentrations, was applied in carcinogenic risk assessments. Therefore, $R_{ori,As(V)}$ and $R_{ori,As(III)}$ for carcinogenic risk assessments were 5/6 and 1/6, respectively, if assuming that total arsenic only included As(III) and As(V), while in the evaluation of NCR, both $R_{ori,As(V)}$ and $R_{ori,As(III)}$ were 1/2 because the concentration of As(V) and As(III) is similar in groundwater in Bangladesh. In addition, the average percentage of As(V) and As(III) in total analysed arsenic in the selected samples from HS and PK (Figure 4-7B) was regarded as a general situation in the PRD and YRD, respectively, when conducting health risk assessments.

3.3.7 Data analysis

The data were processed using Excel, SPSS Statistics 21, and GraphPad Prism 7. The QQ-plot and Shapiro–Wilk test ($p < 0.05$) were used to evaluate the distribution of the data. Besides, non-parametric tests using Kruskal–Wallis one-way analysis of variance (ANOVA) were employed to compare the differences between the sampling groups.

3.4 Molecular biological analysis

This section provides the detailed procedures of the molecular biological tests applied in this study, including the pretreatment of different samples, the quantification of bacterial loads and certain kinds of environmentally relevant ARGs based on qPCR, the analysis of bacterial community structure based on 16S rDNA sequencing, and the determination of antibiotic resistome structure based on metagenomic sequencing. All the samples collected, including the PM_{2.5} (March 2016 to May 2017)/soil samples for regional

comparisons and PM_{2.5}/sewage/sludge samples in the case study (October to November 2016), were subjected to various biological analyses. Specific analytical assays used for different samples are provided in Table 3-3 and Table 3-4.

3.4.1 Sample pretreatment

For PM_{2.5} samples collected from March 2016 to May 2017 in the PRD, the YRD and Beijing for the regional study, a quarter of each filter sample was cut out except for that from the PRD urban site (TH; one eighth of each sample) and the YRD rural site (LS; half of each sample). A blank filter was treated simultaneously using the same operation that was used for the samples. The PM_{2.5} sample pretreatment followed the well-developed method proposed by Jiang et al. (2015) with slight modifications. Briefly, after the filter was cut into pieces if needed (and finally into one-eighth segments), each portion of the filter samples was sonicated with sterilised 1 × phosphate-buffered saline (PBS) in an ultrasonic bath filled with ice-water. According to He et al. (2021), no significant DNA degradation was caused by this procedure. Each monthly combined extract was then filtered through a 0.2-µm polyethersulfone (PES) membrane disc filter (47 mm, PALL) to ensure enough biological material obtained for downstream analysis, although this option sacrificed the time resolution with the results only indicating the monthly average. For the remaining PM_{2.5} samples from the SCISTW and urban and coastal Hong Kong, as well as their field blanks, the whole filter of each sample was treated following the same method as aforementioned, except that the PBS extracts were concentrated on the membrane disc filter individually by sample.

Soil samples were crushed and sieved to remove stones and other coarse detritus like plant debris. Sewage, effluent and sludge samples stored at 4 °C during transport were

treated immediately upon arrival at the laboratory. Influent, flocculation tank sewage, and sedimentation tank sludge collected from the sludge storage tank (~100 mL) were centrifuged at 9840 g and 4 °C for 10 min; the supernatant was carefully discarded and the pellets were kept. The remaining sedimented sludge was fixed with absolute ethanol at a 1:1 ratio for future use (if needed). For sedimentation tank effluent and de-chlorinated discharge, 250 mL solutions were filtered through 0.2- μ m PES membranes (PALL). All the samples were preserved at -80 °C before DNA extraction. All the tools, consumables, and equipment used in this section were sterilised.

3.4.2 DNA extraction

DNA extraction was conducted using the FastDNA SPIN Kit for Soil (MP Biomedicals, United States) according to the manufacturer's instructions, except for a modified purification step involving the use of Agencourt AMPure XP beads (Beckman Coulter, United States) for PM_{2.5} samples (Cao et al., 2014; Jiang et al., 2015). The 0.2- μ m membrane disc filters of effluent and PM_{2.5} were first cut into pieces, while the sieved soil, the pellet from sewage and sludge, and the sludge cake sample (around 150 mg) were directly used as the input for the DNA kit. For each non-PM_{2.5} samples (soil, sewage, effluent, and sludge), DNA was extracted in triplicate and pooled together to reduce heterogeneity, which was followed by a further purification step using the DNeasy PowerClean CleanUp Kit (QIAGEN, United States).

As described in Section 3.4.1, 15 monthly DNA samples of PM_{2.5} and one DNA sample of the field blank in each sampling site for the regional study (TH, CH, and HS site in the PRD, XW, PK, and LS site in the YRD, and BJ site in Beijing) – together 112 DNA extracts (105 of PM_{2.5} and 7 of control) – were ready for downstream analysis.

Correspondingly, 12 DNA samples of soil (TH, XW, PK, and BJ) were obtained in total. For samples from the SCISTW, PU, and HT in Hong Kong, a different strategy was adopted. PM_{2.5} DNA extracts from samples collected in three or four consecutive days were combined to obtain enough DNA for downstream analysis as well as to minimise the possible heterogeneity in samples collected on different days. Specifically, combined DNA samples of PM_{2.5} from 24 to 26 October (period 1) and 27 to 30 October (period 2) in the SCISTW and HT were gained, respectively, as well as that in PU from 28 to 31 October (period 2), 1 to 2 November (period 3), and 3 to 4 November (period 4). After that, DNA extracts of non-air samples from the same sites were combined corresponding to the time division of PM_{2.5} samples and based on the daily flow of influent. Due to an accidental malfunction of the air sampler in FT at period 1 and one of the two samplers in BF at period 2, as well as the limited project budget, 13 PM_{2.5} DNA samples covering the entire sampling period, 3 DNA samples of the field blank, and 5 sewage/effluent DNA samples and 2 sludge DNA samples covering around half of the sampling period were selected for downstream experiments (Table 3-9). All of the DNA extracts were kept at -80 °C until analysis.

Table 3-9 List of DNA samples from the SCISTW and urban and coastal areas in Hong Kong for downstream analysis.

Sample type	Location	Sampling date (2016)											
		24 Oct	25 Oct	26 Oct	27 Oct	28 Oct	29 Oct	30 Oct	31 Oct	01 Nov	02 Nov	03 Nov	04 Nov
Air samples	Flocculation tank				FT-P2								
	Sedimentation tank	ST-P1			ST-P2								
	Sludge storage tank	SST-P1			SST-P2								
	Barge facility_1	BFN-P1											
	Barge facility_2		BFF-P1		BFF-P2								
	Hok Tsui	HT-P1			HT-P2								
	PolyU					PU-P2		PU-P3		PU-P4			
	Blank_SCISTW					Blank_SCISTW							
	Blank_HT					Blank_HT							
	Blank_PU				Blank-PU								
Sewage samples	Screened sewage (influent)	SERaw-P1											
	Flocculation tank sewage	SEFlo-P1		SEFlo-P2									
	Sedimentation tank effluent	EFSed-P1											
	Final effluent (de-chlorination)	EFDechl-P1											
Sludge samples	CEPT sludge before centrifuge	SluSed-P1											
	Sludge cake collected from truck	SluDew-P1											

3.4.3 Absolute quantification of target genes (16S rRNA gene, ARGs, and MGEs) by qPCR

3.4.3.1 Construction of qPCR standards

Due to the limited amount of DNA extracted from airborne PM_{2.5}, 10 genes, including the 16S rRNA gene serving as an indicator of total bacterial load, six ARGs (*ermB*, *tetW*, *qnrS*, *lnuA*, *bla*_{TEM-1}, and *sulI*), and three MGEs (*intI1*, *tnpA-02*, and *tnpA-04*), were selected as targets. The choice of the six ARGs encoding resistance to different classes of antibiotics was based on their prevalence in the surface and atmospheric environments (Ling et al., 2013; Zhou et al., 2018a). The choice of the three MGEs was based on their dominance as important genetic vectors for the dissemination of ARGs (Xu et al., 2016b; Zhou et al., 2019; Zhu et al., 2017a).

To construct standards for absolute quantification by qPCR, targeted genes were firstly amplified from samples on a Veriti Thermal Cycler (Applied Biosystems, United States) following the procedures provided by a previous study (Chen et al., 2013a). Briefly, the PCR mixture in a 25- μ L volume – which contained 12.5 μ L Premix Taq™ DNA Polymerase (TaKaRa, Japan), forward and reverse primers, and a certain amount of template DNA – was subjected to the following amplification procedure: 5 min at 95 °C; 35 cycles of 15 s at 95 °C, 30 s at the annealing temperature, and 45 s at 72 °C; and a final extension at 72 °C for another 10 min. The primer sets and the corresponding annealing temperature used in this study are listed in Table 3-10.

Targeted amplicons were purified using the MEGAquick-spin™ Total Fragment DNA Purification Kit (iNtRON Biotechnology, Korea), followed by cloning into the pMD™19-T vectors (TaKaRa), and transformation into *Escherichia coli* DH5 α

competent cells (TaKaRa). Plasmids containing targeted genes, which were selected by blue-white screening and extracted by MiniBEST Plasmid Purification Kit Ver.4.0 (TaKaRa), were verified by Sanger sequencing.

Table 3-10 Information about the primer sets used in the present study.

Target	Primer	Sequence (5' → 3')	Annealing temperature (°C)	Classification	Reference
16S rRNA gene	Forward	TCCTACGGGAGGCAGCAGT	60	Total bacteria	(Nadkarni et al., 2002)
	Reverse	GGACTACCAGGGTATCTAATCCTGTT			
<i>ermB</i>	Forward	AAAACCTACCCGCCATACCA	60	Macrolide	(Chen et al., 2015)
	Reverse	TTTGGCGTGTTCATTGCTT			
<i>tetW</i>	Forward	GAGAGCCTGCTATATGCCAGC	62	Tetracycline	(Aminov et al., 2001)
	Reverse	GGGCGTATCCACAATGTTAAC			
<i>qnrS</i>	Forward	GTGAGTAATCGTATGTACTTTTGC	57	Quinolone	(Chen et al., 2015)
	Reverse	AAACACCTCGACTTAAGTCT			
<i>lnuA</i>	Forward	TGACGCTCAACACACTCAAAAA	60	Lincomycin	(Zhu et al., 2017b)
	Reverse	TTCATGCTTAAGTTCCATACGTGAA			
<i>bla_{TEM-1}</i>	Forward	CATTTTCGTGTCGCCCTTAT	60	Beta-lactamase	(Tan et al., 2017)
	Reverse	GGGCGAAAACCTCTCAAGGAT			
<i>sul1</i>	Forward	CGCACCGGAAACATCGCTGCAC	58	Sulphonamide	(Tan et al., 2017)
	Reverse	TGAAGTTCCGCCGCAAGGCTCG			
<i>intI1</i>	Forward	GGCTTCGTGATGCCTGCTT	60	MGE/Integrase	(Luo et al., 2010)
	Reverse	CATTCCTGGCCGTGGTTCT			
<i>tnpA-02</i>	Forward	GGGCGGGTCGATTGAAA	60	MGE/IS4 group	(Zhu et al., 2017b)
	Reverse	GTGGGCGGGATCTGCTT			
<i>tnpA-04</i>	Forward	CCGATCACGGAAAGCTCAAG	60	MGE/IS6 group	(Zhu et al., 2017b)
	Reverse	GGCTCGCATGACTTCGAATC			

3.4.3.2 qPCR detection of target genes

After measuring the DNA concentration using a Qubit 3.0 Fluorometer (Thermo Fisher, United States) with the Qubit™ dsDNA HS Assay Kit (Thermo Fisher), ten target genes (Table 3-10) in DNA samples were quantified using the StepOnePlus Real-Time PCR System (Applied Biosystems). To minimise inhibition, a 10-fold and a 100-fold dilution were applied to DNA extracts of PM_{2.5} and other non-PM_{2.5} samples, respectively, before the gene quantification. The dilution factor was determined by testing a number of randomly selected samples.

The qPCR reaction was performed in a 20-μL volume comprising Power SYBR™ Green PCR Master Mix (10 μL) (Life Technologies, United States), forward and reverse primers, template DNA (1 μL), and a certain amount of PCR-grade water. The target genes were amplified according to the following protocol: 10 min at 95 °C; 40 cycles of 15 s at 95 °C, 1 min at the annealing temperature – except that *qnrS* and *sulI* were annealed at 57 °C and 58 °C for 15 s, respectively – and extension at 72 °C for 45 s. In the end, a melt curve analysis was conducted to verify the specificity of the primer sets. Primer sets and the corresponding annealing temperature used in qPCR were the same as that of traditional PCR (Table 3-10). To quantify the absolute gene copy number in DNA samples, a seven-point standard curve using 10-fold serial dilutions was run with samples for each gene. For genes less than the minimum quantifiable copy number (under the current qPCR conditions) in spiked DNA templates without dilution, their concentrations in the atmosphere were set as the limit of quantification (LOQ) for subsequent analysis (Table 3-11). In brief, 2-fold serial dilutions of standards down to one copy were tested to determine the minimum quantifiable copy number, which is also the lowest point of the

standard curve for each target gene. The LOQ was then calculated according to Equation 3-12.

$$LOQ_i (\text{copy } m^{-3}) = \frac{MQCN_i (\text{copy}) \times \frac{V_{DNA \text{ sample}} (\mu L)}{V_{spiked \text{ DNA template}} (\mu L)}}{V_{sampled \text{ air}} (m^3)}$$

Equation 3-12

In Equation 3-12, *i* represents the target genes for qPCR (16S rRNA gene, *ermB*, *tetW*, *qnrS*, *bla*_{TEM-1}, *sulI*, *lnuA*, *intI1*, *tnpA-02*, and *tnpA-04*). MQCN_{*i*} (copy) means the minimum quantifiable copy number of a specific gene (*i*). V_{DNA sample} (μL) and V_{spiked DNA template} (μL) are the total volume of DNA eluted in the last step of DNA extraction (100 μL in this study) and the volume of DNA template spiked in qPCR tests (1 μL in this study), respectively. V_{sampled air} (m³) refers to the corresponding air volume of PM_{2.5} samples used for DNA extraction, which is converted from the total portion of PM_{2.5} filters used for combination in sample pretreatment.

All of the samples, standards, and negative controls (procedural blanks and field blanks) were run in triplicate, with the efficiency of the amplification ranging from 90% to 105%. Because the copy numbers of the 16S rRNA gene detected in PM_{2.5} samples were at least two orders of magnitude higher than those in blank samples, contamination caused during the sampling and DNA extraction procedure could be ignored. The blank samples were thus excluded from subsequent experiments.

Table 3-11 Minimum quantifiable copy number (qPCR) and LOQ of different target genes in the current method (normalised to air volume).

Target gene	Minimum quantifiable copy number in qPCR	LOQ (copy m ⁻³)			
		Regional study (PM _{2.5})		WWTP study (PM _{2.5})	
		Range	Mean (95% CI)	Range	Mean (95% CI)
16S rRNA gene	400	26.92–86.19	52.43 ± 2.82	8.71–17.36	10.99 ± 1.03
<i>ermB/tetW/qnrS/bla_{TEM-1}/sulI/intI1</i>	8	0.53–1.72	1.05 ± 0.06	0.17–0.35	0.22 ± 0.02
<i>lnuA/tnpA-02/tnpA-04</i>	40	2.69–8.62	5.24 ± 0.28	0.87–1.74	1.10 ± 0.10

3.4.3.3 Assessment of inhalational contribution to the daily intake of bacteria and ARGs

To assess the relative importance of inhalation to total human exposure to external ARGs, the human daily intake of the targeted genes via PM_{2.5}, drinking water, and food items in urban populations in China (Beijing, the YRD, and the PRD) was estimated, coupled with the situation in the United States as a comparison, using Equation 3-14, Equation 3-15, and Equation 3-15, respectively.

$$DI_{PM_{2.5}} (\text{copy } d^{-1}) = \text{Concentration (copy } m^{-3}) \times \text{inhalation rate (} m^3 d^{-1})$$

Equation 3-13

$$DI_{\text{drinking water}} (\text{copy } d^{-1}) = \text{Concentration (copy } L^{-1}) \times \text{ingestion rate (} L d^{-1})$$

Equation 3-14

$$DI_{\text{food}} (\text{copy } d^{-1}) = \text{Concentration (copy } g^{-1}) \times \text{ingestion rate (} g d^{-1})$$

Equation 3-15

In the above equations, DI represents the daily intake of targeted genetic elements. The concentrations of the target genes in urban aerosols are from this project (the PRD, YRD, and Beijing in China) and references for the United States (Echeverria-Palencia et al., 2017; Hospodsky et al., 2012). Those in other intake matrices (e.g., drinking water, aquatic products, and vegetables) are from previous studies (Echeverria-Palencia et al., 2017; He et al., 2016; Huang, 2014; Shi et al., 2013; Su et al., 2018a; Su et al., 2018b; Xi

et al., 2009). The daily inhalation rate was commonly set as $20 \text{ m}^3 \text{ day}^{-1}$ (USEPA, 1989). The ingestion rates for drinking water, aquaculture products, and vegetables in China were 1.6 L day^{-1} ($1.5\text{--}1.7 \text{ L day}^{-1}$), 57.5 g day^{-1} ($40\text{--}75 \text{ g day}^{-1}$), and 400 g day^{-1} ($300\text{--}500 \text{ g day}^{-1}$), respectively, according to the Dietary Guidelines for Chinese Residents (Chinese Nutrition Association, 2016). For U.S. adults, the ingestion rates for drinking water and aquaculture products (finfish) were set as 2 and 12 g day^{-1} , respectively, as recommended by the USEPA (1989). These comparisons were based on the assumption of equal DNA extraction efficiency between matrices across studies.

3.4.4 16S rRNA gene amplicon sequencing

3.4.4.1 Sample preparation and sequencing strategy

In order to compare the regional differences of airborne bacterial community structure, 16S rRNA gene amplicon sequencing was conducted for $\text{PM}_{2.5}$ samples that were continuously collected from March 2016 to May 2017 in the PRD, the YRD, and Beijing. The V3-V4 hypervariable region of the 16S rRNA gene was amplified using KAPA HiFi HotStart ReadyMix (Kapa Biosystems, United States) with primer pair 341F (ACTCCTACGGGAGGCAGCAG)/806R (GGACTACHVGGGTWTCTAAT) on a Veriti Thermal Cycler. Each reaction mixture ($25 \mu\text{L}$) contained $12.5 \mu\text{L}$ of KAPA HiFi HotStart ReadyMix, 200 nM of forward and reverse primers, $5 \mu\text{L}$ of template DNA, and a certain amount of PCR-grade water. The amplification procedure was as follows: 3 min at $95 \text{ }^\circ\text{C}$ for initial denaturation; 35 cycles of 20 s at $98 \text{ }^\circ\text{C}$, 30 s at $55 \text{ }^\circ\text{C}$, and 50 s at $72 \text{ }^\circ\text{C}$; and a final extension at $72 \text{ }^\circ\text{C}$ for another 5 min. The targeted amplicons (around 460 bp in length) were then purified using the MEGAquick-spinTM Total Fragment DNA Purification Kit and quantified with the QubitTM dsDNA HS Assay Kit after electrophoretic separation in a 1.5% agarose gel. Purified amplicons from the same season

at the same sampling site were pooled on an equal mole basis and sequenced on the Illumina Miseq platform (2×300 bp paired-end run) in the Beijing Genomics Institute (Wuhan, China). The raw sequencing data were preprocessed using in-house scripts of the Beijing Genomics Institute. In brief, sequencing reads were truncated if the average quality score over the sliding window (30 bp) was less than 20. The trimmed reads were removed if they were shorter than 75% of their original size. Afterwards, the remaining data were further filtered to remove adapters and reads with ambiguous bases or low complexity (with 10 same bases consecutively). The clean data acquired were deposited in the National Center for Biotechnology Information (NCBI) BioProject database (<https://www.ncbi.nlm.nih.gov/bioproject/>) with the accession number of PRJNA485473. For soil samples collected in the same urban sites, their DNA extracts were directly sent to the Beijing Genomics Institute for 16S rRNA gene amplicon sequencing with the same primer pair and sequencing platform as that of PM_{2.5}. The sequencing data were then subject to the same preprocessing procedure as that of PM_{2.5}.

3.4.4.2 Taxonomy annotation and source tracking

The structure of the bacterial community in the samples was characterised by the Basic Local Alignment Search Tool for nucleotide sequence (BLASTn) (Altschul et al., 1997) against the Silva SSU database (version 111) with an E-value cut-off of $1e-20$ (Mackelprang et al., 2011). The sequences from the BLAST results were assigned to NCBI taxonomies via MEGAN (version 4.67.5) (Huson et al., 2007) using the lowest common ancestor (LCA) algorithm with the default cut-off of BLAST bitscore 50 and 10% of the top 50 hits. MEGAN directly classifies sequencing reads into taxonomic bins without generations of operational taxonomic units or amplicon sequencing variants (Mitra et al., 2011). In addition, SourceTracker2 (Knights et al., 2011), a quantitative

method developed based on a Bayesian approach to track the proportion of biological elements from source environments, was applied as a supplement with default parameters to estimate the contribution of terrestrial origins (soil/dust) to PM_{2.5}-associated bacteria. The bacterial taxonomy information (genus level) of PM_{2.5} and soil samples were used as the model input; the PM_{2.5} and soil samples were set as sink and source samples, respectively.

3.4.5 Metagenomic sequencing

3.4.5.1 Sequencing strategy

Unlike the regional studies where the PM_{2.5} samples were divided for both chemical and biological analysis, samples from the SCISTW and urban and coastal Hong Kong were fully used for DNA extraction (Section 3.4.2) in order to obtain enough DNA amount for metagenomic sequencing and thus capture the antibiotic resistome. Around 25–100 ng DNA of each combined sample from these three sites in Hong Kong were sent to Beijing Genomics Institute for low-input library construction and metagenome shotgun sequencing on an Illumina Hiseq X Ten platform with the PE150 (2 × 150 bp paired-end run) strategy. The sequencing data were firstly filtered using fastp (Chen et al., 2018) to remove reads with low quality, short in length, or with low complexity (--qualified_quality_phred 20; --unqualified_percent_limit 40; --n_base_limit 5; --length_required 75; --complexity_threshold 30), as well as removing contaminations from adapters and duplication. After quality control procedures, 432 GB of clean data in total from 20 samples were obtained and uploaded to the NCBI BioProject database (<https://www.ncbi.nlm.nih.gov/bioproject/>) with the accession number of PRJNA693982.

The rarefaction curves proved that the sequencing strategy applied in this study was able to capture sufficiently the bacterial community at the genus level and most of the ARG subtypes (Figure 3-6).

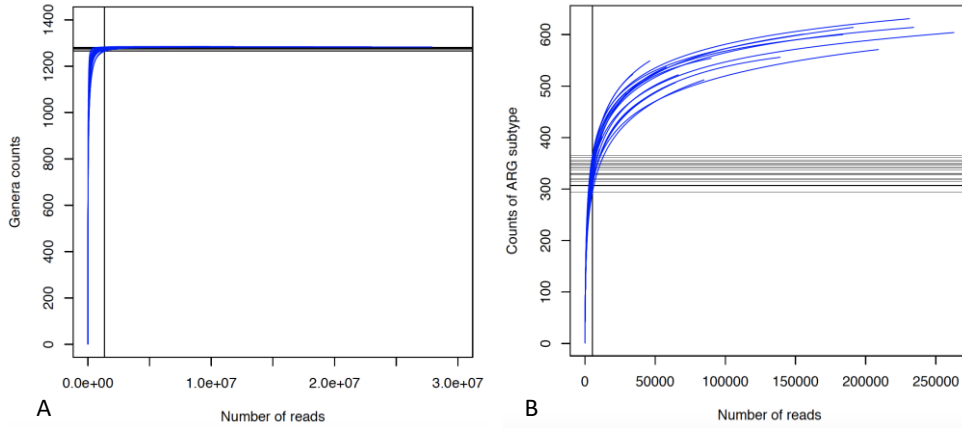


Figure 3-6 Rarefaction curves of (A) bacterial genera and (B) ARG subtype diversity analysed using the “vegan” package in R.

3.4.5.2 Bioinformatic analysis

Taxonomy classification and estimation of the relative abundance of bacteria were conducted in Kraken 2 (Wood et al., 2019) and Bracken 2.5 (Lu et al., 2017) using the standard Kraken 2 database. Venn diagrams revealing the intersections of bacterial communities among different samples were drawn using jvenn (Bardou et al., 2014). ARGs were predicted using the DeepARG online platform (Arango-Argoty et al., 2018) with default parameters (--identity 50%; --E-value 1e-10; --coverage 5%; --minimum probability 0.8). The relative abundance of ARGs normalised to the 16S rRNA gene calculated by DeepARG was based on Equation 3-16 (Li et al., 2015a).

$$Relative\ abundance\ (ARGs) = \sum_1^n \frac{N_{ARG-like\ read} \times \frac{L_{ARG-like\ read}}{L_{ARG\ reference\ sequence}}}{N_{16S\ rDNA\ read} \times \frac{L_{16S\ rDNA\ read}}{L_{16S\ rDNA\ reference\ sequence}}}$$

Equation 3-16

In Equation 3-16, n means the number of mapped ARG reference sequences that belong to a particular ARG subtype; $N_{\text{ARG-like read}}$ represents the number of ARG-like reads annotated to a specific ARG reference sequence; while $L_{\text{ARG-like read}}$ and $L_{\text{ARG reference sequence}}$ mean the length of the specific ARG-like read and the corresponding ARG reference sequence, respectively. $N_{16S \text{ rDNA read}}$ is the number of identified 16S rDNA reads, and $L_{16S \text{ rDNA reference sequence}}$ refers to the length of the 16S rDNA reference sequence (1432 bp used in DeepARG). According to Li et al. (2015a), the relative abundance of ARGs generated based on this method could be comparable to that from qPCR.

Afterwards, non-metric multidimensional scaling (NMDS) analysis was conducted to analyse the differentiation of taxonomy and ARG profile between different sample types or sampling locations, followed by further identification of the determined biomarkers, which were determined by a linear discriminant analysis (LDA) effect size (LEfSe) method (Segata et al., 2011).

To evaluate the co-occurrence patterns of ARGs, MGEs, and human pathogens, clean sequencing data were then assembled on the MetaStorm platform (Arango-Argoty et al., 2016) using iterative de Bruijn graph *de novo* assembler for short reads sequencing data with highly uneven sequencing depth (IDBA-UD) (Peng et al., 2012). The output scaffolds were then deposited in the NanoARG platform (Arango-Argoty et al., 2019) for annotation (identity ≥ 50) of ARGs, MGEs, and putative human pathogens, especially for ESKAPE pathogens (*Enterococcus faecium*, *Staphylococcus aureus*, *Klebsiella pneumoniae*, *Acinetobacter baumannii*, *Pseudomonas aeruginosa*, and *Enterobacter* spp.) and other WHO priority pathogens (*Enterobacteriaceae*, *Helicobacter pylori*, *Campylobacter* spp., *Salmonellae*, *Neisseria gonorrhoeae*, *Streptococcus pneumoniae*,

Haemophilus influenzae, and *Shigella* spp.) in urgent need of novel antibiotics for treatment. Meanwhile, the assembled data were uploaded to the online MetaCompare platform to evaluate the potential horizontal dissemination risks of ARGs, particularly for their transfer to human pathogens (Oh et al., 2018). This computational software proposed a conceptual risk score based on the distance in a three-dimensional (3D) space between the dot of the analysed sample and the dot symbolising the theoretical maximum resistome risk. The three coordinate axes of the 3D space represented the relative abundance of scaffolds containing: 1) ARG-like sequences, 2) ARG- and MGE-like sequences, and 3) ARG-, MGE-, and pathogen-like sequences, respectively. The relative abundance here was expressed as the number of scaffolds embracing such biological elements normalised to the number of total assembled scaffolds.

Furthermore, SourceTracker2 (Knights et al., 2011) was adopted with default parameters to explore the contributions of different putative sources to the airborne bacteria and ARGs. The data used in source tracking were downloaded from NCBI and MG-RAST databases and listed in Appendix 1. All the downloaded data were subjected to the same pipeline of quality control (fastp), taxonomy annotation (Kraken 2 and Bracken 2.5), and ARG identification (DeepARG) as the SCISTW samples. The taxonomy profile at the genus level and ARG profile at the subtype level were used as the input for SourceTracker2, with the PM_{2.5} and other non-air samples as sink and source samples, respectively.

3.4.6 Statistical analysis

NMDS analysis was performed in R (version 3.2.2) using the “vegan” package to capture the regional differentiation in PM_{2.5}-associated bacterial and ARG profiles, as well as

their differences across sample types; one-way analysis of similarities (ANOSIM), permutational multivariate analysis of variance (PERMANOVA), and permutational analysis of multivariate dispersions (PERMDISP) were conducted with 999 random permutations using the “vegan” package to test the statistical significance; the “ggplot2” package was used for the visualisation. RDA was performed using CANOCO (version 4.5) and R (version 3.2.2) (“vegan” package) to explore the correlations between chemical compositions and bacterial communities and between bacterial genera and the analysed ARGs. Other statistical analyses were conducted in R and GraphPad Prism 7.

Chapter 4 Chemical Characterisation and Metal-based Health Risk-oriented Source Apportionment of PM_{2.5} across Geographical Locations in the YRD and PRD

The spatiotemporal variations in PM_{2.5} concentrations and chemical compositions were investigated in the YRD and PRD during a one-year period from March 2016 to February 2017. There were inter-regional differences in PM_{2.5} pollution characteristics and intra-regional disparities with change in land-use impacts from a chemical perspective. Furthermore, based on the analysis of metal(loid) and bioaccessible metal(loid) contents, health risk-oriented source apportionment was conducted to pinpoint the major source contributors of inhalational health risks derived from PM_{2.5}-associated metals using a modified risk assessment model, which considered the speciation and bioaccessibility of metals.

4.1 Inter-regional and intra-regional comparisons of the concentrations and chemical composition profiles of PM_{2.5}

As a whole, residents in both the PRD and YRD were exposed to polluted air during almost the entire evaluated year (March 2016 to February 2017) with excessive PM_{2.5} concentrations relative to the WHO guideline value (25 µg m⁻³ for 24-h samples) (Figure 4-1). Most of the highly polluted days in which PM_{2.5} concentrations were above the Grade II value of the Chinese National Ambient Air Quality Standard (NAAQS) (75 µg m⁻³ for 24-h samples) fell in spring and winter, indicating seasonal characteristics in PM pollution. In general, the PM_{2.5} concentrations seemed to share similar patterns of fluctuation within the same region, with the exception of occasional site-specific episodes of pollution, such as the relatively high PM_{2.5} concentrations in the semirural-industrial

site (HS) in the PRD in winter (Figure 4-1). In terms of the annual average PM_{2.5} concentration (Figure 4-2), the HS site (69.0 µg m⁻³) in the PRD and the PK site (68.6 µg m⁻³) in the YRD presented the heaviest air pollution in their respective region. These two sites under industrial influences showed a significantly higher PM_{2.5} concentration compared with the suburban (CH, 46.7 µg m⁻³) and rural (LS, 47.9 µg m⁻³) areas, while the PM_{2.5} concentration in the urban sites ranked in the middle (TH, 50.0 µg m⁻³; XW, 61.1 µg m⁻³). Such discrepancies among different land-use zones likely reveal the exacerbation of air pollution as a result of anthropogenic activities. When focusing on the urban sites of these two regions, PM_{2.5} concentrations were 20% higher in the YRD than in the PRD in terms of annual average values (t-test, $p < 0.05$), suggesting that urban residents in the YRD are vulnerable to air pollution exposure.

Echoing the variations in PM_{2.5} concentrations, the inter-regional differences in chemical composition profiles were more pronounced than the intra-regional ones (Figure 4-3). There was a higher proportion of WSI relevant to secondary inorganic aerosols (NO₃⁻, SO₄²⁻, and NH₄⁺) and a lower proportion of carbonaceous materials (OC and EC) presumably from combustion activities to the total identified components in the YRD compared with the PRD. Such regional differentiation had been observed in these two regions regardless of the land-use type of the sampling locations (Table 4-1) (Du et al., 2017; Ming et al., 2017; Tao et al., 2017). The inter-regional heterogeneity in the dominant mass contributors of PM_{2.5} (OC/EC and WSI) underscored the regional PM_{2.5} pollution characteristics and the discrepancies in the major source contributors to PM_{2.5} between the two regions.

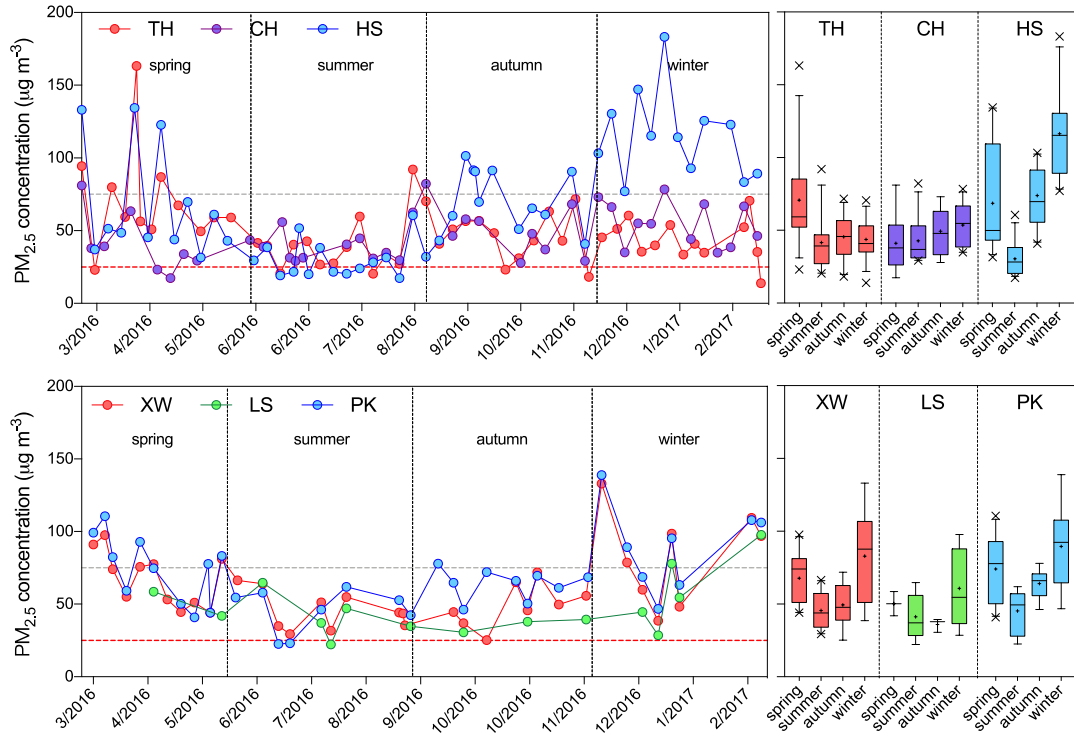


Figure 4-1 Spatiotemporal variations in $PM_{2.5}$ concentrations at the studied sites in the PRD (TH, CH, and HS) and YRD (XW, PK, and LS). The red dashed line represents the WHO guideline value for $PM_{2.5}$ concentrations ($25 \mu\text{g m}^{-3}$) based on short-time monitoring (24 h), while the grey dashed line is the Grade II level ($75 \mu\text{g m}^{-3}$) for 24-h sampling according to China's Air Quality Standard.

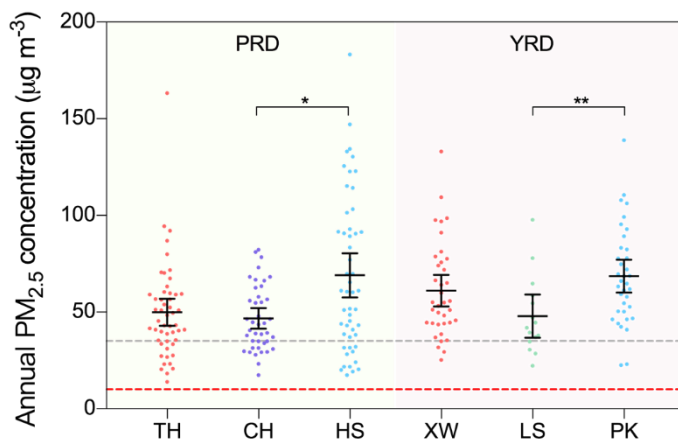


Figure 4-2 Annual average $PM_{2.5}$ concentrations at the studied sites in the PRD (TH, CH, and HS) and YRD (XW, PK, and LS). Line and error bars represent the mean with the

95% CI. Non-parametric Kruskal–Wallis tests were conducted in GraphPad Prism 7 (* $p < 0.05$; ** $p < 0.01$). The red dashed line represents the WHO guideline value for PM_{2.5} concentrations (10 $\mu\text{g m}^{-3}$) on an annual average basis, while the grey dashed line indicates the Grade II level (35 $\mu\text{g m}^{-3}$) for annual mean according to the Chinese NAAQS.

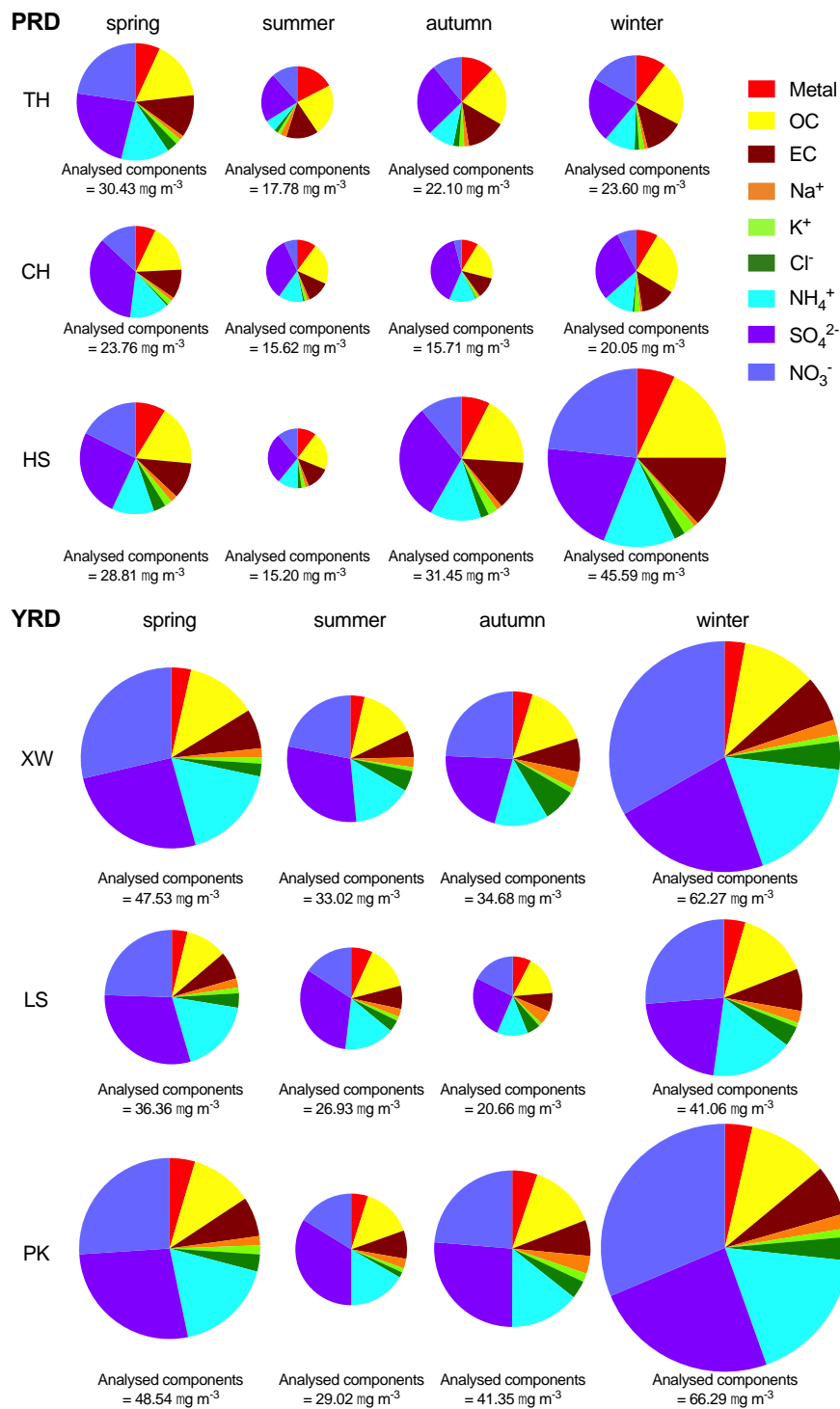


Figure 4-3 Seasonal variations in major chemical components analysed in PM_{2.5} in the PRD and YRD. The pie charts are divided according to the proportion of each analysed component over the total analysed components regarding their concentrations in PM_{2.5} samples.

Table 4-1 Comparisons of chemical compositions of PM_{2.5} in the PRD and YRD in different studies (μg m⁻³).

Region	Location (land-use type)	Sampling period	PM _{2.5}	OC	EC	Na ⁺	NH ₄ ⁺	K ⁺	Cl ⁻	NO ₃ ⁻	SO ₄ ²⁻	Carbonaceous material (%)	WSI (%)	Reference
PRD	Guangzhou (urban)	Jan 2014–Dec 2014	48	8.2	4	0.4	3.8	0.7	0.2	2.2	9.3	25.4%	34.6%	(Tao et al., 2017)
	Zhuhai (suburban)	Apr 2014–Jan 2015	45	9.4	2.6	0.3	3.6	0.4	0.3	2.7	8.1	26.7%	34.2%	(Tao et al., 2017)
	Shanghai	Oct 2013–Jul 2014	94.6	9.89	1.63	-- ^a	8.13	1.28	2.64	18	14.5	12.2%	47.1%	(Ming et al., 2017)
	Shanghai	2015 spring	74.38	11.31	2.83	1.87	5.69	0.19	1.27	11.18	8.69	19.0%	38.8%	
	Nanjing	2015 spring	82.52	11.48	2.65	2.65	7.91	1.52	1.62	16.11	21.39	17.1%	62.0%	
	Ningbo	2015 spring	68.3	9.86	2.27	2.58	4.17	0.75	1.59	7.41	8.72	17.8%	36.9%	
YRD	Lin'an (background)	2015 spring	55.18	9.63	2.4	3.19	4.73	0.44	0.63	7.96	22.26	21.8%	71.1%	(Du et al., 2017)
	Shanghai	2014 winter	102.55	17.93	4.04	1.77	14.42	1.48	6.94	25.44	18.26	21.4%	66.6%	
	Nanjing	2014 winter	99.78	14.73	3.85	1.33	12.3	1.35	4.04	16.39	11.72	18.6%	47.2%	
	Ningbo	2014 winter	97.98	14.38	3.69	2.63	10.56	1.03	4.26	16.34	17.03	18.4%	52.9%	
	Lin'an (background)	2014 winter	83.85	12.17	3.16	2.78	8.55	1.24	2.08	14.48	19.29	18.3%	57.7%	

^a unmeasured

4.2 Regional comparisons of the characteristics of PM_{2.5}-associated metal(loid)s

As a follow-up to the inter-regional and intra-regional comparisons of PM_{2.5} chemical components in the previous section, trace metal(loid)s that might pose significant health impacts – even though accounting for a relatively low mass percentage of PM_{2.5} – were picked out for further analysis. Considering that trace metals may not all be available for biochemical reactions after moving into the human body via inhalation, their bioaccessible fractions extracted by Gamble's Solution were analysed in the meanwhile so as to conduct downstream assessments of inhalational health risks. Hence, this section presents regional comparisons of both the total and bioaccessible concentrations of targeted metal(loid)s.

4.2.1 Total metal(loid) concentrations

In the PRD, the annual average concentrations of the highly enriched ($EF > 100$) and some of the moderately enriched ($10 < EF < 100$) elements, such as Zn, Pb, As, and Cd, were significantly higher in the semirural HS site compared with the suburban and urban sites ($p < 0.05$) (Figure 4-4A, Table 4-2). Nevertheless, the remaining trace metals, such as Cu, Cr, Ni, V, Mn, and Co, exhibited the lowest concentrations in the suburban CH site ($p < 0.01$) but showed elevated concentrations in the semirural (HS) and urban (TH) areas. The highest concentrations of Zn, Pb, As, and Cd (regarded as industrial tracers), which were found in HS, could be explained by the spread of industries containing electroplating factories and hardware and battery manufacturers in this sampling district. When comparing the situation in the YRD with that in the PRD, there were noticeable differences. As an important tracer of anthropogenic sources, such as metal manufacturing and wear abrasions in transport activities, the Cu concentration was highest in the PK site, while the concentrations of other highly or moderately enriched

elements (Cd, As, Pb, Zn, Cr, and Ni) as well as V were either comparable or slightly higher in the suburban-industrial PK site compared with the urban XW site, but significantly lower in the rural LS area ($p < 0.01$). The intra-regional differences in anthropogenic metal profiles in both the PRD and YRD indicate the spatial heterogeneity of potential sources of emissions and their contributions to local pollution. In contrast to some studies conducted in other countries where the decreased metal concentration faithfully followed the urban–suburban–rural gradient (Hueglin et al., 2005), the highest concentration of many highly and moderately enriched elements as industrial and urban signals was found in the semirural site in the PRD and the suburban site in the YRD in this study. Chan et al. (2006) reported similar trends when targeting other pollutants in the PRD. This finding can be explained by mixed land use and/or the expansion of urbanisation and industrialisation to the outskirts of cities, including suburban and even rural areas in certain regions of China. Furthermore, as mentioned above, the featured elements were different in the PRD and YRD. On the basis of inter-regional comparisons, in the PRD there was a high abundance of Ni, which is an indicator of heavy oil usage (ship emissions in the PRD), and Co in the polluted areas, especially As at the semirural-industrial site (Figure 4-4A), corresponding to their higher enrichment in this region (Figure 4-5). By contrast, there was a significant accumulation of Cr, Pb, Cd, and Cu in terms of absolute concentrations in non-rural sites in the YRD. Such differences are likely to reflect regionally distinctive patterns of pollution determined by disparities in sources of emissions and their underlying structure, affecting the risks of exposure to airborne metals by residents in different regions. In addition, Table 4-2 also provides the previous metal concentrations in the sampling cities collected from the literature. It was observed that the concentrations of most targeted metals generally decreased over the years (from 2013 to 2017) in the selected cities in both regions, particularly for the urban sites. Such

findings are not surprising because of the implementation of the Air Pollution Prevention and Control Action Plan (State Council of the People's Republic of China, 2013) in China since 2013. According to the action plan, the PRD and YRD, two of the critical regions of concern, had undergone a series of pollution source control policies. Major strategies include progressive changes in energy consumption structure (*e.g.*, substituting part of coal with natural gas in electricity generation), optimisation of industrial layout (*e.g.*, relocating polluting industries, like metallurgical and petrochemical plants, out of town), reinforcement of vehicular emission control (*e.g.*, implementing the Fifth Stage National Vehicle Emission Standard), and so on. Although metal is not the target pollutant in the action plan, the air pollution control policies implemented were also conducive to reducing PM_{2.5}-associated metal concentrations.

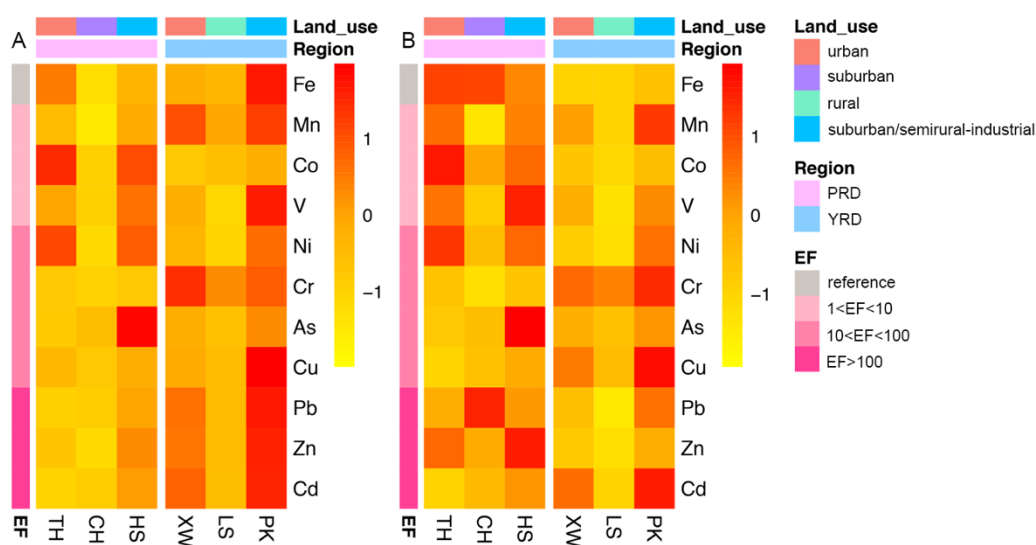


Figure 4-4 Comparisons of the (A) total and (B) bioaccessible metal/metalloid concentrations in PM_{2.5} in the PRD and YRD region based on annual average figures. The concentration value of each element was normalised independently prior to plotting figures in R using the pheatmap package. The original data can be found in Table 4-2 and Table 4-3. Metals presented here were grouped based on the mean value of the EFs in all the sampling sites.

Table 4-2 The average concentrations of trace elements in PM_{2.5} in the PRD and YRD in different studies (ng m⁻³).

Region	Sampling sites	Type	Sampling period	PM _{2.5} (µg m ⁻³)	Fe	As	Cd	Co	Cr	Cu	Mn	Ni	Pb	V	Zn	Reference
PRD	Tianhe	Urban	2013/9–2014/8	81.9	741.54	12.37	2.56	2.51	13.09	43.62	30.69	5.87	78.27	9.66	228.55	(Ming, 2017)
	Tianhe		2016/3–2017/2	55.0	493.95	4.39	0.74	0.53	10.12 ^b	16.37	13.02	5.72	25.52	4.79	127.31	This study
	Yuexiu		2015/1–2015/12	78	443	10	2		13	28	27	3	59		306	(Li et al., 2016b)
	Conghua	Suburban	2012–2013						26.2 ^a	28.6 ^a			77.2 ^a		224.8 ^a	(Lai et al., 2016)
	Conghua		2016/3–2017/2	46.7	296.29	5.34	0.83	0.27	3.68 ^b	10.20	7.34	2.62	26.95	3.20	95.54	This study
	Panyu		2015/1–2015/12	57	285	11	2		3	26	30	3	51		233	(Li et al., 2016b)
	Heshan	Semirural (industrial)	2013/9–2014/8	86.1	674.49				7.91	28.74	117.41	4.59	75.66	6.02	297.41	(Ming, 2017)
	Heshan		2016/3–2017/2	69.0	399.93	13.41	1.44	0.49	9.73 ^b	20.38	15.08	5.42	42.61	5.85	197.92	This study
YRD	Gulou	Urban	2010/4–2010/9			8.88	2.85	6.08	20.93	104.02	71.73	13.40	157.77		362.70	(Hu et al., 2012)
	Gulou		2013/4–2013/5	109.8	872.5	10.61	4.36		26.14	61.8	66.44	14.65	205.2		462.6	(Li et al., 2015b)
	Xuanwu		2013/9–2014/8	97.8	942	6.04	4.71	5.51	13.21	24.7	47.16	9.25	90.87	9.71	247.32	(Ming, 2017)
	Xuanwu		2016/3–2016/7	61.1	411.79	6.44	1.88	0.29	77.46 ^b	20.99	21.79	3.73	54.72	4.44	212.76	This study
	Pukou	Suburban (industrial)	2010/6–2010/9			10.08	3.33	6.65	19.30	85.88	94.63	15.05	212.58		861.25	(Hu et al., 2012)
	Pukou		2012/7–2013/6	125		6.3	2.09		24.76	29.44	58.97	8.1	67.37	3.95	254.8	(Qi et al., 2016)
	Pukou		2016/3–2017/2	68.6	625.44	8.07	2.34	0.35	60.74 ^b	55.76	22.96	5.14	74.54	7.56	283.56	This study
	Xianlin	Suburban	2013/4–2013/5	123.1	1048	10.86	4.94		26.62	68.9	76.3	15.59	215.8		510.2	(Qi et al., 2016)
	Lishui	Rural	2016/4–2017/2	47.9	397.56	5.11	1.03	0.31	42.69 ^b	15.22	15.59	2.79	33.32	2.94	142.92	This study

^a re-calculated based on the data provided in the article

^b conversion based on Cr recovery

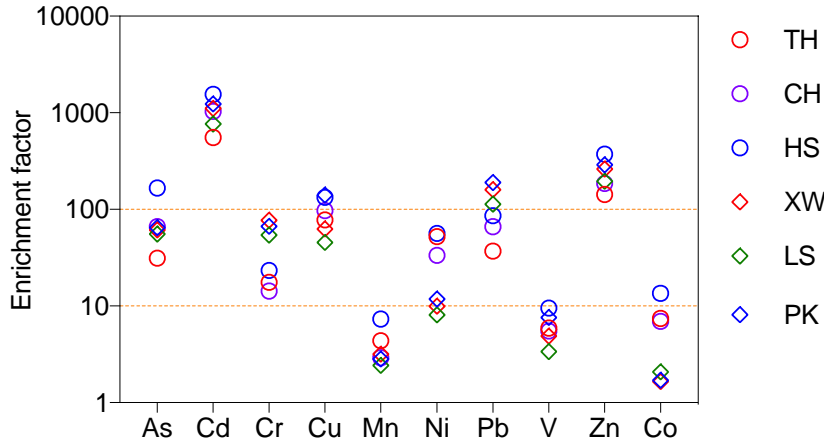


Figure 4-5 EFs of the analysed trace elements (Fe concentration as reference), shown as their annual average.

4.2.2 Bioaccessibility and bioaccessible concentrations of targeted metal(loid)s

Bioaccessibility varied considerably among the targeted elements (Figure 4-6); this property refers to the modulation of the fraction of their bulk concentrations that can be readily available to lung cells in the human body. In general, the targeted elements exhibited spatially consistent bioaccessibility, with the highest for As (>60%), intermediate for Cu, Ni, Cd, and Co (20%–60%), and low for Zn, Fe, Cr, and Pb (<20%). In turn, the spatial trend of the bioaccessible concentrations of these elements followed that of their total concentrations (Figure 4-4B and Figure 4-6, Table 4-3). In contrast, the bioaccessibility of Mn and V differed regionally, which was higher (>60%) in the PRD and lower (20%–60%) in the YRD. The impact from the regional difference in their total concentrations (higher in the YRD than in the PRD) was thus offset. Our results are in agreement with those of previous studies, where As and V had high accessibility and Pb had the lowest accessibility in variably sized airborne particles in Gamble’s solution (Wiseman et al., 2014). It is possible that a large portion of the As, V, and Mn in PM_{2.5} in this study existed as soluble ions, while the other studied metals were probably in

refractory or non-dissolved forms. As mentioned earlier, the bioaccessibility of a metal depends largely on its chemical form only if the properties of the metal are considered. For example, Pb and Zn tending to be enriched in submicron particles are primarily in the form of oxides (Labrada-Delgado et al., 2012) and difficult to leach out. This factor may partially explain the lower bioaccessibility of these two metal elements. Spatially, the bioaccessibility of most of the metals was consistent between sites within the YRD or within the PRD, a result that is in agreement with the intra-regional PM_{2.5} pollution patterns reflected by the consistent chemical profile across regional scales (Figure 4-3).

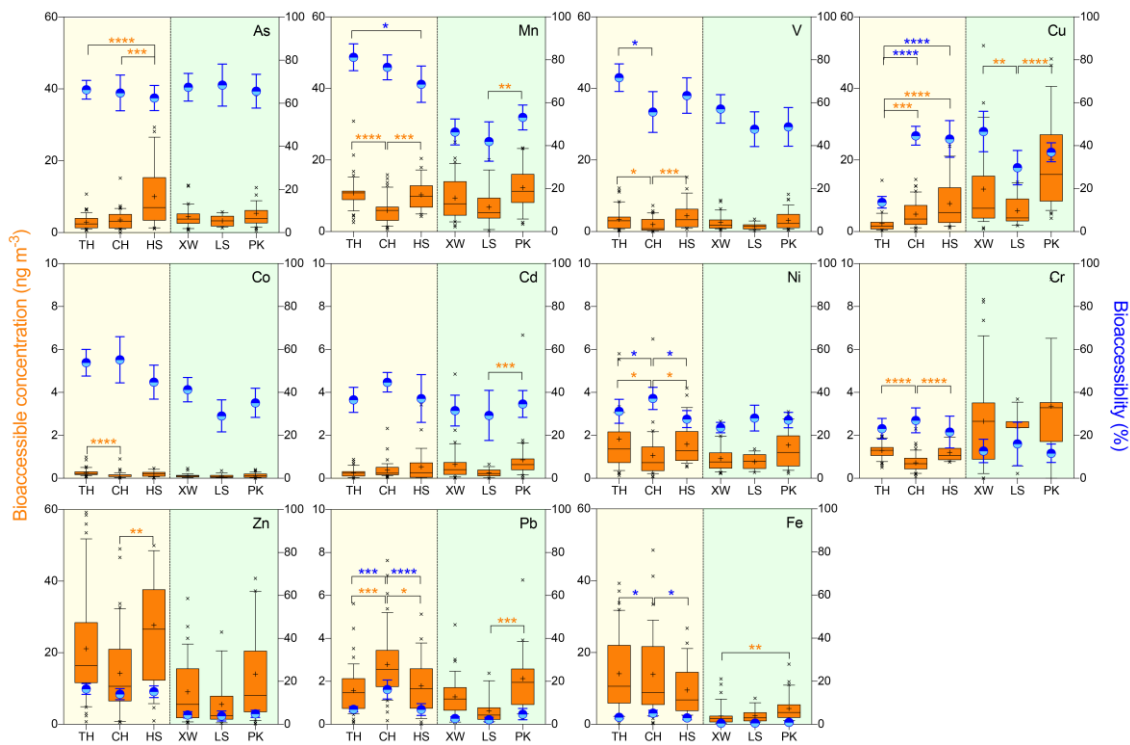


Figure 4-6 Bioaccessible metal concentrations extracted by Gamble’s solution and their corresponding bioaccessibility (%) in PM_{2.5} in the PRD and YRD. The orange box plots represent the bioaccessible concentrations (left Y-axis), while the blue dots indicate the bioaccessibility (right Y-axis). The box plots with whiskers cover data from the 10th to 90th percentile. The error bars for dot plots represent the 95% CI. Non-parametric Kruskal–Wallis tests were conducted in GraphPad Prism 7 (* $p < 0.05$; ** $p < 0.01$; *** $p < 0.001$; **** $p < 0.0001$).

Table 4-3 Annual average bioaccessible concentrations of metal(loid)s in PM_{2.5} in the PRD and YRD.

Region	Sites	Land-use type	Bioaccessible concentration (ng m ⁻³) (mean ± standard deviation)										
			Fe	As	Cd	Cr	Cu	Mn	Ni	Pb	V	Zn	Co
PRD	TH	Urban	14.14 ± 10.70	2.90 ± 1.96	0.25 ± 0.21	1.30 ± 0.39	2.28 ± 2.54	10.81 ± 4.44	1.83 ± 2.48	1.57 ± 1.08	3.41 ± 3.02	21.13 ± 15.35	0.27 ± 0.18
	CH	Suburban	13.92 ± 11.62	3.53 ± 2.81	0.38 ± 0.40	0.72 ± 0.43	4.85 ± 3.77	5.92 ± 3.59	1.06 ± 1.1	2.79 ± 1.62	1.95 ± 1.97	14.23 ± 11.86	0.16 ± 0.14
	HS	Semirural-industrial	9.57 ± 7.07	10.02 ± 8.14	0.53 ± 0.76	1.20 ± 0.41	7.82 ± 7.07	10.27 ± 4.14	1.59 ± 0.99	1.79±1.23	4.45±3.80	27.68 ± 18.33	0.21 ± 0.12
YRD	XW	Urban	2.38 ± 2.94	4.40 ± 2.92	0.65 ± 0.88	2.65 ± 2.25	11.87 ± 12.17	9.40 ± 5.87	0.92 ± 0.63	1.28 ± 0.98	2.61 ± 2.18	9.10 ± 8.94	0.12 ± 0.09
	LS	Rural	2.42 ± 1.89	3.29 ± 1.37	0.25 ± 0.18	2.35 ± 0.89	5.82 ± 4.28	6.83 ± 5.29	0.77 ± 0.35	0.63 ± 0.65	1.45 ± 0.92	5.56 ± 7.11	0.10 ± 0.09
	PK	Suburban-industrial	4.44 ± 3.69	5.38 ± 6.22	0.86 ± 1.10	3.36 ± 3.17	20.18 ± 14.54	12.25 ± 6.93	1.55 ± 1.80	2.13 ± 1.96	3.13 ± 2.63	14.05 ± 15.16	0.13 ± 0.11

4.3 Speciation-adjusted risk assessment of metal(loid)s

The inhalational health risks posed by PM_{2.5}-associated metal(loid)s were calculated in all of the sampling sites based on the annual average bioaccessible concentrations for each targeted element, with a focus on both the CR and NCR for adults. Regarding the effect potency of different metals, the benchmark from the USEPA, coupled with other standards, generally correlated with our previous cell-based toxicity assays, with the exception of Cr and Cu (Figure 4-7A). Of note, the USEPA guidelines for some metals were based on their most toxic form or on a bulk application in which the disregard of metal speciation could result in a bias in the risk assessment. The LCF of the XANES spectra (Figure 4-7B) revealed that the predominant form of arsenic was the less toxic pentavalent arsenic, which on average accounted for 90% of the total arsenic (As(III) + As(V)) content in the PRD and almost 100% in the YRD. This finding is comparable to previous observations made in the PRD (Huang et al., 2014a). After modifying the arsenic-induced CR and NCR based on the above-mentioned speciation information, at all sites the accumulated CR exceeded the safety limit of 10^{-6} , ranging from 2.1×10^{-6} (suburban CH) to 4.6×10^{-6} (semirural-industrial HS) in the PRD, and from 3.2×10^{-6} (rural LS) to 4.8×10^{-6} (suburban-industrial PK) in the YRD. These data imply the comparable level of exposure risk for residents in these two regions. If the current exposure scenarios are sustained, around two to five adults out of every one million in the population of the PRD and YRD (represented by the selected sites) are at risk of developing cancer due to lifetime exposures to airborne metals (Figure 4-8A). Without modifications of the assessment model based on As and Cr speciation, the exposure risk could be highly overestimated, especially for the carcinogenic risk with an approximate 10-fold overestimation (Figure 4-8A). Among the potentially carcinogenic elements under consideration, chromium alone posed a cancer risk exceeding the acceptable level

(10^{-6}) in all the sampling locations (Figure 4-9), accounting for over 76%–80% of the total CR in the YRD and 55% in urban PRD. In contrast, arsenic was responsible for more than half of the total CR (51%–65%) in the other two sites in the PRD. (Figure 4-8B). For NCR that was lower than unity at all sites, manganese took the place of chromium as the predominant contributor, with a risk contribution ranging from 40% at the CH site to 55% at the LS site. The only exception was the HS site, where arsenic became the top contributor to the NCR (39%). In addition, the lower toxic potencies of Fe and Zn, while at high concentrations, resulted in negligible cancer risks compared with other elements (Figure 4-10).

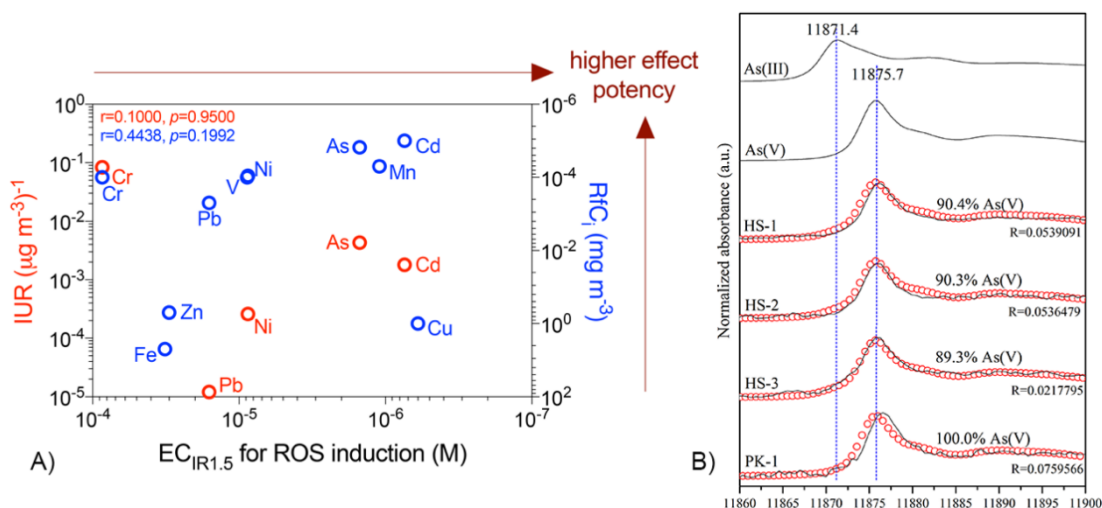


Figure 4-7 Toxicity potency of metals with regard to their speciation. Panel (A) presents the correlation (spearman r and p values are shown) between the effect concentration for reactive oxygen species (ROS) induction ($EC_{IR1.5}$; units: M) of different metals (Jin et al., 2019) and the IUR ($\mu\text{g m}^{-3}$)⁻¹, as well as the inhalation-relevant RfC (mg m^{-3}) of various metals specified in the documents of the USEPA (2018a) and other national standards (Oosthuizen et al., 2015) that are given in Table 3-8. The $EC_{IR1.5}$ data of different metals used here are based on certain kinds of speciation, *i.e.*, Pb(II), V(V), Ni(II), As(V), Mn(II), Cr(III), Cd(II), Fe(III), Cu(II), and Zn(II). Panel (B) presents the dominant speciation of

arsenic in three PM_{2.5} samples with high concentrations of arsenic in the semirural-industrial site (HS) in the PRD and one in the suburban-industrial site (PK) in the YRD, illustrated by XANES spectra (black solid line). The red dotted lines represent the LCF results. The spectra of two standards (As(III) and As(V)) were obtained from a previous study (Cui et al., 2013).

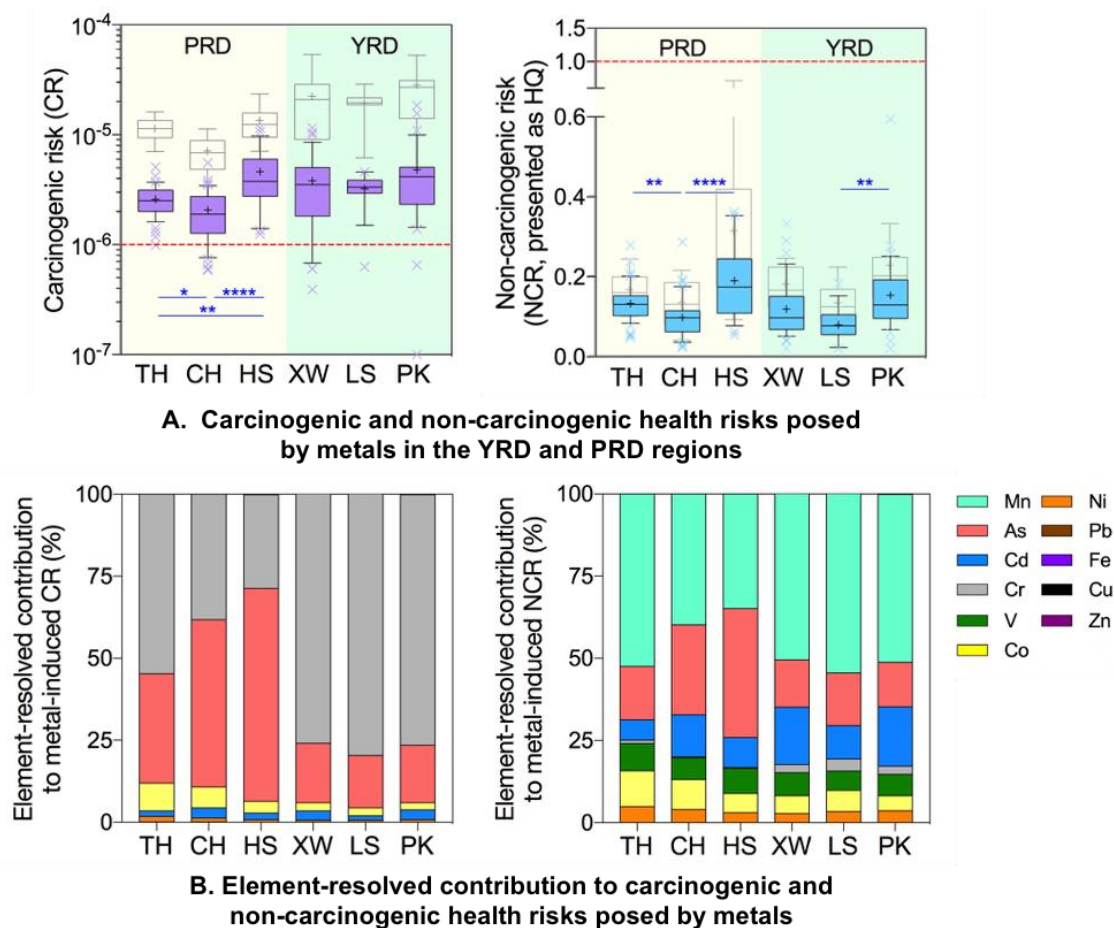


Figure 4-8 The CR and NCR posed by PM_{2.5}-associated metals in the PRD and YRD. Panel (A) presents the CR and NCR posed by metals across geographical locations under different land-use impacts in the two studied regions, based on annual bioaccessible metal concentrations with modifications according to As and Cr speciation. The box plots with whiskers cover data from the 10th to 90th percentiles, with outliers marked by crosses. The red dashed lines stand for the acceptable risk level for a carcinogen (10⁻⁶) and the reference HQ level (1.0) for non-cancer effects recommended by the USEPA. The grey

box plots show the original assessment results without speciation adjustment. Panel (B) indicates the relative contributions of various metals to the total CR and NCR in the six sampling sites.

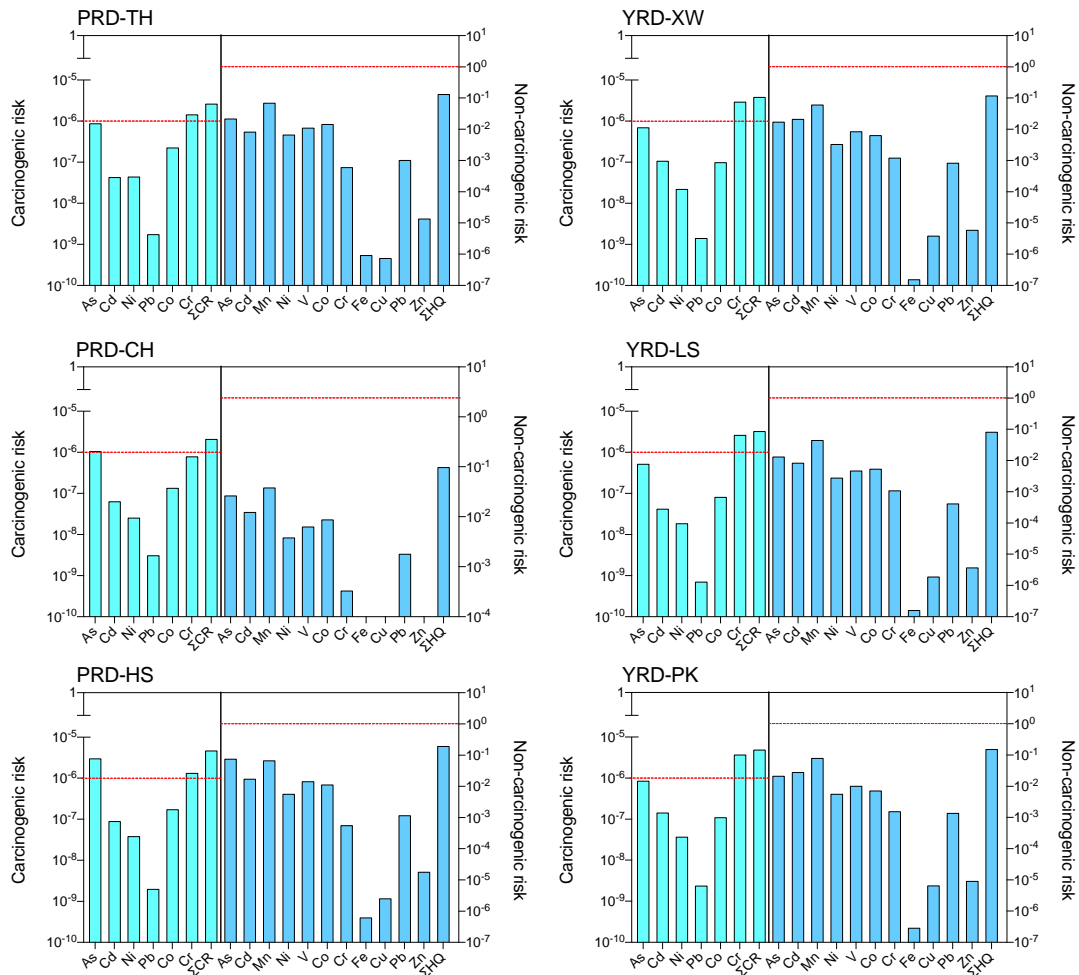


Figure 4-9 CR and NCR (presented as the HQ) values from different metals in $PM_{2.5}$ based on their bioaccessible concentrations. The red dotted lines represent the acceptable risk levels for a carcinogen (10^{-6}) and the reference HQ level (1.0) for non-cancer effects recommended by the USEPA.

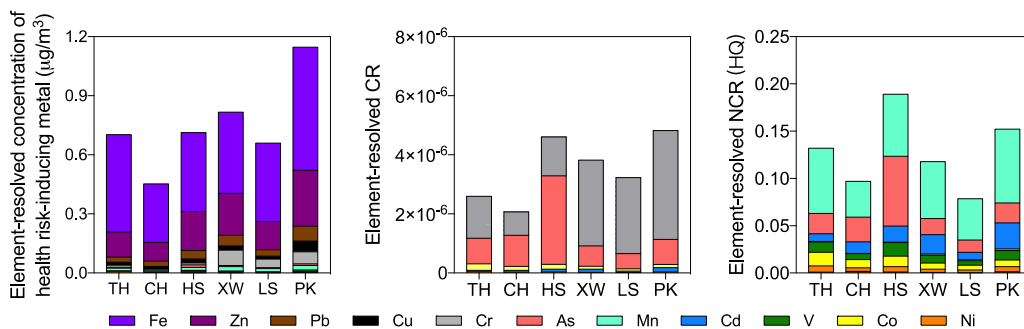


Figure 4-10 Element-resolved metal mass profile and risk (CR and NCR) profile in the PRD and YRD (absolute abundance).

4.4 Contribution of emission sources to metal-induced health risks

To link the emission sources to the consequent health risks, two urban sites (TH in the PRD and XW in the YRD) and the two sites with strong industrial impacts (HS in the PRD and PK in the YRD) were selected in this section for further study. Source apportionment of $\text{PM}_{2.5}$ based on the chemical components, especially for trace metals, was deployed using the PMF model. Afterwards, the health risk posed by each metal calculated in Section 4.3 was individually assigned to different source categories according to the source-resolved metal profiles identified by PMF to obtain the source-resolved risk profiles. Detailed interpretations of the PMF results (*e.g.*, identification of emission sources on the basis of their chemical fingerprints), as well as the regional comparisons and urban–industrial contrast of the major source contributors of metal-derived risks via $\text{PM}_{2.5}$ inhalation, are entirely given as follows.

4.4.1 Identification of emission sources of major chemical components in $\text{PM}_{2.5}$, with a particular focus on trace metals

In the PRD, six source factors were identified in both urban TH and semirural-industrial HS, as shown in Figure 4-11A and Figure 4-11B. The first factor with high amounts of

crustal elements, including Al, Fe, Ca, Mg, Mn, and Co, and the presence of some other trace elements, was identified as fugitive dust from soil, construction, and possibly industry. This factor accounted for 25.0% and 20.3% of the total PM_{2.5} mass concentration in TH and HS, respectively. The second factor could be secondary nitrate formation – given the dominance of nitrate and ammonium – which contributed 18.6% of the particle concentration in TH and 17.8% in HS. The third factor appeared to represent the use of heavy oil by trucks and ships, considering the relatively high abundance of V and Ni and the existence of OC and EC. In view of the relatively high loads of Cu and Zn that are usually from friction braking of vehicles, Cr from decorations, and a certain amount of carbonaceous materials, the fourth factor in TH was distinguished as vehicular emissions. The former two factors in TH and the third factor in HS representing the emissions from traffic and transportation resulted in 26.4% and 14.5% of the PM_{2.5} mass in TH and HS, respectively. The fifth factor in TH and the fourth factor in HS – denoted by high loads of Na⁺, Cl⁻, and a certain amount of other WSI, could be sea salt (12.2% in TH and 9.3% in HS of PM_{2.5} mass concentration). The sixth factor in TH and the fifth factor in HS were dominated by trace metals like As, Cr, Pb, Zn, and Cd, OC/EC, which were attributed to coal combustion and waste incineration, K⁺ as a marker of biomass burning, and a high abundance of SO₄²⁻. This factor was thus identified as a mix of non-traffic combustion (coal, waste, and biomass) and secondary sulphate, which accounted for 17.8% and 22.8% of PM_{2.5} mass in TH and HS, respectively. The last factor in the HS site – with various kinds of heavy metals, but with low abundance of carbon – could be industrial emissions (15.4% of PM_{2.5}), because of the locally rapid developments of hardware and electroplating industries and manufacture of transport equipment and home appliances.

There were also six source factors classified in the urban XW and industrial PK sites in the YRD (Figure 4-11C and Figure 4-11D). Analogous to the analysis in features of source profiles in the PRD, the first to fifth factors in the urban XW site were identified as fugitive dust (17.1% of the PM_{2.5} mass concentration; Al, Ca, and Mg enriched), secondary aerosol formation (31.5%; high abundance of NH₄⁺, SO₄²⁻, and NO₃⁻), fuel oil usage (11.6%; denoted by Ni and V), vehicular emission (7.8%; high load of Cu, coupled with Pb, Zn, and carbonaceous materials), and combustion and incineration activities (22.1%; coal, waste, and biomass burning; denoted by carbonaceous materials, K⁺, Cl⁻, and a series of heavy metals). By contrast, the last factor distinguished as industrial emission (10.0%) was characterised by high Mn, Fe, and Cr loads, which is reasonable due to the existence of certain steel plants in Nanjing in the YRD. In general, the resolved source profile in the industrial PK site is similar to that in the urban XW site, despite the inconsistency in PM_{2.5} contributions from different sources. The contributions to PM_{2.5} of the aforementioned six major sources in PK in sequence were 23.2%, 30.9%, 8.2%, 12.5%, 18.1%, and 7.1%, respectively.

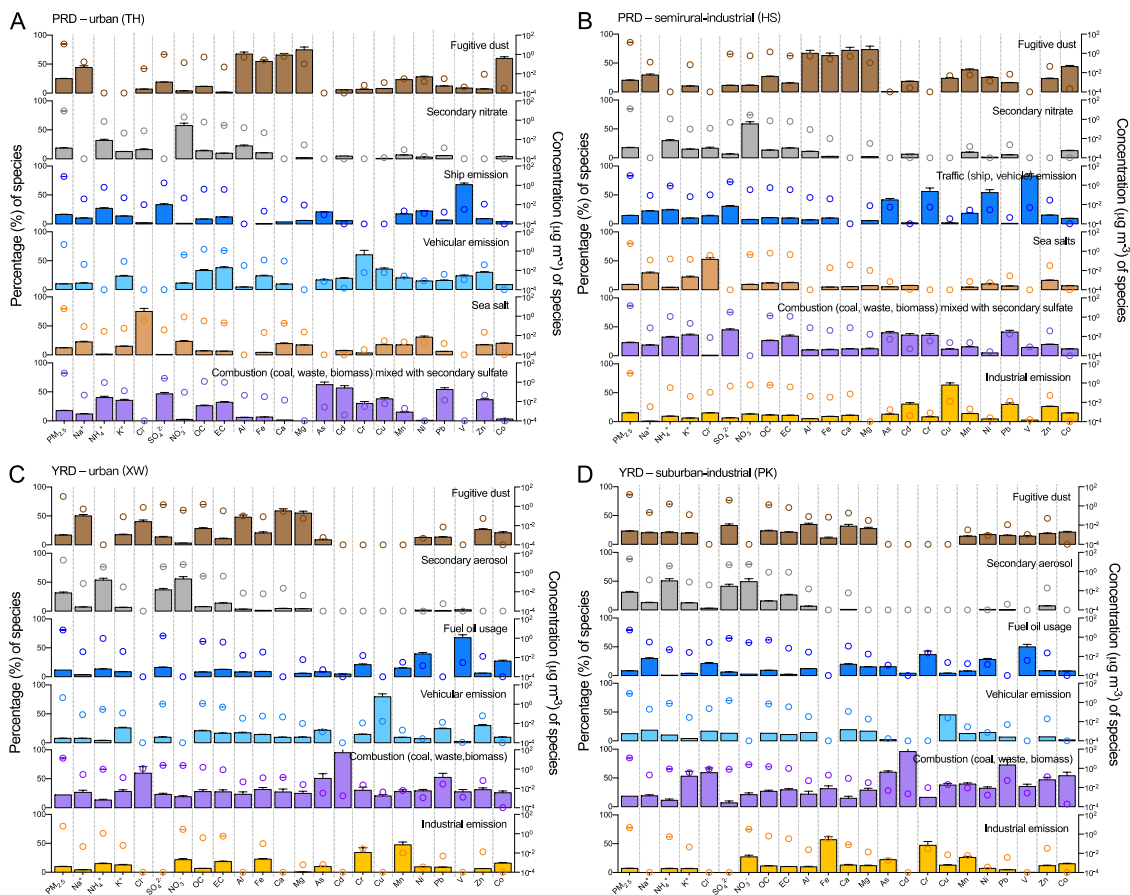


Figure 4-11 Resolved source profiles of major chemical components in $PM_{2.5}$ for: (A) the urban TH site in the PRD, (B) the semirural-industrial HS site in the PRD, (C) the urban XW site in the YRD, and (D) the suburban-industrial PK site in the YRD. The coloured bar represents the percentage of certain species contributed by different sources (left Y-axis), while the circle indicates the corresponding concentration of species that originated from these sources (right Y-axis). Error bars represent the 95% CI estimated by the bootstrap method in PMF.

4.4.2 Source-resolved metal-induced risk profiles based on PMF results

First, for better spatial comparisons, sources identified in Section 4.4.1 with analogous attributes were combined and finally condensed into a total of five sources: fugitive dust and sea salts, industrial emissions, traffic emissions (vehicular emissions and fuel oil combustion by trucks and ships), non-traffic combustion (coal combustion, biomass

burning, and waste incineration), and the formation of secondary aerosol (secondary sulphate, nitrate, and OC). The three typical anthropogenic sources, namely traffic emissions, non-traffic combustion, and industrial emissions, contributed a similar share (~50%) of the PM_{2.5} mass concentration in both the YRD and PRD. However, the contribution of these sources to the mass concentration of risk-inducing metals differed between the two regions (<50% for the YRD and >75% for the PRD) (Figure 4-12B and Figure 4-13). The non-traffic combustion identified in the TH and HS sites was partially mixed with secondary sulphate, thus leading to an overestimated contribution to PM_{2.5} mass from non-traffic combustion and an underestimation from secondary aerosols to some extent in these two sites. Nevertheless, there was a negligible influence on the source-resolved profile of trace metal mass and metal-induced risks, because the metal contribution from secondary sulphate could be relatively low. For both the CR and NCR, the source-resolved contribution was regionally distinct between the YRD and PRD, and relatively consistent between sites of different land use within each region (Figure 4-12A and Figure 4-13), reiterating the regional patterns of pollution. In the PRD, the first three largest source contributors to the CR were traffic emissions (44%–47%), non-traffic combustion (37%–39%), and industrial emissions (0%–12%). By contrast, there was an elevated contribution from industrial activities to the CR in the YRD (28% in XW and 40% in PK); this factor ranked first among the source contributors in suburban-industrial PK and contributed comparably with traffic emissions (35%) and non-traffic combustion (34%) in urban areas. With regard to the NCR, the risk-based source profile appeared to be similar to the mass-based source profile of risk-posing metals (Figure 4-12). Traffic emissions (39% in TH and 31% in HS) and non-traffic combustion (22% in TH and 26% in HS) remained the predominant contributors to the NCR of metals at most of the sites in the PRD, the only exception being urban TH, where fugitive dust and sea salts (35%)

outranked non-traffic combustion. In the YRD, the major source contributor to the NCR was non-traffic combustion activities (43% in XW and 52% in PK), followed by comparable contributions from traffic and industrial emissions. The regional differences in source-resolved metal mass/risk profile reflected the different industrial and energy structures. For example, coal consumption was greater in the YRD than in the PRD (National Bureau of Statistics of China, 2014), resulting in a greater share of non-traffic combustion activities in the mass concentration and the NCR of metals in the YRD. Previous studies had demonstrated that industrial coal combustion accounted for the considerable metal-induced health risks in another industrial city (Foshan) of the PRD (Zhou et al., 2018c) and identified coal combustion and traffic emission as the most dominant sources of health risks posed by metals during wintertime PM_{2.5} episodes in Beijing (Huang et al., 2018). More importantly, these studies highlight the significant discrepancies between mass concentration-oriented and health risk-oriented source apportionment of PM_{2.5}-associated metals. Such discrepancies were also observed for other toxic components, such as polycyclic aromatic hydrocarbons (PAHs) in urban Nanjing (Zhuo et al., 2017), with the disproportionate contribution to mass profile and risk profile by each source category. These findings prompted us to rethink the current framework of mass concentration-oriented source apportionment and emission reduction for PM_{2.5} pollution. Given that dominant mass fractions (*e.g.*, NO₃⁻ and SO₄²⁻) are not necessarily toxicologically relevant, there is an imminent need for identification of key toxic components and associated sources to support health risk-oriented source apportionment and mitigation strategies (Li et al., 2019b).

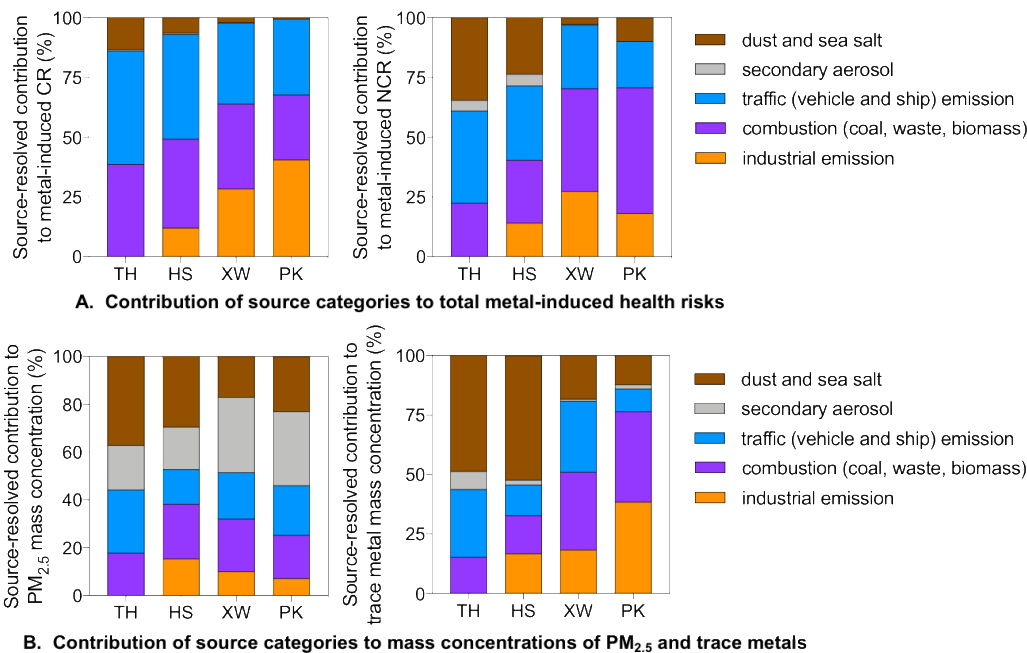


Figure 4-12 Contribution of different emission sources to the mass and risk profile of PM_{2.5}-associated metals in the PRD and YRD. Panel (A) highlights the urban–industrial contrast in source-specific health risks posed by trace metals in the PRD and YRD. Panel (B) supplements the source-resolved mass profiles of PM_{2.5} and risk-inducing trace metals (Mn, As, Cd, Cr, V, Co, Ni, Pb, Fe, Cu, and Zn).

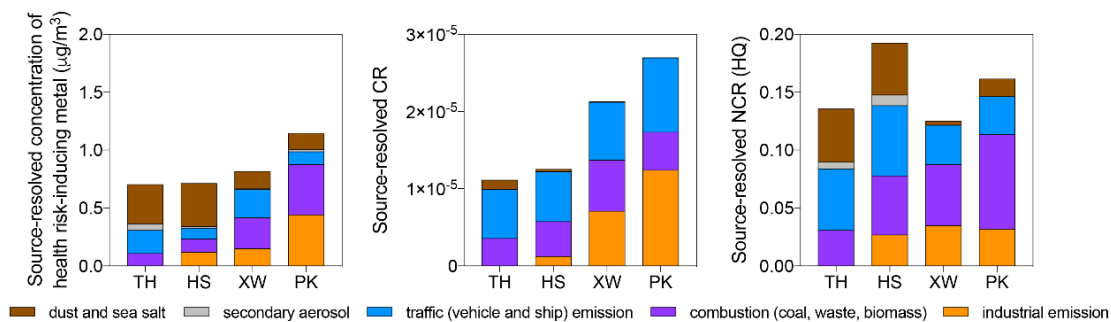


Figure 4-13 Source-resolved metal mass profile and risk (CR and NCR) profile in the PRD and YRD (absolute abundance).

4.5 Summary

This chapter presented the results from investigating the PM_{2.5} pollution between the PRD (south China) and YRD (east China), represented by selected typical cities in each region, from a chemical perspective. An overall comparative picture of regional patterns of PM_{2.5} chemical compositions – particularly for the associated metals, as well as their variations affected by land-use types in the selected cities in these two studied regions – was provided. By incorporating bioaccessibility and speciation information of metal elements into health risk assessments, this study tried to assign the metal-induced risks, which were based on the bioaccessible metal concentrations, to various emission sources according to the source apportionment result resolved by the PMF model. The major findings of the current chapter are listed as follows.

1. Both the PRD and YRD were subject to PM_{2.5} pollution ($>25 \mu\text{g m}^{-3}$ standardised by the WHO) during almost the entire sampling period, with a clear seasonal characteristic that most of the highly polluted days fell in spring and winter. Within each region, there was an increasing trend in PM_{2.5} concentration from suburban (PRD)/rural (YRD) to urban and industrial areas.
2. There were different regional patterns of PM_{2.5} chemical composition profiles in the two studied regions, in contrast to the less pronounced intra-regional variations. Briefly, there was a higher proportion of WSI relevant to secondary inorganic aerosols (NO_3^- , SO_4^{2-} , and NH_4^+) and a lower proportion of carbonaceous materials (OC and EC), presumably from combustion activities to the total identified components, in the YRD compared with the PRD.

3. The particulate trace metal profiles reflected the land-use impacts within each region, with the highest concentrations of anthropogenically enriched metals (*e.g.*, Zn, Pb, As, and Cd in the PRD and Cu in the YRD) at the industrial sites, a comparable or slightly lower concentration in urban sites, and a decreased concentration in the rural areas. Such intra-regional differences in anthropogenic metal profiles indicate the spatial heterogeneity of potential sources of emissions and their contributions to local pollution.

4. Except that Mn and V presented a higher bioaccessibility (>60%) in the PRD and lower bioaccessibility (20%–60%) in the YRD region, the bioaccessibility of most of the other targeted elements generally exhibited a spatial consistency, with the highest for As (>60%); intermediate for Cu, Ni, Cd, and Co (20%–60%); and low for Zn, Fe, Cr, and Pb (<20%) in both regions. In other words, the spatial trend of the bioaccessible concentrations of these elements followed that of their total concentrations. In addition, As(V) was the predominant arsenic species in both regions according to XANES analysis.

5. The metal-induced CR was generally comparable between the YRD and PRD. By applying model modification, the overestimation from the traditional model could be better controlled. In general, chromium was the dominant contributor to the total excessive cancer risks posed by metals except for the non-urban sites in the PRD affected more by arsenic, whereas manganese accounted for a large proportion of the NCR in the selected cities in both regions (within safety value). There was an elevated contribution from industrial emissions in the YRD sites, while traffic emissions and non-traffic combustion (coal/waste/biomass burning) were the common dominant sources of the CR and NCR posed by metals in both regions. It indicated the primary sources to be

controlled for the mitigation of metal-induced risks in the two regions. Meanwhile, the metal risk-based source profile shifted from the metal mass-based source profile.

In summary, this chapter presented the regional differentiation of PM_{2.5} pollution in the PRD and YRD based on the observations in selected cities in these two regions, from the characterisation of chemical compositions, to the identification of their potential emission sources, and then the determination of source-resolved contributions to metal-induced health risks via PM_{2.5} inhalation. The incorporation of metal speciation information in this chapter further highlighted the importance of model modification based on speciation distribution in risk assessment studies to control bias better. However, the ratio of Cr(III) to Cr(VI) used in this study was based on the assumption from the USEPA; it prompts us to look for robust methods for metal speciation identification in air samples to further reduce errors. Nevertheless, the current quantitative connection between the major source categories and the resultant health risks of the key metal content in PM_{2.5} still somehow provides practical implications for the precise mitigation of targeted sources and metal components to alleviate the consequent health risks adaptive to site-specific scenarios. The differentiation in source contribution profiles between metal mass concentration and metal-induced risk further urges us to think about the situation extrapolated to the whole PM_{2.5}. The risk-based source profile of the whole PM_{2.5} is very likely to significantly shift from its mass concentration-based source profile. This inference indicates the need for a paradigm shift on PM_{2.5} pollution mitigation from mass concentration-based source control (*e.g.*, sources of SO₄²⁻, NO₃⁻, and NH₄⁺) to risk-oriented source control. However, only the chemical proportion of PM_{2.5} was discussed in this chapter. For an integrated risk assessment, it is still required to investigate the biological counterpart, which may also pose considerable health impacts but lacks extensive exploration. Therefore,

biological analysis of PM_{2.5} samples from the same sampling sites in the PRD and YRD, including the bacterial community and the associated genetic pollutants like ARGs, will be conducted in the next chapter (Chapter 5) to provide a relatively comprehensive portrait of PM_{2.5} pollution in these two regions with an integrated characterisation from both chemical and biological perspectives. Meanwhile, a temperate site will be added as a supplement to explore the climate impact on the geographical distributions of biological components in PM_{2.5}. Further in Chapter 6, there will be a focus on the contribution of potential sources to the PM_{2.5}-associated bacteria and ARGs.

Chapter 5 Biological Components of PM_{2.5}, from Associated Airborne Bacteria to ARGs in the YRD and PRD

Following up on the chemical investigations in Chapter 4, the same batch of PM_{2.5} samples (March 2016–February 2017) and an additional batch extending to the next quarter (March–May 2017) in the YRD and PRD were subject to biological analysis in this chapter, including bacteria and ARGs, some of which can be potential environmental and biological hazards. In brief, to shed light on the geographical fingerprints of airborne bacteria and antibiotic resistance relevant to fine particulates, spatial and seasonal variations in the total loads of PM_{2.5}-associated bacteria – and certain kinds of the common ARG subtypes (*e.g.*, *ermB*, *tetW*, *qnrS*, *lnuA*, *bla*_{TEM-1}, and *sulI*) and MGEs (*e.g.*, *intI1*, *tnpA-02*, and *tnpA-04*) – were explored based on qPCR, as well as the bacterial community structure using 16S rRNA amplicon sequencing approach. Meanwhile, an urban site (Beijing) in the temperate zone in China was used as a comparison for discussion of climate impacts. Furthermore, the daily intake of ARGs and bacteria via inhalation was compared to other exposure pathways (*e.g.*, drinking water and food ingestion) in different locations, thus addressing site-specific exposure risks.

5.1 Regional differences in PM_{2.5}-associated bacterial loads and community structure

5.1.1 Intra-regional urban–rural contrast of PM_{2.5}-associated bacterial loads

Intra-regional comparisons of total bacterial loads associated with PM_{2.5} were conducted across land-use transects in the YRD and PRD (Figure 5-1). In the YRD, seasonal variations in the absolute concentrations of the 16S rRNA gene (a well-verified indicator of bacteria) were most pronounced at the rural LS site, with an evident decrease in the

winter season and a rapid recovery in the following spring. This pattern contrasts with the less distinct seasonal fluctuations in the urban XW and industrial PK sites. Similarly to the situation in the YRD, the most significant variations in airborne bacterial loads were in the semirural HS site of the PRD, but the differences decreased from semirural to suburban and urban sites. With intense anthropogenic activities in urban areas, contributions of natural sources (*e.g.*, vegetation) to the airborne microbes were likely replaced by those from anthropogenic sources (*e.g.*, WWTPs, composting facilities, and livestock farms) that are more stable across seasons, thus flattening the seasonal rhythms of bacterial loads observed in (sub)urban and industrial areas. The intra-regional patterns of airborne bacterial loads seemed not to correspond to the spatial variations in chemical pollutions across sites under different land-use impacts illustrated in Chapter 4. PM_{2.5} concentrations may not be a critical factor regulating the spatiotemporal dynamics of the airborne bacteria therein, as the abundance of the 16S rRNA gene did not correlate with the concentration of PM_{2.5} across the studied regions (Figure 5-2A). Given that a bacterial genome has on average 4.2 copies of the 16S rRNA genes (Větrovský et al., 2013) and a bacterial cell is around 10⁻¹² g in weight (Elert, 2009), the bacterial content accounted for less than 0.05% of the PM_{2.5} concentrations (Figure 5-2B). It might be worth mentioning that some single-copy marker genes in bacteria (*e.g.*, *rpoB*) are promising to be used in the future for a better estimation of bacterial cell concentrations in case the accuracy is verified (Ogier et al., 2019). Returning to the previous point, the differentiation of the regional pattern between the chemical and biological constituents in PM_{2.5} implies that these two kinds of compositions might originate from distinct emission sources. Therefore, it was not surprising that although the HS site in the PRD suffered from certain industrial influence, as noticed in Chapter 4, the bacterial changes seemed to be affected more by the semirural characteristics, such as a high level of vegetation coverage. Hence,

in the following discussions of the biologically relevant contents, HS is mentioned as a semirural site.

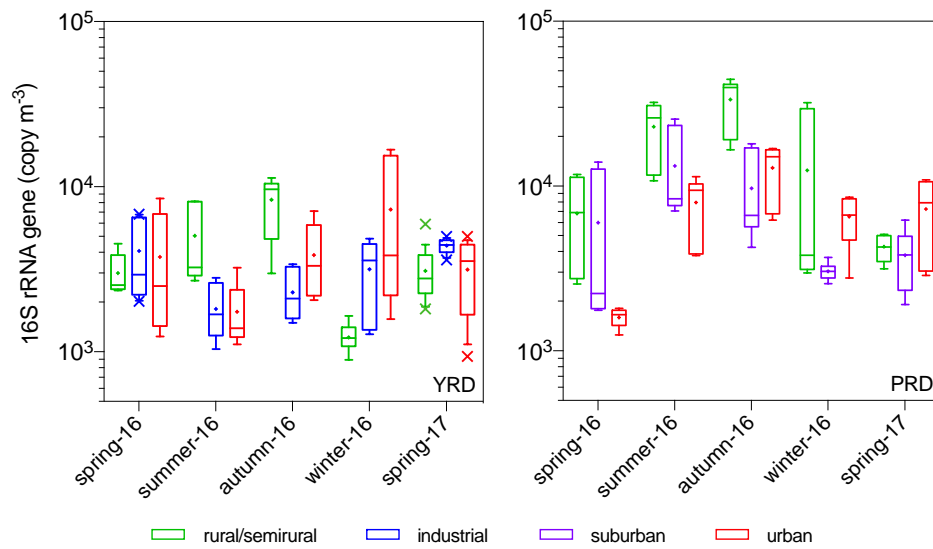


Figure 5-1 Intra-regional rural–urban contrasts of PM_{2.5}-associated 16S rRNA gene abundance (an indicator of bacteria) in the YRD and PRD.

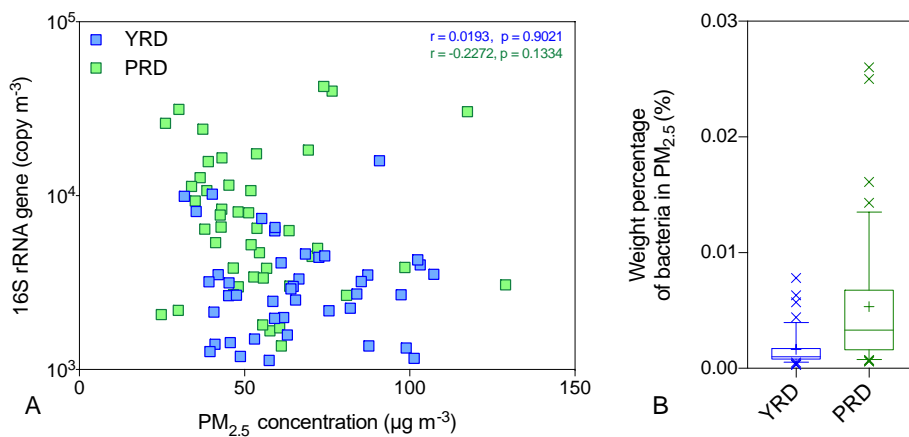


Figure 5-2 (A) Relationship between the abundance of the 16S rRNA gene and the concentration of PM_{2.5} and (B) the bacterial weight proportion of PM_{2.5}.

5.1.2 Inter-regional comparisons of PM_{2.5}-associated bacteria in urban areas

When focusing on the urban sites, the absolute abundance of the 16S rRNA gene seemed to be relatively consistent over the sampling period, with narrow fluctuations constrained to one order of magnitude (10^3 to 10^4 copy m^{-3}) in both the YRD and PRD. By contrast, the seasonality of the total bacterial load was more apparent in an urban Beijing site located in the North Temperate Zone, where the absolute concentration of the 16S rRNA gene declined from spring to winter by nearly three orders of magnitude and recovered in the following spring (Figure 5-3). Zhen et al. (2017) reported a similar seasonal trend of the bacterial concentrations in TSP in urban Beijing, and other authors have noted a larger span of airborne bacterial loads in different sampling time under a broader geographical comparison within the North Temperate Zone (Gao et al., 2017; Wei et al., 2019; Xu et al., 2019) (Figure 5-4). It was thus speculated that the relative consistency of airborne bacterial loads over seasons in the urban YRD and PRD in contrast to the dramatic changes in urban Beijing – which also corresponded to fewer seasonal variations of the bacterial community structure (at the phylum level) in the PRD and YRD (Figure 5-5) – could be partly due to the climate impact regarding their geographical locations. More specifically, local sources such as soil and vegetation might be more critical influential factors that drove the abundance of ambient airborne bacteria (Bowers et al., 2013; Bowers et al., 2011b). For example, the phylum Cyanobacteria, which is partially derived from plants and soil/dust, dropped from 24% of total bacteria in the spring (8.5×10^4 copies m^{-3}) to less than 1% in the winter (3 copies m^{-3}) and recovered to 47% in the next spring (6.3×10^4 copies m^{-3}) in urban Beijing (Figure 5-5). Du et al. (2018) reported similar trends in Beijing: the relative abundance of Cyanobacteria/Chloroplast dropped from the spring (32%) to the winter (2%) in the identified PM_{2.5}-associated bacteria. By contrast, the relative abundance of the phylum Cyanobacteria varied less among seasons

in the subtropical YRD and PRD (Figure 5-5). In addition, contributions from terrestrial origins (here referring to soil and dust) predicted by SourceTracker2 exhibited a corresponding seasonal change in the Beijing site, with a high input from soil/dust in the spring – when dust storms frequently occurred – but significantly decreasing input in the winter when the surface soil was likely to be covered by snow. On the contrary, the contribution from this source in the YRD and PRD was relatively consistent across seasons (Figure 5-6). All the above-mentioned observations provide evidence of the seasonal dependence of vegetative and other terrestrial contributions to airborne bacteria, typically in the temperate regions due to the distinct climate features, whose impact is likely to conceal the effect arisen from human activities in urban areas.

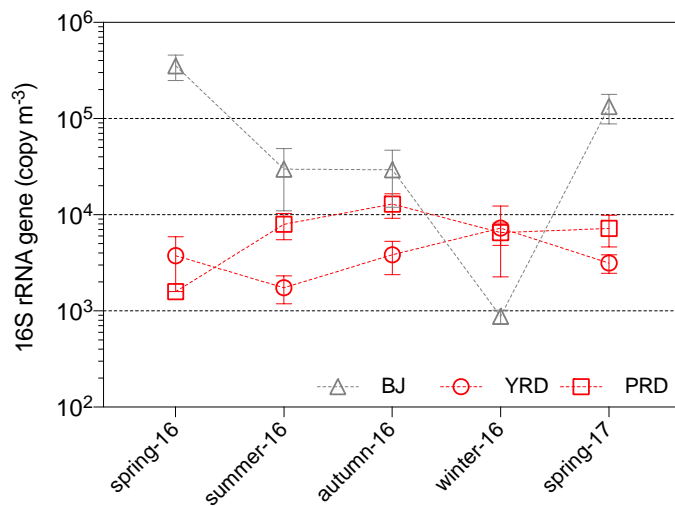


Figure 5-3 Inter-regional comparisons of PM_{2.5}-associated 16S rRNA gene abundance in urban areas in the YRD and PRD, with an urban site in the temperate zone (Beijing) as a comparison.

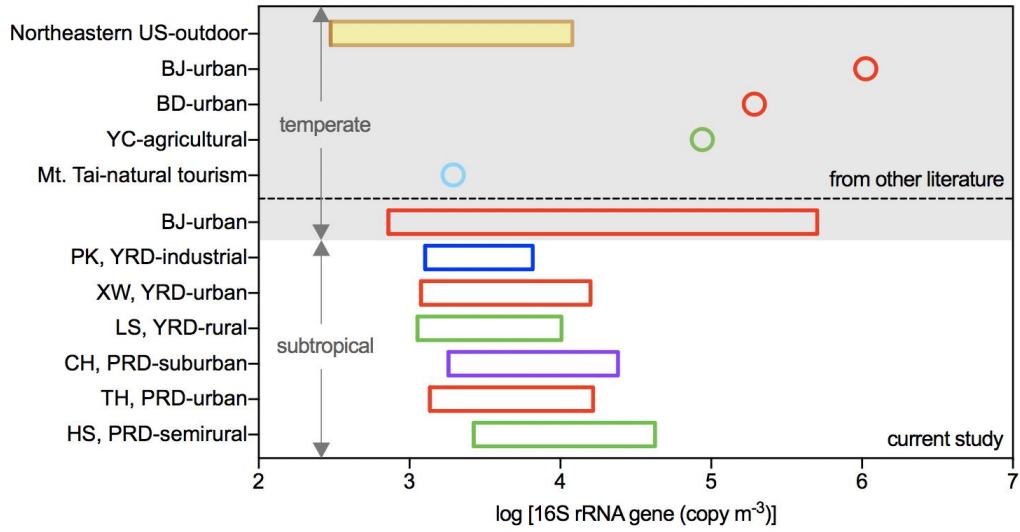


Figure 5-4 Comparisons of the 16S rRNA gene abundance in PM_{2.5} of different regions in different climate zones. Data for comparisons were sought from the literature (Gao et al., 2017; Hospodsky et al., 2012; Wei et al., 2019; Xu et al., 2019). BD: Baoding, Hebei; YC: Yucheng, Shandong; Mt. Tai: Mountain Tai, Shandong.

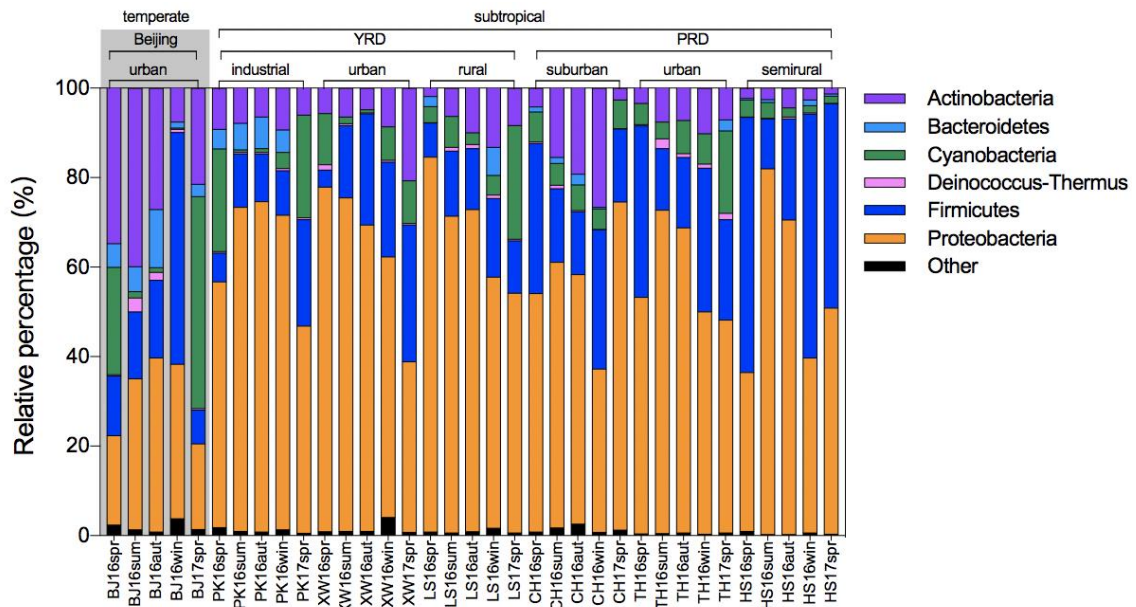


Figure 5-5 Spatiotemporal patterns of PM_{2.5}-associated bacterial communities at the phylum level in the YRD and PRD in the subtropical zone, compared with bacterial communities in Beijing (the temperate zone).

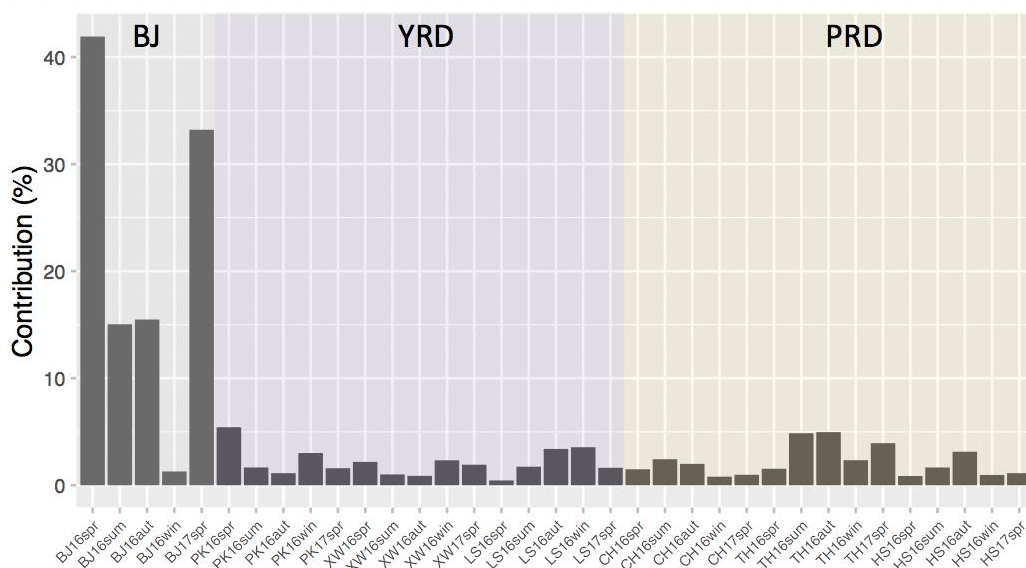


Figure 5-6 Seasonal variations in the contribution from terrestrial sources (soil/dust) in different sampling sites predicted by SourceTracker2.

5.1.3 Relationship between chemical components and bacterial community structures in PM_{2.5}

Previous studies indicate that chemical pollutants in the atmosphere could also pose effects on airborne bacterial loads and community structures, although the influence of this factor might not be as significant as that of emission sources and climate/meteorological conditions. To explore the possible linkage between the chemical and biological compositions of PM_{2.5}, RDA was conducted in the YRD and PRD (Figure 5-7). Based on the analysis, OC in the YRD and Cl⁻ and NO₃⁻ in the PRD could be the relatively important factors among the carbonaceous and ion components to influence the airborne bacterial communities in these two regions. Such components were found as nutrients to promote bacterial growth in the atmosphere (Zhang et al., 2019c). Apart from the effect of possible nutrients, the changes in airborne bacterial communities in both regions could also be relevant to crustal elements. For example, a high proportion of the

most abundant bacterial genera seemed to be correlated to crustal elements, including Al, Fe, and Ca; this finding indicates that these genera might originate from the same source of crustal elements, such as soil and dust. This result reiterates the source contribution from soil/dust predicted by SourceTracker2. However, only around 19% of the variance in bacterial community structures in the YRD and 27% in the PRD can be explained by the analysed chemical components, as revealed by the adjusted R^2 in the RDA results. There is still a large proportion of variance that fails to be well explained by the current known factors. Furthermore, there is no denying that the biological effects (*e.g.*, bacterial interactions), which was not considered in RDA, could also influence the model results.

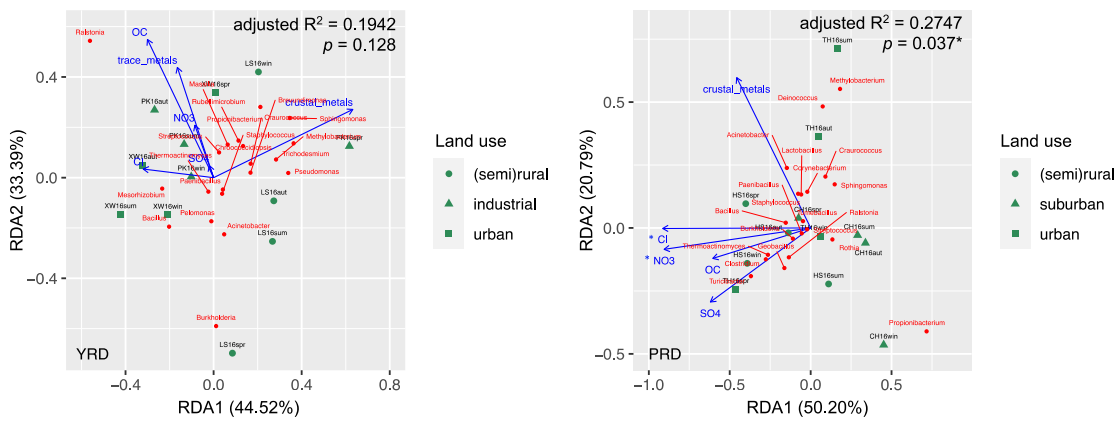


Figure 5-7 RDA reveals the relationship between the bacterial community and chemical compositions in $PM_{2.5}$ (999 permutations, $*p < 0.05$). Here only the top 20 bacterial genera were used for analysis. The “adjusted R^2 ” on the figures represents the proportion of variance explained by the explanatory variables (chemical components) in the total variance of response variables (bacterial taxa). The percentage marked in the axis means the proportion of variance explained by the certain RDA component in the total explained variance.

5.2 Regional fingerprints of ARG profiles with relevance to potential hosts

5.2.1 Regional comparisons of the concentration and composition of PM_{2.5}-associated ARGs

The annual average concentrations of the total analysed PM_{2.5}-associated ARGs were generally highest in the (semi)rural areas and gradually decreased in the other two sites under different land-use impacts in the selected cities within each region. This trend was incredibly pronounced in the PRD across the semirural–urban–suburban transect (Figure 5-8A). However, similar levels of PM_{2.5}-borne ARG content were found among the urban sites in the PRD, the YRD and Beijing, indicating that the annual levels of airborne ARGs were relatively consistent across different regions in human-impacted areas.

Echoing the disparities in airborne bacterial communities at the genus level (Figure 5-9A), the corresponding ARG profiles exhibited different regional patterns among the PRD, the YRD, and the urban Beijing site (Figure 5-10). Unlike *lnuA* dominating in the detected PM_{2.5}-associated ARGs in Beijing, *lnuA* and *sulI* collectively played a leading role in the PRD. By contrast, *ermB* had the dominant position in the YRD, except in the urban area, where *bla*_{TEM-1} was as dominant as *ermB*. Regional differentiation in airborne ARG profiles related to airborne fine particulate matter was also demonstrated by the NMDS and PERMANOVA test based on the Bray–Curtis dissimilarity (Figure 5-9B, Table 5-1) with tests of dispersion effects by PERMDISP (Table 5-2). It was found that the ARG profiles, as well as the bacterial community structures, were significantly different among regions with no obvious dispersion effects. Recently, the terrestrial resistome in natural environments has been found to differ between temperate and subtropical regions and to be regulated by plants and soil bacterial communities (Hu et al., 2018a). As an important source of atmospheric bacteria and ARGs, soil with different resistomes among the

regions might play a prominent role in the formation of regionally different airborne ARG profiles. However, the differentiation of the detected ARG profiles between the PRD and YRD sampling sites within the subtropical zone likely hints at a significant influence from other more anthropogenically relevant emission sources with regional characteristics independent from climate impact to some extent. In contrast to the regional disparities, the annual average ARG profile within a region, based on limited detected subtypes, was generally less diverse; this finding suggests that the regional impacts could overwrite local influences.

The seasonality of the relative abundance of the detected airborne ARGs is presented in Figure 5-11. In short, the relative abundance of ARGs normalised to the 16S rRNA gene indicates the proportion of ARB in the total bacterial community, if it is given that one ARB only carries one ARG. Overall, except for the rural LS in the YRD – where the relative abundance of ARGs evolved from spring to winter along a seasonal cycle – the seasonal contrast of most of the predominant airborne ARGs was not distinct (variations within one half to one order of magnitude) in all the remaining sampling sites. In turn, variations in concentrations of most ARGs were likely to follow the general changes in total bacterial loads. These findings suggest either that the dominant emission sources of airborne bacteria were also the major contributors of airborne ARB or that both the major emission sources of total airborne bacteria and ARB were subject to similar regulations by certain factors. However, to determine the specific reasons, further studies are warranted regarding the potential sources of airborne bacteria and ARGs as well as the regulatory processes they undergo in the atmosphere after escapes from emission sources.

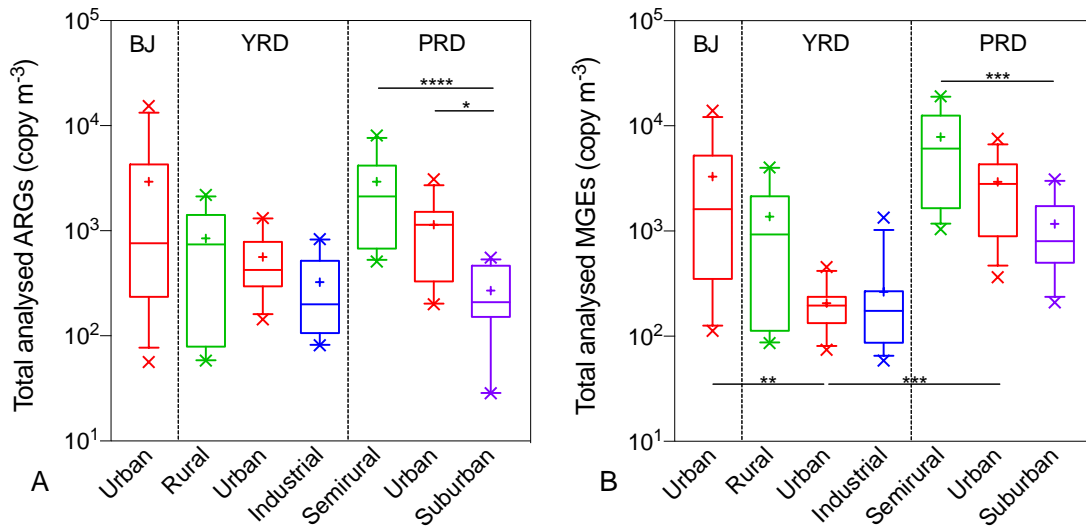


Figure 5-8 Annual average (the first four seasons included) concentrations of (A) ARGs and (B) MGEs in the YRD and PRD (subtropical) compared with urban Beijing (temperate) (* $p < 0.05$; **** $p < 0.0001$).

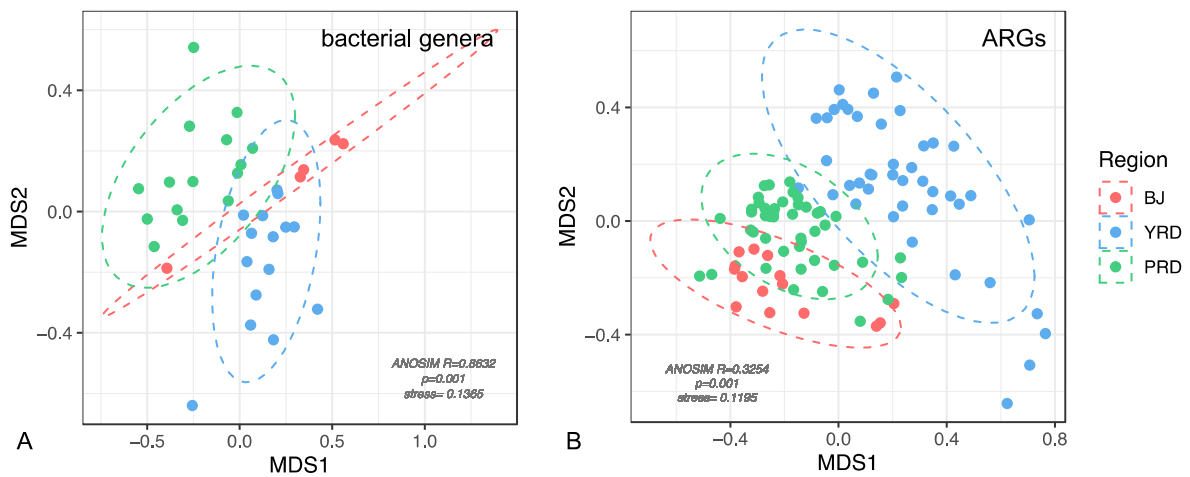


Figure 5-9 NMDS analysis (Bray-Curtis dissimilarity) based on (A) bacterial communities at the genus level and (B) ARGs profiles, respectively; the ellipse represents the 95% confidence level.

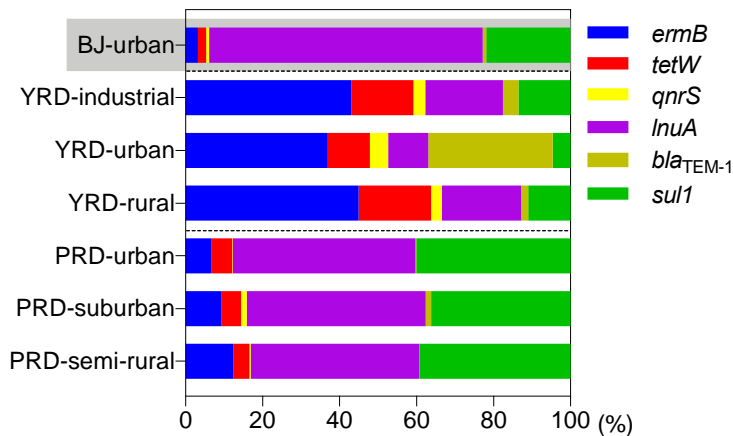


Figure 5-10 Regional signatures of airborne ARG profiles. The relative percentage of each gene is an annual average of all of the samples.

Table 5-1 PERMANOVA (Bray–Curtis dissimilarity) test results of the regional differentiation in bacterial and ARG profiles (* $Pr < 0.05$; ** $Pr < 0.01$; *** $Pr < 0.001$).

Bacteria			ARGs		
Group	R ²	Pr(>F)	Group	R ²	Pr(>F)
PRD/YRD	0.0598	0.098	PRD/YRD	0.1735	0.001***
PRD/BJ	0.1369	0.022*	PRD/BJ	0.1775	0.001***
YRD/BJ	0.1080	0.040*	YRD/BJ	0.0483	0.030*
All	0.4280	0.001***	All	0.1945	0.001***

Table 5-2 PERMDISP test (“betadisper” and “PERMUTEST” function in the “vegan” package) on the dispersion effects in NMDS analysis of regional differentiation in bacterial and ARG profiles. For the pairwise comparisons, observed and permuted p -value are presented below and above diagonal, respectively.

Bacteria				ARGs			
	F	Permutation	Pr(>F)		F	Permutation	Pr(>F)
All	2.3496	999	0.094	All	0.877	999	0.4130
Pairwise comparisons				Pairwise comparisons			
Group	BJ	PRD	YRD	Group	BJ	PRD	YRD
BJ		0.8790	0.1270	BJ		0.2590	0.3460
PRD	0.8707		0.0390	PRD	0.2471		0.4960
YRD	0.1338	0.0408		YRD	0.3469	0.5034	

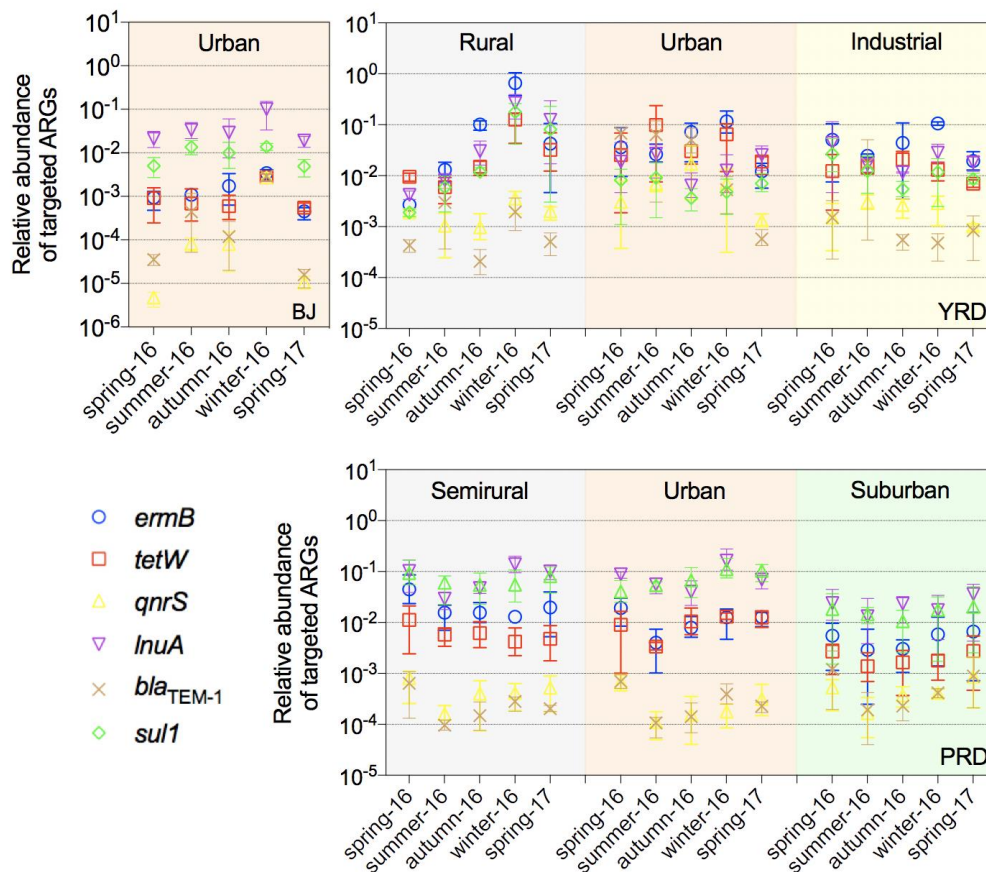


Figure 5-11 Seasonal variability of relative abundance of airborne ARGs normalised to the 16S rRNA gene.

5.2.2 Relationship between airborne bacteria and the detected ARGs

RDA was conducted to explore the relationships between airborne bacterial genera and ARGs. Despite the regionally divergent bacterial communities, there may be a limited number of core taxa members that could be potential ARG hosts, as suggested by the

association between the currently analysed ARGs and specific bacterial genera independent of seasons and land-use types (Figure 5-12). The relative compositions of these potential hosts within the airborne bacterial community of each region may explain the regionally specific signature of ARG profiles (as discussed above). In addition, there were significant positive correlations between most of the analysed ARGs and between most of the bacterial genera (Figure 5-13), suggesting the co-abundance relationship between the ARGs and between the bacterial genera. Therefore, the RDA should be interpreted with caution due to potential co-correlation between ARGs and bacterial genera. Nevertheless, it is still worth noting that some of the identified bacterial genera significantly associated with the analysed ARGs, such as *Acinetobacter*, *Burkholderia*, *Clostridium*, *Sphingomonas*, and *Staphylococcus*, include certain clinically important pathogenic species. However, some environmental bacteria harbour intrinsic resistance to endogenous or naturally occurring antibiotics (Allen et al., 2010). For example, *Pseudomonas aeruginosa* has high intrinsic resistance in the presence of a β -lactamase-encoding gene on chromosomes, in addition to its outer-membrane barrier and the efflux pumps (Hancock et al., 2000; Okamoto et al., 2001). These natural resistance mechanisms have also been discovered in other species like *Burkholderia pseudomallei*, *Burkholderia cepacia*, and *Stenotrophomonas maltophilia* (Poole, 2001). It is therefore imperative in future studies to distinguish intrinsic and acquired resistance and ascertain the mobility of ARGs as well as the identities of ARG-carrying bacteria (pathogen or non-pathogen) in PM_{2.5}. Moreover, a recent study, which reanalysed some rare PM_{2.5} metagenomic data from Beijing, pointed out that the 24-h fine particles could harbour a high diversity of ARGs from around 40 subtypes in non-polluted days to over 90 subtypes in hazy days (Hu et al., 2018b). This result suggested that the targeted ARGs in this study, though involving six ARG types, could cover less than 7% of the ARG subtypes in PM_{2.5} at a

conservative estimate. All the issues mentioned above prompt us to try metagenomic sequencing in future research for a better understanding of airborne antibiotic resistance and its health relevance.

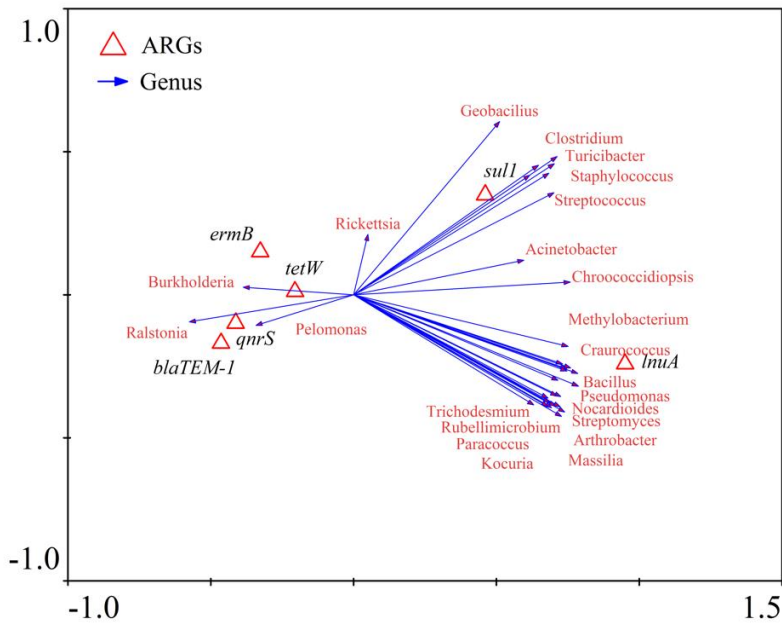


Figure 5-12 RDA identifying the relationships between bacterial genera and ARGs in PM_{2.5} ($p < 0.05$).

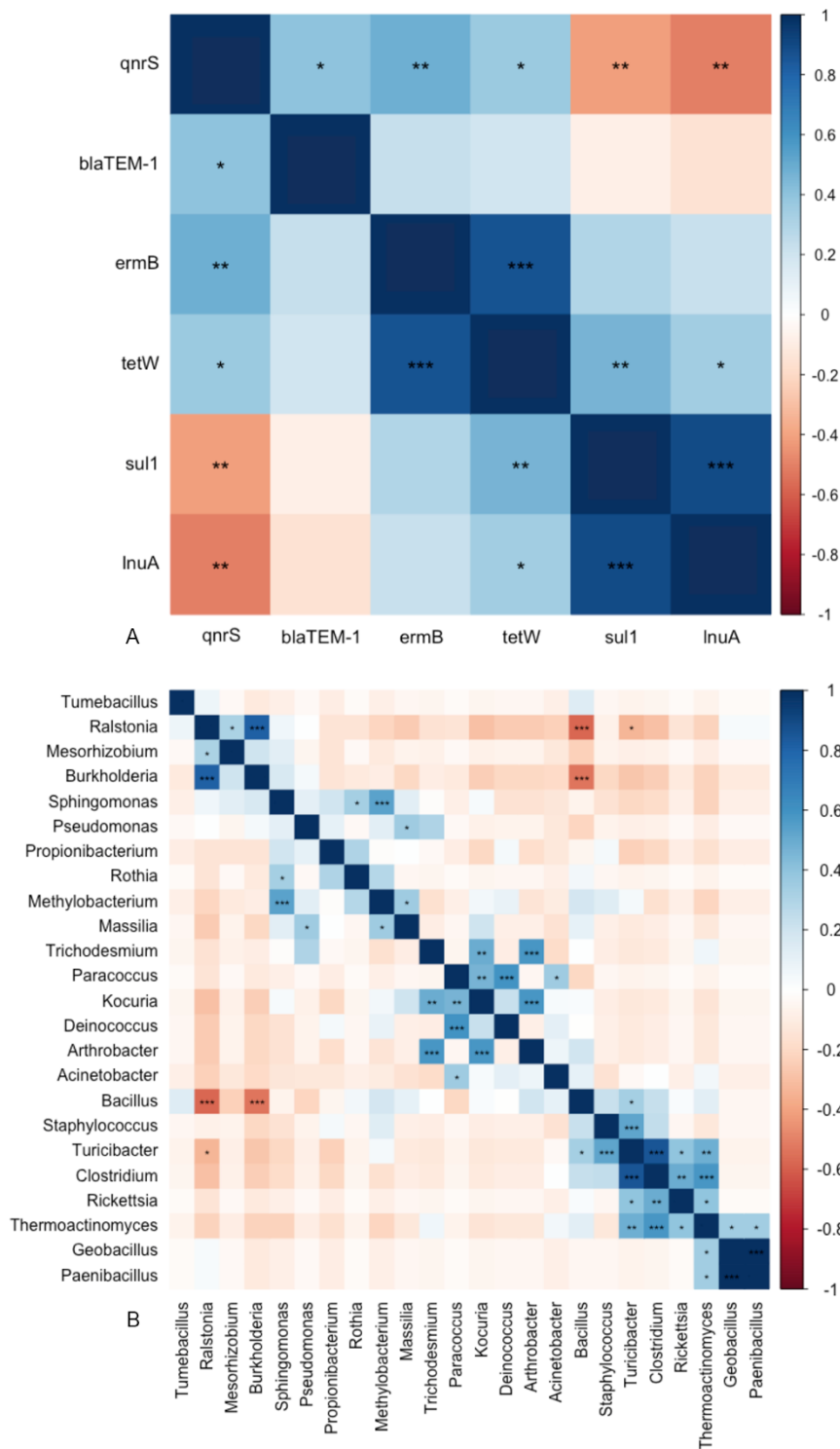


Figure 5-13 Spearman correlation matrices (A) between targeted ARGs and (B) between dominant genera (>5%). The asterisks indicate the significant levels (* $p < 0.05$; ** $p < 0.01$; *** $p < 0.001$).

5.3 Enrichment of ARGs and MGEs in PM_{2.5} in the studied regions

Integrations and transposons are important MGEs responsible for the dissemination of ARGs in the environment. In this study, *intI1* and *tnpA* belonging to the IS4 or IS6 group were widely detected in all the sampling sites. The absolute abundance of the total analysed MGEs generally varied against land-use types and spanned two orders of magnitude considering all sites in the YRD and PRD (Figure 5-8B). When turning to the urban areas, the YRD exhibited a significantly lower annual mean compared with urban PRD and Beijing ($p < 0.05$). The differences in MGEs concentrations possibly imply spatially and temporally different prospects for the potential of HGT in the atmospheric environment. In addition, there were significant correlations between the relative abundance of the total analysed ARGs and MGEs normalised to the 16S rRNA gene across most of the land-use types, with the exception of insignificance at the industrial and urban site of the YRD (Figure 5-14). These findings point to a co-occurrence pattern of ARGs and MGEs prevalent in the atmosphere. It should, however, be noted that the co-abundance of MGEs and ARGs does not necessarily mean the occurrence of HGT. Future studies are warranted to verify the mobility and transferability of these ARGs and, if so, to elucidate the genetic context (*e.g.*, types of MGEs) underlying the transfer mechanism (*e.g.*, plasmid-mediated conjugative transfer).

The relative abundance of ARGs normalised to the 16S rRNA gene and *intI1* normalised to cell numbers based on metagenomic sequencing was previously found to increase from natural environments to engineered systems and human and animal excreta samples (Figure 5-15 and Figure 5-16). This trend coincides with an increase in the level of anthropogenic impacts to exert selective pressure for the development of antibiotic resistance (Li et al., 2015a; Ma et al., 2017). However, the relative abundance of ARGs

and MGEs in outdoor PM_{2.5} seemed to break this trend. The median relative abundance of ARGs detected in PM_{2.5} samples is comparable to that in wastewater systems, with variability covering the entire span of all other sample types (Figure 5-15). This was also the case for the PM_{2.5}-associated *intI1* (Figure 5-16). The qPCR analysis used in this study only targeted a limited set of ARGs, whereas all of the identifiable ARG or ARG-like sequences in the other three groups of matrices based on metagenomics were included in this comparison. Therefore, the relative abundance of total airborne ARGs could be even higher. In addition, considering soil, wastewater, and faeces to be potential sources of airborne bacteria and ARGs (Bowers et al., 2011a; Bowers et al., 2011b; Joung et al., 2017; Li et al., 2016a), the large variability in the relative abundance of ARGs in the PM_{2.5} samples is an indication of the mixing effects of these surface sources. The current findings reaffirm the importance of the atmosphere as a potential gateway for surface sources of ARGs and as a key transmission route for human exposure. Future investigations of airborne ARGs in the vicinity of typical surface sources coupled with atmospheric dispersion modelling are warranted to identify their contribution to the ambient airborne ARGs.

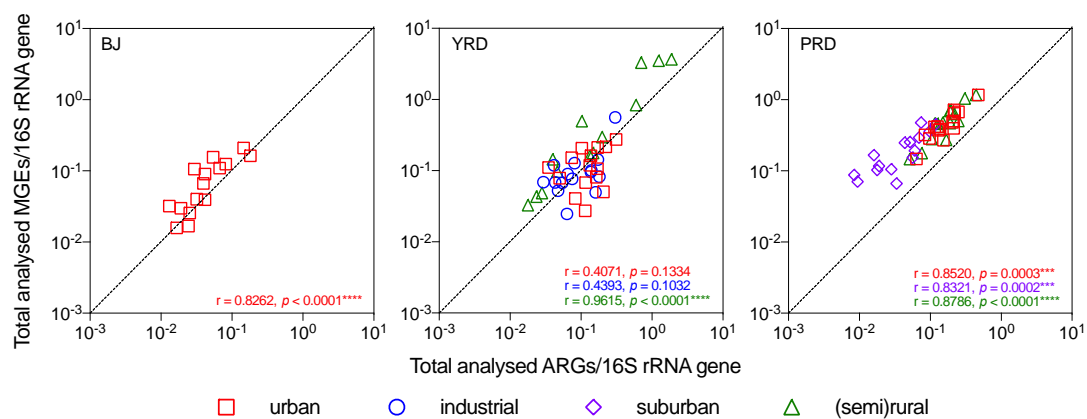


Figure 5-14 Relationships between ARGs and MGEs in PM_{2.5} across the studied sites.

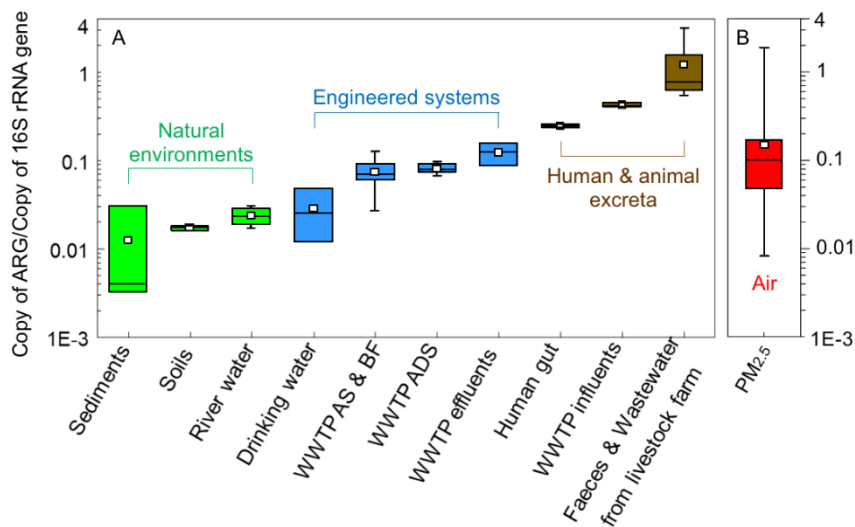


Figure 5-15 Relative abundance of ARGs normalised to the 16S rRNA gene in different environmental matrices. Panel (A) was adapted from Li et al. (2015a) (Copyright 2015 International Society for Microbial Ecology). Note that the data in (A) are based on metagenomic sequencing, while the data in (B) are based on qPCR analyses from this study.

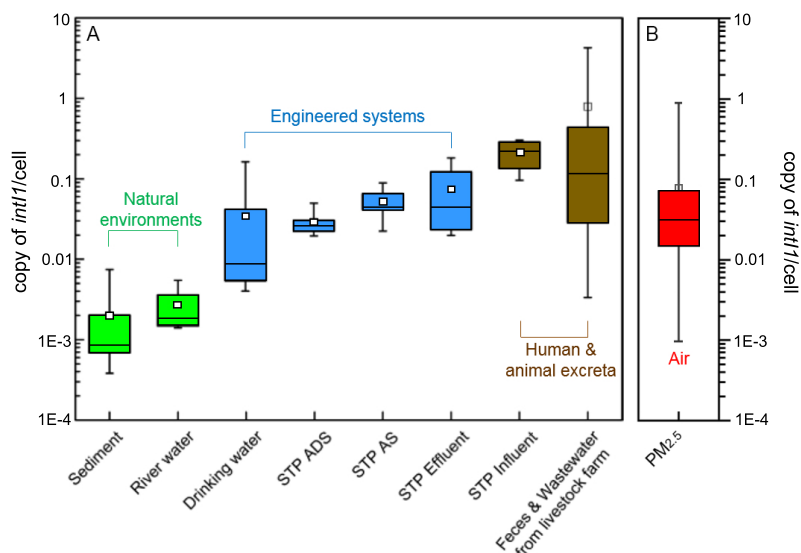


Figure 5-16 Comparisons of *intI1* copy number per cell (assuming on average 4.2 copies of the 16S rRNA gene per cell) between different environmental matrices. Panel (A) was

adapted from Ma et al. (2017) (Copyright 2017 American Chemical Society). In (A), *intI1* was identified based on metagenomic sequencing, while in (B) the gene was quantified by qPCR in the current study.

5.4 Human exposure to environmental ARGs from inhalation and other pathways in the YRD and PRD

The contribution of PM_{2.5} exposure to the total daily intake of ARGs from various pathways varied between the YRD and PRD (Figure 5-17) because of regional differentiation in airborne ARG profiles as well as the possible differences of ARG contamination in water and food between regions. Furthermore, the daily intake of ARGs via ingestion (drinking water and the intestines of aquaculture products) exceeded that of inhalation in most circumstances, with the exception of a comparable level for *ermB* and *bla_{TEM}* between drinking water and PM_{2.5} occurring in the YRD indicating the unequal roles of these pathways for human exposure. This is similar to the situation in the United States – PM_{2.5} exposure plays a non-negligible role compared with other pathways, based on the limited data for the 16S rRNA gene and ARGs in urban airborne particles and other intake-relevant matrices. It is stressed, however, that the intestines of aquaculture species are rarely consumed directly. Including this ingestion pathway represents a worst-case exposure scenario that is subject to the availability of data. The processing of drinking water (often boiled in China) and food (normally well-cooked around the world) might further modify the magnitude of exposure to bacteria and ARGs through ingestion, in contrast to the direct inhalation of PM_{2.5}-associated bacteria and ARGs without any prior treatment. Therefore, it is imperative to perform a daily basket survey of waterborne and foodborne bacteria and ARGs, considering the effects of cooking/boiling, to conduct a more comprehensive analysis of exposure pathways. On the other hand, bacteria and

the associated ARGs inhaled through the respiratory tract may have different fates from their ingested counterparts that must travel through the gastrointestinal tract. The ultimate effects of these external uptakes, which may complicate medication-induced ARGs, warrant more systematic research in the future. Despite these uncertainties, comparisons of daily intake in the YRD and PRD in the current study provide a first-tier screening of the relevance of the respective pathways to human aggregate exposure to environmental ARGs in region-specific scenarios. The inclusion of inhalable and ingestible ARGs in the full range of exposure sources would make the environmental framework of ARGs more relevant to human health and eventually make possible communication to the clinical framework of ARGs.

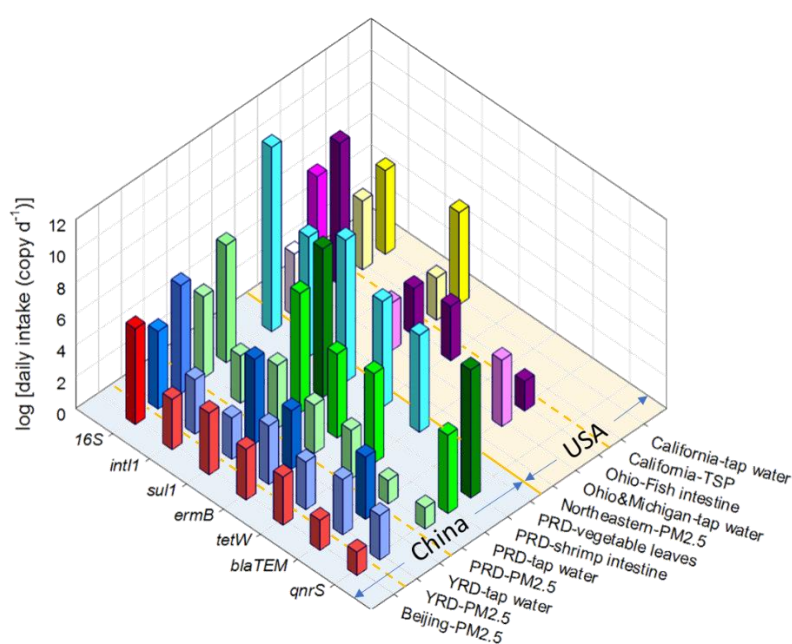


Figure 5-17 Regional comparisons of the human daily intake of ARGs and the 16S rRNA genes between inhalation and ingestion, coupled with a contrast with the U.S. situation. The calculations are based on Equation 3-13, Equation 3-14, and Equation 3-15. Annual average concentrations of targeted genes in the PRD, the YRD, and Beijing generated in this study were used to estimate the daily intake via inhalation. The raw data on the concentrations of the targeted genes in tap water in the YRD and PRD were from Shi et

al. (2013) and Su et al. (2018b), respectively. The raw data for samples of shrimp intestines and washed vegetable leaves in the PRD were from Su et al. (2018a) and He et al. (2016), respectively. The U.S. data were obtained from Hospodsky et al. (2012), Xi et al. (2009), Huang (2014), and Echeverria-Palencia et al. (2017).

5.5 Summary

The results in this chapter reaffirmed the ubiquity of ARGs in the atmosphere across spatiotemporal scales, including the inhalation-relevant fine particle fraction ($PM_{2.5}$). The Earth's atmosphere serves as a habitat for bacteria where ARGs can be highly enriched, and fine aerosols act as a transmission vector for human exposure to bacteria and environmentally disseminated ARGs. These findings contribute to our awareness of the link between bioaerosols and human health and supplement the previous understanding of health impacts posed by airborne particulates, which used to be considered mainly from chemical perspectives. Some major findings of this chapter are listed below.

1. Seasonal variations in airborne bacterial loads were most pronounced at the (semi)rural site compared with other land-use types in both the YRD and PRD. Anthropogenic activities that were more seasonally independent were likely to flatten the seasonal rhythms of bacterial loads and explain the less distinct seasonal fluctuations observed in (sub)urban and industrial areas.

2. When focusing on the urban site, seasonal variations in airborne bacterial loads were comparable in the YRD and PRD in the subtropical zone (10^3 to 10^4 copies m^{-3}), in contrast to the significant fluctuation in another city in the temperate region (10^3 to $>10^5$ copies m^{-3}), which was similar to the observations in bacterial communities. Climate

condition could be a critical influential factor by regulating the seasonal changes of the dominant sources themselves – like vegetation – or influencing the seasonal input of the rather stable emission sources – like soil/dust – to modulate their seasonal contributions to airborne bacteria.

3. While the airborne ARG profiles exhibited different regional patterns between the YRD (dominated by *ermB*) and the PRD (rich in *lnuA* and *sulI*), they seemed relatively consistent within each region independent of seasonal cycles and land-use impacts. Meanwhile, the targeted ARGs were correlated to limited bacterial genera, a finding that might hint at the possible ARG hosts. However, the current results were based on limited ARGs analysed. A comprehensive scan of antibiotic resistome by metagenomic sequencing is required in the future to get a full picture of ARG hosts.

4. There were common correlations between ARGs and MGEs across regions. PM_{2.5} was at the higher end of ARG and MGE enrichment across various environmental media, with the variability covering the entire span of all of the other types of samples, including those from natural environments or engineering systems, as well as human/animal faeces. This finding indicates the mixing effects of these surface sources on airborne ARGs and MGEs.

5. The spatiotemporally differentiated bacterial communities and ARG abundance and the composition, mobility, and potential hosts of ARGs in the atmosphere have substantial implications for human inhalational exposure over spatiotemporal scales. Compared with other contributing pathways for ARG intake (*e.g.*, drinking water and food ingestion), inhalation could be another non-negligible pathway with region-specific importance.

In short, this chapter extensively explored the spatiotemporal features of PM_{2.5}-associated bacteria and certain kinds of ARGs in the YRD and PRD, which might not be necessarily consistent with the spatiotemporal variations of the chemical components of PM_{2.5}. The ubiquitous presence of bacteria and ARGs, as well as their enrichment in airborne particles, triggers concerns about the consequent exposure risks. Based on current observations, it is speculated that emission sources could play an important role in affecting the abundance and structure of airborne bacteria and ARGs. However, limited by the detection technique (qPCR), only six ARG subtypes were analysed in this chapter. What the major emission sources are and how much these potential sources could contribute to the ambient airborne microbiome and antibiotic resistome remain unclear based on the current results, which require further investigations. Therefore, the next chapter presents an additional study implemented in a typical WWTP in Hong Kong in the PRD, which is considered as a representative anthropogenic ARG source. Coupled with the literature data on other potential sources downloaded from the NCBI database, the next chapter aims to explore the contribution of different potential sources, especially for WWTPs, to the atmospheric bacteria and ARGs. Meanwhile, in contrast to limited kinds of ARGs quantified in this chapter as constrained by DNA amount, PM_{2.5} samples collected in the WWTP will be fully used in DNA extraction for metagenomic sequencing to obtain a comprehensive profile of airborne ARGs and to elucidate the dissemination potentials of ARGs in the atmosphere based on the co-occurrence pattern of ARGs and MGEs.

Chapter 6 Typical Urban Anthropogenic Sources of PM_{2.5}-associated Bacteria and ARGs – A Case Study in a WWTP in Hong Kong

To further explore the contributions of potential emission sources to PM_{2.5}-associated bacteria and ARGs in urban areas – which were less explored in Chapter 5 – a case study was conducted in a WWTP, which is considered as an urban ARG hotspot. With a high level of urbanisation, Hong Kong is a suitable city in the PRD to deploy such an investigation. In this study, the largest WWTP, the SCISTW, which serves half of the population in Hong Kong, was selected as a representative. PM_{2.5} samples collected near various treatment facilities within the SCISTW in late October 2016, as well as the sewage, sludge, and effluent samples along the wastewater treatment process, were subjected to multiple molecular biological analyses, including quantification of the 16S rRNA gene abundance and metagenomic sequencing. For comparisons, PM_{2.5} samples were also acquired simultaneously in an urban (PU) and a coastal mountain (HT) site. Based on the metagenomic sequencing data, the contrast in bacterial community structure and ARG profile among different sample types and that among various sampling locations are discussed. In addition, the co-occurrence pattern of PM_{2.5}-associated bacteria, ARGs, and MGEs was analysed to speculate on the potential hosts of PM_{2.5}-associated ARGs and to estimate the dissemination potential of ARGs through HGT by comparing the conceptualised risk scores. Finally, contributions of different emission sources to PM_{2.5}-borne bacteria and the associated ARGs, especially for WWTPs, were quantified using SourceTracker2.

6.1 Distinctive features of the microbial community structure among PM_{2.5}, sewage, sludge, and effluent

As shown in Figure 6-1, although there was a higher relative abundance of eukaryotes in the whole microbial community in PM_{2.5} samples, especially in the coastal site, bacteria were still the predominant organisms regardless of sample types, which made up 85%–95% of reads in PM_{2.5} samples and over 99% in sewage/effluent and sludge samples. When focusing on the bacterial community, there was an extremely high degree of overlap in bacterial diversity at the genus level between sewage/sludge/treated effluent and PM_{2.5} samples regardless of the sampling locations in Hong Kong (Figure 6-2A), suggesting that PM_{2.5} could be an important bacterial habitat and possibly a vector of frequent bacteria exchange between the atmosphere and other environments. When further shedding light on the bacterial community structure, it was clear that samples from the same environmental media shared a more similar structure than that of the same sampling location (Figure 6-3A). NMDS analysis revealed that samples were clustered more by sample type at the phylum and genus level (Figure 6-3B). Based on the categorisation by sample type, LEfSe analysis identified Actinobacteria at both the phylum and class level as discriminative features of PM_{2.5} – with higher abundance than in other samples ($p < 0.05$) (Figure 6-3C). It is also worth noting that coastal PM_{2.5} samples distinctively separated from urban/SCISTW PM_{2.5} samples at the genus level might imply different dominant sources of airborne microbes between the coastal areas and the other two sites impacted by intense human activities. The significant increase in PM_{2.5}-associated bacterial loads (represented by the 16S rRNA gene abundance) in urban/SCISTW compared with coastal areas (Figure 6-2B) also highlights the contributions of anthropogenic sources to airborne microbes.

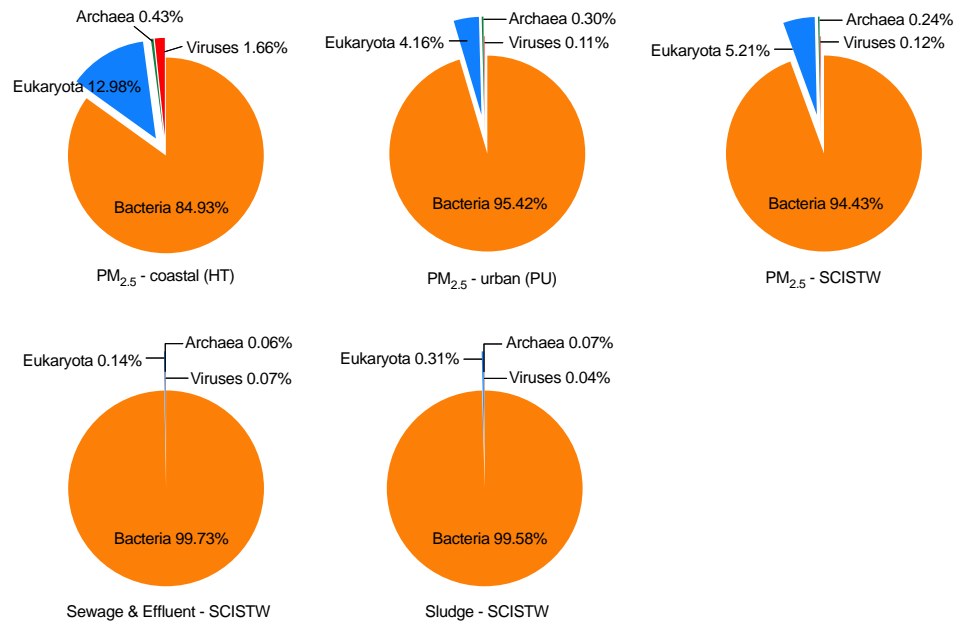


Figure 6-1 Relative abundance of microbial communities at the domain level assigned by kraken2 (read-based).

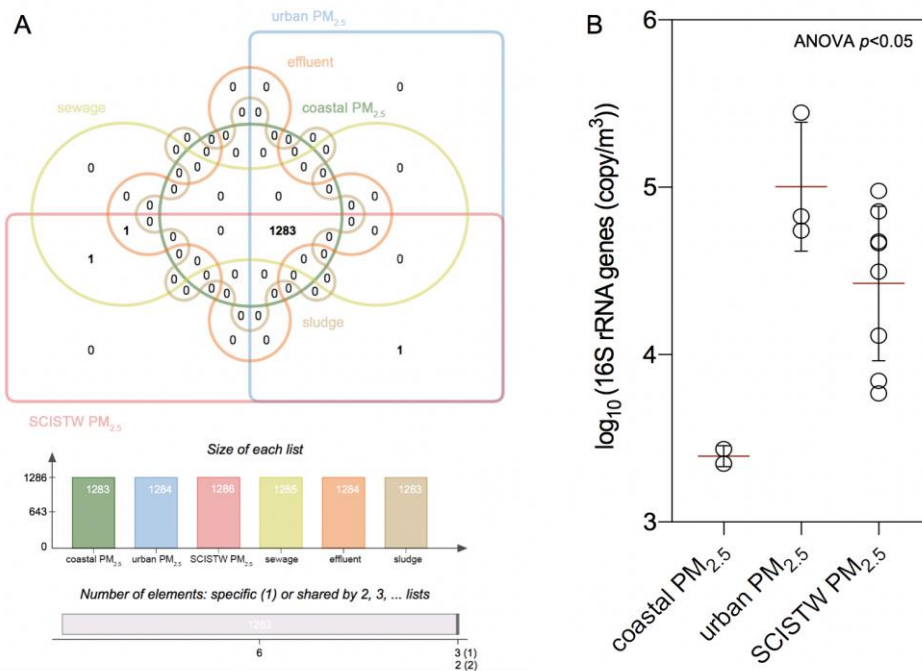


Figure 6-2 (A) The number of shared bacterial genera revealed by a Venn diagram and (B) comparisons of PM_{2.5}-associated bacterial loads among different sampling locations.

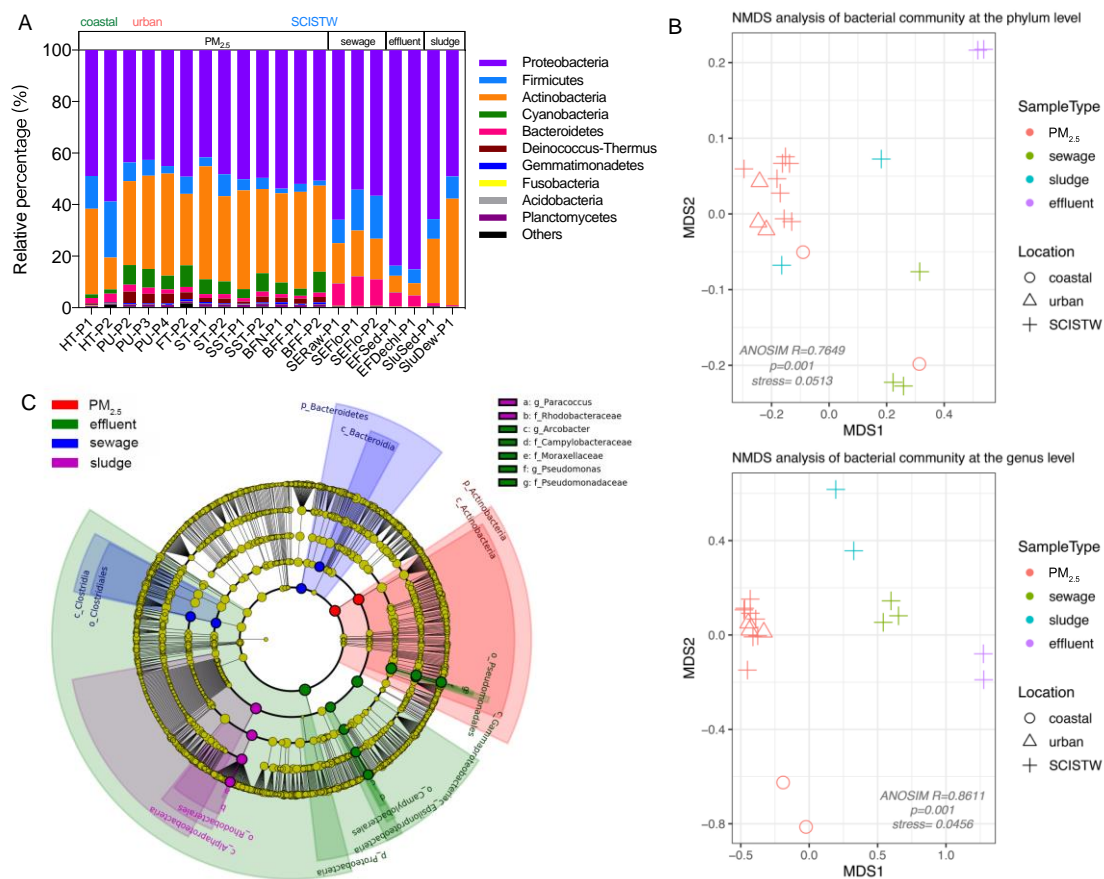


Figure 6-3 Shift in bacterial community structure among sample types: (A) the relative abundance of the profiled bacteria at the phylum level; (B) the NMDS results of the bacterial community at the phylum and genus levels; (C) the taxonomic differentiation among different sample types at the statistically significant level of 0.05 using LefSe analysis (LDA score > 4.6).

6.2 Discrimination of ARG profiles across environmental matrices and sampling locations

ARGs encoding resistance to different antibiotics were widely found with high diversity in all the samples irrespective of environmental matrices and sampling locations. However, there were more unique ARG subtypes in PM_{2.5} compared with sewage/sludge (Figure 6-4A), as well as in SCISTW PM_{2.5} compared with coastal/urban PM_{2.5} (Figure 6-4B). It seems that all the samples shared a generally similar pattern of the most abundant

antibiotic resistance types, of which the relative abundance was in descending order of multidrug resistance (1.81–4.36 copies/16S rRNA gene) > MLS (macrolide-lincosamide-streptogramin)/peptide resistance (0.36–1.18 copies/16S rRNA gene) \geq rifamycin/tetracycline resistance in PM_{2.5} (0.30–0.95 copy/16S rRNA gene)/sludge (0.64–0.71 copy/16S rRNA gene) and beta-lactam/tetracycline resistance in sewage/effluent (0.30–0.55 copy/16S rRNA gene) (Figure 6-5A and Figure 6-5C). Compared with other studies on airborne particles in urban areas/poultry farms/hospitals (He et al., 2020; Hu et al., 2018b; Yang et al., 2018), there was a significantly higher relative abundance of ARGs (orders of magnitude) and more ARG subtypes in PM_{2.5} samples in this study. These differences could be due to the more comprehensively curated ARG database and the novel machine learning-based algorithm (DeepARG) for ARG annotation adopted in this study to capture as many potential ARGs as possible (Arango-Argoty et al., 2018).

These findings echo the disparities in bacterial community structure among various sample types. As disclosed by cluster analysis, PM_{2.5} samples were segregated from sewage/sludge/effluent samples from the SCISTW based on drug resistance type or ARG subtype (Figure 6-5A and Figure 6-6). Considering that there was an elevated amount of unique ARGs and distinct bacterial community structures in PM_{2.5}, perhaps airborne particles are a unique environmental reservoir for ARGs with associations to their potential hosts. The atmosphere could also simultaneously provide selective pressures to reshape the profiles of airborne ARGs and the bacterial community after the emissions of microbes, including ARB and non-ARB, to the atmosphere from their source environments like WWTPs. Illustrated by LEfSe results (Figure 6-7), a series of ARGs as featured biomarkers were likely to be internally responsible (to a certain extent) for the

discrimination of the ARG profile between airborne particles and other samples, such as *rpoB2* conferring resistance to rifamycin; *tetA(48)* conferring resistance to tetracycline; *bcrA* conferring resistance to peptide antibiotics; *oleC* conferring resistance to MLS; and *mtrA*, *arlR*, *mexF*, and *abcA* conferring resistance to multiple antibiotics. Yang et al. (2018) reported comparable phenomena: multidrug resistance genes, bacitracin (a kind of polypeptide) resistance genes, and MLS resistance genes were dominant in airborne antibiotic resistance profiles in WWTPs and urban areas. Remarkably, some multidrug resistance genes like *mexF* were prevalent and enriched in airborne particles in poultry farms and WWTPs compared with those in animal faeces and activated sludge, respectively (Yang et al., 2018). Coupled with the similar observations in this study, there might be a potential commonality for the airborne antibiotic resistome, especially in such potential source environments. Furthermore, the increasing trend in the relative abundance of total detected PM_{2.5}-associated ARGs (normalised to the 16S rRNA gene) across the coastal–urban–SCISTW gradient (Figure 6-5B) indicates the impacts of human activities on ARG accumulation in the atmosphere. This finding is also consistent with former investigations that airborne ARGs were enriched in animal farms and hospitals compared with downtown areas and suburban communities (He et al., 2020; Yang et al., 2018). Collectively, the findings demonstrate that WWTPs could be a notable ARG hotspot with contributions to the nearby airborne antibiotic resistome.

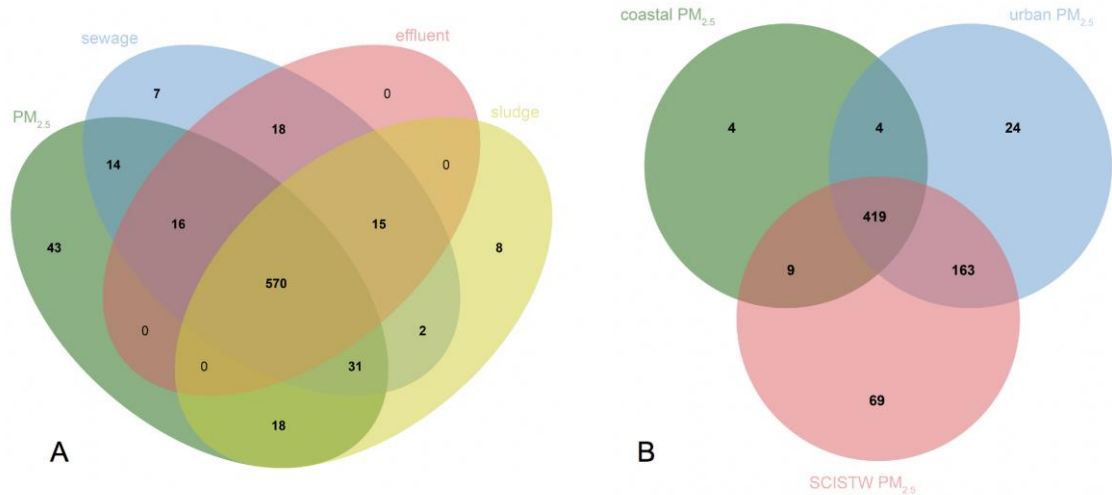


Figure 6-4 The number of shared ARG subtypes of samples (A) from different environmental matrices and (B) among PM_{2.5} samples collected in different locations.

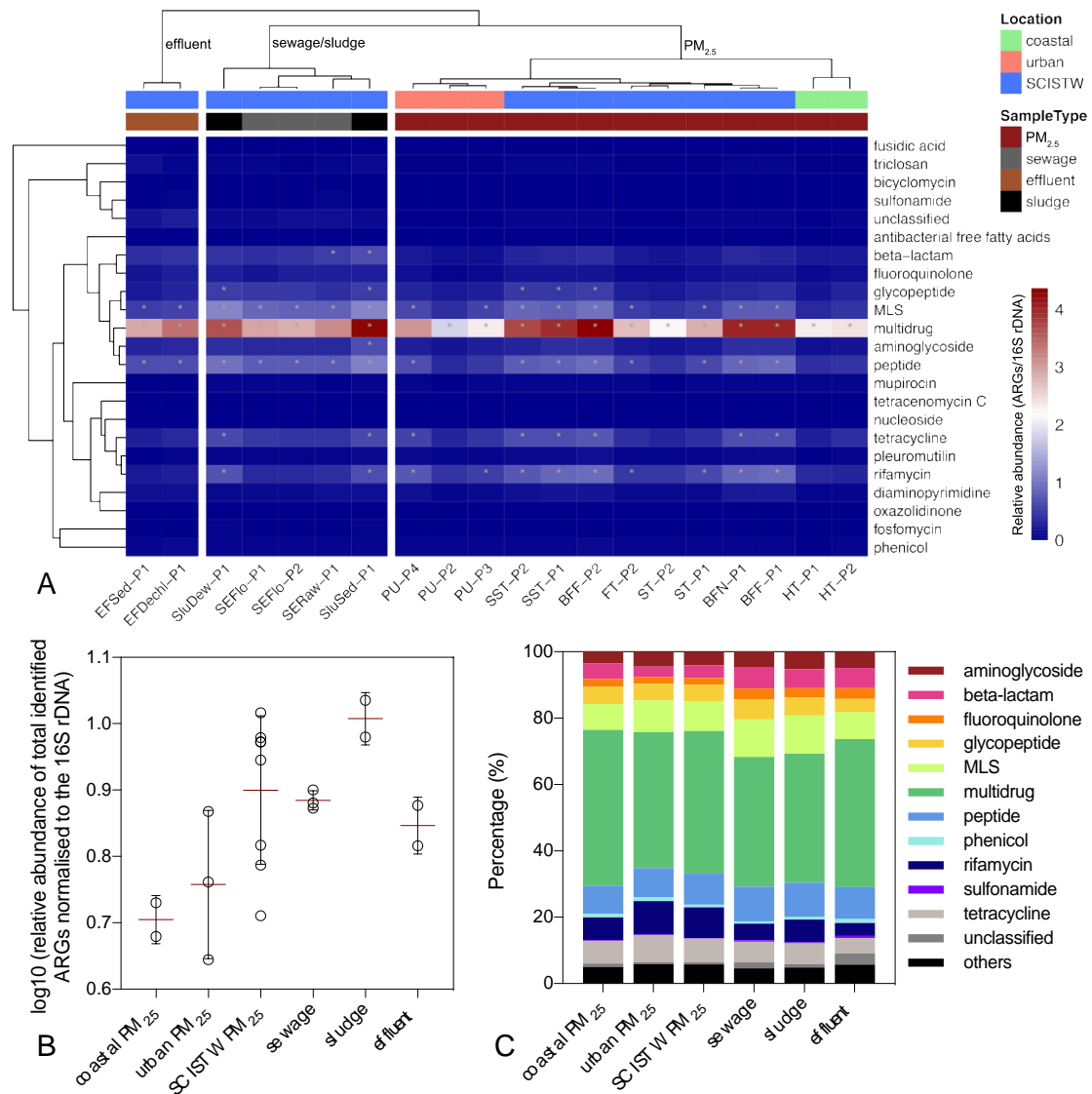


Figure 6-5 Antibiotic resistance profiles of samples across environmental matrices and sampling locations according to the drug class. In (A), ARGs at the type level with the relative abundance no less than 0.5 (normalised to the 16S rRNA gene) are marked with asterisks in the corresponding cells. The correlation-based distance was considered in average-linkage clustering. Panel (B) presents the relative abundance of total identified ARGs normalised to the 16S rRNA gene among sample types and sampling locations. The brown line represents the mean value. Panel (C) shows the contributions of various ARG types to the total ARG abundance in different samples.

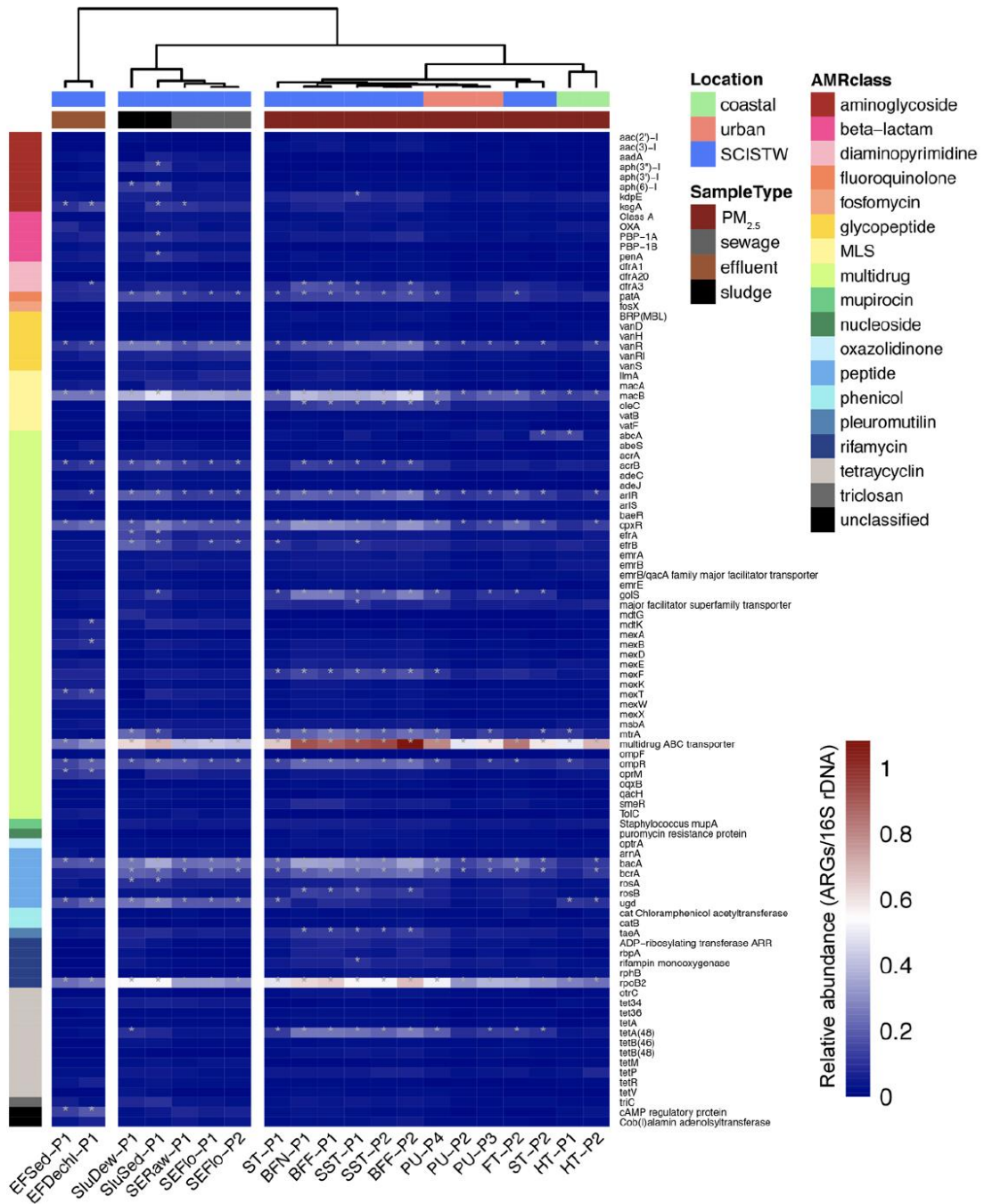


Figure 6-6 Profiles of the top 100 ARGs with the highest relative abundance (normalised to the 16S rRNA gene) in samples across environmental matrices and sampling locations at the ARG subtype level. ARGs with a relative abundance no less than 0.1 (normalised to the 16S rRNA gene) are marked with asterisks. The correlation-based distance was considered in average-linkage clustering.

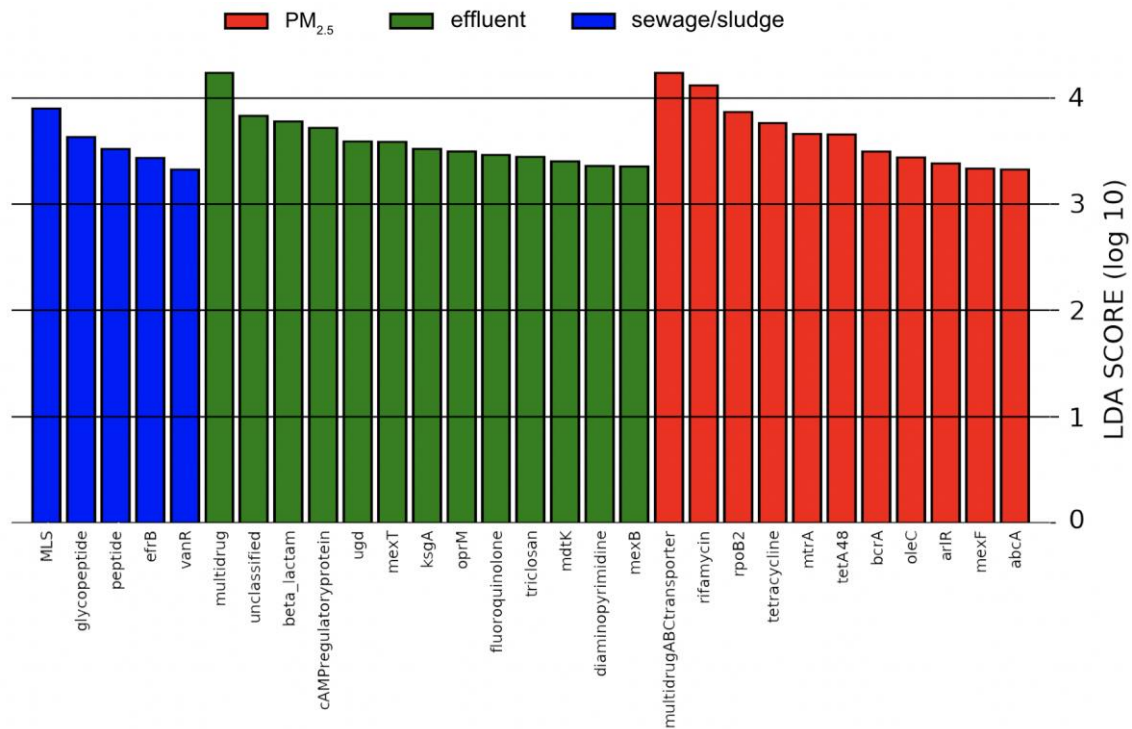


Figure 6-7 Major significantly discriminative ARGs and resistance types between different sample types revealed by LefSe analysis (LDA score > 3.3).

6.3 Co-occurrence patterns of ARGs, MGEs, and potential hosts to indicate the environmental resistome risks

To evaluate the horizontal dissemination potential of ARGs and their latent risks as health hazards, the mobility and the potential host(s) of ARGs were investigated according to the co-occurrence relationship of ARGs, MGEs, and bacteria on the assembled scaffolds using NanoARG. Here “co-occurrence” means these elements were detected on the same scaffold. First, with regard to the ARG profile, the results predicted from the assembled scaffolds were generally comparable to those from direct annotations of short sequencing reads (Figure 6-5C and Figure 6-8A), which indicates the output consistency of these two processing pipelines in the identification of ARGs. In this section, the co-occurrence relationship of the targeted objects and the evaluation of the ARG resistome risk are discussed based on the assembled results.

6.3.1 Overview of the co-occurrence relationship of ARGs, MGEs and bacteria

According to the co-occurrence pattern shown in Figure 6-8C, only a small minority of the identified ARGs, around $\leq 2\%$ in urban/SCISTW samples and none in coastal PM_{2.5}, were potentially mobile. This finding suggests a relatively low probability of HGT of ARGs happening between bacteria whether in air, sewage, or sludge. Similar phenomena have been previously observed: there was only a small portion of ARGs on MGEs (*e.g.*, integrons and plasmids), although ARGs and MGEs were widely detected and frequently found correlated in environmental samples (Ma et al., 2017; Zhang et al., 2020a).

Moreover – not analogous to the total ARG profile, which was comparable in all the studied samples with the predominant position taken by multidrug resistance genes – over 50% of the potentially mobile ARGs (PM-ARGs) seemed to confer resistance to rifamycin in urban and SCISTW PM_{2.5}. By contrast, behind the multidrug resistance genes, there was an elevated proportion of PM-ARGs belonging to glycopeptide, tetracycline, and beta-lactam resistance categories in non-air samples (Figure 6-8A). The differences between the total ARG and PM-ARG profile hint at the inequivalent dissemination risks of different ARGs regarding their linkage with MGEs apart from the influence of environmental media. In addition, there were apparent disparities in the host structures between ARGs and PM-ARGs in PM_{2.5} samples (Figure 6-8B). Echoing the pattern of rifamycin resistance genes, Actinobacteria, which was responsible for 25% of the total ARGs in PM_{2.5}, outpaced Proteobacteria to be the most abundant host taxa (38%–50%) in the corresponding PM-ARG profile. This discernible synchronicity could be explained by Actinobacteria possibly being the predominant host of mobile rifamycin resistance genes (Figure 6-8D) in the studied samples, which was not surprising because

some Actinobacteria naturally produce rifamycin (Kim et al., 2006). Although the co-occurrence pattern of ARGs, MGEs, and their potential hosts was uncovered to some extent here, the interactive mechanisms of these complicated connections and the driving factors differentiating PM_{2.5} and other samples are still hidden in the mist. Hence, this issue warrants intensive study in the future.

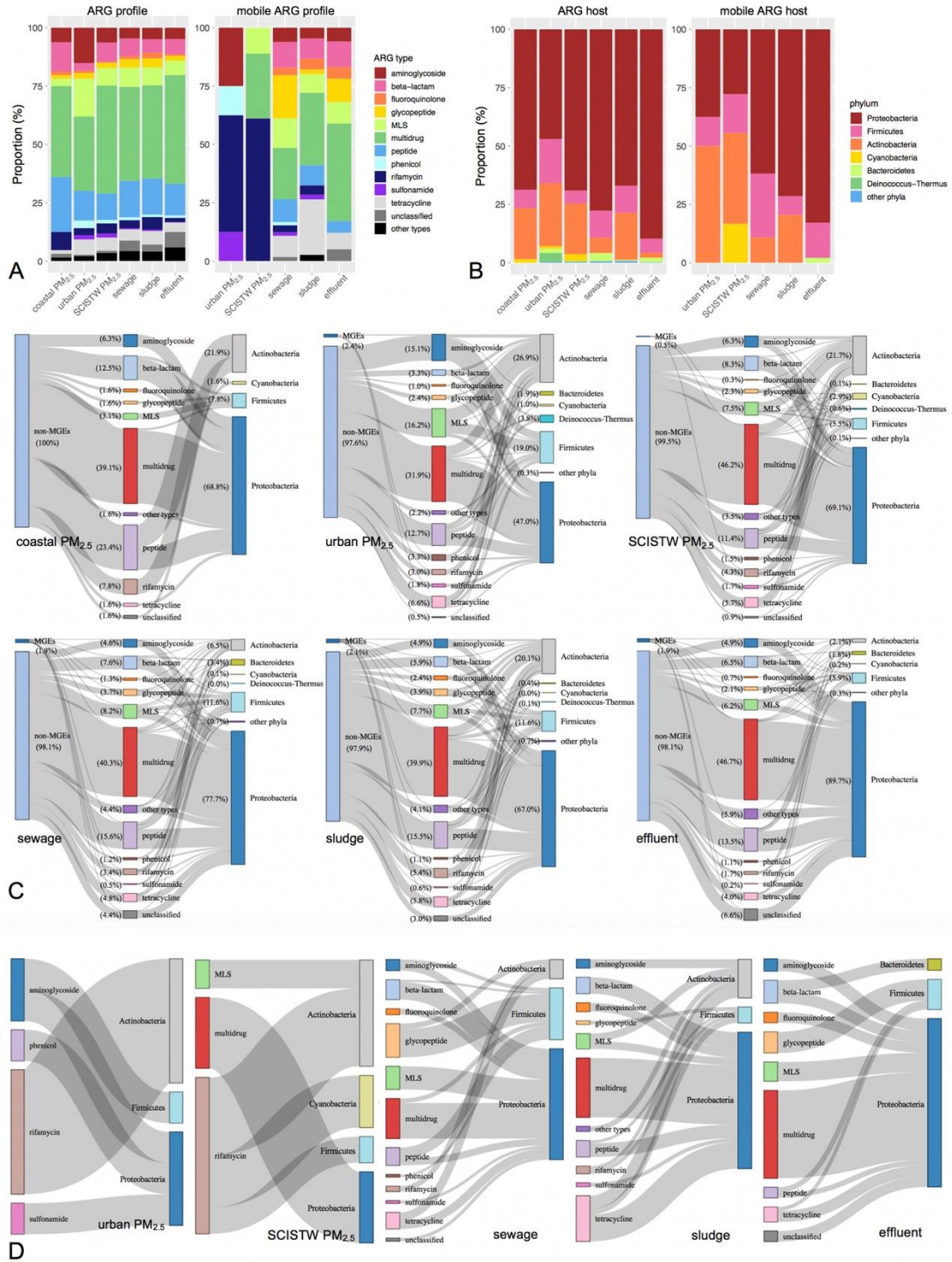


Figure 6-8 Co-occurrence patterns of ARGs, MGEs, and potential bacterial hosts at the phylum level based on assembled scaffolds (analysed by NanoARG). Panel (A) shows the differences between the ARG profile and the mobile ARG profile, while (B) presents the differences in their host profiles. Panel (C) and (D) demonstrate the detailed co-occurrence patterns of ARGs and mobile ARGs with their potential hosts in Sankey

diagrams, respectively. In (C), the left column shows whether the identified ARGs are co-localised with MGEs on the assembled scaffolds, whereas the middle and right columns are the profiles of ARGs and their potential hosts, respectively, the same as the left panel of (A) and (B). Analogously, the first and second column of each subfigure in (D) exhibit the mobile ARG profile and their potential hosts, the same as shown in the right side of (A) and (B), respectively.

6.3.2 Evaluation of resistome risks across sample types and sampling locations

To evaluate and compare the HGT potential and health hazards of ARGs among different sample types, MetaCompare was employed to rank their resistome risk based on the association of ARGs, MGEs, and putative pathogens. The results were visualised on a 3D hazard space and turned into a conceptual risk score. Compared with sewage, sludge, and effluent samples, PM_{2.5} samples generally exhibited a lower relative abundance of scaffolds with targeted elements in three aspects, regardless of whether the scaffolds contain ARGs, both ARGs and MGEs, or pathogen-like sequences with co-localised ARGs and MGEs (Figure 6-9A). Correspondingly, the integrated risk score reflects that the antibiotic resistome hazard was relatively lower in the PM_{2.5} samples, whereas there were no significant changes among PM_{2.5} samples collected in different sites. Such observations, from a metagenomic perspective, might imply a relatively common phenomenon that HGT events of ARGs, including their propagations to putative human pathogens, could be less likely to occur in the atmosphere – in coastal areas or human-impacted sites – compared with other more compact media in potential ARG emission sources, such as sewage and sludge in WWTPs. However, as mentioned in Chapter 5, ARG-associated bacteria dwelling in the atmosphere could enter the human body directly via inhalation without any pretreatment, which is different from other exposure pathways.

Therefore, when considering ARGs as a kind of biological hazard with regard to human health, ARG dissemination via HGT in the atmosphere may still be worthy of attention, even though there is a low probability that it will occur.

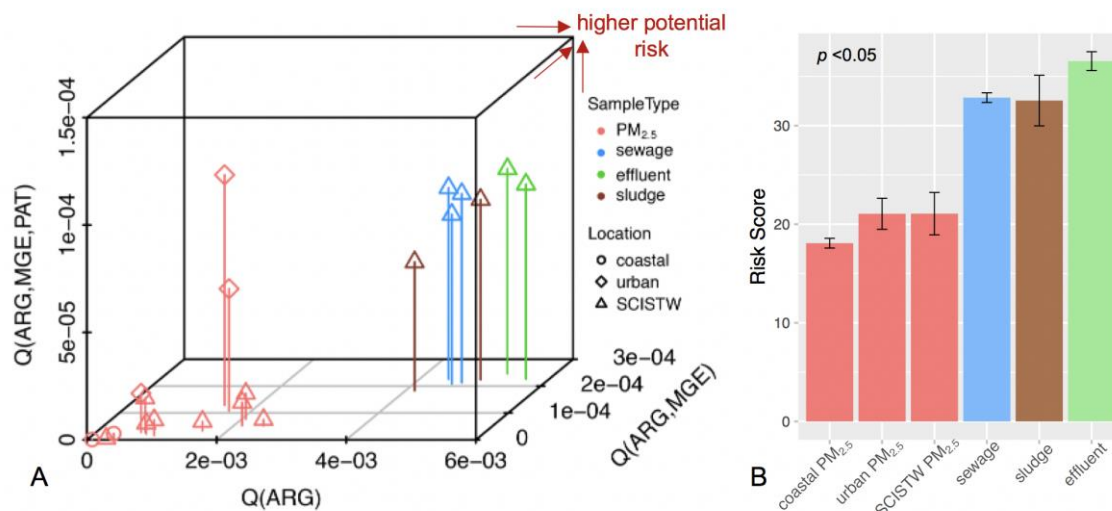


Figure 6-9 Estimated dissemination risks of ARGs proposed by MetaCompare. The X-, Y- and Z-axes in (A) represent the co-occurrence probability of the targeted components – ARGs, ARGs–MGEs, ARGs–MGEs–putative pathogens, respectively – identified in the samples. This information is expressed as the scaffold number with critical components divided by the total assembled scaffold number. The normalised risk scores evaluating the dissemination potential of ARGs and their latent association with putative pathogens are shown in (B). Detailed information of the relevant algorithms could be found in a previous study (Oh et al., 2018).

6.3.3 Exploration of ARG-associated priority pathogens in urban and WWTP PM_{2.5}

In recent years, ESKAPE and other priority pathogens emphasised by the WHO (listed in Table 6-1) have attracted more and more attention of researchers and medical personnel, because of their rapid acquisition of resistance to commonly used antibiotics that make medical therapy ineffective against pathogenic infection. This phenomenon had increased

the need to explore new antibiotics. In view of this, scaffolds containing both ARG-like and priority-pathogen-like sequences were sorted out from the NanoARG results to further analyse the spread of antibiotic resistance in these pathogens. As shown in Figure 6-10, in all samples except PM_{2.5} in coastal areas, ARGs co-occurred with at least four kinds of pathogens from the list of concerns. In general, the relative abundance of the total identified antibiotic-resistant pathogens (normalised to the total scaffold number) was significantly higher in non-PM_{2.5} samples, across which the profiles of the critical pathogens with antibiotic resistance, as well as that of resistance types identified in these pathogens, seemed to be comparably consistent (Figure 6-10). In contrast to *Klebsiella pneumoniae* as the predominant species in sewage/sludge/effluent, *Acinetobacter baumannii* was the main antibiotic-resistant pathogenic species in SCISTW PM_{2.5}, which was also present in sewage/sludge/effluent but undetectable in urban PM_{2.5}. Although the sludge storage tanks and flocculation/sedimentation tanks are covered for odour control, it seemed that such measures could not simultaneously control the emission of bacteria of concern from sewage/sludge to the surrounding air in an effective manner. In urban PM_{2.5}, staphylococcus aureus was witnessed as the featured antibiotic-resistant pathogen. It was worth noting that there has been a remarkable growth in hospital-associated cases of methicillin-resistant *Staphylococcus aureus* in Hong Kong over the past few years, as well as the noticeable detection rate of carbapenem-resistant *Acinetobacter* and extended-spectrum β -lactamase (ESBL)-producing *Escherichia coli* (Centre for Health Protection, 2017). Fortunately, the types of ARGs co-occurring with the priority pathogens in PM_{2.5} samples in this study were distinguishable from the clinical cases, indicating that the pathogens with acquired resistance of clinical concern have not yet been disseminated to the atmospheric environment on a wide scale. Moreover, the ARG profile of pathogens exhibited distinct divergence among samples with a stepwise increase in multidrug

resistance and a sharp decrease in aminoglycoside resistance from urban PM_{2.5}, to SCISTW PM_{2.5}, and then other samples in the SCISTW. Such a gradient might also imply the contribution of sewage/sludge in WWTPs to antibiotic-resistant pathogens in the ambient air. This eventuality would correspond with the result noted in the previous section that SCISTW could be an important contributor to airborne bacteria and the associated antibiotic resistance.

Table 6-1 List of priority pathogens with increasing concern of antimicrobial resistance proposed by the WHO, categorised by the urgency of the need for novel antibiotics.

Level	Pathogen	Antimicrobial resistance type
Critical	<i>Acinetobacter baumannii</i>	carbapenem-resistant (beta-lactam)
	<i>Pseudomonas aeruginosa</i>	carbapenem-resistant (beta-lactam)
	<i>Enterobacteriaceae</i>	carbapenem-resistant (beta-lactam), ESBL-producing (Extended spectrum beta-lactamases)
High	<i>Enterococcus faecium</i>	vancomycin-resistant (glycopeptide)
	<i>Staphylococcus aureus</i>	methicillin-resistant (beta-lactam), vancomycin-intermediate and resistant (glycopeptide)
	<i>Helicobacter pylori</i>	clarithromycin-resistant (MLS)
	<i>Campylobacter</i> spp.	fluoroquinolone-resistant
	<i>Salmonellae</i>	fluoroquinolone-resistant
	<i>Neisseria gonorrhoeae</i>	cephalosporin-resistant (beta-lactam), fluoroquinolone-resistant
Medium	<i>Streptococcus pneumoniae</i>	penicillin-non-susceptible (beta-lactam)
	<i>Haemophilus influenzae</i>	ampicillin-resistant (beta-lactam)
	<i>Shigella</i> spp.	fluoroquinolone-resistant

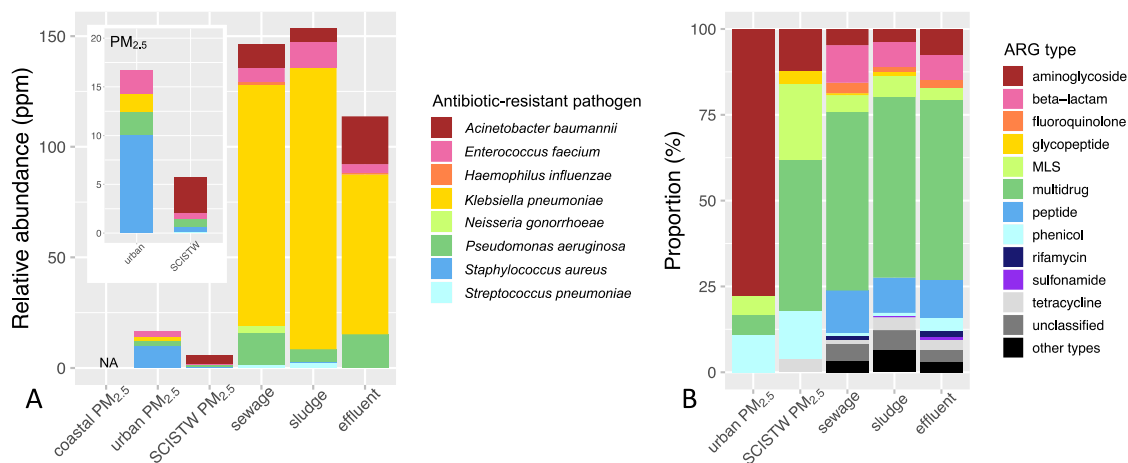


Figure 6-10 (A) Antibiotic-resistant pathogens and (B) the corresponding resistance profile at the ARG type level identified based on the co-occurrence pattern of critical pathogens (ESKAPE and WHO priority pathogens) and ARGs in different samples via NanoARG. The Y-axis of (A) represents the relative abundance of antibiotic-resistant pathogens described in the unit of “ppm”, which means the hit number of these antibiotic-resistant pathogens found in one million assembled scaffolds. Panel (B) shows the distribution of ARGs identified in critical pathogens.

6.4 Contributions of WWTP and other potential sources to airborne bacteria and ARGs

To quantify the contributions of potential sources to the PM_{2.5}-associated bacteria and ARGs in the studied sites, 104 metagenomes of samples collected from different environments were regarded as representatives of various source categories. Besides sewage, sludge, and effluent samples from the WWTP, other sequencing data downloaded from MG-RAST and NCBI databases covered a wide range of environmental samples, including that from anthropogenic sources like landfill leachate and others from more natural environments such as freshwater, seawater, sediment, and soil (detailed project ID listed in Appendix 1). To focus on the local situation, most of the

samples were from Hong Kong and South China, except the seawater samples that were selected from the Pacific Ocean and the Indian Ocean because of a lack of suitable metagenomic data of marine samples from Hong Kong. These samples collectively formed a database of the potential sources of airborne bacteria and ARGs, which was used as an input in the subsequent source tracking procedure. As revealed by NMDS analysis, samples tended to be clustered by their environmental types whether based on the bacterial community structure or the ARG profile (Figure 6-11), indicating that samples from different environmental sources generally had distinct features in bacterial and ARG structures.

According to the results of SourceTracker2, approximately 60% of the PM_{2.5}-associated bacteria in the SCISTW and half in the urban site could be traced back to the currently selected sources, while only 25% in the coastal site could be explained (Figure 6-12A). Corresponding to the comparable bacterial community structure in PM_{2.5} samples between the urban and the SCISTW sites (Figure 6-3), the source profiles of PM_{2.5}-associated bacteria were also relatively consistent in these two sites, where soils were the dominant contributor accounting for 22%–29%. However, this proportion was compressed to only 5% in coastal areas. In addition, there was an elevated contribution of WWTP to the ambient airborne bacteria, presented as the combination of sewage, sludge, and effluent, ranging from 14% in the coastal site to 18% in the urban and the SCISTW sites. Specifically, sludge was the biggest contributor (13%) to bacteria in urban and SCISTW PM_{2.5} among WWTP matrices, followed by sewage (3%–4%) and effluent (<2%). It was not unexpected that a large portion of the PM_{2.5}-associated bacteria was apportioned to unknown sources because other important potential sources, like nearby vegetation and skin/exhaled air from Hong Kong residents, were not included into the

model due to their lack of metagenomic analysis. In contrast to the differentiation of bacterial source profile between the coastal site and the other two sites under intense human impacts, the ARG source profile was more comparable among the three sampling sites with <12% of the PM_{2.5}-associated ARGs from undetermined sources (Figure 6-12B). It was generally discerned that more than 36% of the PM_{2.5}-associated ARGs could be ascribed to WWTP (comparable shares from sewage, sludge, and effluent), followed by freshwater and landfill leachate. The disparities between the source profiles of PM_{2.5}-associated bacteria and ARGs might reveal different enrichment levels of ARGs in various source environments. Specifically, WWTPs, represented by the SCISTW in this study, were responsible for up to 18% of the PM_{2.5}-associated bacteria but a much higher proportion of ARGs in the three sites as mentioned above. This finding might confirm that WWTPs are an important urban ARG hotspot and could be a major anthropogenic source of ARGs to the atmospheric environment. There were similar phenomena of ARG enrichment at different levels in other sources except for soil (Figure 6-12). Based on the current resolved sources, the PM_{2.5}-associated bacteria in urban Hong Kong were more likely to have a terrestrial origin, while the ARGs relevant to ARB might be more attributed to aquatic systems.

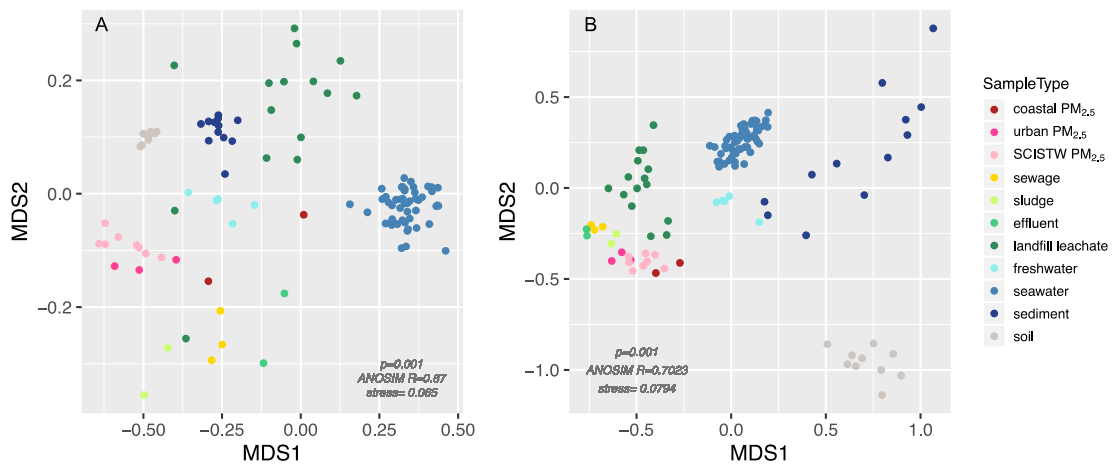


Figure 6-11 NMDS analysis of (A) the bacterial community structure at the genus level and (B) the ARG profile at the subtype level of different sample types used in source tracking.

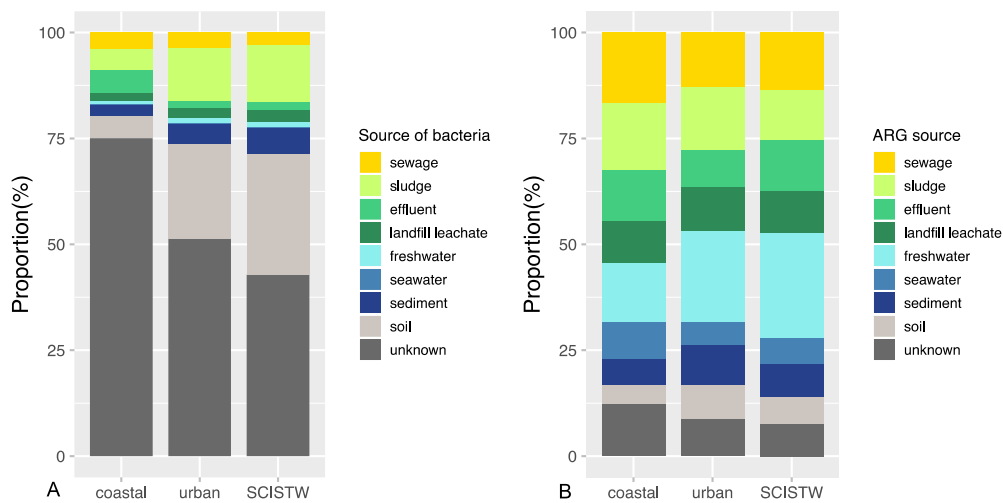


Figure 6-12 Contributions of various potential sources to (A) PM_{2.5}-associated bacteria and (B) ARGs in coastal, urban, and SCISTW sites analysed by SourceTracker2.

6.5 Summary

The SCISTW in Hong Kong, a highly developed city in the PRD, was selected as a representative to conduct further investigations on the contributions of potential anthropogenic sources to airborne bacteria and associated ARGs in urban areas. PM_{2.5},

sewage, sludge, and effluent samples from the SCISTW, as well as PM_{2.5} samples in an urban site and a coastal site as background reference, were collected simultaneously for molecular biological experiments and bioinformatic analysis. This study highlights the dissemination of ARGs and the hosted bacteria from typical urban sources like WWTPs to the ambient atmosphere and provides a quantitative source profile of airborne bacteria and ARGs in PM_{2.5} in Hong Kong. The major results of this chapter are provided below.

1. There was a high degree of overlap in bacterial taxa at the genus level between PM_{2.5} and non-PM_{2.5} (sewage/sludge/effluent) samples, which indicates that PM_{2.5} could be an important bacterial habitat with a high level of bacterial richness. According to the bacterial community structure, PM_{2.5} with a higher abundance of Actinobacteria were generally distinguished from other non-air samples. When making comparisons among PM_{2.5} from different sampling sites, urban and SCISTW PM_{2.5}, with heavier bacterial loads, showed incompletely similar bacterial profiles from the coastal reference PM_{2.5}. This phenomenon could be due to the stronger anthropogenic influence on the airborne microbes in these two sites.

2. In general, the most enriched ARG types presented a similar pattern across different sample types with the relative abundance in descending order of multidrug resistance > MLS/peptide resistance ≥ rifamycin/tetracycline resistance in PM_{2.5}/sludge and beta-lactam/tetracycline resistance in sewage/effluent. However, the total resistome profile on the basis of drug resistance type or ARG subtype segregated PM_{2.5} from other non-air samples. More unique ARGs and different bacterial community structures in PM_{2.5} indicate that airborne particles are a unique environmental reservoir for ARGs with associations to their potential hosts. There was an increasing trend for the relative

abundance of total detected PM_{2.5}-associated ARGs across the coastal–urban–SCISTW gradient; this finding illustrates the impacts of human activities on ARG accumulation in the atmosphere.

3. Only a small minority of ARGs were co-localised with MGEs on assembled scaffolds – whether in PM_{2.5} or non-PM_{2.5} samples – except the coastal PM_{2.5} with no mobile ARGs detected. Among the potentially mobile ARGs, >50% encoded resistance to rifamycin in PM_{2.5}, in contrast to an elevated proportion of glycopeptide and tetracycline resistance genes following multidrug resistance genes in sewage/effluent and sludge, respectively. The disparities between the total ARG and mobile ARG profiles suggest the inequivalent dissemination risks of different ARGs through HGT.

4. Considering the occurrence frequencies of ARGs, ARGs–MGEs, and ARGs–MGEs–putative pathogens, there was a lower estimated resistome risk score of PM_{2.5} compared with non-PM_{2.5} samples, while it was comparable within PM_{2.5} samples from different locations. From a metagenomic perspective, this outcome might indicate a lower probability of HGT events of ARGs, including their propagation to putative human pathogens that occurs in the atmosphere.

5. Some ESKAPE and WHO priority pathogens with antibiotic resistance were detected in urban and SCISTW PM_{2.5}. Fortunately, none of them harboured antibiotic resistance with clinical concerns; this finding illustrates that pathogens with clinically acquired resistance had not yet been transmitted to the atmospheric environment according to the current study.

6. According to the results of source tracking, liquid/solid matrices in WWTP (sewage, sludge, and effluent) contributed ~18% to the PM_{2.5}-associated bacteria (dominant contribution from sludge) and >36% to the relevant airborne ARGs (comparable contribution from the three matrices in WWTPs) in urban areas and within the WWTP. This finding confirms that WWTP as an important urban ARG hotspot could be a major anthropogenic source of ARGs in the atmospheric environment.

In conclusion, following up with the discussions of inter-regional and intra-regional disparities in bacterial load and ARG burden limited to certain common subtypes in PM_{2.5} in Chapter 5, the investigations in the current chapter narrowed down the scope and focused on one of the typical urban ARG hotspots (WWTPs), with literature data on other potential sources as supplements, to provide a quantitative view on the contributions of different emission sources to the ambient PM_{2.5}-associated bacteria and ARGs. Both the resolved source profiles of PM_{2.5}-associated bacteria and ARGs were found different from sources of chemical components in PM_{2.5}; such a disparity highlights different source control strategies adaptive to these two kinds of PM_{2.5} components. This chapter pointed out that WWTPs could be an important source of biological contents in PM_{2.5}, especially the bacterially associated ARGs. Sludge was the key matrix responsible for the PM_{2.5}-associated bacteria emitted from WWTPs. In contrast, the higher contribution to airborne ARG from WWTPs (36%) was comparably shared by sludge, sewage, and effluent. Therefore, additional measures are required in the future to control the aerosolisation of sludge-borne and sewage-borne biological contaminants and their emission to the atmosphere.

Chapter 7 Conclusions and Recommendations

7.1 Overall summary and major conclusions

The current one-year study on PM_{2.5} pollution in the YRD and PRD – two of the most densely populated regions in China – aimed to characterise the geographical disparities in PM_{2.5} from both chemical and biological perspectives and further link the potential health risks to their sources. First, based on the selected cities, the spatiotemporal variations in PM_{2.5} chemical compositions were compared between the two regions and across geographical locations under different land-use impacts within each region. By incorporating metal speciation and bioaccessibility information, health risk-oriented source apportionment was conducted to identify the source contributors of inhalational risks derived from PM_{2.5}-associated metals (Chapter 4). Then, the biological components of PM_{2.5}, including bacteria and several kinds of associated ARGs and MGEs that were less explored but had critical health implications, were measured for their geographical distributions and region-specific exposure risks (Chapter 5). Third, to estimate the contributions of putative sources to PM_{2.5}-associated bacteria and ARGs, a typical WWTP in Hong Kong in the PRD as an urban ARG hotspot was selected for extensive studies using metagenomic approaches (Chapter 6). Collectively, this thesis provided a panorama of PM_{2.5} pollution in the YRD and PRD by chemical and biological characterisations and connected the potential emission sources and the consequent health implications. This integrated approach could be expanded to pinpoint the key health-relevant sources of PM_{2.5}, which has important implications for the formulation of source control strategies to reduce human health risks. The major findings and conclusions of this thesis are listed below.

1. PM_{2.5} pollution in the YRD and PRD regions exhibited clear seasonal and spatial characteristics regarding concentration and chemical compositions. PM_{2.5} concentrations were found to peak in the spring and winter and to vary across geographical locations, the highest of which was in sites under industrial influence. The regional patterns of PM_{2.5} chemical composition (including OC, EC, WSI, and metals) were differentiated, with a higher contribution from secondary inorganic aerosols and a lower contribution from carbonaceous matters in the YRD compared with the PRD.

2. Metals could be a key chemical component of PM_{2.5} that pose adverse health effects on humans. Disparities in PM_{2.5}-associated metal profiles between selected sites within each region reflected the influence of land use, with anthropogenically enriched metals (*e.g.*, Zn, Pb, As, and Cd in the PRD and Cu in the YRD) accumulating superlatively at the industrial sites. By contrast, the bioaccessibility of most analysed metals was generally spatially consistent both within and between regions. When the metal bioaccessibility and speciation information was incorporated into the risk assessment model, the estimated CR over the safety level could be attributable to chromium and arsenic. Traffic emission and non-traffic combustion (coal/waste/biomass burning) were the common dominant sources of metal-induced CR across selected cities in the two regions, besides an elevated contribution from industrial emissions in the YRD sites. The differentiation between the source-resolved risk profile and source-resolved mass profile of PM_{2.5}-associated metals further implied that regulatory control of PM_{2.5} should shift from mass concentration-based framework to risk-based paradigm for real public health benefit.

3. Motivated by the importance of an integrated understanding of PM_{2.5} pollution to mitigate health impact, attention was then turned to the less explored biological fractions. Bacteria and associated-ARGs were found to be ubiquitous in PM_{2.5} across spatiotemporal scales. The more pronounced seasonal variations in airborne bacterial load at the (semi)rural sites in both regions, revealing the natural rhythm, could be flattened by anthropogenic activities in urban areas. Emission sources and climate conditions played an important role in regulating the bacterial abundance and structure, while the chemical composition of PM_{2.5} had limited effects. In contrast, the ARG profile based on limited target genes was independent of seasonal cycles and land-use types within each region. Despite inter-regional differences in the fingerprints of antibiotic resistance, the studied ARGs were commonly correlated with MGEs across regions and speculatively associated with limited bacterial genera. PM_{2.5} was at the higher end of ARG and MGE enrichment across various environmental media and human excreta. Based on comparisons with ingestion of drinking water and food, inhalation of PM_{2.5} could be an important exposure pathway for ARG intake. Therefore, the spatiotemporal difference in bacterial and ARG abundance could imply region-specific importance of inhalation in bacterial and ARG exposure.

4. Finally, the WWTP study using metagenomic sequencing revealed the disparate bacterial and ARG profiles between PM_{2.5} and non-air samples (sewage/sludge/effluent), though multidrug-resistance genes were commonly dominant in the antibiotic resistome. The increasing relative abundance of identified ARGs in PM_{2.5} across the coastal–urban–WWTP gradient indicates the impacts of human activities on ARG accumulation in the atmosphere. Fortunately, the co-occurrence analysis of ARGs, MGEs and putative pathogens suggests a low probability of HGT events of ARGs in the atmosphere,

especially for the transfer to pathogens. Lastly, the significant contribution of sewage, sludge, and effluent in WWTP to PM_{2.5}-associated bacteria and ARGs confirm that WWTPs could be a major anthropogenic source of ARGs in the atmospheric environment. The great differences in source profiles of chemical and microbial hazards in PM_{2.5} motivate us to adopt different source control strategies in the future.

7.2 Limitations of the current study and future perspectives

Although the PM_{2.5} pollution in selected cities in the YRD and PRD was collectively investigated from both the chemical and the biological perspective and extended to emission sources and health implications, which could be more comprehensive than the previous studies that mainly explored the chemical compartment of PM_{2.5}, the current results are restricted by certain aspects like the models and experimental techniques applied, the experimental settings, and so on. Some limitations and the relevant recommendations are briefly discussed below.

The assessment of metal-induced exposure risks in this thesis was based on the USEPA standard guidelines and quantitatively adjusted according to arsenic speciation detected via the XANES technique. The low concentration of Cr did not support the XANES analysis of its speciation. Therefore, the quantitative share of Cr(VI) in total Cr (1/7) assumed by the USEPA (2018b) was adopted. Although the refined method can significantly reduce the overestimation of metal-induced risks, certain biases still exist in the result since the Cr species was not determined from our real samples. This uncertainty highlights the need for more robust characterisations of toxic metal forms in PM_{2.5} or adjustments of the future sampling strategy to acquire airborne particles with enough Cr content for XANES analysis. In addition, other heavy metals like Fe and Cu had been

identified as dominant drivers of metal-derived oxidative stress in human lung cells exposed to urban PM_{2.5} (Jin et al., 2019). This finding contrasts with the current observation in the present study that these elements contributed little to the health risks posed by PM_{2.5}-associated metals. This is understandable because of the inconsistencies in the relative toxic potencies of metals between the two assessment systems and because of the incorporation of bioaccessibility in lieu of total concentrations in this study. It is therefore imperative to develop robust predictive models to reconcile the data on *in vitro* toxicity and the safety limits derived from human epidemiological studies on inhalable metals. Moreover, our adjusted model for health-oriented source apportionment still relied on a number of default exposure and population parameters and the assumption of the equal bioaccessibility of a certain metal for various source categories. Thus, it is necessary to refine the relevant parameters to reflect local scenarios, investigate the speciation profile of metals in different sources, and apportion the health risks to emission sources according to a more realistic basis – source-specific metal bioavailability.

Compared with the relatively well-studied chemical part, the (micro)biological fraction has been far less investigated and remains a lot for exploration and standardisation. First, the comparisons of absolute abundance of bacterial and ARG loads in PM_{2.5} in the current study were based on the assumption of equal DNA extraction efficiency across samples, while the *de facto* extraction performances were unknown. To improve the current assessment method, internal standards like a model bacterium containing an artificial gene fragment can be added into samples in future applications. By quantifying the copy number of artificial genes in DNA extracts, the extraction efficiency can be used as an adjustment factor to correct the absolute abundance of the target gene context. Analogously, the mock bacterial community can be used to estimate the sequencing

performance. Limited by traditional qPCR, the current investigations of the ARG profile in PM_{2.5} between the two studied regions only targeted certain kinds of ARGs. To obtain a comprehensive ARG profile across geographical locations, either metagenomic sequencing or high-throughput qPCR is desired to conduct a broader-spectrum scan of ARGs in PM_{2.5} with extension to a national, continental, and even global scale. Moreover, the pretreatment method before DNA extraction in the current study captured the microbial cells retained on 0.2- μ m PES membrane disc filters; other biological contents were discarded along with the filtrate. This process means that this study only presented the spatiotemporal dynamics of intracellular ARGs. However, the extracellular fraction (*e.g.*, free ARGs and those ARGs carried by viruses that have not infected any potential hosts) could serve as another important portion in the whole PM_{2.5}-associated antibiotic resistome (He et al., 2021). With a much smaller size (PM_{0.1} level), the extracellular ARGs could penetrate deeper into the human respiratory tract and become an additional source for pulmonary microbial communities to acquire antibiotic resistance via HGT (*e.g.*, transformation and transduction).

In the third part of this project, SourceTracker2 was applied to estimate quantitatively the contributions of various sources to PM_{2.5}-associated bacteria and ARGs based on the taxonomy and ARG profile of sink and source samples. However, the complex interactions between bacterial taxa and how environmental stress alters the bacterial communities after their aerosolisation from putative sources seemed not to be considered extensively in the algorithm. A combination of aerodynamic transport models and monitoring of the dynamic process of aerosolisation in different heights above sources may help to further resolve the flux and dissemination of bacteria and ARGs from urban spots to the ambient atmosphere. In addition, some of the sequencing data of source

samples were obtained from studies conducted in nearby provinces or even in a farther region due to the limited available metagenomic data. As mentioned in Chapter 5, the microbial and ARG profile of environmental samples could be subject to local and regional influences and exhibited geographically dependent features. Thus, the application of these data in the source tracking model may result in certain biases. In consideration of this eventuality, it is important to conduct a metagenomic-based survey in various local putative sources, including those not involved in the current study, like vegetation, hospitals, and humans (exhaled air and skin), to further fill the unknown fractions with more sources. Benefit from the development of sequencing technologies, metagenomic next-generation sequencing of the genomic content in PM_{2.5} (with low DNA input for library construction) became feasible in this case study. Based on the co-occurrence pattern of the targeted genetic context on assembled scaffolds, various ARG-carrying bacteria, especially for pathogenic hosts with prior clinical relevance, were identified in the PM_{2.5} samples in the urban and WWTP sites. However, culture-dependent techniques are still required to confirm the viability of these hosts and the expression of antibiotic resistance. The integration of genotypic and phenotypic analysis by metagenomic sequencing and culture-dependent methods in the future can thus help to better understand the environmental fate and health effect of antibiotic resistance and other critical airborne microbial hazards, especially for human pathogens, including pathogenic fungi and viruses that are not yet explored from the metagenomic data in the current study.

Finally, regarding the PM_{2.5} compositions with health implications, this thesis only selected certain types of chemical (*e.g.*, heavy metals) and microbial components (*e.g.*, bacteria and associated ARGs) for intensive study. To achieve a comprehensive health

risk-oriented air quality management, a thorough dissection of both chemical and microbial toxicity-driving components in PM_{2.5} is necessarily required. After that, it is of significance to develop robust models for integrated risk assessment of chemical and microbial hazards, with consideration of their joint toxicity, in order for the better health impact-oriented source control of PM_{2.5} pollution.

Appendix 1

Detailed information of the source data used in SourceTracker2 besides the samples collected from the SCISTW in this study.

Source category	SRA study	Run/Sample name	Description	Database
Freshwater	SRP033730	SRR1047946	Influent for drinking water treatment in Hong Kong	NCBI
		SRR1047948		
		SRR1047951		
		SRR1047952		
		SRR1047954		
Sediment	SRP061803	SRR2134631	Marine sediment in Hong Kong	NCBI
		SRR2134632		
		SRR2134633		
		SRR2134637		
		SRR2134639		
		SRR2134640		
		SRR2134642		
		SRR2134644		
		SRR2134634		
		SRR2134636		
		SRR2134641		
		SRR2134643		
Seawater	ERP001736	ERR598943	Surface seawater (<5 m) collected in the Pacific and Indian Ocean	NCBI
		ERR598954		
		ERR598966		
		ERR598967		
		ERR598970		
		ERR598978		
		ERR598979		
		ERR598989		
		ERR598992		
		ERR598997		
		ERR599011		
		ERR599012		
		ERR599019		
		ERR599024		
		ERR599029		
ERR599030				

Source category	SRA study	Run/Sample name	Description	Database
Seawater	ERP001736	ERR599036	Surface seawater (<5 m) collected in the Pacific and Indian Ocean	NCBI
		ERR599038		
		ERR599039		
		ERR599045		
		ERR599050		
		ERR599052		
		ERR599054		
		ERR599057		
		ERR599058		
		ERR599063		
		ERR599064		
		ERR599066		
		ERR599069		
		ERR599074		
		ERR599075		
		ERR599077		
		ERR599080		
		ERR599088		
		ERR599091		
		ERR599093		
		ERR599098		
		ERR599102		
		ERR599114		
		ERR599118		
		ERR599119		
		ERR599120		
		ERR599138		
ERR599139				
ERR599141				
ERR599142				
ERR599143				
ERR599146				
ERR599150				
ERR599151				
ERR599158				
ERR599160				
ERR599162				
ERR599163				
ERR599169				
Soil	SRP039858	SRR1190308	Paddy soil collected in south China	NCBI

Source category	SRA study	Run/Sample name	Description	Database
Soil	SRP039858	SRR1190311	Paddy soil collected in south China	NCBI
		SRR1190316		
		SRR1190334		
		SRR1190336		
		SRR1190349		
		SRR1190350		
		SRR1190383		
		SRR1190384		
		SRR1190306		
Landfill leachate	mgp21084	SWL_1	Leachate collected in landfills in China	MG-RAST
		SWL_3		
		SWL_4		
		SWL_5		
		SWL_6		
		SWL_7		
		SWL_8		
		SWL_10		
		SWL_11		
		SWL_14		
		SWL_15		
		SWL_16		
		SWL_17		
		SWL_18		
SWL_19				

Appendix 2

This section provides a database of the experimental results of the thesis.

1. Concentrations of carbonaceous materials and WSI ($\mu\text{g m}^{-3}$; mean \pm standard deviation)

Site	Season	OC	EC	Na ⁺	NH ₄ ⁺	K ⁺	Cl ⁻	SO ₄ ²⁻	NO ₃ ⁻
TH	spring	4.96 \pm 2.24	3.57 \pm 2.01	0.36 \pm 0.20	4.04 \pm 3.27	0.47 \pm 0.27	0.90 \pm 0.65	7.14 \pm 3.50	6.90 \pm 8.16
	summer	4.10 \pm 1.58	2.57 \pm 0.99	0.50 \pm 0.28	0.94 \pm 1.01	0.25 \pm 0.12	0.30 \pm 0.17	3.96 \pm 2.21	2.06 \pm 1.75
	autumn	4.73 \pm 2.13	3.11 \pm 1.57	0.39 \pm 0.17	2.11 \pm 1.06	0.41 \pm 0.23	0.47 \pm 0.37	5.83 \pm 2.75	2.41 \pm 1.81
	winter	5.22 \pm 2.19	3.17 \pm 1.35	0.29 \pm 0.17	2.50 \pm 1.03	0.41 \pm 0.18	0.37 \pm 0.23	5.26 \pm 2.00	3.92 \pm 2.20
	annual	4.74 \pm 2.02	3.08 \pm 1.50	0.39 \pm 0.22	2.34 \pm 2.09	0.38 \pm 0.22	0.50 \pm 0.45	5.48 \pm 2.82	3.76 \pm 4.58
CH	spring	4.07 \pm 2.43	2.46 \pm 1.32	0.29 \pm 0.14	3.27 \pm 1.59	0.41 \pm 0.22	0.16 \pm 0.08	8.35 \pm 2.72	3.06 \pm 3.00
	summer	3.38 \pm 1.54	1.82 \pm 1.20	0.21 \pm 0.15	2.03 \pm 1.60	0.20 \pm 0.14	0.13 \pm 0.15	5.20 \pm 3.62	1.06 \pm 1.50
	autumn	3.18 \pm 1.60	1.73 \pm 1.07	0.10 \pm 0.06	2.19 \pm 1.22	0.25 \pm 0.18	0.07 \pm 0.12	6.19 \pm 3.23	0.63 \pm 0.96
	winter	5.04 \pm 2.67	2.80 \pm 1.46	0.18 \pm 0.08	2.38 \pm 1.09	0.46 \pm 0.23	0.14 \pm 0.10	5.80 \pm 3.03	1.53 \pm 1.13
	annual	3.93 \pm 2.16	2.21 \pm 1.31	0.20 \pm 0.13	2.43 \pm 1.42	0.32 \pm 0.22	0.13 \pm 0.12	6.27 \pm 3.29	1.53 \pm 1.92
HS	spring	5.11 \pm 3.01	3.02 \pm 1.60	0.58 \pm 0.43	3.53 \pm 2.23	0.62 \pm 0.39	1.03 \pm 0.86	7.36 \pm 3.10	5.05 \pm 5.18
	summer	3.17 \pm 1.17	1.94 \pm 1.07	0.29 \pm 0.11	1.66 \pm 1.24	0.32 \pm 0.15	0.33 \pm 0.27	4.24 \pm 2.44	1.69 \pm 1.76
	autumn	5.83 \pm 2.21	4.02 \pm 1.81	0.46 \pm 0.19	4.18 \pm 2.48	0.78 \pm 0.37	0.68 \pm 0.50	9.71 \pm 5.21	3.43 \pm 2.66
	winter	8.23 \pm 2.73	5.96 \pm 3.20	0.37 \pm 0.17	5.95 \pm 2.93	0.98 \pm 0.46	0.92 \pm 0.52	9.38 \pm 3.77	10.64 \pm 8.8
	annual	5.39 \pm 2.89	3.59 \pm 2.43	0.42 \pm 0.27	3.67 \pm 2.67	0.65 \pm 0.42	0.71 \pm 0.61	7.48 \pm 4.29	4.85 \pm 5.90
PK	spring	5.42 \pm 1.37	3.43 \pm 1.02	0.81 \pm 0.15	8.56 \pm 2.82	0.78 \pm 0.37	1.48 \pm 1.12	13.22 \pm 4.44	12.63 \pm 6.11
	summer	4.24 \pm 1.66	2.38 \pm 0.90	0.82 \pm 0.20	4.83 \pm 1.99	0.35 \pm 0.15	0.46 \pm 0.47	9.82 \pm 4.12	4.69 \pm 2.77
	autumn	5.73 \pm 1.52	3.07 \pm 1.18	1.51 \pm 0.97	5.94 \pm 2.62	0.74 \pm 0.34	1.53 \pm 1.18	10.83 \pm 4.06	9.78 \pm 3.62

Site	Season	OC	EC	Na ⁺	NH ₄ ⁺	K ⁺	Cl ⁻	SO ₄ ²⁻	NO ₃ ⁻
PK	winter	6.89 ± 2.42	4.34 ± 2.41	1.26 ± 0.31	11.84 ± 4.56	0.74 ± 0.31	2.05 ± 0.86	15.94 ± 4.98	20.76 ± 12.13
	annual	5.56 ± 1.90	3.31 ± 1.55	1.09 ± 0.59	7.81 ± 3.95	0.67 ± 0.34	1.39 ± 1.09	12.47 ± 4.79	11.96 ± 8.70
XW	spring	6.03 ± 1.37	3.35 ± 0.91	0.79 ± 0.19	8.25 ± 3.27	0.52 ± 0.22	1.08 ± 0.57	12.21 ± 4.4	13.62 ± 6.50
	summer	4.67 ± 1.64	2.27 ± 0.75	0.82 ± 0.20	4.99 ± 2.68	0.35 ± 0.15	1.71 ± 1.19	9.80 ± 4.04	7.21 ± 3.41
	autumn	5.31 ± 1.46	2.80 ± 1.45	1.39 ± 0.44	4.47 ± 2.29	0.43 ± 0.14	2.77 ± 1.30	7.35 ± 2.61	8.42 ± 4.11
	winter	6.48 ± 2.61	4.02 ± 2.38	1.31 ± 0.26	11.05 ± 5.31	0.60 ± 0.26	2.45 ± 0.65	13.73 ± 5.97	20.67 ± 11.97
	annual	5.65 ± 1.80	3.13 ± 1.54	1.05 ± 0.39	7.28 ± 4.27	0.48 ± 0.22	1.93 ± 1.14	10.9 ± 4.85	12.58 ± 8.63
LS	spring	3.64 ± 1.30	2.44 ± 1.19	0.80 ± 0.01	6.52 ± 1.18	0.50 ± 0.03	1.26 ± 0.09	10.91 ± 2.29	8.91 ± 1.20
	summer	3.81 ± 0.89	1.97 ± 0.67	0.69 ± 0.18	4.29 ± 3.02	0.37 ± 0.06	0.99 ± 0.82	8.72 ± 4.70	4.25 ± 3.66
	autumn	3.34 ± 0.64	1.59 ± 0.38	1.16 ± 0.30	2.61 ± 0.08	0.28 ± 0.06	1.11 ± 0.41	5.35 ± 1.24	3.63 ± 2.15
	winter	5.99 ± 6.01	3.56 ± 3.10	1.02 ± 0.11	6.92 ± 3.74	0.38 ± 0.12	1.70 ± 0.73	8.85 ± 3.65	10.76 ± 4.98
	annual	4.42 ± 3.48	2.48 ± 1.92	0.91 ± 0.25	5.13 ± 3.12	0.37 ± 0.10	1.29 ± 0.68	8.38 ± 3.70	6.92 ± 4.73

2. Total metal(loid) concentrations (ng m⁻³; mean ± standard deviation)

Site	Season	Al	Fe	As	Cd	Cr*	Cu
TH	spring	552.18 ± 350.30	376.75 ± 262.83	4.74 ± 2.55	0.72 ± 0.54	4.24 ± 2.09	18.38 ± 11.89
	summer	833.41 ± 439.37	601.69 ± 339.75	2.54 ± 1.24	0.44 ± 0.23	12.29 ± 10.10	13.52 ± 6.86
	autumn	778.77 ± 410.55	503.78 ± 248.98	5.18 ± 2.99	0.89 ± 0.40	6.61 ± 3.29	18.32 ± 11.01
	winter	892.96 ± 460.21	477.04 ± 281.65	5.33 ± 3.04	0.95 ± 0.49	16.44 ± 12.95	15.8 ± 8.33
	annual	769.56 ± 426.10	493.95 ± 290.74	4.39 ± 2.72	0.74 ± 0.46	10.12 ± 9.65	16.37 ± 9.53
CH	spring	593.84 ± 357.93	332.64 ± 247.07	5.49 ± 2.83	0.68 ± 0.50	3.07 ± 1.59	10.9 ± 7.73
	summer	566.00 ± 547.86	326.11 ± 378.21	2.93 ± 2.74	0.47 ± 0.35	2.70 ± 1.95	7.82 ± 4.67
	autumn	429.41 ± 205.04	281.79 ± 204.31	6.44 ± 7.99	0.97 ± 1.05	4.76 ± 4.56	10.85 ± 9.03
	winter	902.37 ± 460.21	245.87 ± 281.65	6.97 ± 3.04	1.22 ± 0.49	4.36 ± 12.95	11.68 ± 8.33

Site	Season	Al	Fe	As	Cd	Cr*	Cu
CH	annual	632.37 ± 414.72	296.29 ± 261.17	5.34 ± 4.66	0.83 ± 0.71	3.68 ± 2.72	10.2 ± 7.73
	spring	879.51 ± 1114.58	337.49 ± 401.24	15.39 ± 15.51	1.05 ± 0.66	9.39 ± 7.41	14.71 ± 9.08
HS	summer	626.57 ± 616.94	272.74 ± 149.88	8.95 ± 5.93	0.83 ± 1.09	8.57 ± 11.08	7.29 ± 2.62
	autumn	665.01 ± 321.37	459.27 ± 242.59	18.69 ± 15.38	1.79 ± 1.48	13.63 ± 9.70	21.06 ± 15.34
	winter	1076.01 ± 435.90	571.35 ± 271.05	11.1 ± 5.39	2.28 ± 1.16	7.07 ± 1.97	43.63 ± 31.12
	annual	792.82 ± 688.95	399.93 ± 289.3	13.41 ± 11.86	1.44 ± 1.25	9.73 ± 8.71	20.38 ± 21.17
PK	spring	294.33 ± 233.79	652.34 ± 459.12	7.82 ± 3.74	2.17 ± 0.89	13.85 ± 9.03	38.36 ± 18.95
	summer	173.39 ± 85.19	376.79 ± 255.19	5.58 ± 3.75	1.54 ± 1.15	22.96 ± 20.82	35.42 ± 16.78
	autumn	229.94 ± 95.01	531.95 ± 206.82	10.16 ± 12.06	3.55 ± 2.88	92.62 ± 52.50	59.69 ± 36.08
	winter	222.88 ± 99.32	942.30 ± 1099.20	8.53 ± 5.30	2.01 ± 1.07	127.11 ± 87.23	95.63 ± 52.32
	annual	235.48 ± 152.04	625.44 ± 603.51	8.07 ± 6.95	2.34 ± 1.78	60.74 ± 67.44	55.76 ± 39.51
XW	spring	246.3 ± 105.41	432.20 ± 146.20	7.5 ± 3.27	1.84 ± 0.96	10.06 ± 6.47	20.78 ± 9.77
	summer	157.34 ± 45.05	295.33 ± 98.91	6.33 ± 3.16	1.62 ± 1.07	9.00 ± 3.73	16.64 ± 16.28
	autumn	195.50 ± 62.23	440.48 ± 181.44	5.00 ± 4.12	1.65 ± 0.96	117.83 ± 109.80	17.15 ± 7.90
	winter	232.42 ± 156.52	471.51 ± 217.87	6.53 ± 3.64	2.41 ± 1.88	198.21 ± 91.38	29.47 ± 29.68
	annual	211.18 ± 103.79	411.79 ± 170.91	6.44 ± 3.50	1.88 ± 1.23	77.46 ± 102.97	20.99 ± 17.37
LS	spring	255.82 ± 159.7	304.67 ± 166.58	5.83 ± 1.72	0.98 ± 0.26	6.26 ± 0.73	10.15 ± 3.30
	summer	329.53 ± 71.53	372.91 ± 147.86	5.31 ± 2.21	0.96 ± 0.36	11.08 ± 7.21	15.29 ± 17.10
	autumn	190.37 ± 34.01	400.16 ± 164.91	4.25 ± 2.48	0.77 ± 0.03	60.88 ± 1.59	18.95 ± 9.75
	winter	243.83 ± 193.76	457.80 ± 314.48	5.15 ± 3.01	1.27 ± 0.95	77.96 ± 33.93	14.94 ± 8.52
	annual	320.20 ± 130.48	591.21 ± 207.65	6.94 ± 2.31	1.89 ± 0.58	79.42 ± 37.49	26.17 ± 11.20

*Conversion based on Cr recovery

Site	Season	Mn	Ni	Pb	V	Zn	Co
TH	spring	18.01 ± 10.38	7.84 ± 4.86	25.00 ± 16.07	9.21 ± 6.24	148.16 ± 77.79	0.65 ± 0.57
	summer	12.99 ± 10.84	6.61 ± 5.31	15.98 ± 8.44	4.55 ± 2.51	106.18 ± 38.13	0.60 ± 0.32
	autumn	10.44 ± 4.44	4.76 ± 3.14	31.05 ± 17.00	2.39 ± 2.07	135.51 ± 49.43	0.49 ± 0.27

Site	Season	Mn	Ni	Pb	V	Zn	Co
TH	winter	10.82 ± 5.56	3.69 ± 1.57	31.18 ± 14.79	3.18 ± 3.19	123.25 ± 47.90	0.37 ± 0.23
	annual	13.02 ± 8.65	5.72 ± 4.23	25.52 ± 15.25	4.79 ± 4.51	127.31 ± 55.20	0.53 ± 0.37
CH	spring	8.27 ± 4.97	3.92 ± 2.49	21.74 ± 16.76	6.01 ± 2.97	94.59 ± 46.83	0.36 ± 0.36
	summer	6.28 ± 6.54	2.60 ± 1.12	15.74 ± 10.81	3.43 ± 2.45	83.08 ± 46.40	0.20 ± 0.19
	autumn	7.92 ± 6.17	2.40 ± 1.45	34.46 ± 39.14	2.04 ± 2.19	99.47 ± 69.53	0.18 ± 0.10
	winter	7.27 ± 5.56	1.74 ± 1.57	37.29 ± 14.79	1.61 ± 3.19	106.70 ± 47.90	0.35 ± 0.23
	annual	7.34 ± 5.41	2.62 ± 1.68	26.95 ± 24.23	3.20 ± 2.73	95.54 ± 55.60	0.27 ± 0.23
HS	spring	18.49 ± 14.05	7.16 ± 4.70	28.35 ± 15.08	8.83 ± 4.10	199.56 ± 95.12	0.52 ± 0.39
	summer	10.58 ± 5.15	4.46 ± 3.55	16.58 ± 7.98	4.81 ± 3.45	97.08 ± 38.17	0.24 ± 0.13
	autumn	14.38 ± 8.53	5.39 ± 4.73	61.31 ± 39.93	6.26 ± 5.92	242.31 ± 129.42	0.46 ± 0.22
	winter	18.33 ± 6.57	4.88 ± 2.29	71.53 ± 34.01	3.54 ± 1.81	281.20 ± 160.87	0.82 ± 0.26
	annual	15.08 ± 9.39	5.42 ± 3.99	42.61 ± 34.77	5.85 ± 4.44	197.92 ± 129.16	0.49 ± 0.33
PK	spring	14.88 ± 8.43	3.9 ± 1.73	93.08 ± 47.24	6.7 ± 3.97	338.21 ± 214.49	0.37 ± 0.22
	summer	10.71 ± 5.80	2.97 ± 1.65	44.13 ± 20.82	4.23 ± 2.88	207.57 ± 161.06	0.21 ± 0.13
	autumn	32.88 ± 12.40	7.41 ± 3.67	83.63 ± 70.06	11.56 ± 11.90	318.94 ± 116.76	0.38 ± 0.11
	winter	35.15 ± 18.00	6.45 ± 3.50	69.23 ± 27.00	7.59 ± 4.42	244.61 ± 155.70	0.44 ± 0.25
	annual	22.96 ± 15.53	5.14 ± 3.20	74.54 ± 48.37	7.56 ± 7.02	283.56 ± 170.95	0.35 ± 0.20
XW	spring	14.11 ± 5.42	3.32 ± 1.78	59.29 ± 24.30	4.41 ± 2.97	226.66 ± 80.44	0.32 ± 0.28
	summer	13.85 ± 8.97	2.79 ± 2.01	40.92 ± 18.98	4.05 ± 3.18	180.40 ± 106.80	0.18 ± 0.12
	autumn	30.88 ± 14.26	4.77 ± 1.48	50.46 ± 35.69	4.97 ± 2.57	234.47 ± 90.23	0.33 ± 0.13
	winter	31.18 ± 15.01	4.19 ± 1.45	66.48 ± 33.67	4.33 ± 3.58	204.31 ± 99.22	0.32 ± 0.15
	annual	21.79 ± 13.69	3.73 ± 1.79	54.72 ± 28.84	4.44 ± 2.96	212.76 ± 91.60	0.29 ± 0.20
LS	spring	9.90 ± 1.43	1.92 ± 0.49	38.43 ± 10.22	1.61 ± 0.47	142.82 ± 21.24	0.22 ± 0.12
	summer	9.98 ± 4.81	2.02 ± 0.55	26.09 ± 9.20	2.29 ± 1.22	136.91 ± 40.74	0.31 ± 0.26
	autumn	18.88 ± 9.09	3.89 ± 1.15	34.58 ± 20.00	4.14 ± 1.39	153.54 ± 51.28	0.31 ± 0.17
	winter	21.49 ± 13.47	3.23 ± 0.98	37.75 ± 16.87	3.39 ± 1.69	142.60 ± 87.32	0.35 ± 0.15
	annual	23.82 ± 10.05	4.10 ± 1.10	57.99 ± 14.14	4.74 ± 1.52	225.94 ± 55.65	0.35 ± 0.18

3. Bioaccessible metal(loid) concentration (ng m⁻³; mean ± standard deviation)

Site	Season	Fe	As	Cd	Cr	Cu	Mn
TH	spring	11.29 ± 8.12	2.48 ± 1.73	0.29 ± 0.18	1.27 ± 0.47	4.87 ± 4.29	12.83 ± 8.48
	summer	11.24 ± 7.85	1.89 ± 0.95	0.15 ± 0.12	1.32 ± 0.50	1.35 ± 1.05	12.56 ± 5.60
	autumn	19.59 ± 12.38	3.88 ± 2.63	0.37 ± 0.30	1.23 ± 0.48	1.72 ± 1.54	10.38 ± 3.34
	winter	14.41 ± 12.44	3.34 ± 1.88	0.27 ± 0.27	1.36 ± 0.58	1.77 ± 1.02	8.69 ± 3.99
	annual	14.14 ± 10.70	2.90 ± 1.99	0.25 ± 0.22	1.30 ± 0.48	2.28 ± 2.54	10.81 ± 5.53
CH	spring	19.33 ± 14.18	3.55 ± 2.34	0.32 ± 0.20	1.04 ± 0.34	5.47 ± 3.99	8.70 ± 5.18
	summer	11.79 ± 10.89	2.20 ± 1.89	0.22 ± 0.15	0.88 ± 0.58	3.96 ± 3.49	5.84 ± 4.96
	autumn	10.46 ± 8.64	4.37 ± 4.29	0.52 ± 0.70	0.61 ± 0.17	4.82 ± 4.29	5.18 ± 3.98
	winter	14.03 ± 12.44	4.04 ± 1.88	0.48 ± 0.27	0.39 ± 0.58	5.35 ± 1.02	5.32 ± 3.99
	annual	13.92 ± 11.62	3.53 ± 2.96	0.38 ± 0.41	0.72 ± 0.43	4.85 ± 3.77	5.92 ± 4.08
HS	spring	8.72 ± 8.72	8.92 ± 8.48	0.06 ± 0.12	1.22 ± 0.36	9.51 ± 5.94	10.91 ± 5.51
	summer	6.05 ± 2.69	7.07 ± 4.82	0.71 ± 1.08	1.10 ± 0.41	2.18 ± 0.85	7.10 ± 1.38
	autumn	12.47 ± 5.08	18.66 ± 8.29	0.90 ± 0.75	1.43 ± 0.53	8.33 ± 6.06	11.67 ± 3.32
	winter	17.14 ± 8.36	5.28 ± 1.66	0.69 ± 0.14	1.00 ± 0.24	18.63 ± 9.04	13.22 ± 3.40
	annual	9.57 ± 7.07	10.02 ± 8.14	0.53 ± 0.77	1.20 ± 0.41	7.82 ± 7.07	10.27 ± 4.39
PK	spring	3.27 ± 1.40	3.97 ± 2.40	0.46 ± 0.19	2.13 ± 1.33	18.69 ± 10.60	11.01 ± 4.27
	summer	3.72 ± 3.31	4.18 ± 3.15	0.44 ± 0.31	1.79 ± 1.74	9.30 ± 3.18	6.10 ± 4.38
	autumn	3.95 ± 3.36	7.73 ± 12.45	1.66 ± 1.97	3.85 ± 3.31	20.67 ± 14.53	15.28 ± 8.83
	winter	7.73 ± 5.47	6.31 ± 3.09	0.95 ± 0.40	7.07 ± 6.46	32.58 ± 18.18	15.62 ± 6.98
	annual	4.44 ± 3.69	5.38 ± 6.40	0.86 ± 1.10	3.36 ± 3.67	20.18 ± 14.54	12.25 ± 7.24
XW	spring	1.18 ± 1.03	4.66 ± 2.61	0.34 ± 0.23	1.49 ± 1.31	23.17 ± 6.03	7.41 ± 2.97
	summer	1.47 ± 1.05	3.87 ± 2.00	0.29 ± 0.21	1.93 ± 1.82	10.18 ± 11.71	5.42 ± 3.92
	autumn	2.82 ± 2.78	4.16 ± 3.80	0.61 ± 0.46	3.46 ± 2.97	5.26 ± 3.78	11.59 ± 6.30
	winter	4.56 ± 4.76	4.95 ± 4.19	1.45 ± 1.54	7.24 ± 1.03	12.89 ± 16.54	13.92 ± 6.81
	annual	2.38 ± 2.94	4.40 ± 3.01	0.65 ± 0.88	2.65 ± 2.53	11.87 ± 12.17	9.40 ± 5.87
LS	spring	2.09 ± 1.18	3.71 ± 1.22	0.14 ± 0.03	3.69 ± 0.00	3.33 ± 0.70	4.38 ± 0.18

Site	Season	Fe	As	Cd	Cr	Cu	Mn
LS	summer	1.87 ± 1.90	3.47 ± 1.51	0.21 ± 0.17	1.84 ± 1.32	6.18 ± 6.60	3.93 ± 2.44
	autumn	2.88 ± 1.44	3.70 ± 2.26	0.36 ± 0.08	2.51 ± 0.00	7.18 ± 3.87	8.86 ± 1.93
	winter	2.81 ± 2.60	2.32 ± 0.90	0.28 ± 0.25	3.38 ± 0.00	5.79 ± 4.58	9.49 ± 8.04
	annual	2.71 ± 1.89	4.59 ± 1.48	0.64 ± 0.18	3.03 ± 1.26	12.4 ± 4.28	9.99 ± 5.29

Site	Season	Ni	Pb	V	Zn	Co
TH	spring	3.88 ± 4.76	2.13 ± 1.28	6.03 ± 4.47	13.90 ± 8.12	0.45 ± 0.31
	summer	1.88 ± 1.22	1.05 ± 0.62	4.08 ± 2.23	15.09 ± 7.93	0.27 ± 0.13
	autumn	1.08 ± 0.57	1.53 ± 1.13	2.05 ± 2.09	30.02 ± 15.26	0.27 ± 0.13
	winter	0.84 ± 0.73	1.73 ± 1.11	1.99 ± 2.37	25.00 ± 20.75	0.16 ± 0.09
	annual	1.83 ± 2.50	1.57 ± 1.08	3.41 ± 3.15	21.13 ± 15.35	0.27 ± 0.19
CH	spring	2.07 ± 1.81	2.62 ± 1.07	3.18 ± 2.41	15.80 ± 9.46	0.38 ± 0.29
	summer	1.14 ± 0.62	1.98 ± 0.93	2.35 ± 2.03	12.37 ± 8.78	0.17 ± 0.17
	autumn	0.65 ± 0.60	2.52 ± 1.69	1.44 ± 1.93	13.33 ± 15.79	0.08 ± 0.05
	winter	0.50 ± 0.73	3.94 ± 1.11	0.97 ± 2.37	15.54 ± 20.75	0.11 ± 0.09
	annual	1.06 ± 1.12	2.79 ± 1.64	1.95 ± 2.00	14.23 ± 11.86	0.16 ± 0.18
HS	spring	1.54 ± 0.70	0.76 ± 0.59	4.25 ± 2.72	27.13 ± 15.37	0.18 ± 0.10
	summer	1.22 ± 0.81	1.98 ± 0.81	3.41 ± 3.18	16.42 ± 10.04	0.12 ± 0.09
	autumn	2.36 ± 1.43	2.81 ± 1.52	7.30 ± 5.84	32.63 ± 16.68	0.27 ± 0.11
	winter	1.28 ± 0.78	2.56 ± 1.04	1.05 ± 0.00	53.37 ± 27.24	0.41 ± 0.02
	annual	1.59 ± 0.99	1.79 ± 1.23	4.45 ± 3.94	27.68 ± 18.33	0.21 ± 0.13
PK	spring	1.03 ± 0.87	2.18 ± 1.66	3.13 ± 3.28	12.16 ± 12.23	0.11 ± 0.12
	summer	0.81 ± 0.61	1.66 ± 1.31	1.95 ± 2.03	5.13 ± 4.55	0.07 ± 0.06
	autumn	2.61 ± 3.18	2.78 ± 3.67	3.79 ± 2.02	21.8 ± 22.79	0.14 ± 0.10
	winter	1.80 ± 0.80	1.92 ± 1.28	3.56 ± 2.87	18.33 ± 13.04	0.23 ± 0.08
	annual	1.55 ± 1.80	2.13 ± 2.05	3.13 ± 2.63	14.05 ± 15.16	0.13 ± 0.11
XW	spring	0.82 ± 0.66	1.05 ± 0.69	2.18 ± 2.00	3.76 ± 2.33	0.11 ± 0.12

Site	Season	Ni	Pb	V	Zn	Co
XW	summer	0.62 ± 0.55	0.90 ± 0.71	1.95 ± 2.62	5.87 ± 8.93	0.06 ± 0.07
	autumn	1.23 ± 0.51	1.42 ± 1.45	3.38 ± 1.70	13.87 ± 8.95	0.17 ± 0.10
	winter	1.06 ± 0.69	1.79 ± 0.97	3.09 ± 2.42	16.42 ± 9.41	0.14 ± 0.04
	annual	0.92 ± 0.63	1.28 ± 1.00	2.61 ± 2.18	9.10 ± 8.94	0.12 ± 0.10
LS	spring	0.72 ± 0.29	0.35 ± 0.11	0.82 ± 0.15	1.47 ± 0.15	0.06 ± 0.01
	summer	0.55 ± 0.33	0.59 ± 0.68	0.78 ± 0.48	2.94 ± 2.87	0.10 ± 0.14
	autumn	1.14 ± 0.21	0.44 ± 0.43	2.57 ± 0.87	7.20 ± 7.60	0.12 ± 0.07
	winter	0.79 ± 0.34	1.08 ± 1.17	1.69 ± 0.75	9.66 ± 11.06	0.10 ± 0.05
	annual	0.95 ± 0.35	1.32 ± 0.70	2.55 ± 0.92	9.43 ± 7.11	0.13 ± 0.09

4. Bioaccessibility of metal(loid)s (mean ± standard deviation; expressed as bioaccessible metal(loid) concentration divided by total metal(loid) concentration)

Site	Season	Fe	As	Cd	Cr	Cu	Mn
TH	spring	0.04 ± 0.02	0.54 ± 0.13	0.54 ± 0.11	0.37 ± 0.16	0.29 ± 0.07	0.8 ± 0.16
	summer	0.03 ± 0.03	0.73 ± 0.14	0.37 ± 0.22	0.20 ± 0.15	0.10 ± 0.06	0.79 ± 0.24
	autumn	0.04 ± 0.01	0.72 ± 0.09	0.30 ± 0.18	0.24 ± 0.11	0.08 ± 0.03	0.89 ± 0.09
	winter	0.03 ± 0.03	0.64 ± 0.16	0.21 ± 0.16	0.26 ± 0.25	0.11 ± 0.04	0.79 ± 0.20
	annual	0.03 ± 0.02	0.66 ± 0.15	0.36 ± 0.21	0.27 ± 0.17	0.14 ± 0.09	0.81 ± 0.18
CH	spring	0.06 ± 0.02	0.63 ± 0.29	0.51 ± 0.11	0.40 ± 0.17	0.49 ± 0.13	0.89 ± 0.09
	summer	0.06 ± 0.07	0.70 ± 0.29	0.46 ± 0.13	0.35 ± 0.18	0.44 ± 0.16	0.79 ± 0.14
	autumn	0.03 ± 0.01	0.76 ± 0.10	0.46 ± 0.16	0.20 ± 0.11	0.41 ± 0.13	0.70 ± 0.16
	winter	0.05 ± 0.03	0.53 ± 0.16	0.38 ± 0.16	0.12 ± 0.25	0.45 ± 0.04	0.77 ± 0.20
	annual	0.05 ± 0.04	0.65 ± 0.25	0.45 ± 0.14	0.26 ± 0.18	0.45 ± 0.14	0.77 ± 0.16
HS	spring	0.03 ± 0.03	0.55 ± 0.13	0.07 ± 0.16	0.21 ± 0.17	0.57 ± 0.29	0.63 ± 0.22
	summer	0.03 ± 0.02	0.75 ± 0.11	0.60 ± 0.19	0.31 ± 0.25	0.33 ± 0.15	0.78 ± 0.20

Site	Season	Fe	As	Cd	Cr	Cu	Mn
HS	autumn	0.03 ± 0.01	0.62 ± 0.15	0.41 ± 0.18	0.12 ± 0.14	0.40 ± 0.10	0.59 ± 0.18
	winter	0.03 ± 0.02	0.52 ± 0.05	0.37 ± 0.16	0.13 ± 0.05	0.37 ± 0.10	0.74 ± 0.23
	annual	0.03 ± 0.02	0.62 ± 0.15	0.35 ± 0.28	0.22 ± 0.19	0.43 ± 0.22	0.68 ± 0.21
PK	spring	0.01 ± 0.01	0.49 ± 0.12	0.22 ± 0.06	0.18 ± 0.12	0.48 ± 0.15	0.67 ± 0.17
	summer	0.01 ± 0.01	0.72 ± 0.19	0.29 ± 0.20	0.17 ± 0.25	0.29 ± 0.10	0.53 ± 0.14
	autumn	0.01 ± 0.01	0.68 ± 0.31	0.41 ± 0.19	0.07 ± 0.06	0.33 ± 0.07	0.44 ± 0.12
	winter	0.02 ± 0.02	0.76 ± 0.16	0.51 ± 0.13	0.07 ± 0.06	0.34 ± 0.08	0.48 ± 0.13
	annual	0.01 ± 0.01	0.65 ± 0.23	0.35 ± 0.18	0.14 ± 0.14	0.37 ± 0.13	0.53 ± 0.16
	annual	0.01 ± 0.01	0.65 ± 0.23	0.35 ± 0.18	0.14 ± 0.14	0.37 ± 0.13	0.53 ± 0.16
XW	spring	0.00 ± 0.00	0.59 ± 0.13	0.18 ± 0.07	0.18 ± 0.17	0.83 ± 0.10	0.54 ± 0.17
	summer	0.01 ± 0.00	0.61 ± 0.20	0.20 ± 0.16	0.25 ± 0.20	0.52 ± 0.25	0.38 ± 0.14
	autumn	0.01 ± 0.01	0.81 ± 0.12	0.42 ± 0.19	0.04 ± 0.06	0.29 ± 0.11	0.42 ± 0.18
	winter	0.01 ± 0.01	0.79 ± 0.22	0.51 ± 0.20	0.04 ± 0.03	0.37 ± 0.11	0.49 ± 0.19
	annual	0.01 ± 0.01	0.68 ± 0.19	0.32 ± 0.21	0.15 ± 0.17	0.47 ± 0.24	0.46 ± 0.18
LS	spring	0.01 ± 0.00	0.63 ± 0.02	0.14 ± 0.01	0.54 ± 0.00	0.33 ± 0.04	0.45 ± 0.08
	summer	0.00 ± 0.00	0.66 ± 0.12	0.23 ± 0.22	0.23 ± 0.17	0.27 ± 0.10	0.37 ± 0.13
	autumn	0.01 ± 0.01	0.85 ± 0.10	0.47 ± 0.12	0.04 ± 0.00	0.37 ± 0.05	0.51 ± 0.13
	winter	0.01 ± 0.00	0.78 ± 0.20	0.31 ± 0.24	0.05 ± 0.00	0.37 ± 0.09	0.40 ± 0.24
	annual	0.01 ± 0.00	0.67 ± 0.14	0.32 ± 0.21	0.15 ± 0.20	0.42 ± 0.08	0.46 ± 0.17

Site	Season	Ni	Pb	V	Zn	Co
TH	spring	0.42 ± 0.19	0.12 ± 0.05	0.73 ± 0.15	0.11 ± 0.05	0.62 ± 0.19
	summer	0.35 ± 0.24	0.07 ± 0.05	0.84 ± 0.11	0.15 ± 0.09	0.44 ± 0.19
	autumn	0.24 ± 0.09	0.04 ± 0.02	0.76 ± 0.18	0.21 ± 0.06	0.57 ± 0.18
	winter	0.21 ± 0.12	0.05 ± 0.02	0.58 ± 0.25	0.18 ± 0.10	0.52 ± 0.23
	annual	0.30 ± 0.19	0.07 ± 0.04	0.73 ± 0.20	0.16 ± 0.09	0.53 ± 0.20
CH	spring	0.51 ± 0.12	0.17 ± 0.10	0.53 ± 0.28	0.17 ± 0.07	0.73 ± 0.14
	summer	0.41 ± 0.13	0.17 ± 0.09	0.60 ± 0.39	0.16 ± 0.09	0.48 ± 0.33

Site	Season	Ni	Pb	V	Zn	Co
CH	autumn	0.27 ± 0.15	0.12 ± 0.10	0.54 ± 0.29	0.11 ± 0.08	0.49 ± 0.28
	winter	0.28 ± 0.12	0.12 ± 0.02	0.55 ± 0.25	0.13 ± 0.10	0.33 ± 0.23
	annual	0.36 ± 0.16	0.15 ± 0.09	0.56 ± 0.30	0.14 ± 0.08	0.47 ± 0.29
HS	spring	0.26 ± 0.13	0.02 ± 0.01	0.51 ± 0.19	0.13 ± 0.04	0.34 ± 0.11
	summer	0.29 ± 0.10	0.15 ± 0.08	0.75 ± 0.19	0.17 ± 0.07	0.49 ± 0.32
	autumn	0.30 ± 0.06	0.04 ± 0.02	0.66 ± 0.16	0.14 ± 0.07	0.55 ± 0.10
	winter	0.22 ± 0.01	0.05 ± 0.04	0.43 ± 0.01	0.18 ± 0.13	0.46 ± 0.01
	annual	0.28 ± 0.10	0.07 ± 0.07	0.61 ± 0.21	0.15 ± 0.07	0.45 ± 0.20
PK	spring	0.24 ± 0.10	0.02 ± 0.01	0.39 ± 0.21	0.03 ± 0.02	0.26 ± 0.12
	summer	0.26 ± 0.08	0.03 ± 0.04	0.51 ± 0.29	0.03 ± 0.05	0.26 ± 0.17
	autumn	0.29 ± 0.14	0.02 ± 0.02	0.53 ± 0.30	0.06 ± 0.06	0.35 ± 0.19
	winter	0.31 ± 0.09	0.03 ± 0.03	0.55 ± 0.29	0.07 ± 0.06	0.53 ± 0.17
	annual	0.27 ± 0.11	0.03 ± 0.03	0.49 ± 0.27	0.05 ± 0.05	0.34 ± 0.19
XW	spring	0.23 ± 0.07	0.02 ± 0.01	0.48 ± 0.15	0.02 ± 0.01	0.32 ± 0.07
	summer	0.22 ± 0.07	0.02 ± 0.01	0.43 ± 0.21	0.03 ± 0.02	0.32 ± 0.08
	autumn	0.26 ± 0.06	0.03 ± 0.03	0.70 ± 0.14	0.07 ± 0.05	0.51 ± 0.15
	winter	0.24 ± 0.09	0.03 ± 0.02	0.71 ± 0.07	0.08 ± 0.03	0.47 ± 0.23
	annual	0.24 ± 0.07	0.02 ± 0.02	0.57 ± 0.19	0.04 ± 0.04	0.40 ± 0.15
LS	spring	0.41 ± 0.26	0.01 ± 0.00	0.52 ± 0.06	0.01 ± 0.00	0.32 ± 0.13
	summer	0.26 ± 0.08	0.03 ± 0.03	0.33 ± 0.09	0.02 ± 0.03	0.24 ± 0.16
	autumn	0.30 ± 0.03	0.01 ± 0.01	0.62 ± 0.07	0.05 ± 0.05	0.34 ± 0.00
	winter	0.24 ± 0.08	0.03 ± 0.02	0.53 ± 0.12	0.06 ± 0.05	0.27 ± 0.14
	annual	0.23 ± 0.11	0.02 ± 0.02	0.55 ± 0.15	0.04 ± 0.04	0.39 ± 0.13

5. CR and NCR induced by metal(loid)s

CR	TH	CH	HS	PK	XW	LS
As*	8.66E-07	1.05E-06	2.99E-06	8.46E-07	6.91E-07	5.17E-07
Cd	4.19E-08	6.26E-08	8.76E-08	1.42E-07	1.06E-07	4.14E-08
Ni	4.35E-08	2.52E-08	3.77E-08	3.67E-08	2.19E-08	1.83E-08
Pb	1.72E-09	3.05E-09	1.96E-09	2.34E-09	1.40E-09	6.95E-10
Co	2.22E-07	1.34E-07	1.71E-07	1.09E-07	9.81E-08	8.00E-08
Cr*	1.42E-06	7.89E-07	1.32E-06	3.69E-06	2.91E-06	2.57E-06
sum	2.59E-06	2.07E-06	4.61E-06	4.82E-06	3.83E-06	3.23E-06

* Adjusted based on speciation information

HQ	TH	CH	HS	PK	XW	LS
As*	2.14E-02	2.60E-02	7.38E-02	2.09E-02	1.71E-02	1.28E-02
Cd	8.14E-03	1.22E-02	1.70E-02	2.76E-02	2.06E-02	8.05E-03
Mn	6.91E-02	3.79E-02	6.57E-02	7.83E-02	6.01E-02	4.37E-02
Ni	6.50E-03	3.77E-03	5.63E-03	5.49E-03	3.27E-03	2.73E-03
V	1.09E-02	6.24E-03	1.42E-02	1.00E-02	8.34E-03	4.62E-03
Co	1.44E-02	8.65E-03	1.11E-02	7.07E-03	6.36E-03	5.18E-03
Cr*	5.92E-04	3.29E-04	5.49E-04	1.54E-03	1.21E-03	1.07E-03
Fe	9.04E-07	8.90E-07	6.12E-07	2.84E-07	1.52E-07	1.54E-07
Cu	7.29E-07	1.55E-06	2.50E-06	6.45E-06	3.79E-06	1.86E-06
Pb	1.00E-03	1.78E-03	1.14E-03	1.36E-03	8.17E-04	4.05E-04
Zn	1.35E-05	9.10E-06	1.77E-05	8.98E-06	5.82E-06	3.56E-06
sum	1.32E-01	9.68E-02	1.89E-01	1.52E-01	1.18E-01	7.85E-02

* Adjusted based on speciation information

6. PMF result (source contribution profiles for each chemical component; unit: %)

TH	Fugitive dust	Secondary nitrate	Ship emission	Vehicular emission	Sea salt	Combustion (coal/waste/biomass) mixed with secondary sulphate
PM _{2.5}	24.98	18.59	16.53	9.89	12.24	17.77
Na ⁺	44.07	0.00	10.23	11.28	22.32	12.10
NH ₄ ⁺	0.00	31.69	26.94	0.00	1.14	40.24
K ⁺	0.00	12.45	13.72	23.42	14.84	35.58
Cl ⁻	6.98	16.06	2.05	0.00	74.91	0.00
SO ₄ ²⁻	18.94	0.00	33.59	0.00	0.73	46.73
NO ₃ ⁻	3.92	57.59	1.31	11.25	23.42	2.51
OC	11.42	13.98	8.49	32.93	7.03	26.16
EC	1.66	9.65	12.38	37.83	6.55	31.93
Al	67.38	22.38	0.00	4.31	0.00	5.94
Fe	54.70	10.28	0.44	23.69	4.32	6.57
Ca	65.70	0.00	3.55	9.52	19.73	1.50
Mg	74.84	1.98	6.20	0.00	16.98	0.00
As	0.00	0.00	20.66	16.51	0.26	62.57
Cd	5.66	4.77	5.66	19.49	7.55	56.88
Cr	6.32	0.00	0.00	60.04	3.48	30.16
Cu	7.71	0.82	0.00	35.59	17.76	38.12
Mn	23.33	6.66	17.43	20.23	17.27	15.08
Ni	27.97	3.09	22.45	14.87	30.75	0.87
Pb	12.30	5.41	6.57	15.75	6.02	53.96
V	8.51	0.00	68.04	23.46	0.00	0.00
Zn	7.24	0.00	9.17	29.70	17.38	36.52
Co	59.94	4.18	3.98	8.54	19.97	3.39

HS	Fugitive dust	Secondary nitrate	Traffic emission	Sea salt	Combustion (coal/waste/biomass) mixed with secondary sulphate	Industrial emission
PM _{2.5}	20.26	17.76	14.55	9.26	22.79	15.39
Na ⁺	29.31	0.00	22.06	29.37	18.40	0.86
NH ₄ ⁺	0.00	29.93	24.25	4.28	32.08	9.45
K ⁺	10.20	15.02	10.06	22.30	35.99	6.42
Cl ⁻	0.00	16.94	14.06	52.75	1.08	15.18
SO ₄ ²⁻	11.48	6.77	30.36	0.00	44.88	6.52
NO ₃ ⁻	11.53	58.88	7.42	9.10	0.00	13.07
OC	26.63	13.47	10.54	11.72	26.06	11.57
EC	15.50	17.04	9.92	12.37	34.18	11.00
Al	66.80	11.13	6.85	0.00	10.06	5.17
Fe	62.74	2.59	10.05	4.91	10.70	9.01
Ca	71.93	0.00	0.00	5.52	11.70	10.85
Mg	73.17	2.19	5.40	7.19	12.05	0.00
As	0.69	0.00	41.34	5.27	39.79	12.91
Cd	18.25	6.35	1.68	7.62	35.84	30.26
Cr	0.00	0.00	56.19	0.00	35.38	8.43
Cu	23.56	0.00	1.67	0.00	11.41	63.35
Mn	38.15	9.88	18.08	4.67	15.31	13.90
Ni	25.03	1.33	54.13	10.05	4.93	4.54
Pb	16.03	5.35	1.06	6.60	41.13	29.83
V	0.01	0.00	82.85	0.00	14.40	2.74
Zn	23.07	0.00	14.99	16.35	19.55	26.04
Co	43.97	12.65	9.57	7.01	11.72	15.09

XW	Fugitive dust	Secondary aerosol	Fuel oil usage	Vehicular emission	Combustion (coal/waste/biomass)	Industrial emission
PM _{2.5}	17.09	31.50	11.59	7.78	22.07	9.96
Na ⁺	50.22	7.17	3.74	7.86	26.57	4.43
NH ₄ ⁺	0.00	53.83	13.41	4.06	13.46	15.25
K ⁺	17.58	6.75	8.88	25.76	28.08	12.95
Cl ⁻	40.24	0.00	0.00	0.00	59.76	0.00
SO ₄ ²⁻	13.82	36.95	16.34	9.87	23.02	0.00
NO ₃ ⁻	3.15	55.75	0.00	0.00	19.09	22.02
OC	28.41	7.77	8.45	20.87	27.70	6.81
EC	10.95	13.87	12.72	16.41	27.64	18.42
Al	47.76	3.59	8.23	17.08	23.35	0.00
Fe	20.73	1.57	9.07	14.38	31.60	22.66
Ca	58.82	4.64	0.00	9.34	27.20	0.00
Mg	54.85	4.15	5.95	9.78	24.68	0.60
As	9.01	0.00	8.62	21.56	50.70	10.10
Cd	0.00	0.00	5.03	0.00	94.97	0.00
Cr	0.00	0.00	21.08	14.53	30.06	34.33
Cu	0.00	0.00	0.00	79.56	20.44	0.00
Mn	0.00	0.00	15.11	9.53	27.69	47.67
Ni	12.97	1.70	39.56	7.14	29.10	9.54
Pb	13.34	1.10	0.00	24.38	52.32	8.86
V	0.00	2.31	67.77	2.45	27.47	0.00
Zn	26.31	0.00	6.25	29.89	31.33	6.22
Co	21.17	0.00	27.19	9.86	25.74	16.05

PK	Fugitive dust	Secondary aerosol	Fuel oil usage	Vehicular emission	Combustion (coal/waste/biomass)	Industrial emission
PM _{2.5}	23.15	30.90	8.22	12.49	18.11	7.12
Na ⁺	20.08	12.85	29.44	18.52	19.11	0.00
NH ₄ ⁺	20.47	50.58	0.64	10.16	11.22	6.94
K ⁺	19.59	12.36	3.85	4.23	53.01	6.95
Cl ⁻	0.00	3.03	21.00	16.71	59.26	0.00
SO ₄ ²⁻	32.77	41.39	6.15	13.15	6.54	0.00
NO ₃ ⁻	0.00	49.25	2.35	0.00	21.13	27.27
OC	23.70	15.78	9.24	13.12	26.62	11.53
EC	21.03	26.09	2.20	10.80	29.64	10.24
Al	34.57	6.72	11.95	14.64	21.96	10.17
Fe	11.24	0.00	0.00	0.00	31.51	57.26
Ca	31.88	1.04	19.67	19.27	14.94	13.20
Mg	27.48	0.00	15.06	16.78	28.74	11.93
As	0.00	0.00	15.34	2.11	60.01	22.54
Cd	0.00	0.00	4.06	0.00	95.94	0.00
Cr	0.00	0.00	36.62	0.00	16.20	47.18
Cu	0.00	0.00	4.20	45.25	37.58	12.97
Mn	14.18	0.00	7.70	12.77	39.27	26.07
Ni	17.21	0.93	28.13	14.48	32.14	7.10
Pb	15.53	0.53	0.00	6.70	72.35	4.89
V	14.56	0.00	49.94	0.00	35.15	0.35
Zn	18.81	7.08	8.29	6.90	46.89	12.03
Co	21.36	0.00	7.95	1.43	53.82	15.44

7. Monthly average concentrations of target genes (copy m⁻³) analysed by qPCR

Site	Month	16S rRNA gene	<i>ermB</i>	<i>tetW</i>	<i>qnrS</i>	<i>lnuA</i>	<i>bla</i> _{TEM-1}	<i>sul1</i>	<i>int11</i>	<i>tnpA-02</i>	<i>tnpA-04</i>
TH	Mar 2016	1.37E+03	2.60E+01	1.30E+01	8.62E-01	1.35E+02	8.62E-01	3.41E+01	5.40E+00	4.41E+01	3.21E+02
	Apr 2016	1.67E+03	5.06E+01	2.76E+01	7.65E-01	1.55E+02	8.52E-01	1.12E+02	1.74E+01	5.09E+01	7.39E+02
	May 2016	1.74E+03	1.49E+01	1.76E+00	1.63E+00	1.28E+02	1.63E+00	5.18E+01	8.72E+00	2.25E+01	6.90E+02
	Jun 2016	9.33E+03	6.92E+01	3.79E+01	1.01E+00	5.30E+02	1.21E+00	5.87E+02	8.40E+01	2.34E+02	3.17E+03
	Jul 2016	1.07E+04	1.09E+01	3.07E+01	5.34E-01	7.87E+02	5.78E-01	6.45E+02	5.21E+01	3.40E+02	3.74E+03
	Aug 2016	3.84E+03	1.40E+01	1.22E+01	6.80E-01	1.41E+02	5.26E-01	1.55E+02	2.52E+01	9.37E+01	1.11E+03
	Sept 2016	1.65E+04	8.42E+01	9.51E+01	6.66E-01	3.58E+02	1.12E+00	5.08E+02	6.16E+01	1.27E+02	2.24E+03
	Oct 2016	1.57E+04	8.69E+01	1.01E+02	1.12E+00	5.14E+02	1.45E+00	8.22E+02	8.09E+01	3.59E+02	4.05E+03
	Nov 2016	6.60E+03	8.66E+01	1.27E+02	2.34E+00	4.33E+02	1.74E+00	7.82E+02	8.25E+01	3.43E+02	4.35E+03
	Dec 2016	6.50E+03	3.03E+01	7.48E+01	5.58E-01	1.80E+03	4.04E+00	1.19E+03	5.73E+01	3.85E+02	7.18E+03
	Jan 2017	4.70E+03	7.07E+01	7.30E+01	1.18E+00	5.02E+02	1.18E+00	3.52E+02	4.92E+01	1.73E+02	2.14E+03
	Feb 2017	8.37E+03	1.54E+02	1.02E+02	1.69E+00	8.89E+02	2.55E+00	6.49E+02	7.99E+01	2.27E+02	3.02E+03
	Mar 2017	7.99E+03	1.26E+02	1.01E+02	1.49E+00	6.72E+02	1.35E+00	1.11E+03	9.69E+01	2.84E+02	4.99E+03
	Apr 2017	1.07E+04	8.95E+01	8.59E+01	1.59E+00	4.91E+02	2.56E+00	6.80E+02	7.23E+01	2.50E+02	4.16E+03
	May 2017	2.99E+03	4.20E+01	5.06E+01	1.82E+00	2.39E+02	8.27E-01	3.27E+02	3.77E+01	1.50E+02	1.74E+03
CH	Mar 2016	1.81E+03	2.08E+00	1.71E+00	1.17E+00	2.01E+01	1.17E+00	2.74E+00	2.06E+00	7.61E+00	2.93E+02
	Apr 2016	2.07E+03	2.01E+01	7.05E+00	1.56E+00	9.25E+01	5.74E+00	7.59E+01	1.02E+01	1.59E+01	7.17E+02
	May 2016	1.27E+04	7.23E+01	4.74E+01	2.37E+00	2.12E+02	2.50E+00	2.18E+02	4.73E+01	1.99E+02	2.90E+03
	Jun 2016	2.41E+04	5.95E+00	1.67E+01	1.32E+00	9.25E+01	9.69E-01	3.41E+02	2.60E+01	1.27E+02	2.67E+03
	Jul 2016	7.74E+03	5.71E+01	1.97E+01	2.59E+00	2.30E+02	3.25E+00	1.53E+02	2.56E+01	7.28E+01	1.40E+03
	Aug 2016	8.06E+03	8.89E+00	7.38E+00	9.05E-01	4.91E+01	9.05E-01	7.63E+01	7.71E+00	3.97E+01	7.81E+02
	Sept 2016	1.74E+04	6.01E+01	4.92E+01	9.56E+00	1.70E+02	2.04E+00	2.04E+02	2.80E+01	6.00E+01	1.75E+03
	Oct 2016	6.43E+03	6.77E+00	2.36E+00	2.26E+00	1.85E+02	2.26E+00	1.63E+01	6.23E+00	5.92E+01	3.61E+02
	Nov 2016	5.22E+03	2.37E+01	9.25E+00	1.13E+00	1.69E+02	1.13E+00	9.08E+01	1.10E+01	1.93E+01	7.70E+02

Site	Month	16S rRNA gene	<i>ermB</i>	<i>tetW</i>	<i>qnrS</i>	<i>lnuA</i>	<i>bla</i> _{TEM-1}	<i>sul1</i>	<i>int11</i>	<i>tnpA-02</i>	<i>tnpA-04</i>
CH	Dec 2016	3.41E+03	1.13E+01	7.81E+00	1.13E+00	4.59E+01	1.13E+00	1.09E+02	1.61E+01	1.61E+01	8.36E+02
	Jan 2017	3.02E+03	4.23E+00	2.23E+00	1.51E+00	1.39E+01	1.51E+00	5.22E+00	3.09E+00	1.34E+01	1.96E+02
	Feb 2017	2.70E+03	3.45E+01	6.27E+00	1.13E+00	9.23E+01	1.13E+00	5.21E+01	7.31E+00	1.57E+01	7.69E+02
	Mar 2017	3.82E+03	6.03E+01	2.08E+01	1.17E+00	1.83E+02	1.44E+00	1.93E+02	2.01E+01	5.60E+01	1.65E+03
	Apr 2017	2.19E+03	7.30E+00	5.25E+00	4.53E+00	1.24E+02	4.53E+00	1.77E+01	7.62E+00	4.82E+01	9.85E+02
	May 2017	5.37E+03	3.85E+00	2.51E+00	1.13E+00	2.32E+01	1.13E+00	1.36E+01	3.45E+00	1.64E+01	4.48E+02
HS	Mar 2016	2.67E+03	6.44E+01	6.53E+00	2.90E+00	2.73E+02	2.90E+00	1.59E+02	3.61E+01	1.84E+02	1.63E+03
	Apr 2016	6.29E+03	5.40E+02	1.33E+02	6.85E+00	1.06E+03	4.45E+00	1.04E+03	2.83E+02	5.90E+02	6.48E+03
	May 2016	1.15E+04	2.71E+02	1.16E+02	2.97E+00	4.48E+02	1.52E+00	6.28E+02	1.72E+02	3.74E+02	4.74E+03
	Jun 2016	3.13E+04	5.51E+02	1.88E+02	3.97E+00	9.88E+02	2.41E+00	2.44E+03	4.80E+02	8.38E+02	1.18E+04
	Jul 2016	2.61E+04	5.71E+02	2.04E+02	3.12E+00	1.01E+03	3.15E+00	2.15E+03	5.13E+02	8.81E+02	1.10E+04
	Aug 2016	1.13E+04	8.00E+01	3.86E+01	2.64E+00	2.04E+02	1.04E+00	2.56E+02	6.70E+01	1.12E+02	1.47E+03
	Sept 2016	3.99E+04	3.99E+02	1.98E+02	3.01E+00	1.69E+03	3.58E+00	1.88E+03	4.01E+02	7.80E+02	1.00E+04
	Oct 2016	1.83E+04	2.27E+02	5.90E+01	1.31E+01	6.79E+02	1.39E+00	4.18E+02	1.38E+02	2.08E+02	2.89E+03
	Nov 2016	4.24E+04	1.04E+03	4.36E+02	1.76E+01	2.64E+03	1.18E+01	3.97E+03	8.45E+02	1.12E+03	1.80E+04
	Dec 2016	3.04E+04	3.28E+02	2.38E+02	5.61E+00	2.86E+03	5.48E+00	3.25E+03	5.26E+02	9.74E+02	1.76E+04
	Jan 2017	3.07E+03	4.39E+01	6.83E+00	1.94E+00	6.13E+02	9.94E-01	1.01E+02	4.14E+01	1.04E+02	1.39E+03
	Feb 2017	3.87E+03	5.30E+01	9.79E+00	1.63E+00	4.85E+02	1.32E+00	9.78E+01	1.77E+01	3.78E+01	9.98E+02
	Mar 2017	4.48E+03	2.35E+01	7.98E+00	7.95E-01	3.14E+02	7.95E-01	1.70E+02	3.79E+01	8.88E+01	1.95E+03
	Apr 2017	4.99E+03	7.30E+01	1.92E+01	4.44E+00	4.81E+02	9.94E-01	4.00E+02	8.85E+01	1.35E+02	3.38E+03
	May 2017	3.36E+03	1.33E+02	2.93E+01	1.72E+00	4.52E+02	7.95E-01	4.16E+02	1.34E+02	2.43E+02	3.12E+03
XW	Mar 2016	1.37E+03	1.20E+02	5.60E+01	1.06E+01	6.10E+01	4.38E+01	1.39E+01	7.89E+01	1.57E+01	2.01E+02
	Apr 2016	2.51E+03	2.88E+01	1.55E+01	2.77E+00	1.89E+01	2.24E+02	2.77E+00	7.55E+01	2.77E+00	9.27E+01
	May 2016	7.40E+03	7.18E+01	2.18E+01	2.77E+00	3.45E+01	6.13E+02	9.94E+01	1.27E+02	3.17E+00	7.12E+01

Site	Month	16S rRNA gene	<i>ermB</i>	<i>tetW</i>	<i>qnrS</i>	<i>lnuA</i>	<i>bla</i> _{TEM-1}	<i>sul1</i>	<i>int11</i>	<i>tnpA-02</i>	<i>tnpA-04</i>
XW	Jun 2016	1.19E+03	4.96E+01	1.39E+01	1.15E+01	3.72E+01	8.29E+01	9.23E+00	6.92E+01	2.77E+00	1.79E+02
	Jul 2016	2.66E+03	5.06E+01	2.01E+01	1.76E+01	2.39E+01	3.19E+02	4.02E+00	7.88E+01	4.02E+00	1.33E+02
	Aug 2016	1.40E+03	2.60E+01	2.43E+01	6.88E+00	5.74E+01	4.28E+00	2.55E+01	5.96E+01	9.09E+00	2.22E+02
	Sept 2016	2.14E+03	1.95E+02	8.55E+01	7.31E+00	8.06E+00	6.00E+01	7.31E+00	6.26E+01	7.31E+00	1.60E+02
	Oct 2016	3.16E+03	5.95E+01	2.43E+01	2.89E+01	1.27E+01	2.73E+02	1.75E+01	1.37E+02	4.86E+00	2.35E+02
	Nov 2016	6.28E+03	6.71E+02	7.15E+01	2.44E+02	7.14E+01	2.27E+02	1.28E+01	1.84E+02	4.86E+00	1.27E+02
	Dec 2016	1.59E+04	1.10E+03	8.40E+01	4.99E+00	7.44E+01	2.89E+01	2.73E+01	3.06E+02	1.78E+01	3.21E+02
	Jan 2017	1.99E+03	3.72E+02	1.37E+02	2.70E+01	5.11E+01	1.89E+01	1.71E+01	3.36E+02	4.86E+00	2.04E+02
	Feb 2017	4.00E+03	3.77E+02	7.42E+01	3.02E+01	3.02E+01	1.85E+01	1.61E+01	1.92E+02	7.30E+00	4.47E+02
	Mar 2017	3.50E+03	6.15E+01	1.82E+01	3.64E+00	1.35E+02	3.06E+00	3.86E+01	3.95E+01	3.72E+01	4.55E+02
	Apr 2017	3.21E+03	4.23E+01	1.82E+01	3.65E+00	7.97E+01	1.39E+00	1.55E+01	2.45E+01	2.68E+01	2.02E+02
	May 2017	2.72E+03	1.56E+01	2.43E+01	4.86E+00	3.49E+01	1.15E+00	1.43E+01	9.44E+00	2.62E+01	2.66E+02
PK	Mar 2016	2.69E+03	2.81E+02	7.00E+01	3.71E+00	3.11E+02	2.79E+00	1.45E+02	1.66E+02	4.50E+01	1.29E+03
	Apr 2016	2.18E+03	8.86E+01	1.91E+01	6.21E+00	2.93E+01	7.04E+00	2.61E+01	8.62E+01	6.75E+00	1.84E+02
	May 2016	6.56E+03	4.97E+01	1.39E+01	2.22E+00	3.08E+01	1.53E+00	9.42E+01	1.82E+02	4.16E+00	2.68E+02
	Jun 2016	1.27E+03	3.11E+01	1.39E+01	2.78E+00	2.73E+01	1.73E+00	5.71E+00	1.68E+01	3.83E+00	9.36E+01
	Jul 2016	1.50E+03	3.45E+01	3.15E+01	6.31E+00	2.47E+01	7.65E+01	3.66E+01	6.89E+01	6.31E+00	7.51E+01
	Aug 2016	2.68E+03	7.16E+01	3.64E+01	7.29E+00	3.16E+01	1.46E+00	2.14E+01	7.56E+00	8.52E+00	5.01E+01
	Sept 2016	1.58E+03	3.15E+01	2.43E+01	4.86E+00	1.78E+01	9.73E-01	6.13E+00	2.25E+01	8.47E+00	7.49E+01
	Oct 2016	1.97E+03	6.83E+00	3.41E+01	6.83E+00	2.34E+01	1.37E+00	9.31E+00	5.44E+01	7.98E+00	1.72E+02
	Nov 2016	3.32E+03	3.60E+02	9.90E+01	4.86E+00	3.86E+01	1.14E+00	2.56E+01	1.84E+01	6.23E+00	1.39E+02
	Dec 2016	1.33E+03	1.52E+02	2.43E+01	4.86E+00	3.31E+01	9.72E-01	1.51E+01	2.06E+01	4.86E+00	1.65E+02
	Jan 2017	4.62E+03	4.99E+02	3.67E+01	4.86E+00	1.94E+02	9.72E-01	9.96E+01	7.59E+01	1.62E+01	2.89E+02
	Feb 2017	3.53E+03	3.47E+02	4.53E+01	1.41E+01	6.51E+01	1.76E+00	8.81E+00	8.41E+01	9.41E+00	2.44E+02

Site	Month	16S rRNA gene	<i>ermB</i>	<i>tetW</i>	<i>qnrS</i>	<i>lnuA</i>	<i>bla</i> _{TEM-1}	<i>sulI</i>	<i>intI1</i>	<i>tnpA-02</i>	<i>tnpA-04</i>
PK	Mar 2017	4.28E+03	1.27E+02	3.56E+01	4.85E+00	9.92E+01	7.03E+00	4.79E+01	1.04E+02	1.29E+01	2.10E+02
	Apr 2017	4.42E+03	7.04E+01	2.98E+01	3.64E+00	5.41E+01	2.88E+00	3.02E+01	6.05E+01	1.55E+01	2.26E+02
	May 2017	4.51E+03	5.84E+01	2.67E+01	4.86E+00	8.80E+01	9.72E-01	3.47E+01	3.58E+01	7.37E+00	1.92E+02
LS	Apr 2016	2.47E+03	5.53E+00	2.76E+01	5.53E+00	1.24E+01	1.36E+00	5.53E+00	5.53E+00	5.53E+00	9.57E+01
	May 2016	3.52E+03	1.12E+01	2.75E+01	5.51E+00	1.20E+01	1.10E+00	5.51E+00	2.93E+01	5.51E+00	8.07E+01
	Jun 2016	3.01E+03	2.30E+01	2.76E+01	5.52E+00	2.14E+01	1.10E+00	5.86E+00	3.03E+01	6.54E+00	1.09E+02
	Jul 2016	8.12E+03	1.49E+02	2.31E+01	1.99E+00	7.57E+01	4.57E+01	8.02E+01	6.87E+01	9.38E+00	7.07E+02
	Sept 2016	9.91E+03	1.06E+03	1.00E+02	5.74E+00	1.60E+02	1.52E+00	1.41E+02	1.42E+02	4.06E+01	1.58E+03
	Oct 2016	3.20E+03	3.80E+02	6.17E+01	5.72E+00	1.54E+02	1.14E+00	3.43E+01	1.29E+02	1.84E+01	7.97E+02
	Nov 2016	1.02E+04	8.01E+02	1.62E+02	5.65E+00	2.75E+02	1.16E+00	1.10E+02	1.84E+02	3.70E+01	1.42E+03
	Dec 2016	1.43E+03	5.37E+02	6.18E+01	5.65E+00	1.85E+02	1.20E+00	6.02E+01	1.38E+02	1.75E+01	1.04E+03
	Jan 2017	1.13E+03	6.34E+02	1.92E+02	2.03E+00	3.09E+02	1.53E+00	2.59E+02	2.32E+02	8.60E+01	3.65E+03
	Feb 2017	1.16E+03	1.23E+03	1.92E+02	5.72E+00	4.61E+02	4.25E+00	3.06E+02	2.61E+02	8.17E+01	3.94E+03
	Mar 2017	2.25E+03	1.04E+01	2.76E+01	5.52E+00	3.85E+01	1.10E+00	6.83E+00	1.76E+01	1.28E+01	2.92E+02
	Apr 2017	2.91E+03	3.09E+02	2.03E+02	6.52E+00	8.67E+02	2.20E+00	6.67E+02	5.26E+02	1.63E+02	8.93E+03
May 2017	4.11E+03	7.02E+01	5.98E+01	5.52E+00	2.40E+02	1.10E+00	4.50E+01	8.70E+01	3.71E+01	1.91E+03	

8. Concentrations of certain kinds of genes in PM_{2.5}/sewage/sludge samples in the SCISTW study (by qPCR).

Sample type	Sample ID	PM _{2.5} (µg m ⁻³)	Target gene concentration (copy m ⁻³)									
			16S rRNA gene	<i>ermB</i>	<i>sulI</i>	<i>lnuA</i>	<i>tetW</i>	<i>qnrS</i>	<i>bla</i> _{TEM-1}	<i>tnpA-02</i>	<i>tnpA-04</i>	<i>intI1</i>
PM _{2.5}	FT-P2	25.98	6.99E+03	8.64E+01	4.35E+02	3.13E+02	3.34E+01	6.30E+00	2.78E-01	7.54E+01	1.42E+03	1.26E+02

Sample type	Sample ID	PM _{2.5} (µg m ⁻³)	Target gene concentration (copy m ⁻³)									
			16S rRNA gene	<i>ermB</i>	<i>sul1</i>	<i>lnuA</i>	<i>tetW</i>	<i>qnrS</i>	<i>bla</i> _{TEM-1}	<i>tnpA-02</i>	<i>tnpA-04</i>	<i>int11</i>
PM _{2.5}	ST-P1	23.38	1.30E+04	2.09E+01	1.78E+02	1.23E+02	5.00E+00	9.04E+00	4.72E-01	7.92E+01	1.41E+03	1.11E+02
	ST-P2	23.95	5.86E+03	9.90E+01	7.03E+02	3.09E+02	1.53E+01	5.51E+00	6.40E-01	1.34E+02	2.12E+03	3.77E+02
	BFN-P1	26.24	7.19E+04	5.20E+01	1.07E+03	2.16E+02	6.92E+00	1.40E+01	5.26E-01	5.29E+02	4.64E+03	8.75E+02
	BFF-P1	26.69	4.64E+04	4.38E+01	6.95E+02	3.08E+02	7.47E+00	6.68E+00	7.94E-01	4.83E+02	3.95E+03	4.66E+02
	BFF-P2	29.03	9.52E+04	1.34E+02	1.83E+03	4.34E+02	1.79E+01	4.95E+00	1.96E-01	7.92E+02	9.47E+03	1.21E+03
	SST-P1	24.06	4.75E+04	9.60E+00	3.23E+02	3.01E+02	7.96E+00	3.87E+00	3.35E-01	1.64E+02	3.07E+03	2.22E+02
	SST-P2	25.44	3.14E+04	1.83E+02	1.07E+03	1.12E+03	3.13E+01	3.33E+00	3.10E-01	2.51E+02	4.82E+03	8.19E+02
	HT-P1	31.79	2.74E+03	2.12E+01	1.69E+01	7.37E+01	1.43E+00	6.64E+00	2.33E-01	3.49E+01	3.69E+02	3.36E+01
	HT-P2	28.75	2.23E+03	1.23E+01	3.76E+01	2.28E+01	3.11E+00	2.81E+00	1.85E-01	3.01E+01	1.70E+02	6.31E+01
	PU-P2	62.31	5.51E+04	1.00E+03	5.09E+03	3.85E+03	1.22E+02	3.74E+01	5.47E+00	2.08E+03	2.44E+04	1.87E+03
	PU-P3	90.83	2.80E+05	6.85E+03	4.23E+04	1.18E+04	1.03E+03	1.25E+01	1.59E+01	7.41E+03	1.54E+05	1.56E+04
	PU-P4	60.26	6.72E+04	6.75E+02	3.08E+03	1.68E+03	1.32E+02	9.18E+00	2.79E+00	5.03E+02	1.37E+04	1.33E+03

Sample type	Sample ID	Unit	16S rRNA gene	<i>ermB</i>	<i>sul1</i>	<i>lnuA</i>	<i>tetW</i>	<i>qnrS</i>	<i>bla</i> _{TEM-1}	<i>tnpA-02</i>	<i>tnpA-04</i>	<i>int11</i>
Sewage	SERaw-P1	copy mL ⁻¹ sewage or sludge	6.53E+08	2.92E+07	1.14E+08	6.56E+05	4.24E+06	3.43E+07	1.01E+06	5.21E+08	8.50E+07	1.06E+08
	SEFlo-P1		1.15E+09	9.98E+07	1.27E+08	9.44E+05	1.22E+07	2.96E+07	2.11E+06	5.45E+08	1.61E+08	1.05E+08
	SEFlo-P2		5.01E+08	4.98E+07	7.42E+07	4.74E+05	6.12E+06	2.87E+07	1.01E+06	2.83E+08	7.36E+07	6.56E+07
Effluent	EFSeD-P1		9.08E+08	1.19E+07	1.24E+08	1.18E+05	1.79E+06	2.47E+07	9.71E+05	8.13E+08	1.59E+07	1.15E+08
	EFDechl-P1		9.97E+08	2.13E+07	1.70E+08	1.76E+05	3.00E+06	5.99E+07	8.23E+05	6.89E+08	1.48E+07	1.71E+08
Sludge	SluSed-P1		1.10E+10	6.08E+08	8.81E+08	1.18E+07	8.25E+07	2.38E+07	5.28E+06	1.06E+10	2.88E+09	8.86E+08

Sample type	Sample ID	Unit	16S rRNA gene	<i>ermB</i>	<i>sulI</i>	<i>lnuA</i>	<i>tetW</i>	<i>qnrS</i>	<i>bla</i> _{TEM-1}	<i>tnpA-02</i>	<i>tnpA-04</i>	<i>intI1</i>
Sludge	SluDew-P1	copy mg ⁻¹ sludge	1.57E+08	6.19E+06	8.71E+06	4.14E+05	5.37E+05	2.62E+05	9.39E+04	5.29E+07	3.76E+07	6.89E+06

References

- Agerso, Y. & Petersen, A. (2007). The tetracycline resistance determinant Tet 39 and the sulphonamide resistance gene *sulIII* are common among resistant *Acinetobacter* spp. isolated from integrated fish farms in Thailand. *J. Antimicrob. Chemother.*, *59*, 23-27.
- Allen, H. K., Donato, J., Wang, H. H., Cloud-Hansen, K. A., Davies, J., & Handelsman, J. (2010). Call of the wild: antibiotic resistance genes in natural environments. *Nat. Rev. Microbiol.*, *8*, 251-259.
- Aller, J. Y., Kuznetsova, M. R., Jahns, C. J., & Kemp, P. F. (2005). The sea surface microlayer as a source of viral and bacterial enrichment in marine aerosols. *J. Aerosol Sci.*, *36*, 801-812.
- Altschul, S. F., Madden, T. L., Schäffer, A. A., Zhang, J. H., Zhang, Z., Miller, W., & Lipman, D. J. (1997). Gapped BLAST and PSI-BLAST: a new generation of protein database search programs. *Nucleic Acids Res.*, *25*, 3389-3402.
- Amann, R. I., Ludwig, W., & Schleifer, K. H. (1995). Phylogenetic identification and in-situ detection of individual microbial-cells without cultivation. *Microbiol. Rev.*, *59*, 143-169.
- Aminov, R., Garrigues-Jeanjean, N., & Mackie, R. (2001). Molecular ecology of tetracycline resistance: development and validation of primers for detection of tetracycline resistance genes encoding ribosomal protection proteins. *Appl. Environ. Microbiol.*, *67*, 22-32.
- Arango-Argoty, G., Dai, D. J., Pruden, A., Vikesland, P., Heath, L. S., & Zhang, L. Q. (2019). NanoARG: a web service for detecting and contextualizing antimicrobial resistance genes from nanopore-derived metagenomes. *Microbiome*, *7*, 88.
- Arango-Argoty, G., Garner, E., Pruden, A., Heath, L. S., Vikesland, P., & Zhang, L. Q. (2018). DeepARG: a deep learning approach for predicting antibiotic resistance genes from metagenomic data. *Microbiome*, *6*, 1-15.
- Arango-Argoty, G., Singh, G., Heath, L. S., Pruden, A., Xiao, W. D., & Zhang, L. Q. (2016). MetaStorm: a public resource for customizable metagenomics annotation. *PLoS One*, *11*, e0162442.
- ArcGIS Desktop (2012). v.10.1. Environmental Systems Research Institute, Inc.: Redlands, CA.
- Ariya, P., Sun, J., Eltouny, N., Hudson, E., Hayes, C., & Kos, G. (2009). Physical and chemical characterization of bioaerosols – Implications for nucleation processes. *Int. Rev. Phys. Chem.*, *28*, 1-32.
- Ariya, P. A., Nepotchatykh, O., Ignatova, O., & Amyot, M. (2002). Microbiological degradation of atmospheric organic compounds. *Geophys. Res. Lett.*, *29*, 2077.

- Atkinson, R., Kang, S., Anderson, H., Mills, I., & Walton, H. (2014). Epidemiological time series studies of PM_{2.5} and daily mortality and hospital admissions: a systematic review and meta-analysis. *Thorax*, *69*, 660-665.
- Bakutis, B., Monstvilienė, E., & Januskeviciene, G. (2004). Analyses of airborne contamination with bacteria, endotoxins and dust in livestock barns and poultry houses. *Acta Vet. Brno*, *73*, 283-289.
- Bär, M., Hardenberg, J., Meron, E., & Provenzale, A. (2002). Modelling the survival of bacteria in drylands: the advantage of being dormant. *Proc. R. Soc. B.*, *269*, 937-942.
- Baral, D., Dvorak, B. I., Admiraal, D., Jia, S. G., Zhang, C., & Li, X. (2018). Tracking the sources of antibiotic resistance genes in an urban stream during wet weather using shotgun metagenomic analyses. *Environ. Sci. Technol.*, *52*, 9033-9044.
- Bardou, P., Mariette, J., Escudié, F., Djemiel, C., & Klopp, C. (2014). jvenn: an interactive Venn diagram viewer. *BMC bioinformatics*, *15*, 293.
- Bauer, H., Fuerhacker, M., Zibuschka, F., Schmid, H., & Puxbaum, H. (2002). Bacteria and fungi in aerosols generated by two different types of wastewater treatment plants. *Water Res.*, *36*, 3965-3970.
- Beijing Municipal Bureau of Statistics (2017a). Beijing regional statistical yearbook 2017 (in Chinese). Beijing, China. China Statistics Press. Retrieved from <http://nj.tjj.beijing.gov.cn/nj/qxnj/2017/zk/indexch.htm>
- Beijing Municipal Bureau of Statistics (2017b). Beijing statistical yearbook 2017 (in Chinese). Beijing, China. China Statistics Press. Retrieved from <http://nj.tjj.beijing.gov.cn/nj/main/2017-tjnj/zk/indexch.htm>
- Berglund, B. (2015). Environmental dissemination of antibiotic resistance genes and correlation to anthropogenic contamination with antibiotics. *Infect. Ecol. Epidemiol.*, *5*, 28564.
- Bertolini, V., Gandolfi, I., Ambrosini, R., Bestetti, G., Innocente, E., Rampazzo, G., & Franzetti, A. (2013). Temporal variability and effect of environmental variables on airborne bacterial communities in an urban area of Northern Italy. *Appl. Microbiol. Biotechnol.*, *97*, 6561-6570.
- Bowers, R. M., Clements, N., Emerson, J. B., Wiedinmyer, C., Hannigan, M. P., & Fierer, N. (2013). Seasonal variability in bacterial and fungal diversity of the near-surface atmosphere. *Environ. Sci. Technol.*, *47*, 12097-12106.
- Bowers, R. M., Lauber, C. L., Wiedinmyer, C., Hamady, M., Hallar, A. G., Fall, R., Knight, R., & Fierer, N. (2009). Characterization of airborne microbial communities at a high-elevation site and their potential to act as atmospheric ice nuclei. *Appl. Environ. Microb.*, *75*, 5121-5130.

- Bowers, R. M., McLetchie, S., Knight, R., & Fierer, N. (2011a). Spatial variability in airborne bacterial communities across land-use types and their relationship to the bacterial communities of potential source environments. *ISME J.*, *5*, 601-612.
- Bowers, R. M., Sullivan, A. P., Costello, E. K., Collett, J. L., Jr., Knight, R., & Fierer, N. (2011b). Sources of bacteria in outdoor air across cities in the Midwestern United States. *Appl. Environ. Microbiol.*, *77*, 6350-6356.
- Cao, C., Jiang, W. J., Wang, B. Y., Fang, J. H., Lang, J. D., Tian, G., Jiang, J. K., & Zhu, T. F. (2014). Inhalable microorganisms in Beijing's PM_{2.5} and PM₁₀ pollutants during a severe smog event. *Environ. Sci. Technol.*, *48*, 1499-1507.
- Census and Statistics Department (2017). Summary results of 2016 population by-census. HKSAR Government. Retrieved from <https://www.byccensus2016.gov.hk/en/index.html>
- Census and Statistics Department (2018). Gross domestic product (yearly) (2017 edition). HKSAR Government. Retrieved from <https://www.censtatd.gov.hk/hkstat/sub/sp250.jsp?productCode=B1030002>
- Centre for Health Protection (2017). Hong Kong strategy and action plan on antimicrobial resistance 2017-2022. Department of Health, HKSAR Government. Retrieved from https://www.chp.gov.hk/files/pdf/amr_action_plan_eng.pdf
- Chan, L. Y., Chu, K. W., Zou, S. C., Chan, C. Y., Wang, X. M., Barletta, B., Blake, D. R., Guo, H., & Tsai, W. Y. (2006). Characteristics of nonmethane hydrocarbons (NMHCs) in industrial, industrial-urban, and industrial-suburban atmospheres of the Pearl River Delta (PRD) region of south China. *J. Geophys. Res. Atmos.*, *111*.
- Chang, Y. H., Huang, K., Deng, C. R., Zou, Z., Liu, S. D., & Zhang, Y. L. (2017). First long-term and near real-time measurement of atmospheric trace elements in Shanghai, China. *Atmos. Chem. Phys.*, *18*, 11793-11812.
- Chen, B. W., Liang, X. M., Huang, X. P., Zhang, T., & Li, X. D. (2013a). Differentiating anthropogenic impacts on ARGs in the Pearl River Estuary by using suitable gene indicators. *Water Res.*, *47*, 2811-2820.
- Chen, B. W., Liang, X. M., Nie, X. P., Huang, X. P., Zou, S. C., & Li, X. D. (2015). The role of class I integrons in the dissemination of sulfonamide resistance genes in the Pearl River and Pearl River Estuary, South China. *J. Hazard. Mater.*, *282*, 61-67.
- Chen, B. W., Yang, Y., Liang, X. M., Yu, K., Zhang, T., & Li, X. D. (2013b). Metagenomic profiles of antibiotic resistance genes (ARGs) between human impacted estuary and deep ocean sediments. *Environ. Sci. Technol.*, *47*, 12753-12760.
- Chen, B. W., Yuan, K., Chen, X., Yang, Y., Zhang, T., Wang, Y. W., Luan, T. G., Zou, S. C., & Li, X. D. (2016). Metagenomic analysis revealing antibiotic resistance genes (ARGs) and their genetic compartments in the tibetan environment. *Environ. Sci. Technol.*, *50*, 6670-6679.

- Chen, J. M., Tan, M. G., Li, Y. L., Zheng, J., Zhang, Y. M., Shan, Z. C., Zhang, G. L., & Li, Y. (2008). Characteristics of trace elements and lead isotope ratios in PM_{2.5} from four sites in Shanghai. *J. Hazard. Mater.*, *156*, 36-43.
- Chen, S. F., Zhou, Y. Q., Chen, Y. R., & Gu, J. (2018). fastp: an ultra-fast all-in-one FASTQ preprocessor. *Bioinformatics*, *34*, i884-i890.
- Chen, X. Y., Ran, P. X., Ho, K. F., Lu, W. J., Li, B., Gu, Z. P., Song, C. J., & Wang, J. (2012). Concentrations and size distributions of airborne microorganisms in Guangzhou during summer. *Aerosol Air Qual. Res.*, *12*, 1336-1344.
- Chinese Nutrition Association (2016). The food guide pagoda for Chinese residents (2016). *Dietary guidelines for Chinese residents 2016 (in Chinese)*. Beijing, China. People's Medical Publishing House. pp.3.
- Colombo, C., Monhemius, A. J., & Plant, J. A. (2008). Platinum, palladium and rhodium release from vehicle exhaust catalysts and road dust exposed to simulated lung fluids. *Ecotoxicol. Environ. Saf.*, *71*, 722-730.
- Cong, Z. Y., Kang, S. C., Luo, C. L., Li, Q., Huang, J., Gao, S. P., & Li, X. D. (2011). Trace elements and lead isotopic composition of PM₁₀ in Lhasa, Tibet. *Atmos. Environ.*, *45*, 6210-6215.
- Cui, J. L., Du, J. J., Tian, H. X., Chan, T. S., & Jing, C. Y. (2018). Rethinking anaerobic As (III) oxidation in filters: Effect of indigenous nitrate respirers. *Chemosphere*, *196*, 223-230.
- Cui, J. L., Shi, J. B., Jiang, G. B., & Jing, C. Y. (2013). Arsenic levels and speciation from ingestion exposures to biomarkers in Shanxi, China: implications for human health. *Environ. Sci. Technol.*, *47*, 5419-5424.
- de la Campa, A. S., de la Rosa, J., Sánchez-Rodas, D., Oliveira, V., Alastuey, A., Querol, X., & Ariza, J. G. (2008). Arsenic speciation study of PM_{2.5} in an urban area near a copper smelter. *Atmos. Environ.*, *42*, 6487-6495.
- Du, P. R., Du, R., Ren, W. S., Lu, Z. D., & Fu, P. Q. (2018). Seasonal variation characteristic of inhalable microbial communities in PM_{2.5} in Beijing city, China. *Sci. Total Environ.*, *610*, 308-315.
- Du, W. J., Zhang, Y. R., Chen, Y. T., Xu, L. L., Chen, J. S., Deng, J. J., Hong, Y. W., & Xiao, H. (2017). Chemical characterization and source apportionment of PM_{2.5} during spring and winter in the Yangtze River Delta, China. *Aerosol Air Qual. Res.*, *17*, 2165-2180.
- Echeverria-Palencia, C. M., Thulsiraj, V., Tran, N., Ericksen, C. A., Melendez, I., Sanchez, M. G., Walpert, D., Yuan, T., Ficara, E., & Senthilkumar, N. (2017). Disparate antibiotic resistance gene quantities revealed across 4 major cities in California: A survey in drinking water, air, and soil at 24 public parks. *ACS Omega*, *2*, 2255-2263.

- Eduard, W., Douwes, J., Mehl, R., Heederik, D., & Melbostad, E. (2001). Short term exposure to airborne microbial agents during farm work: exposure-response relations with eye and respiratory symptoms. *Occup. Environ. Med.*, *58*, 113-118.
- Egorova, K. S. & Ananikov, V. P. (2017). Toxicity of metal compounds: knowledge and myths. *Organometallics*, *36*, 4071-4090.
- Elert, G. (2009). The physics factbook. Hypertextbook. Retrieved from <https://hypertextbook.com/facts/>.
- Esri (Cartographer). (2009). World Imagery [basemap]. "World Imagery". December 13. Retrieved from <https://www.arcgis.com/home/item.html?id=10df2279f9684e4a9f6a7f08febac2a9>
- Fan, Y., Mei, L. S., Ling, H. H., & Ping, C. (2014). Heavy metal and antibiotic resistance in bacteria isolated from the environment of swine farms. *J. Chem. Soc. Pakistan*, *36*, 360-364.
- Fang, Z. G., Ouyang, Z. Y., Zheng, H., Wang, X. K., & Hu, L. F. (2007). Culturable airborne bacteria in outdoor environments in Beijing, China. *Microb. Ecol.*, *54*, 487-496.
- Fathi, S., Hajizadeh, Y., Nikaeen, M., & Gorbani, M. (2017). Assessment of microbial aerosol emissions in an urban wastewater treatment plant operated with activated sludge process. *Aerobiologia*, *33*, 507-515.
- Feng, X. D., Dang, Z., Huang, W. L., & Yang, C. (2009). Chemical speciation of fine particle bound trace metals. *Int. J. Environ. Sci. Tech.*, *6*, 337-346.
- Franzetti, A., Gandolfi, I., Gaspari, E., Ambrosini, R., & Bestetti, G. (2011). Seasonal variability of bacteria in fine and coarse urban air particulate matter. *Appl. Microbiol. Biotechnol.*, *90*, 745-753.
- Galbreath, K. C. & Zygarlicke, C. J. (2004). Formation and chemical speciation of arsenic-, chromium-, and nickel-bearing coal combustion PM_{2.5}. *Fuel Process. Technol.*, *85*, 701-726.
- Gandolfi, I., Bertolini, V., Bestetti, G., Ambrosini, R., Innocente, E., Rampazzo, G., Papacchini, M., & Franzetti, A. (2015). Spatio-temporal variability of airborne bacterial communities and their correlation with particulate matter chemical composition across two urban areas. *Appl. Microbiol. Biotechnol.*, *99*, 4867-4877.
- Gandolfi, I., Franzetti, A., Bertolini, V., Gaspari, E., & Bestetti, G. (2011). Antibiotic resistance in bacteria associated with coarse atmospheric particulate matter in an urban area. *J. Appl. Microbiol.*, *110*, 1612-1620.
- Gao, J. F., Fan, X. Y., Li, H. Y., & Pan, K. L. (2017). Airborne bacterial communities of PM_{2.5} in Beijing-Tianjin-Hebei megalopolis, China as revealed By Illumina MiSeq sequencing: A case study. *Aerosol Air Qual. Res.*, *17*, 788-798.

- Gao, M., Jia, R. Z., Qiu, T. L., Han, M. L., Song, Y., & Wang, X. M. (2015). Seasonal size distribution of airborne culturable bacteria and fungi and preliminary estimation of their deposition in human lungs during non-haze and haze days. *Atmos. Environ.*, *118*, 203-210.
- Gao, X. L., Shao, M. F., Luo, Y., Dong, Y. F., Ouyang, F., Dong, W. Y., & Li, J. (2016). Airborne bacterial contaminations in typical Chinese wet market with live poultry trade. *Sci. Total Environ.*, *572*, 681-687.
- Gat, D., Mazar, Y., Cytryn, E., & Rudich, Y. (2017). Origin-dependent variations in the atmospheric microbiome community in Eastern Mediterranean dust storms. *Environ. Sci. Technol.*, *51*, 6709-6718.
- Gibbs, S. G., Green, C. F., Tarwater, P. M., Mota, L. C., Mena, K. D., & Scarpino, P. V. (2006). Isolation of antibiotic-resistant bacteria from the air plume downwind of a swine confined or concentrated animal feeding operation. *Environ. Health Perspect.*, *114*, 1032-1037.
- Gilbert, Y., Veillette, M., & Duchaine, C. (2010). Airborne bacteria and antibiotic resistance genes in hospital rooms. *Aerobiologia*, *26*, 185-194.
- Gillings, M. R., Gaze, W. H., Pruden, A., Smalla, K., Tiedje, J. M., & Zhu, Y. G. (2015). Using the class 1 integron-integrase gene as a proxy for anthropogenic pollution. *ISME J.*, *9*, 1269-1279.
- Godelitsas, A., Nastos, P., Mertzimekis, T., Toli, K., Simon, R., & Göttlicher, J. (2011). A microscopic and Synchrotron-based characterization of urban particulate matter (PM₁₀-PM_{2.5} and PM_{2.5}) from Athens atmosphere, Greece. *Nucl. Instrum. Methods Phys. Res. B*, *269*, 3077-3081.
- Gotkowska-Płachta, A., Filipkowska, Z., Korzeniewska, E., Janczukowicz, W., Dixon, B., Golaś, I., & Szwalgin, D. (2013). Airborne microorganisms emitted from wastewater treatment plant treating domestic wastewater and meat processing industry wastes. *Clean–Soil, Air, Water*, *41*, 429-436.
- Guangdong Geological Survey (2010). Multi-purposes geochemical survey: Pearl River Delta, Guangdong province.
- Guangdong Statistics Bureau (2017). Guangdong statistical yearbook 2017. Beijing, China. China Statistics Press. Retrieved from http://stats.gd.gov.cn/gdtjnj/content/post_1424896.html
- Guo, S., Hu, M., Zamora, M. L., Peng, J. F., Shang, D. J., Zheng, J., Du, Z. F., Wu, Z. J., Shao, M., Zeng, L. M., Molina, M. J., & Zhang, R. Y. (2014). Elucidating severe urban haze formation in China. *Proc. Natl. Acad. Sci. U. S. A.*, *111*, 17373-17378.
- Gusareva, E. S., Acerbi, E., Lau, K. J. X., Luhung, I., Premkrishnan, B. N. V., Kolundžija, S., Purbojati, R. W., Wong, A., Houghton, J. N. I., Miller, D., Gaultier, N. E., Heinle, C. E., Clare, M. E., Vettath, V. K., Kee, C., Lim, S. B. Y., Chénard, C., Phung, W. J., Kushwaha, K. K., Ang, P. N., Putra, A., Panicker, D., Koh, Y., Yap, Z. H., Lohar, S. R.,

- Kuwata, M., Kim, H. L., Yang, L., Uchida, A., Drautz-Moses, D. I., Junqueira, A. C. M., & Schuster, S. C. (2019). Microbial communities in the tropical air ecosystem follow a precise diel cycle. *Proc. Natl. Acad. Sci. U. S. A.*, *116*, 23299-23308.
- Han, I. & Yoo, K. (2020). Metagenomic profiles of antibiotic resistance genes in activated sludge, dewatered sludge and bioaerosols. *Water*, *12*, 1516.
- Han, Y. P., Yang, T., Chen, T. Z., Li, L., & Liu, J. X. (2019). Characteristics of submicron aerosols produced during aeration in wastewater treatment. *Sci. Total Environ.*, *696*, 134019.
- Hancock, R. E. & Speert, D. P. (2000). Antibiotic resistance in *Pseudomonas aeruginosa*: mechanisms and impact on treatment. *Drug Resist. Updates*, *3*, 247-255.
- Harrison, R. M., Jones, A. M., Biggins, P. D. E., Pomeroy, N., Cox, C. S., Kidd, S. P., Hobman, J. L., Brown, N. L., & Beswick, A. (2005). Climate factors influencing bacterial count in background air samples. *Int. J. Biometeorol.*, *49*, 167-178.
- He, L. Y., Ying, G. G., Liu, Y. S., Su, H. C., Chen, J., Liu, S. S., & Zhao, J. L. (2016). Discharge of swine wastes risks water quality and food safety: Antibiotics and antibiotic resistance genes from swine sources to the receiving environments. *Environ. Int.*, *92*, 210-219.
- He, P., Wu, Y., Huang, W. Z., Wu, X. W., Lv, J. Y., Liu, P. D., Bu, L., Bai, Z. J., Chen, S. Y., & Feng, W. R. (2020). Characteristics of and variation in airborne ARGs among urban hospitals and adjacent urban and suburban communities: A metagenomic approach. *Environ. Int.*, *139*, 105625.
- He, T. T., Jin, L., Xie, J. W., Yue, S. Y., Fu, P. Q., & Li, X. D. (2021). Intracellular and extracellular antibiotic resistance genes in airborne PM_{2.5} for respiratory exposure in urban areas. *Environ. Sci. Technol. Lett.*, *8*, 128-134.
- Health Effects Institute (2020). State of Global Air 2020. Retrieved from <https://www.stateofglobalair.org>.
- Hospodsky, D., Qian, J., Nazaroff, W. W., Yamamoto, N., Bibby, K., Rismani-Yazdi, H., & Peccia, J. (2012). Human occupancy as a source of indoor airborne bacteria. *PLoS One*, *7*, e34867.
- Hu, H. W., Wang, J. T., Singh, B. K., Liu, Y. R., Chen, Y. L., Zhang, Y. J., & He, J. Z. (2018a). Diversity of herbaceous plants and bacterial communities regulates soil resistome across forest biomes. *Environ. Microbiol.*, *20*, 3186-3200.
- Hu, J. L., Zhao, F. Z., Zhang, X. X., Li, K., Li, C. R., Ye, L., & Li, M. (2018b). Metagenomic profiling of ARGs in airborne particulate matters during a severe smog event. *Sci. Total Environ.*, *615*, 1332-1340.
- Hu, X., Zhang, Y., Ding, Z. H., Wang, T. J., Lian, H. Z., Sun, Y. Y., & Wu, J. C. (2012). Bioaccessibility and health risk of arsenic and heavy metals (Cd, Co, Cr, Cu, Ni, Pb, Zn and Mn) in TSP and PM_{2.5} in Nanjing, China. *Atmos. Environ.*, *57*, 146-152.

- Huang, M. J., Chen, X. W., Zhao, Y. G., Chan, C. Y., Wang, W., Wang, X. M., & Wong, M. H. (2014a). Arsenic speciation in total contents and bioaccessible fractions in atmospheric particles related to human intakes. *Environ. Pollut.*, *188*, 37-44.
- Huang, R. J., Cheng, R., Jing, M., Yang, L., Li, Y. J., Chen, Q., Chen, Y., Yan, J., Lin, C. S., Wu, Y. F., Zhang, R. J., Haddad, I. E., Prevot, A. S. H., O'Dowd, C. D., & Cao, J. J. (2018). Source-specific health risk analysis on particulate trace elements: Coal combustion and traffic emission as major contributors in wintertime Beijing. *Environ. Sci. Technol.*, *52*, 10967-10974.
- Huang, R. J., Zhang, Y. L., Bozzetti, C., Ho, K. F., Cao, J. J., Han, Y. M., Daellenbach, K. R., Slowik, J. G., Platt, S. M., Canonaco, F., Zotter, P., Wolf, R., Pieber, S. M., Bruns, E. A., Crippa, M., Ciarelli, G., Piazzalunga, A., Schwikowski, M., Abbaszade, G., Schnelle-Kreis, J., Zimmermann, R., An, Z. S., Szidat, S., Baltensperger, U., Haddad, I. E., & Prévôt, A. S. H. (2014b). High secondary aerosol contribution to particulate pollution during haze events in China. *Nature*, *514*, 218-222.
- Huang, X., Betha, R., Tan, L., & Balasubramanian, R. (2016a). Risk assessment of bioaccessible trace elements in smoke haze aerosols versus urban aerosols using simulated lung fluids. *Atmos. Environ.*, *125*, 505-511.
- Huang, X., Betha, R., Tan, L. Y., & Balasubramanian, R. (2016b). Risk assessment of bioaccessible trace elements in smoke haze aerosols versus urban aerosols using simulated lung fluids. *Atmos. Environ.*, *125*, 505-511.
- Huang, X., Cheng, J., Bo, D., Betha, R., & Balasubramanian, R. (2016c). Bioaccessibility of Airborne Particulate-Bound Trace Elements in Shanghai and Health Risk Assessment. *Front. Environ. Sci.*, *4*, 76.
- Huang, X., Cheng, J. P., Bo, D. D., Betha, R., & Balasubramanian, R. (2016d). Bioaccessibility of airborne particulate-bound trace elements in Shanghai and health risk assessment. *Front. Environ. Sci.*, *4*, 76.
- Huang, Y. (2014). Antibiotic resistance in aquaculture production. (Doctoral dissertation). The Ohio State University. Retrieved from <https://etd.ohiolink.edu/>
- Hueglin, C., Gehrig, R., Baltensperger, U., Gysel, M., Monn, C., & Vonmont, H. (2005). Chemical characterisation of PM_{2.5}, PM₁₀ and coarse particles at urban, near-city and rural sites in Switzerland. *Atmos. Environ.*, *39*, 637-651.
- Huson, D. H., Auch, A. F., Qi, J., & Schuster, S. C. (2007). MEGAN analysis of metagenomic data. *Genome Res.*, *17*, 377-386.
- Impellitteri, C. A. (2005). Effects of pH and phosphate on metal distribution with emphasis on As speciation and mobilization in soils from a lead smelting site. *Sci. Total Environ.*, *345*, 175-190.
- Imshenetsky, A., Lysenko, S., & Kazakov, G. (1978). Upper boundary of the biosphere. *Appl. Environ. Microbiol.*, *35*, 1-5.

Itani, G. N. & Smith, C. A. (2016). Dust rains deliver diverse assemblages of microorganisms to the Eastern Mediterranean. *Sci. Rep.*, *6*, 22657.

Jacobson-Kram, D. & Montalbano, D. (1985). The reproductive effects assessment group's report on the mutagenicity of inorganic arsenic. *Environ. Mutagen.*, *7*, 787-804.

Jaenicke, R. (2005). Abundance of cellular material and proteins in the atmosphere. *Science*, *308*, 73.

Jan, A., Azam, M., Siddiqui, K., Ali, A., Choi, I., & Haq, Q. (2015). Heavy metals and human health: mechanistic insight into toxicity and counter defense system of antioxidants. *Int. J. Mol. Sci.*, *16*, 29592-29630.

Ji, X. L., Shen, Q. H., Liu, F., Ma, J., Xu, G., Wang, Y. L., & Wu, M. H. (2012). Antibiotic resistance gene abundances associated with antibiotics and heavy metals in animal manures and agricultural soils adjacent to feedlots in Shanghai; China. *J. Hazard. Mater.*, *235*, 178-185.

Jiang, W. J., Liang, P., Wang, B. Y., Fang, J. H., Lang, J. D., Tian, G., Jiang, J. K., & Zhu, T. F. (2015). Optimized DNA extraction and metagenomic sequencing of airborne microbial communities. *Nat. Protoc.*, *10*, 768-779.

Jiang, Z. J., Jolleys, M. D., Fu, T. M., Palmer, P. I., Ma, Y. P., Tian, H., Li, J., & Yang, X. (2020). Spatiotemporal and probability variations of surface PM_{2.5} over China between 2013 and 2019 and the associated changes in health risks: An integrative observation and model analysis. *Sci. Total Environ.*, *723*, 137896.

Jiangmen Statistics Bureau (2017). Statistical communique of Jiangmen on the 2016 national economic and social development (in Chinese). Retrieved from http://www.jiangmen.gov.cn/bmpd/jmstjj/zwzk/tjgybyfx/content/post_906092.html

Jin, L., Luo, X. S., Fu, P. Q., & Li, X. D. (2017). Airborne particulate matter pollution in urban China: A chemical mixture perspective from sources to impacts. *Natl. Sci. Rev.*, *4*, 593-610.

Jin, L., Xie, J. W., Wong, C. K. C., Chan, S. K., Abbaszade, G., Schnelle-Kreis, J., Zimmermann, R., Li, J., Zhang, G., Fu, P. Q., & Li, X. D. (2019). Contributions of city-specific PM_{2.5} to differential in vitro oxidative stress and toxicity implications between Beijing and Guangzhou of China. *Environ. Sci. Technol.*, *53*, 2881-2891.

Joung, Y. S., Ge, Z. F., & Buie, C. R. (2017). Bioaerosol generation by raindrops on soil. *Nat. Commun.*, *8*, 14668.

Kendall, M., Pala, K., Ucakli, S., & Gucer, S. (2011). Airborne particulate matter (PM_{2.5} and PM₁₀) and associated metals in urban Turkey. *Air Qual., Atmos. Health*, *4*, 235-242.

Kim, T. K., Hewavitharana, A. K., Shaw, P. N., & Fuerst, J. A. (2006). Discovery of a new source of rifamycin antibiotics in marine sponge actinobacteria by phylogenetic prediction. *Appl. Environ. Microbiol.*, *72*, 2118-2125.

- Knights, D., Kuczynski, J., Charlson, E. S., Zaneveld, J., Mozer, M. C., Collman, R. G., Bushman, F. D., Knight, R., & Kelley, S. T. (2011). Bayesian community-wide culture-independent microbial source tracking. *Nat. Methods*, *8*, 761.
- Labrada-Delgado, G., Aragon-Pina, A., Campos-Ramos, A., Castro-Romero, T., Amador-Munoz, O., & Villalobos-Pietrini, R. (2012). Chemical and morphological characterization of PM_{2.5} collected during MILAGRO campaign using scanning electron microscopy. *Atmos. Pollut. Res.*, *3*, 289-300.
- Lai, S. C., Zhao, Y., Ding, A. J., Zhang, Y. Y., Song, T. L., Zheng, J. Y., Ho, K. F., Lee, S. C., & Zhong, L. J. (2016). Characterization of PM_{2.5} and the major chemical components during a 1-year campaign in rural Guangzhou, Southern China. *Atmos. Res.*, *167*, 208-215.
- Lee, S.-H., Lee, H.-J., Kim, S.-J., Lee, H. M., Kang, H., & Kim, Y. P. (2010). Identification of airborne bacterial and fungal community structures in an urban area by T-RFLP analysis and quantitative real-time PCR. *Sci. Total Environ.*, *408*, 1349-1357.
- Li, B., Yang, Y., Ma, L. P., Ju, F., Guo, F., Tiedje, J. M., & Zhang, T. (2015a). Metagenomic and network analysis reveal wide distribution and co-occurrence of environmental antibiotic resistance genes. *ISME J.*, *9*, 2490-2502.
- Li, D. H., Li, Y. J., Li, G. L., Zhang, Y., Li, J., & Chen, H. S. (2019a). Fluorescent reconstitution on deposition of PM_{2.5} in lung and extrapulmonary organs. *Proc. Natl. Acad. Sci. U. S. A.*, *116*, 2488-2493.
- Li, H. M., Wang, J. H., Wang, Q. G., Qian, X., Qian, Y., Yang, M., Li, F. Y., Lu, H., & Wang, C. (2015b). Chemical fractionation of arsenic and heavy metals in fine particle matter and its implications for risk assessment: A case study in Nanjing, China. *Atmos. Environ.*, *103*, 339-346.
- Li, J., Cao, J. J., Zhu, Y. G., Chen, Q. L., Shen, F. X., Wu, Y., Xu, S. Y., Fan, H. Q., Da, G., Huang, R. J., Wang, J., de Jesus, A. L., Morawska, L., Chan, C. K., Peccia, J., & Yao, M. S. (2018a). Global survey of antibiotic resistance genes in air. *Environ. Sci. Technol.*, *52*, 10975-10984.
- Li, J., Zhou, L. T., Zhang, X. Y., Xu, C. J., Dong, L. M., & Yao, M. S. (2016a). Bioaerosol emissions and detection of airborne antibiotic resistance genes from a wastewater treatment plant. *Atmos. Environ.*, *124*, 404-412.
- Li, L. G., Yin, X. L., & Zhang, T. (2018b). Tracking antibiotic resistance gene pollution from different sources using machine-learning classification. *Microbiome*, *6*, 93.
- Li, L. Y., Wang, Q., Bi, W. J., Hou, J., Xue, Y. G., Mao, D. Q., Das, R., Luo, Y., & Li, X. D. (2020). Municipal solid waste treatment system increases ambient airborne bacteria and antibiotic resistance genes. *Environ. Sci. Technol.*, *54*, 3900-3908.

- Li, M., Lian, X. W., Wang, J., Su, G. N., Guo, Z. Z., & Guo, L. C. (2016b). Pollution characteristics of metal components in PM_{2.5} in two districts of Guangzhou (in Chinese). *J. Environ. Occup. Med.*, *33*, 650-656.
- Li, T., Hu, R., Chen, Z., Li, Q. Y., Huang, S. X., Zhu, Z., & Zhou, L. F. (2018c). Fine particulate matter (PM_{2.5}): The culprit for chronic lung diseases in China. *Chronic Dis. Transl. Med.*, *4*, 176-186.
- Li, X. D., Jin, L., & Kan, H. D. (2019b). Air pollution: a global problem needs local fixes. *Nature*, *570*, 437-439.
- Li, Y. P., Zhang, H. F., Qiu, X. H., Zhang, Y. R., & Wang, H. R. (2013). Dispersion and risk assessment of bacterial aerosols emitted from rotating-brush aerator during summer in a wastewater treatment plant of Xi'an, China. *Aerosol Air Qual. Res.*, *13*, 1807-1814.
- Liang, Z. S., Yu, Y., Ye, Z. K., Li, G. Y., Wang, W. J., & An, T. C. (2020). Pollution profiles of antibiotic resistance genes associated with airborne opportunistic pathogens from typical area, Pearl River Estuary and their exposure risk to human. *Environ. Int.*, *143*, 105934.
- Liao, Q. L., Liu, C., Jin, Y., Hua, M., Zheng, L. C., Pan, Y. M., & Huang, S. S. (2011). On geochemical regionalization of soils in Jiangsu (in Chinese). *J. Geol.*, *35*, 225-235.
- Ling, A. L., Pace, N. R., Hernandez, M. T., & LaPara, T. M. (2013). Tetracycline resistance and class 1 integron genes associated with indoor and outdoor aerosols. *Environ. Sci. Technol.*, *47*, 4046-4052.
- Liu, J. W., Li, J., Zhang, Y. L., Liu, D., Ding, P., Shen, C. D., Shen, K. J., He, Q. F., Ding, X., Wang, X. M., Chen, D. H., Szidat, S., & Zhang, G. (2014). Source apportionment using radiocarbon and organic tracers for PM_{2.5} carbonaceous aerosols in Guangzhou, South China: Contrasting local-and regional-scale haze events. *Environ. Sci. Technol.*, *48*, 12002-12011.
- Liu, K. K., Shang, Q. M., & Wan, C. Y. (2018). Sources and health risks of heavy metals in PM_{2.5} in a campus in a typical suburb area of Taiyuan, North China. *Atmosphere*, *9*, 46.
- Liu, P. P., Lei, Y. L., Ren, H. R., Gao, J. J., Xu, H. M., Shen, Z. X., Zhang, Q., Zheng, C. L., Liu, H. X., Zhang, R. J., & Pan, H. (2017). Seasonal variation and health risk assessment of heavy metals in PM_{2.5} during winter and summer over Xi'an, China. *Atmosphere*, *8*, 91.
- Lu, J., Breitwieser, F. P., Thielen, P., & Salzberg, S. L. (2017). Bracken: estimating species abundance in metagenomics data. *PeerJ Comput. Sci.*, *3*, e104.
- Lu, S. L., Liu, D. Y., Zhang, W. C., Liu, P. W., Fei, Y., Gu, Y., Wu, M. H., Yu, S., Yonemochi, S., Wang, X. J., & Wang, Q. Y. (2015). Physico-chemical characterization of PM_{2.5} in the microenvironment of Shanghai subway. *Atmos. Res.*, *153*, 543-552.

- Lu, S. L., Yao, Z. K., Chen, X. H., Wu, M. H., Sheng, G. Y., Fu, J. M., & Daly, P. (2008). The relationship between physicochemical characterization and the potential toxicity of fine particulates (PM_{2.5}) in Shanghai atmosphere. *Atmos. Environ.*, *42*, 7205-7214.
- Luhung, I., Wu, Y., Ng, C. K., Miller, D., Cao, B., & Chang, V. W. C. (2015). Protocol improvements for low concentration DNA-based bioaerosol sampling and analysis. *PLoS One*, *10*, e0141158.
- Luo, Y., Mao, D. Q., Rysz, M., Zhou, Q. X., Zhang, H. J., Xu, L., & JJ Alvarez, P. (2010). Trends in antibiotic resistance genes occurrence in the Haihe River, China. *Environ. Sci. Technol.*, *44*, 7220-7225.
- Lymperopoulou, D. S., Adams, R. I., & Lindow, S. E. (2016). Contribution of vegetation to the microbial composition of nearby outdoor air. *Appl. Environ. Microbiol.*, *82*, 3822-3833.
- Lyu, X. P., Chen, N., Guo, H., Zeng, L. W., Zhang, W. H., Shen, F., Quan, J. H., & Wang, N. (2016). Chemical characteristics and causes of airborne particulate pollution in warm seasons in Wuhan, central China. *Atmos. Chem. Phys.*, *16*, 10671-10687.
- Ma, J. H., Xu, J. M., & Qu, Y. H. (2020). Evaluation on the surface PM_{2.5} concentration over China mainland from NASA's MERRA-2. *Atmos. Environ.*, 117666.
- Ma, L. P., Li, A. D., Yin, X. L., & Zhang, T. (2017). The prevalence of integrons as the carrier of antibiotic resistance genes in natural and man-made environments. *Environ. Sci. Technol.*, *51*, 5721-5728.
- Mackelprang, R., Waldrop, M. P., DeAngelis, K. M., David, M. M., Chavarria, K. L., Blazewicz, S. J., Rubin, E. M., & Jansson, J. K. (2011). Metagenomic analysis of a permafrost microbial community reveals a rapid response to thaw. *Nature*, *480*, 368-371.
- Mao, Y. X., Ding, P., Wang, Y. B., Ding, C., Wu, L. P., Zheng, P., Zhang, X., Li, X., Wang, L. Y., & Sun, Z. K. (2019). Comparison of culturable antibiotic-resistant bacteria in polluted and non-polluted air in Beijing, China. *Environ. Int.*, *131*, 104936.
- Marques, M. R., Loebenberg, R., & Almukainzi, M. (2011). Simulated biological fluids with possible application in dissolution testing. *Dissolut. Technol.*, *18*, 15-28.
- Martinez, J. L. & Baquero, F. (2000). Mutation frequencies and antibiotic resistance. *Antimicrob. Agents Chemother.*, *44*, 1771-1777.
- Martinez, J. L., Fajardo, A., Garmendia, L., Hernandez, A., Linares, J. F., Martinez-Solano, L., & Sanchez, M. B. (2009). A global view of antibiotic resistance. *FEMS Microbiol. Rev.*, *33*, 44-65.
- Mazar, Y., Cytryn, E., Erel, Y., & Rudich, Y. (2016). Effect of dust storms on the atmospheric microbiome in the Eastern Mediterranean. *Environ. Sci. Technol.*, *50*, 4194-4202.

- McEachran, A. D., Blackwell, B. R., Hanson, J. D., Wooten, K. J., Mayer, G. D., Cox, S. B., & Smith, P. N. (2015). Antibiotics, bacteria, and antibiotic resistance genes: Aerial transport from cattle feed yards via particulate matter. *Environ. Health Perspect.*, *123*, 337-343.
- Melbostad, E., Eduard, W., Skogstad, A., Sandven, P., Lassen, J., Sjøstrand, P., & Haldal, K. (1994). Exposure to bacterial aerosols and work-related symptoms in sewage workers. *Am. J. Ind. Med.*, *25*, 59-63.
- Menon, S., Hansen, J., Nazarenko, L., & Luo, Y. (2002). Climate effects of black carbon aerosols in China and India. *Science*, *297*, 2250-2253.
- Ming, L. L. (2017). Fine atmospheric particles (PM_{2.5}) in large city clusters, China: chemical compositions, temporal-spatial variations and regional transport. (Doctoral dissertation). The Hong Kong Polytechnic University. Retrieved from <https://theses.lib.polyu.edu.hk/handle/200/9004>
- Ming, L. L., Jin, L., Li, J., Fu, P. Q., Yang, W. Y., Liu, D., Zhang, G., Wang, Z. F., & Li, X. D. (2017). PM_{2.5} in the Yangtze River Delta, China: Chemical compositions, seasonal variations, and regional pollution events. *Environ. Pollut.*, *223*, 200-212.
- Mitra, S., Stärk, M., & Huson, D. H. (2011). Analysis of 16S rRNA environmental sequences using MEGAN. *BMC genomics*, *12*, 1-7.
- Murata, K. & Zhang, D. Z. (2016). Concentration of bacterial aerosols in response to synoptic weather and land-sea breeze at a seaside site downwind of the Asian continent. *J. Geophys. Res. Atmos.*, *121*, 11,636-611,647.
- Nadkarni, M. A., Martin, F. E., Jacques, N. A., & Hunter, N. (2002). Determination of bacterial load by real-time PCR using a broad-range (universal) probe and primers set. *Microbiology*, *148*, 257-266.
- Nanjing Municipal Statistics Bureau (2017). Nanjing statistical yearbook 2017 (in Chinese). Nanjing, China. Nanjing Press. Retrieved from <http://221.226.86.104/file/2017/quxian/index.htm>
- National Bureau of Statistics of China (2014). China energy statistical yearbook 2014. Beijing, China. China Statistics Press. Retrieved from <http://www.stats.gov.cn/tjsj/ndsj/2014/indexeh.htm>
- Nicholas, A. B., Thissen, J. B., Fofanov, V. Y., Allen, J. E., Rojas, M., Golovko, G., Fofanov, Y., Koshinsky, H., & Jaing, C. J. (2015). Metagenomic analysis of the airborne environment in urban spaces. *Microb. Ecol.*, *69*, 346-355.
- Nocoń, K., Rogula-Kozłowska, W., & Widziewicz, K. (2018). Research on chromium and arsenic speciation in atmospheric particulate matter: short review. E3S Web Conf., EDP Sciences.

- Norris, G., Duvall, R., Brown, S., & Bai, S. (2014a). EPA Positive Matrix Factorization (PMF) 5.0 fundamentals and User Guide Prepared for the US Environmental Protection Agency Office of Research and Development, Washington, DC. *Inc., Petaluma*.
- Norris, G. A., Duvall, R., Brown, S. G., & Bai, S. (2014b). EPA positive matrix factorization (PMF) 5.0 fundamentals and user guide. U.S. Environmental Protection Agency, Washington, DC.
- OEHHA (2014). Inorganic arsenic reference exposure levels California EPA, Sacramento, CA. Retrieved from <https://oehha.ca.gov/media/downloads/cmr/appendixd1final.pdf>
- Ogier, J.-C., Pagès, S., Galan, M., Barret, M., & Gaudriault, S. (2019). rpoB, a promising marker for analyzing the diversity of bacterial communities by amplicon sequencing. *BMC Microbiol.*, *19*, 171.
- Oh, M., Pruden, A., Chen, C. Q., Heath, L. S., Xia, K., & Zhang, L. Q. (2018). MetaCompare: a computational pipeline for prioritizing environmental resistome risk. *FEMS Microbiol. Ecol.*, *94*, fiy079.
- Okamoto, K., Gotoh, N., & Nishino, T. (2001). Pseudomonas aeruginosa reveals high intrinsic resistance to penem antibiotics: penem resistance mechanisms and their interplay. *Antimicrob. Agents Chemother.*, *45*, 1964-1971.
- Oosthuizen, M. A., Wright, C. Y., Matooane, M., & Phala, N. (2015). Human health risk assessment of airborne metals to a potentially exposed community: a screening exercise. *Clean Air J.*, *25*, 51-57.
- Ouyang, W. Y., Huang, F. Y., Zhao, Y., Li, H., & Su, J. Q. (2015). Increased levels of antibiotic resistance in urban stream of Jiulongjiang River, China. *Appl. Microbiol. Biotechnol.*, *99*, 5697-5707.
- Pace, N. R. (1997). A molecular view of microbial diversity and the biosphere. *Science*, *276*, 734-740.
- Pal, C., Bengtsson-Palme, J., Kristiansson, E., & Larsson, D. J. (2016). The structure and diversity of human, animal and environmental resistomes. *Microbiome*, *4*, 54.
- Pan, Y. P., Tian, S. L., Li, X. R., Sun, Y., Li, Y., Wentworth, G. R., & Wang, Y. S. (2015). Trace elements in particulate matter from metropolitan regions of Northern China: Sources, concentrations and size distributions. *Sci. Total Environ.*, *537*, 9-22.
- Park, E.-j., Kim, D.-s., & Park, K. (2008). Monitoring of ambient particles and heavy metals in a residential area of Seoul, Korea. *Environ. Monit. Assess.*, *137*, 441-449.
- Patterson, A. J., Colangeli, R., Spigaglia, P., & Scott, K. P. (2007). Distribution of specific tetracycline and erythromycin resistance genes in environmental samples assessed by macroarray detection. *Environ. Microbiol.*, *9*, 703-715.
- Peng, X., Shi, G. L., Liu, G. R., Xu, J., Tian, Y. Z., Zhang, Y. F., Feng, Y. C., & Russell, A. G. (2017). Source apportionment and heavy metal health risk (HMHR) quantification

from sources in a southern city in China, using an ME2-HMHR model. *Environ. Pollut.*, *221*, 335-342.

Peng, Y., Leung, H. C., Yiu, S. M., & Chin, F. Y. (2012). IDBA-UD: a de novo assembler for single-cell and metagenomic sequencing data with highly uneven depth. *Bioinformatics*, *28*, 1420-1428.

Poole, K. (2001). Multidrug efflux pumps and antimicrobial resistance in *Pseudomonas aeruginosa* and related organisms. *J. Mol. Microbiol. Biotechnol.*, *3*, 255-264.

Pruden, A., Pei, R. T., Storteboom, H., & Carlson, K. H. (2006). Antibiotic resistance genes as emerging contaminants: Studies in northern Colorado. *Environ. Sci. Technol.*, *40*, 7445-7450.

Qi, L., Chen, M. D., Ge, X. L., Zhang, Y. F., & Guo, B. F. (2016). Seasonal variations and sources of 17 aerosol metal elements in suburban Nanjing, China. *Atmosphere*, *7*, 153.

Rahman, M. A., Paul, S. C., Siddique, N. E. A., & Alam, A. M. S. (2008). Voltammetric study of arsenic (III) and arsenic (V) in ground water of Hajigonj and Kalkini in Bangladesh. *Pak. J. Anal. Environ. Chem.*, *9*, 7.

Ravel, B. & Newville, M. (2005). ATHENA, ARTEMIS, HEPHAESTUS: data analysis for X-ray absorption spectroscopy using IFEFFIT. *J. Synchrotron Radiat.*, *12*, 537-541.

Rizzo, M. J. & Scheff, P. A. (2007). Utilizing the chemical mass balance and positive matrix factorization models to determine influential species and examine possible rotations in receptor modeling results. *Atmos. Environ.*, *41*, 6986-6998.

Salyers, A. A. & Amabile-Cuevas, C. F. (1997). Why are antibiotic resistance genes so resistant to elimination? *Antimicrob. Agents Chemother.*, *41*, 2321-2325.

Samanta, G., Chowdhury, T. R., Mandal, B. K., Biswas, B. K., Chowdhury, U. K., Basu, G. K., Chanda, C. R., Lodh, D., & Chakraborti, D. (1999). Flow injection hydride generation atomic absorption spectrometry for determination of arsenic in water and biological samples from arsenic-affected districts of West Bengal, India, and Bangladesh. *Microchem. J.*, *62*, 174-191.

Sánchez-Rodas, D., de la Campa, A. M. S., Jesús, D., Oliveira, V., Gómez-Ariza, J. L., Querol, X., & Alastuey, A. (2007). Arsenic speciation of atmospheric particulate matter (PM10) in an industrialised urban site in southwestern Spain. *Chemosphere*, *66*, 1485-1493.

Schaeffer, J., Reynolds, S. J., Magzamen, S., VanDyke, A., Gottel, N., Gilbert, J., Owens, S., Hampton-Marcell, J. T., & Volckens, J. (2017). Size, composition, and source profiles of inhalable bioaerosols from Colorado dairies. *Environ. Sci. Technol.*, *51*, 6430-6440.

Schages, L., Wichern, F., Kalscheuer, R., & Bockmühl, D. (2020). Winter is coming – Impact of temperature on the variation of beta-lactamase and mcr genes in a wastewater treatment plant. *Sci. Total Environ.*, *712*, 136499.

- Schmitt, H., Stoob, K., Hamscher, G., Smit, E., & Seinen, W. (2006). Tetracyclines and tetracycline resistance in agricultural soils: Microcosm and field studies. *Microb. Ecol.*, *51*, 267-276.
- Sebat, J. L., Colwell, F. S., & Crawford, R. L. (2003). Metagenomic profiling: Microarray analysis of an environmental genomic library. *Appl. Environ. Microbiol.*, *69*, 4927-4934.
- Segata, N., Izard, J., Waldron, L., Gevers, D., Miropolsky, L., Garrett, W. S., & Huttenhower, C. (2011). Metagenomic biomarker discovery and explanation. *Genome Biol.*, *12*, R60.
- Seinfeld, J. H. & Pandis, S. N. (2016). Atmospheric chemistry and physics: from air pollution to climate change. John Wiley & Sons.
- Shi, P., Jia, S. Y., Zhang, X. X., Zhang, T., Cheng, S. P., & Li, A. M. (2013). Metagenomic insights into chlorination effects on microbial antibiotic resistance in drinking water. *Water Res.*, *47*, 111-120.
- Smets, W., Moretti, S., Denys, S., & Lebeer, S. (2016). Airborne bacteria in the atmosphere: Presence, purpose, and potential. *Atmos. Environ.*, *139*, 214-221.
- Smichowski, P., Polla, G., & Gómez, D. (2005). Metal fractionation of atmospheric aerosols via sequential chemical extraction: a review. *Anal. Bioanal. Chem.*, *381*, 302-316.
- Smith, D. J., Jaffe, D. A., Birmele, M. N., Griffin, D. W., Schuerger, A. C., Hee, J., & Roberts, M. S. (2012). Free tropospheric transport of microorganisms from Asia to North America. *Microb. Ecol.*, *64*, 973-985.
- So, K. L., Guo, H., & Li, Y. S. (2007). Long-term variation of PM_{2.5} levels and composition at rural, urban, and roadside sites in Hong Kong: Increasing impact of regional air pollution. *Atmos. Environ.*, *41*, 9427-9434.
- Sørensen, M., Schins, R. P., Hertel, O., & Loft, S. (2005). Transition metals in personal samples of PM_{2.5} and oxidative stress in human volunteers. *Cancer Epidemiol. Biomarkers Prev.*, *14*, 1340-1343.
- State Council of the People's Republic of China (2013). Air pollution prevention and control action plan (in Chinese). Document NO. GUOFA[2013]37.
- State Council of the People's Republic of China (2019). The outline of the Yangtze River Delta regional integrated development plan.
- Su, H. C., Hu, X. J., Xu, Y., Xu, W. J., Huang, X. S., Wen, G. L., Yang, K., Li, Z. J., & Cao, Y. C. (2018a). Persistence and spatial variation of antibiotic resistance genes and bacterial populations change in reared shrimp in South China. *Environ. Int.*, *119*, 327-333.

- Su, H. C., Liu, Y. S., Pan, C. G., Chen, J., He, L. Y., & Ying, G. G. (2018b). Persistence of antibiotic resistance genes and bacterial community changes in drinking water treatment system: From drinking water source to tap water. *Sci. Total Environ.*, *616*, 453-461.
- Sun, X. Z., Li, D. M., Li, B., Sun, S. J., Yabo, S. D., Geng, J. L., Ma, L. X., & Qi, H. (2020). Exploring the disparity of inhalable bacterial communities and antibiotic resistance genes between hazy days and non-hazy days in a cold megacity in Northeast China. *J. Hazard. Mater.*, 122984.
- Tan, J. H., Duan, J. C., Ma, Y. L., Yang, F. M., Cheng, Y., He, K. B., Yu, Y. C., & Wang, J. W. (2014). Source of atmospheric heavy metals in winter in Foshan, China. *Sci. Total Environ.*, *493*, 262-270.
- Tan, L., Li, L. Y., Ashbolt, N., Wang, X. L., Cui, Y. X., Zhu, X., Xu, Y., Yang, Y., Mao, D. Q., & Luo, Y. (2017). Arctic antibiotic resistance gene contamination, a result of anthropogenic activities and natural origin. *Sci. Total Environ.*, *621*, 1176-1184.
- Tao, J., Zhang, L. M., Cao, J. J., Zhong, L. J., Chen, D. S., Yang, Y. H., Chen, D. H., Chen, L. G., Zhang, Z. S., Wu, Y. F., Xia, Y. J., Ye, S. Q., & Zhang, R. J. (2017). Source apportionment of PM_{2.5} at urban and suburban areas of the Pearl River Delta region, south China-with emphasis on ship emissions. *Sci. Total Environ.*, *574*, 1559-1570.
- Tao, J., Zhang, L. M., Engling, G., Zhang, R. J., Yang, Y. H., Cao, J. J., Zhu, C. S., Wang, Q. Y., & Luo, L. (2013). Chemical composition of PM_{2.5} in an urban environment in Chengdu, China: Importance of springtime dust storms and biomass burning. *Atmos. Res.*, *122*, 270-283.
- The Institute for Health Metrics and Evaluation (2019). Global Burden of Disease (GBD) Project. Retrieved from <http://www.healthdata.org/gbd/2019>.
- Thurston, G. D., Burnett, R. T., Turner, M. C., Shi, Y., Krewski, D., Lall, R., Ito, K., Jerrett, M., Gapstur, S. M., Diver, W. R., & Pope III, C. A. (2016). Ischemic heart disease mortality and long-term exposure to source-related components of US fine particle air pollution. *Environ. Health Perspect.*, *124*, 785-794.
- Tong, Y. Y. & Lighthart, B. (1997). Solar radiation is shown to select for pigmented outdoor atmosphere. *Photochem. Photobiol.*, *65*, 103-106.
- Uetake, J., Tobo, Y., Uji, Y., Hill, T., DeMott, P., Kreidenweis, S., & Misumi, R. (2019). Seasonal changes of airborne bacterial communities over Tokyo and influence of local meteorology. *Front. Microbiol.*, *10*, 1572.
- Urban, R. C., Lima-Souza, M., Caetano-Silva, L., Queiroz, M. E. C., Nogueira, R. F., Allen, A. G., Cardoso, A. A., Held, G., & Campos, M. L. A. (2012). Use of levoglucosan, potassium, and water-soluble organic carbon to characterize the origins of biomass-burning aerosols. *Atmos. Environ.*, *61*, 562-569.
- USEPA (1989). Risk assessment guidance for Superfund. Volume I: Human health evaluation manual (Part A). U.S. Environmental Protection Agency, Washington, D.C.

Retrieved from https://www.epa.gov/sites/production/files/2015-09/documents/rags_a.pdf

USEPA (1994). Health effects notebook for hazardous air pollutants. Office of Air Quality Planning and Standards, U.S. Environmental Protection Agency, Washington, D.C. Retrieved from <https://www.epa.gov/haps/health-effects-notebook-hazardous-air-pollutants>

USEPA (2007). Arsenic, inorganic (CASRN 7440-38-2). U.S. Environmental Protection Agency, Washington, D.C. Retrieved from https://cfpub.epa.gov/ncea/iris/iris_documents/documents/subst/0278_summary.pdf

USEPA (2009). Risk assessment guidance for Superfund. Volume I: Human health evaluation manual. Part F(Final). U.S. Environmental Protection Agency, Washington, D.C. Retrieved from <https://www.epa.gov/risk/risk-assessment-guidance-superfund-rags-part-f>

USEPA (2018a). Regional screening levels (RSLs) – generic tables (2018). U.S. Environmental Protection Agency, Washington, D.C. Retrieved from <https://www.epa.gov/risk/regional-screening-levels-rsls-generic-tables>

USEPA (2018b). Regional Screening Levels (RSLs) – User's Guide. U.S. Environmental Protection Agency, Washington, D.C. Retrieved from <https://www.epa.gov/risk/regional-screening-levels-rsls-users-guide>

Van Hoek, A. H. A. M., Mevius, D., Guerra, B., Mullany, P., Roberts, A. P., & Aarts, H. J. M. (2011). Acquired antibiotic resistance genes: an overview. *Front. Microbiol.*, 2, 203.

Větrovský, T. & Baldrian, P. (2013). The variability of the 16S rRNA gene in bacterial genomes and its consequences for bacterial community analyses. *PLoS One*, 8, e57923.

Wang, G. H., Huang, L. M., Gao, S. X., Gao, S. T., & Wang, L. S. (2002). Measurements of PM₁₀ and PM_{2.5} in urban area of Nanjing, China and the assessment of pulmonary deposition of particle mass. *Chemosphere*, 48, 689-695.

Wang, X. F., He, S. L., Chen, S. C., Zhang, Y. L., Wang, A. H., Luo, J. B., Ye, X. L., Mo, Z., Wu, L. Z., Xu, P. W., Cai, G. F., Chen, Z. J., & Lou, X. M. (2018). Spatiotemporal characteristics and health risk assessment of heavy metals in PM_{2.5} in Zhejiang Province. *Int. J. Environ. Res. Public Health*, 15, 583.

Wang, Y. H., Hu, L. F., & Lu, G. H. (2015). Health risk assessments based on existing data of arsenic, chromium, lead, and zinc in China's air. *Hum. Ecol. Risk Assess.*, 21, 560-573.

Wang, Y. S., Li, A. G., Zhan, Y. X., Wei, L., Li, Y., Zhang, G. L., Xie, Y. N., Zhang, J., Zhang, Y. M., & Shan, Z. C. (2007). Speciation of elements in atmospheric particulate matter by XANES. *J. Radioanal. Nucl. Chem.*, 273, 247-251.

Wang, Y. Z., Wang, C., & Song, L. (2019). Distribution of antibiotic resistance genes and bacteria from six atmospheric environments: Exposure risk to human. *Sci. Total Environ.*, 694, 133750.

Wei, M., Xu, C. H., Xu, X. M., Zhu, C., Li, J. R., & Lv, G. L. (2019). Characteristics of atmospheric bacterial and fungal communities in PM_{2.5} following biomass burning disturbance in a rural area of North China Plain. *Sci. Total Environ.*, 651, 2727-2739.

Wéry, N. (2014). Bioaerosols from composting facilities—a review. *Front. Cell. Infect. Microbiol.*, 4, 42.

WHO (2018). Ambient (outdoor) air quality and health. Retrieved from [https://www.who.int/news-room/fact-sheets/detail/ambient-\(outdoor\)-air-quality-and-health](https://www.who.int/news-room/fact-sheets/detail/ambient-(outdoor)-air-quality-and-health)

Widziewicz, K., Rogula-Kozłowska, W., & Loska, K. (2016). Cancer risk from arsenic and chromium species bound to PM_{2.5} and PM₁—Polish case study. *Atmos. Pollut. Res.*, 7, 884-894.

Wiseman, C. L. S. & Zereini, F. (2014). Characterizing metal (loid) solubility in airborne PM₁₀, PM_{2.5} and PM₁ in Frankfurt, Germany using simulated lung fluids. *Atmos. Environ.*, 89, 282-289.

Witte, W. (1998). Medical consequences of antibiotic use in agriculture. *Science*, 279, 996-997.

Wood, D. E., Lu, J., & Langmead, B. (2019). Improved metagenomic analysis with Kraken 2. *Genome Biol.*, 20, 257.

Wu, D., Huang, X. H., Sun, J. Z., Graham, D. W., & Xie, B. (2017). Antibiotic resistance genes and associated microbial community conditions in aging landfill systems. *Environ. Sci. Technol.*, 51, 12859–12867.

Xi, C. W., Zhang, Y. L., Marrs, C. F., Ye, W., Simon, C., Foxman, B., & Nriagu, J. (2009). Prevalence of antibiotic resistance in drinking water treatment and distribution systems. *Appl. Environ. Microbiol.*, 75, 5714-5718.

Xie, S. S., Gu, A. Z., Cen, T. Y., Li, D., & Chen, J. M. (2019). The effect and mechanism of urban fine particulate matter (PM_{2.5}) on horizontal transfer of plasmid-mediated antimicrobial resistance genes. *Sci. Total Environ.*, 683, 116-123.

Xu, C., Wei, M., Chen, J., Wang, X., Zhu, C., Li, J., Zheng, L., Sui, G., Li, W., Wang, W., Zhang, Q., & Mellouki, A. (2016a). Bacterial characterization in ambient submicron particles during severe haze episodes at Ji'nan, China. *Sci. Total Environ.*, 580, 188-196.

Xu, C. H., Wei, M., Chen, J. M., Zhu, C., Li, J. R., Xu, X. M., Wang, W. X., Zhang, Q. Z., Ding, A. J., Kan, H. D., Zhao, Z. H., & Mellouki, A. (2019). Profile of inhalable bacteria in PM_{2.5} at Mt. Tai, China: Abundance, community, and influence of air mass trajectories. *Ecotoxicol. Environ. Saf.*, 168, 110-119.

- Xu, L. K., Ouyang, W. Y., Qian, Y. Y., Su, C., Su, J. Q., & Chen, H. (2016b). High-throughput profiling of antibiotic resistance genes in drinking water treatment plants and distribution systems. *Environ. Pollut.*, *213*, 119-126.
- Yang, F. X., Mao, D. Q., Zhou, H., Wang, X. L., & Luo, Y. (2016). Propagation of New Delhi metallo- β -lactamase genes (*bla_{NDM-1}*) from a wastewater treatment plant to its receiving river. *Environ. Sci. Technol. Lett.*, *3*, 138-143.
- Yang, G. S., Ma, L. L., Xu, D. D., Li, J., He, T. T., Liu, L. Y., Jia, H. L., Zhang, Y. B., Chen, Y., & Chai, Z. F. (2012). Levels and speciation of arsenic in the atmosphere in Beijing, China. *Chemosphere*, *87*, 845-850.
- Yang, K., Li, L., Wang, Y., Xue, S., Han, Y., & Liu, J. (2019). Airborne bacteria in a wastewater treatment plant: Emission characterization, source analysis and health risk assessment. *Water Res.*, *149*, 596-606.
- Yang, Y., Zhou, R. J., Chen, B. W., Zhang, T., Hu, L. G., & Zou, S. C. (2018). Characterization of airborne antibiotic resistance genes from typical bioaerosol emission sources in the urban environment using metagenomic approach. *Chemosphere*, *213*, 463-471.
- Ye, W. F., Ma, Z. Y., & Ha, X. Z. (2018). Spatial-temporal patterns of PM_{2.5} concentrations for 338 Chinese cities. *Sci. Total Environ.*, *631*, 524-533.
- Zeng, L. W., Offor, F., Zhan, L. X., Lyu, X. P., Liang, Z. R., Zhang, L. Y., Wang, J. Y., Cheng, H. R., & Guo, H. (2019). Comparison of PM_{2.5} pollution between an African city and an Asian metropolis. *Sci. Total Environ.*, *696*, 134069.
- Zereini, F., Wiseman, C. L. S., & Püttmann, W. (2012). In vitro investigations of platinum, palladium, and rhodium mobility in urban airborne particulate matter (PM₁₀, PM_{2.5}, and PM₁) using simulated lung fluids. *Environ. Sci. Technol.*, *46*, 10326-10333.
- Zhang, A. N., Hou, C. J., Negi, M., Li, L. G., & Zhang, T. (2020a). Online searching platform for the antibiotic resistome in bacterial tree of life and global habitats. *FEMS Microbiol. Ecol.*, *96*, fiae107.
- Zhang, K. P., Delgado-Baquerizo, M., Zhu, Y. G., & Chu, H. Y. (2020b). Space is more important than season when shaping soil microbial communities at a large spatial scale. *mSystems*, *5*, e00783-00719.
- Zhang, M. Y., Zuo, J. N., Yu, X., Shi, X. C., Chen, L., & Li, Z. X. (2018). Quantification of multi-antibiotic resistant opportunistic pathogenic bacteria in bioaerosols in and around a pharmaceutical wastewater treatment plant. *J. Environ. Sci.*, *72*, 53-63.
- Zhang, N., Han, B., He, F., Xu, J., Zhao, R., Zhang, Y., & Bai, Z. (2017). Chemical characteristic of PM_{2.5} emission and inhalational carcinogenic risk of domestic Chinese cooking. *Environ. Pollut.*, *227*, 24-30.

- Zhang, S. J., Du, R., Chen, H. L., Ren, W. S., & Du, P. R. (2019a). Seasonal variation of microbial activity and pathogenic bacteria under non-serious pollution levels in Beijing. *Aerosol Air Qual. Res.*, *19*, 1798-1807.
- Zhang, T. & Fang, H. H. P. (2000). Digitization of DGGE (denaturing gradient gel electrophoresis) profile and cluster analysis of microbial communities. *Biotechnol. Lett.*, *22*, 399-405.
- Zhang, T. & Fang, H. H. P. (2005). 16S rDNA clone library screening of environmental sample using melting curve analysis. *J. Chin. Inst. Eng.*, *28*, 1153-1155.
- Zhang, T., Li, X. Y., Wang, M. F., Chen, H. X., Yang, Y., Chen, Q. L., & Yao, M. S. (2019b). Time-resolved spread of antibiotic resistance genes in highly polluted air. *Environ. Int.*, *127*, 333-339.
- Zhang, T., Li, X. Y., Wang, M. F., Chen, H. X., & Yao, M. S. (2019c). Microbial aerosol chemistry characteristics in highly polluted air. *Sci. China Chem.*, *62*, 1051-1063.
- Zhang, Y. L. & Cao, F. (2015). Fine particulate matter (PM_{2.5}) in China at a city level. *Sci. Rep.*, *5*, 14884.
- Zhao, Y. H., Chen, Z. Y., Hou, J., Mao, D. Q., Lin, H., Xue, Y. G., & Luo, Y. (2020). Monitoring antibiotic resistomes and bacterial microbiomes in the aerosols from fine, hazy, and dusty weather in Tianjin, China using a developed high-volume tandem liquid impinging sampler. *Sci. Total Environ.*, *731*, 139242.
- Zhen, Q., Deng, Y., Wang, Y. Q., Wang, X. K., Zhang, H. X., Sun, X., & Ouyang, Z. Y. (2017). Meteorological factors had more impact on airborne bacterial communities than air pollutants. *Sci. Total Environ.*, *601*, 703-712.
- Zhou, H., Wang, X. L., Li, Z. H., Kuang, Y., Mao, D. Q., & Luo, Y. (2018a). Occurrence and distribution of urban dust-associated bacterial antibiotic resistance in northern China. *Environ. Sci. Technol. Lett.*, *5*, 50-55.
- Zhou, J., Wei, J. J., Choy, K. T., Sia, S. F., Rowlands, D. K., Yu, D., Wu, C. Y., Lindsley, W. G., Cowling, B. J., McDevitt, J., Peiris, M., Li, Y. G., & Yen, H. L. (2018b). Defining the sizes of airborne particles that mediate influenza transmission in ferrets. *Proc. Natl. Acad. Sci. U. S. A.*, *115*, E2386-E2392.
- Zhou, S. Z., Davy, P. K., Huang, M. J., Duan, J. B., Wang, X. M., Fan, Q., Chang, M., Liu, Y. M., Chen, W. H., Xie, S. J., Ancelet, T., & Trompetter, W. J. (2018c). High-resolution sampling and analysis of ambient particulate matter in the Pearl River Delta region of southern China: source apportionment and health risk implications. *Atmos. Chem. Phys.*, *18*, 2049-2064.
- Zhou, X., Qiao, M., Su, J. Q., Wang, Y., Cao, Z. H., Cheng, W. D., & Zhu, Y. G. (2019). Turning pig manure into biochar can effectively mitigate antibiotic resistance genes as organic fertilizer. *Sci. Total Environ.*, *649*, 902-908.

Zhu, B. K., Chen, Q. L., Chen, S. C., & Zhu, Y. G. (2017a). Does organically produced lettuce harbor higher abundance of antibiotic resistance genes than conventionally produced? *Environ. Int.*, 98, 152-159.

Zhu, Y. G., Zhao, Y., Li, B., Huang, C. L., Zhang, S. Y., Yu, S., Chen, Y. S., Zhang, T., Gillings, M. R., & Su, J. Q. (2017b). Continental-scale pollution of estuaries with antibiotic resistance genes. *Nat. Microbiol.*, 2, 16270.

Zhuo, S. J., Shen, G. F., Zhu, Y., Du, W., Pan, X. L., Li, T. C., Han, Y., Li, B. G., Liu, J. F., Cheng, H. F., Xing, B. S., & Tao, S. (2017). Source-oriented risk assessment of inhalation exposure to ambient polycyclic aromatic hydrocarbons and contributions of non-priority isomers in urban Nanjing, a megacity located in Yangtze River Delta, China. *Environ. Pollut.*, 224, 796-809.

Publications from the Research Project

1. **Xie, J. W.**[#], Jin, L.[#], Luo, X. S., Zhao, Z., & Li, X. D. (2018). Seasonal disparities in airborne bacteria and associated antibiotic resistance genes in PM_{2.5} between urban and rural sites. *Environ. Sci. Tech. Lett.*, 5, 74-79. ([#]Co-first author) (one of the best papers in *ES&T Letters* in 2018)
2. **Xie, J. W.**, Jin, L., He, T. T., Chen, B. W., Luo, X. S., Feng, B. H., Huang, W., Li, J., Fu, P. Q., & Li, X. D. (2019). Bacteria and antibiotic resistance genes (ARGs) in PM_{2.5} from China: implications for human exposure. *Environ. Sci. Technol.*, 53, 963-972.
3. **Xie, J. W.**, Jin, L., Cui, J. L., Luo, X. S., Li, J., Zhang, G., & Li, X. D. (2020). Health risk-oriented source apportionment of PM_{2.5}-associated trace metals. *Environ. Pollut.*, 114655.
4. Jin, L., **Xie, J. W.**, Wong, C. K. C., Chan, S. K. Y., Abbaszade, G., Schnelle-Kreis, J., Zimmermann, R., Li, J., Zhang, G., Fu, P. Q., & Li, X. D. (2019). Contributions of city-specific PM_{2.5} to differential in vitro oxidative stress and toxicity implications between Beijing and Guangzhou of China. *Environ. Sci. Technol.*, 53, 2881-2891.
5. Luo, X. S., Zhao, Z., **Xie, J. W.**, Luo, J., Chen, Y., Li, H. B., & Jin, L. (2019). Pulmonary bioaccessibility of trace metals in PM_{2.5} from different megacities simulated by lung fluid extraction and DGT method. *Chemosphere*, 218, 915-921.
6. He, T. T., Jin, L., **Xie, J. W.**, Yue, S. Y., Fu, P. Q., & Li, X. D. (2021). Intracellular and extracellular antibiotic resistance genes in airborne PM_{2.5} for respiratory exposure in urban areas. *Environ. Sci. Technol. Lett.*, 8, 128-134.